UNIVERSITY OF CALIFORNIA
RIVERSIDE

Tracking Hemicellulose and Lignin Deconstruction During Hydrothermal Pretreatment of Biomass

A Dissertation submitted in partial satisfaction
of the requirements for the degree of

Doctor of Philosophy

in

Chemical and Environmental Engineering

by

Heather Lorelei McKenzie

June 2012

Dissertation Committee:
Dr. Charles E. Wyman, Chairperson
Dr. Victor Rodgers
Dr. Jianzhong Wu

The Dissertation of Heather Lorelei McKenzie is approved:

_____

_____

_____
Committee Chairperson

University of California, Riverside

ACKNOWLEDGMENTS

This work was supported by and performed as part of the BioEnergy Science Center (BESC). The BioEnergy Science Center is a U.S. Department of Energy Bioenergy Research Center supported by the Office of Biological and Environmental Research in the DOE Office of Science. BESC was an incredible learning opportunity. I would also like to acknowledge the financial support provided by the Natural Sciences and Engineering Research Council of Canada, William R. Pierson Graduate Fellowship, and the Martin Keller Award for Excellence for Student Poster. Support by the Ford Motor Company for the Ford Motor Company Chair in Environmental Engineering was also valuable to the completion of this thesis. Finally, this thesis would have been impossible without the facilities provided by the University of California Riverside College of Engineering Center for Environmental Research and Technology.

I would like to thank my thesis advisor Dr. Wyman for his mentorship over the past five years; when I started I couldn't have imagined all the things that I have accomplished during my Ph.D. I would also like to thank my lab mates, especially Dr. Jaclyn DeMartini, Hongjia Li (who will one day be a doctor), Xiadi Gao (another future doctor), and Dr. Taiying Zhang for many helpful discussions. I worked with many outstanding researchers as part of the BioEnergy Science Center. Their contributions were invaluable and are noted at the start of each chapter. There are many people who helped me get through the rough spots: Dr. Hsiao-yun Yeh, Dr. Sharon Walker, my parents, my sister, and most of all my fiancé, Brandon Trajano. Brandon was always there for me with dinner, a pep talk, a pair of helping hands, or sometimes all three.

ABSTRACT OF THE DISSERTATION

Tracking Hemicellulose and Lignin Deconstruction
During Hydrothermal Pretreatment of Biomass

by

Heather Lorelei McKenzie

Doctor of Philosophy, Graduate Program in Chemical and Environmental Engineering
University of California, Riverside, June 2012
Dr. Charles E. Wyman, Chair

The development of transportation fuels with low greenhouse gas emissions is imperative due to growing demand for transportation fuels, decreasing conventional petroleum supplies, and global warming. Ethanol from cellulosic biomass could address all of these challenges but current conversion technologies are not commercially feasible. Expensive pretreatments and enzymes are needed to recover fermentable sugars from cellulose and hemicellulose. Lignin represents an additional barrier to sugar recovery. The pretreatment step, key to the conversion process, hydrolyzes xylan, part of hemicellulose, and disrupts lignin. Cellulose, hemicellulose, and lignin are closely associated in the cell wall but the effect of these associations during pretreatment has not been studied despite suggestions that they are important. Better knowledge of hemicellulose and lignin deconstruction during pretreatment could lead to breakthroughs that would bring cellulosic ethanol one step closer to reality.

Key to this study of biomass deconstruction was the use of a fixed bed flowthrough pretreatment reactor. Pretreatment products are swept out of the reactor quickly thus facilitating the tracking of products as a function of time, limiting side and degradation reactions, and product precipitation at the end of pretreatments. The implementation of a metal 96 well plate for pretreatment resulted in the implementation of indirect steam heating, which raised questions about the adequacy of fluidized sand baths for heating. The results of pretreatment and enzymatic hydrolysis using each system were not significantly different although indirect steam did prove to be the superior heating system. Confident in the performance of the fluidized sand bath, baseline-operating conditions for flowthrough pretreatment were selected based on review of the literature, modeling, and trial and error. *Populus trichocarpa*, a potential bioenergy crop, was subjected to batch and flowthrough pretreatment along with model substrates: holocellulose, the hemicellulose and cellulose portion of *P. trichocarpa*, birchwood xylan, and cellulolytic enzyme lignin isolated from *P. trichocarpa*. The differences in the pretreatment results among these substrates indicate that the associations between cellulose, hemicellulose, and lignin limit the hydrolysis of xylan but increase the extractability of lignin. The findings of this thesis provide new research directions and suggest new plant modification and pretreatment strategies.

Table of Contents

List of Figures

Chapter 1. Introduction

Chapter 3. Evaluation of options for a high throughput pretreatment and hydrolysis system for screening biomass

Chapter 4. A comparison of the heating performance of a fluidized sand bath and a steam chamber and their effects on the results of pretreatment and enzymatic hydrolysis.

Chapter 5. Data development and modeling to define operating strategies and baseline performance for the study of biomass deconstruction during hydrothermal pretreatment.

List of Tables

Chapter 2. Fundamentals of biomass pretreatment at low pH.

Chapter 3. Evaluation of options for a high throughput pretreatment and hydrolysis system for screening biomass.

Chapter 4. A comparison of the heating performance of a fluidized sand bath and a steam chamber and their effects on the results of pretreatment and enzymatic hydrolysis.

Chapter 5. Data development and modeling to define operating strategies and baseline performance for the study of biomass deconstruction during hydrothermal pretreatment.

Chapter 6. Deconstruction of xylan in *Populus trichocarpa* and model substrates during hydrothermal pretreatment.

Chapter 7. Deconstruction of lignin during hydrothermal pretreatment.

Chapter 8. Cellulosic ethanol and gasoline for 100 years: A comparison of carbon dioxide fluxes associated with production and use of ethanol from cellulosic energy crops grown in different regions of North America to the production and use of gasoline from various fossil fuel feedstocks over 100 years.

Chapter 1.

Introduction

This chapter describes the economic and environmental concerns that make the development of alternative transportation fuels essential; many of these concerns are addressed by ethanol produced from cellulosic biomass. However, the composition and structure of plant cell walls creates a resistance to the release of fermentable sugars; this is commonly referred to as recalcitrance. A sample cellulosic ethanol facility is described; the first step in the process is pretreatment with dilute acid or water at high temperature. Although key to the success of the overall process, pretreatment is poorly understood, particularly the deconstruction of hemicellulose and lignin to soluble fragments. The approach used in this thesis to better understand these mechanisms is outlined.

1.1. The necessity of alternative fuels

Transportation accounts for approximately 27%[1] of the world's total energy consumption and most of this energy is derived from petroleum. The demand for transportation energy is still growing; in the United States demand is expected to increase by 14% from 2008 to 2035[1]. While the demand for petroleum resources increases, resource accessibility is decreasing. Over half of the petroleum used in the United States is imported[2]. A significant portion of the world's petroleum reserves is found in countries where geopolitical issues have and could disrupt petroleum supplies. The importance of unconventional resources, such as the Canadian oil sands, extra-heavy Venezuelan oil or coal to liquids, is growing[3] but these feedstocks are more difficult to recover and process resulting in increased costs and increased greenhouse gas emissions.[4]

The dual challenges of increasing demand and decreasing accessibility and reliability of petroleum resources have stimulated the search for alternative transportation fuels.

The search for alternative fuels is also heavily influenced by climate change concerns. Gases such as carbon dioxide, methane, and nitrous oxide are referred to as greenhouse gases because they absorb radiation and then release it back to the Earth's surface creating a net warming effect analogous to a glass greenhouse. Human activities such as the combustion of fossil fuels and deforestation have resulted in an increase of greenhouse gases. Atmospheric carbon dioxide levels have increased from 280 ppm in pre-industrial times to 382 ppm in 2006[5] leading to increased global temperatures and changes in the climate. Potential effects include the spread of infectious diseases, an increased number of extreme weather events such as tropical cyclones, and reduced air quality[6]. In order to avoid these misfortunes, it is necessary to reduce anthropogenic emissions of greenhouse gases, especially carbon dioxide. Since transportation emissions represent approximately one third of American greenhouse gas emissions[7] reductions in this sector are critical.

Given these concerns, a renewable transportation energy source with low or no greenhouse gas emissions is needed. Bioethanol, particularly cellulosic ethanol, represents one solution.

1.2. Cellulosic ethanol

Replacing motor gasoline is a high priority as it is the primary American transportation fuel; in 2007 it accounted for 64% of the United States' transportation fuel consumption[8]. The lower heating value of ethanol is two thirds that of gasoline but

ethanol has a significantly higher octane number therefore an engine optimized for the combustion of ethanol could likely produce about 75% of the range of a gasoline engine on a volume basis[9]. Domestic production of ethanol would help insulate the United States from petroleum shortages and stimulate rural economies. Due to carbon sequestration by plants, bioethanol typically has much lower life cycle CO_2 emissions.[10] The potential annual supply of cellulosic biomass is estimated to be 33 to 119 million tons[11] and can be produced with minimal agricultural inputs such as pesticides, fertilizers, and water. Finally, ethanol production from cellulosic feedstocks does not represent competition to food production. Given these considerations, the U.S. Renewable Fuels Standards program has mandated that American transportation fuels must annually contain 36 billion gallons of renewable fuels by 2022, 73% of which must be cellulosic fuels such as cellulosic ethanol[12].

One of the most promising cellulosic feedstocks in North America is the genus *Populus,* commonly referred to as poplar. These fast-growing, deciduous trees can be found through out North America[13] and can be grown on forest or economically marginal lands. It has been shown that *Populus* can be grown to high yields without fertilizers or irrigation,[14] and can be harvested and processed with conventional forestry equipment. The *Populus* genome has been sequenced and *Populus* has proven relatively easy to genetically manipulate therefore improved feedstock traits can be readily added. Significant research on the conversion of *Populus* to biofuels has already been conducted. Given the potential of *Populus* as an energy crop, this thesis focused on a sample species, *Populus trichocarpa*.

Like all cellulosic biomass, *Populus* has three major fractions: cellulose, hemicellulose, and lignin. Cellulose is a polymer made up of glucose units covalently linked by 1, 4 glycosidic bonds.[15, 16] Strong intramolecular and intermolecular hydrogen bonds limit the release of glucose monomers during acid hydrolysis.[16] Hemicellulose refers to a collection of shorter, branched polymers made up of pentoses such as xylose and arabinose and hexoses such as glucose and mannose. The amorphous structure of these polymers makes them easily hydrolyzed. Xylans are the major hemicellulose in *Populus*. The third polymer is lignin, which consists of *p*-coumaryl, coniferyl, and sinapyl alcohol in a highly branched structure[17]. Hydrogen bonds form between cellulose and hemicellulose while hemicellulose and lignin share covalent bonds.[17, 18] The structure of the plant cell wall hinders the recovery of sugar monomers; this resistance is referred to as recalcitrance.

To produce ethanol from cellulosic biomass, a biorefinery must overcome this recalcitrance with minimal cost; Figure 1 presents a flow diagram of a possible biorefinery adapted from Humbird et al.[19] The first reactive step, pretreatment, is designed to alter the composition and structure of the biomass so that the enzymatic hydrolysis of the sugar polymers to monomers by cellulase can occur rapidly and with greater yields[20]. Two of the most promising pretreatments are dilute acid pretreatment and hydrothermal pretreatment. Dilute acid pretreatment uses 0.5 to 1.0% sulfuric acid at temperatures ranging from 140 to 190^{o}C[21] while hydrothermal pretreatment is the cooking of biomass in water at temperatures between 180 to 220^{o}C[20]. Both processes result in hydrolysis of a significant portion of hemicellulose. The hydrolysate from dilute

acid pretreatment contains primarily monomers while the hydrolysate from hydrothermal pretreatment contains primarily oligomers. Glucose and nutrients are used to grow a cellulase producing fungus, such as *Trichodermia reesei*. *T. reesei* produces a mixture of cellulase enzymes including endoglucanase, exoglucanase, and β-glucosidase, each of which has a unique role in hydrolyzing cellulose to fermentable glucose. The resulting fermentation broth containing the secreted enzymes is blended with the pretreated solids and hydrolysate. Humbird's[19] process calls for the partial enzymatic hydrolysis of the solids before the slurry is transferred to a batch bioreactor. After enzymatic hydrolysis is completed in the batch reactor, a microorganism such as *Zymomonas mobilis* is added to ferment the available pentoses and hexoses to ethanol. Fermentation produces beer, an aqueous stream containing approximately 5 wt% ethanol as well as unconverted solids. The solids are separated and the ethanol is recovered by distillation and molecular sieve adsorption[19]. The residual solids, consisting primarily of lignin, are burned to provide process steam and power for the biorefinery. The water, or stillage, is treated and recycled.

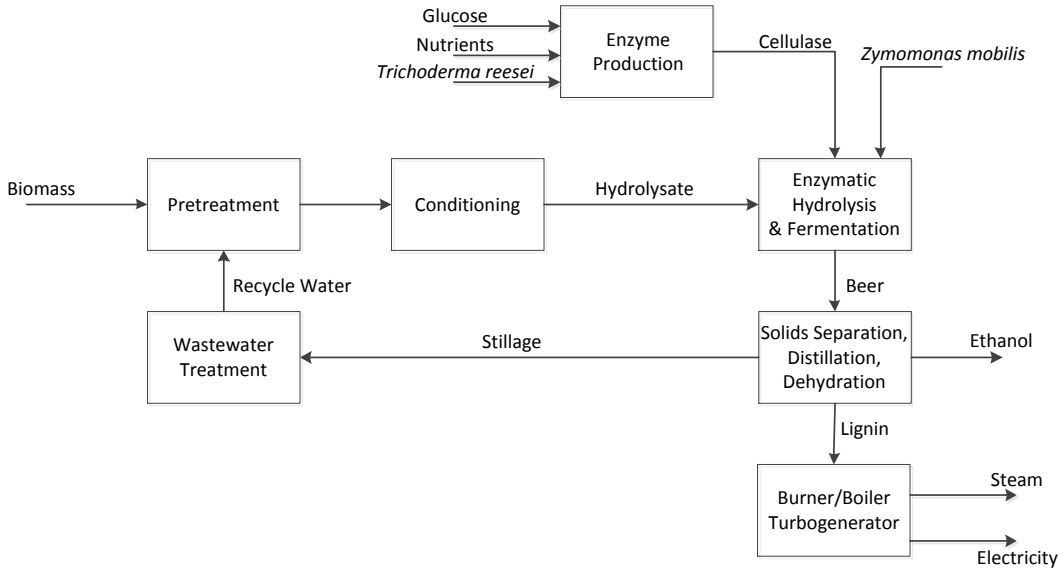

Figure 1.1. Process flow diagram for the production of ethanol from cellulosic biomass. Adapted from Humbird et al.[19]

The pretreatment step must realize high sugar yields for the overall process with multiple crops from various sites over a range of harvest ages with minimum use of heat, pressure, and chemicals. The type of pretreatment influences the type and amount of enzyme needed for saccharification as well as the yield and concentration of sugars.[22] Pretreatment may also lead to the production of inhibitors that can negatively affect saccharification and fermentation operations.[22] The sugar concentrations will dictate the ethanol concentrations and thus the distillation requirements.[22] Pretreatment will also influence the types of residues that must be disposed of or can be used for combustion. Therefore, pretreatment can have a significant impact on the economic competitiveness of a facility.

1.3. Thesis motivation

Despite pretreatment's importance to the economic success of cellulosic ethanol, it is still poorly understood. Both xylan and lignin are reactive during hydrothermal

pretreatment and the removal of xylan and lignin are frequently cited as key pretreatment objectives but the mechanisms are not well defined. Without a clear understanding of the fate of xylan and lignin during pretreatment, it is difficult to develop strategies to improve their removal while realizing low costs. Furthermore, although many kinetic models for the hydrolysis of hemicellulose to monomers and subsequent degradation products exist, the models are highly empirical and are of limited value for scale up. These models treat the hydrolysis of xylan to xylose as a series of homogeneous, first order reactions with Arrhenius kinetics. However, xylan is a complex substrate sharing bonds with both cellulose and lignin. The effects of these interactions on xylan hydrolysis have not been considered. Lignin is an even more complex substrate. It has been suggested that the reduction in the lignin content of biomass following pretreatment is due to depolymerization, a phase change, or dissolution and that the bonds between hemicellulose and lignin may also influence the deconstruction of lignin during pretreatment. However, little effort has been made to analyze these suggestions.

Against this background, the goal of this thesis is to develop greater insight into the mechanisms of biomass deconstruction. The key tool in the pursuit of this knowledge is a flowthrough reactor. The flowthrough reactor is a percolation type reactor and has several advantages over a batch reactor including: the monitoring of the evolution of pretreatment products as a function of time, the limitation of side and degradation reactions, and the removal of pretreatment products prior to reaction quenching thus avoiding precipitation of products. The course of product generation should reflect the recalcitrance of the solid substrate.

1.4. Thesis organization

The first type of pretreatment discussed in this thesis is dilute acid pretreatment, which can be applied to a wide variety of feedstocks in support of enzymatic digestion of biomass to fermentable sugars and other processes. The fundamentals are described in Chapter 2. However, there are several disadvantages to dilute acid pretreatment including the need for expensive, corrosion-resistant equipment, solid and liquid streams often require washing or neutralization, and conditioning process may result in product loss. Therefore, the balance of the thesis focuses on hydrothermal pretreatment. The principles of hydrothermal hydrolysis are very similar to dilute acid hydrolysis.

The results of pretreatment cannot be predicted a priori thus a trial and error approach is required when evaluating combinations of biomass feedstock, pretreatment, and enzymatic hydrolysis. To support this task a high throughput pretreatment and enzymatic hydrolysis system is required. The first step in the development of this system was to evaluate possible systems; this evaluation is presented in Chapter 3. The most promising system, a custom-made metal 96 well plate was selected for further characterization. These details are published elsewhere.[23]

The new 96 well plate led to the introduction of indirect steam as a heating medium. In Chapter 4, heating with indirect steam is compared to heating in a conventional fluidized sand bath.

After establishing the effectiveness of the fluidized sand bath for heating pretreatment reactors, pretreatment operating strategies are developed in Chapter 5. The

effects of temperature, time, and flow rate on the pretreatment of *Populus trichocarpa* are examined with a combination of models and experimental work.

Populus trichocarpa and model substrates are pretreated in Chapters 6 and 7. In Chapter 6, the influence of cellulose and lignin on the hydrolysis of xylan during hydrothermal pretreatment is examined. In Chapter 7, the influence of carbohydrates on the conversion of lignin during hydrothermal pretreatment is examined.

Chapter 8 represents a shift away from the study of pretreatment. One of the major concerns regarding the use of cellulosic ethanol is the greenhouse gas emissions from land use changes. A life cycle analysis of the CO_2 emissions from the production and consumption of ethanol is developed and compared with emissions from the production and consumption of gasoline.

Conclusions and recommendations for future work are presented in Chapter 9.

1.5. References

(1) International Energy Outlook 2011; DOE/EIA-0484(2011); U.S. Energy Information Administration: Washington, DC, September 2011; 9-16.

(2) Wyman CE. Biomass ethanol: technical progress, opportunities and commercial challenges. *Annu. Rev. Energ. Env*. **1999**; *24*: 189-226.

(3) Brandt AR, Farrell AE. Scraping the bottom of the barrel: greenhouse gas emission consequences of a transition to low-quality and synthetic petroleum resources. *Climatic Change*. **2007**; *84*: 241-263.

(4) Brandt AR, Plevin RJ, Farrell AE. Dynamics of the oil transition: Modeling capacity, depletion, and emissions. *Energy*. **2010**; *35*: 2852-2860.

(5) Atmosphere Changes. http://www.epa.gov/climatechange/science/recentac.html (Accessed April 2012), Environmental Protection Agency.

(6) Climate Change- Health and Environmental Effects. http://www.epa.gov/climatechange/effects/health.html (Accessed April 2012), U.S. Environmental Protection Agency.

(7) Emissions of Greenhouse Gases; DOE/EIA-0573(2007); Energy Information Administration, Washington, D.C., December 2008.

(8) Annual Energy Review- Petroleum. http://www.eia.doe.gov/emeu/aer/petro.html (Accessed June 2008), Energy Information Administration, Table 5.13c.

(9) Wyman C. Ethanol Fuel in *Encyclopedia of Energy*; C.J. Cleveland, Ed.; Elsevier Academic Press: Boston, 2004; Vol. 2, 541-555.

(10) Lynd LR. Overview and evaluation of fuel ethanol from cellulosic biomass: Technology, economics, the environment, and policy. *Annu. Rev. Energ. Env*. **1996**; *21*: 403-465.

(11) Perlack RD, Stokes BJ, Eds. *U.S. Billion-Ton Update: Biomass Supply for a Bioenergy and Bioproducts Industry*; ORNL/TM-2011/224; U.S. Department of Energy: Oak Ridge National Laboratory, Oak Ridge, TN, 2011.

(12) EPA Finalizes Regulations for the National Renewable Fuel Standard Program for 2010 and Beyond. http://www.epa.gov/otaq/renewablefuels/420f10007.pdf (accessed April 8, 2012).

(13) Sannigrahi P, Ragauskas AJ, Tuskan GA. Poplar as a feedstock for biofuels: a review of compositional characteristics. *Biofuels, Bioprod. Bioref*. **2010**; *4*: 209-226.

(14) Labrecque M, Teodorescu TI. Field performance and biomass production of 12 willow and poplar clones in short-rotation coppice in southern Quebec (Canada). *Biomass Bioenerg*. **2005**; *29*: 1-9.

(15) Wyman CE, editor. Handbook on bioethanol: production and utilization. United States of America: Taylor and Francis; 1996.

(16) Hallac BB, Ragauskas AJ. Analyzing cellulose degree of polymerization and its relevancy to cellulosic ethanol. *Biofuel. Bioprod. Bior*. **2011**; *5*: 215- 225.

(17) Fenegel D, Wegener G. Lignin in *Wood- Chemistry, Ultrastructure and Reactions*. Walter de Gruyter: New York, 1984; p. 141.

(18) Albersheim P, Darvill A, Roberts K, Sederoff R, Staehelin A. *Plant cell walls from chemistry to biology*. Garland Science: New York, 2011.

(19) Humbird D, Davis R, Tao L, Kinchin C, Hsu D, Aden A, Schoen P, Lukas J, Olthof B, Worley M, Sexton D, Dudgeon D. *Process Design and Economics for Biochemical Conversion of Lignocellulosic Biomass to Ethanol: Dilute-Acid Pretreatment and Enzymatic Hydrolysis of Corn Stover*; NREL/TP-5100-47764; U.S. Department of Energy: National Renewable Energy Laboratory, Golden, CO, 2011.

(20) Mosier N, Wyman C, Dale B, Elander R, Lee YY, Holtzapple M, Ladisch M. Features of promising technologies for pretreatment of lignocellulosic biomass. *Bioresource Technol*. **2005**; *96*: 673-686.

(21) Wyman CE, Dale BE, Elander RT, Holtzapple M, Ladisch MR, Lee YY. Coordinated development of leading biomass pretreatment technologies. *Bioresource Technol*. **2005**; *96*: 1959-1966.

(22) Wyman CE. What is (and is not) vital to advancing cellulosic ethanol. *Trends Biotechnol*. **2007**; *25*: 153-157.

(23) Studer MH, DeMartini JD, Brethauer S, McKenzie HL, Wyman CE. Engineering of a high-throughput screening sysetm to identify cellulosic biomass, pretreatments, and enzyme formulations that enhance sugar release. *Biotechnol. Bioeng*. **2010**; *105*(2): 231-238.

Chapter 2.

Fundamentals of biomass pretreatment at low pH.[*]

[*] Reprinted from *High Throughput Pretreatment and Hydrolysis Systems for Screening*, in *Aqueous Pretreatment of Plant Biomass for Biological and Chemical Conversion to Fuels and Chemicals*, edited by Professor Charles E. Wyman, Copyright (IN PRESS) John Wiley and Sons Ltd. Please contact publishers for details.

2.1. Abstract

Production of fuels and chemicals from lignocellulosic biomass typically requires an initial treatment to produce reactive intermediates. For ethanol production via biological conversion of sugars, this step is referred to as pretreatment and produces a more digestible form of biomass for subsequent enzymatic hydrolysis. Additionally, new developments in catalytic production of hydrocarbons for use as drop-in fuels or chemicals has generated interest in the conversion of biomass to reactive intermediates in addition to sugars such as furfural and levulinic acid that result from sugar dehydration. All of these intermediates can be generated through acid hydrolysis of biomass. In this chapter, changes in cellulose, hemicellulose, lignin, ash and ultrastructure following acid hydrolysis of biomass are described. Furthermore, the evolution of acid treatment objectives is outlined along with common acidifying agents, reaction temperatures and times, and reactor configurations. Kinetic models of these reactions are also reviewed.

2.2. Introduction

A wide variety of conversion processes can be used to generate fuels and chemicals from biomass, with many including a hydrolysis and/or dehydration reaction at low pH as an initial stage. In the case of acid hydrolysis of biomass prior to enzymatic hydrolysis and fermentation, this step is called pretreatment. Due to the diversity of conversion processes, it is difficult to define a single set of objectives, but in general, the goals are to generate reactive intermediates in high yields for subsequent conversion to final products and minimize generation of compounds that interfere with downstream operations. For example, if lignocellulosic biomass is to be converted to ethanol through dilute acid pretreatment, enzymatic hydrolysis, and fermentation, the objectives of pretreatment are to produce high yields of hemicellulose sugars, improve the enzymatic digestibility of the remaining solids to realize high yields of glucose, and avoid generating biological inhibitors such as furfural and acetic acid. On the other hand, if lignocellulosic biomass is to be converted into jet fuel alkanes through cellulose hydrolysis to levulinic acid followed by catalytic processing of levulinic acid to alkanes, the objectives are to generate levulinic acid in high yields and avoid solid catalyst poisons such as mineral acids.

Two of the primary advantages of low pH reactions are the ready availability of catalysts such as H_2SO_4 and SO_2 and high product yields. However, the capital costs of reactors and associated equipment used for low pH reactions are high due to the need for expensive, corrosion-resistant materials. As well, the solid and liquid streams resulting

from low pH pretreatment often require washing or neutralization. Both of these considerations create technical challenges and add cost. Finally, the conditioning process to reduce inhibitors can result in sugar losses as well as added expense. For example, Martinez and coworkers[1] found that the total sugars in pretreatment hydrolysate decreased by 8.74±4.46% after overliming.

This chapter will first explore the earliest use of acid in biomass conversion that provided a foundation for extension to biological conversion of biomass to ethanol, i.e. pretreatment: cellulose hydrolysis to glucose for fermentation to ethanol. Examples of the operating conditions associated with this process will be presented. Emphasis will be placed on the use of SO_2 and H_2SO_4, the most common acidifying agents, given their effectiveness and low price. The evolution of dilute acid pretreatments to support conversion of biomass to hydrocarbon fuels with solid catalysts will also be discussed. Kinetic models of cellulose and hemicellulose hydrolysis at low pH conditions will also be presented. One model of pretreatment makes use of a relationship known as the combined severity (CS) factor, defined as[2,3]:

$$\log(CS) = \log\left(t \exp\left(\frac{T - 100}{14.75}\right)\right) - pH \tag{1}$$

where t is the time in minutes, and T is the temperature in degrees Celsius. This relationship will be discussed further in section 2.6.2; however, it is a useful way of comparing the different pretreatment conditions presented in sections 2.4 and 2.5.

Low pH pretreatment is a diverse field, and references to which could easily fill a book therefore, the objective of this chapter is to provide a summary of key references for

the interested reader to pursue. The selection of pretreatment conditions is a complex problem that depends on factors such as process objectives, biomass species, chemical costs, safety considerations, and local influences such as regulations or chemical availability. It is currently not possible to identify optimum pretreatment conditions without extensive experimental work and process engineering to arrive at the optimal overall system.

2.3. Effects of low pH on biomass

2.3.1. Cellulose

Cellulose is a linear polymer of glucose that typically accounts for 35 to 50% of lignocellulosic biomass.[4] The monomer units are covalently linked by 1, 4 glycosidic bonds.[5] Due to the presence of multiple hydroxyl groups, there is a high degree of intramolecular and intermolecular hydrogen bonding between the glucan chains.[5] The glucan chains form a crystalline core with a semi-crystalline shell[6, 7]

Due to the crystalline nature of cellulose, very low pH, high temperatures, or extended times are required to hydrolyze significant quantities of cellulose to glucose.[8] Under conditions that favor cellulose hydrolysis, the glucose released degrades to products such as levulinic and formic acid.[8] Under less severe hydrolysis conditions, the degree of polymerization has been found to change substantially. Several researchers[9,10,11] hydrolyzed different cellulose substrates such as cotton linters and wood pulp with 2.45 to 5 N HCl or 2.5 N H_2SO_4 at 5 to 105^oC for 0.25 to 480 hours and then calculated the degree of polymerization from cuprammonium viscosity values. These treatments resulted in 2 to 20% loss of cellulose. They found that during hydrolysis the

degree of polymerization decreased rapidly initially and then stabilized at a level-off degree of polymerization (LODP) after 15 to 30 minutes.[9,10,11] It was proposed that the initial decrease in DP was due to the rapid hydrolysis of amorphous cellulose. In his study, Battista subjected wood pulp to mild hydrolysis with 5 N HCl at 18^{o}C for 24 hours to 44 weeks, a drastic hydrolysis with boiling 2.5N HCl for 1 to 15 minutes, or mild hydrolysis followed by drastic hydrolysis.[9] In this case, the weight loss during drastic hydrolysis for the sequential process was lower than the weight loss for the single stage drastic hydrolysis.[9] Based on these observations, Battista proposed that under mild conditions, hydrolysis occurs slowly, and crystallization generates pieces that are more resistant to acid hydrolysis.[9] A study by Bouchard et al. revealed similar trends in the degree of polymerization following hydrolysis of α-cellulose; they also showed that after a period of slow depolymerization, the rate of depolymerization increased.[12] The three phases were attributed to endogenous attack of amorphous cellulose by acid followed by exogenous acid attack of the ends of crystalline cellulose and finally simultaneous endogenous/exogenous hydrolysis of the remaining cellulose.[12] Changes in the degree of polymerization of cellulose in lignocellulosic materials following acid hydrolysis have also been detected. Martínez and colleagues subjected a softwood mixture and almond shells to dilute acid pretreatment and then determined the degree of polymerization from intrinsic viscosity measurements.[13] When Martínez and colleagues plotted the degree of polymerization as a function of severity, they observed the characteristic rapid decrease in degree of polymerization for both substrates.[13] In the case of a softwood mixture, this rapid initial decrease was followed by stabilization at the level-off degree of

polymerization.[13] Almond shells were not pretreated at high severity conditions, so no LODP was observed.[13] Kumar et al. subjected corn stover and poplar to hydrolysis with dilute H_2SO_4 and SO_2.[14] These treatments removed 3.1 to 12.1% of the glucan in biomass and reduced the degree of polymerization by 65 to 85% compared to untreated biomass.[14] The degree of polymerization of cellulose in switchgrass has also been shown to decrease following pretreatment with 0.1 mol/m^3 H_2SO_4 at 160^{o}C.[15]

Mild hydrolysis has also been found to affect biomass crystallinity. In the work by Kumar and associates, the crystallinity index of the pretreated materials was measured by wide-angle X-ray diffraction and FTIR-ATR.[14] The X-ray diffraction measurements showed that the crystallinity index of corn stover and poplar increased while the FTIR spectra indicated that the ratio of amorphous to crystalline cellulose decreased.[14] Therefore, the increase in crystallinity index may reflect removal of amorphous components such as hemicellulose and lignin from biomass and not an increase in cellulose crystallinity.

2.3.2. Hemicellulose

The second most plentiful carbohydrate fraction in most lignocellulosic biomass is hemicellulose and typically accounts for approximately 15 to 35% of biomass.[4] For hardwoods, grasses, and agricultural residues, hemicellulose polymers primarily consist of pentose sugars such as xylose and arabinose. Depending on the substrate, hemicellulose typically also contains the hexose sugars glucose, mannose, and galactose, with these sugars being most prevalent in softwoods. The structure of hemicellulose is

more complex than cellulose and contains many branches. Acetyl is the most common side group.[4]

Due to its branched structure, hemicellulose is amorphous and much more susceptible to acidic hydrolysis than cellulose. In fact, hemicellulose can be almost completely removed with limited damage to cellulose.[16] The extent of hemicellulose removal, of course, depends upon hydrolysis conditions. For example, Öhgren and colleagues were able to recover approximately 65% of the xylan in corn stover by pretreatment with 2% SO_2 at 200^{o}C for 2 minutes, while only an 18% yield was achieved when the same corn stover was pretreated with 2% SO_2 at 170^{o}C for 2 minutes.[17]

The removal of hemicellulose appears to depend upon the acidifying agent. For example, Martín and colleagues found that pretreatment of sugarcane bagasse with H_2SO_4 resulted in complete removal and partial degradation of xylan while SO_2 pretreatment removed less xylan but produced substantially fewer degradation products such as furfural.[18] These differences were likely due to the differences in the amount of H_2SO_4 or SO_2 absorbed by bagasse prior to pretreatment.

Hemicellulose sugars can be released into solution either as oligomers or monomers, with their ratios varying with temperature, time, and acid concentration. For example, as the temperature was increased from 201^{o}C to 225^{o}C for hydrolysis of poplar in 0.4% H_2SO_4, the fraction of monomers in the hydrolysate increased from 55 to 76%.[19] In another study, increasing the H_2SO_4 concentration increased the selective production of xylose from xylooligomers.[20]

Acetyl groups are removed during acid hydrolysis as acetic acid or attached to solubilized hemicellulose.[16, 20, 21] Experimental results indicate that once released, acetic acid does not degrade[16,21,22]; therefore increasing hydrolysis time increases the release of acetyl monomers from hemicellulose. However, there is no consensus on the effect of temperature on the release of acetyl groups. For example, Maloney and co-workers found that the acetyl removal rate from paper birch was slightly faster than that of xylan removal at 100 and 130^{o}C but decreased at 150 and 170^{o}C.[21] In contrast, Aguilar and colleagues showed that increasing the temperature of hydrolysis of sugar cane bagasse from 100 to 122^{o}C with 2-6% H_2SO_4 increased the acetic acid concentration in the hydrolysate, but a second temperature increase to 128^{o}C reduced the acetic acid concentration slightly.[16] These differences may be a reflection of differences in the types of biomass used or the acid concentration.

Once in solution, hemicellulose derived oligomers can react to form products such as furfural that can react with each other or with sugars to form more complex products[23]; for example pentose can be acetalized by furfural.[24] Furfural can further decompose to formic acid or humin char.[25] These decomposition reactions have been observed for numerous types of biomass including corn stover[17, 26], hardwoods,[27] softwoods,[27] and switchgrass[27]. Possible reaction schemes were described by Antal and co-workers[23], Hoydonckx and co-workers[24], and Weingarten and co-workers[25]. As hydrolysis time increases, the extent of these decomposition reactions increases as well. The higher the hydrolysis temperature, the sooner decomposition becomes significant. For example, the maximum xylose production from corn stover was achieved in 2 minutes at 180^{o}C and 5

minutes at 160°C using 0.98% H_2SO_4; for reactions lasting longer than these times, xylose yields dropped due to degradation.[26] Similarly, as acid concentration is increased at a constant temperature, the time to maximum xylose yield or onset of significant degradation drops.[26]

2.3.3. Lignin

Lignin is the third major polymer in biomass but is made up of phenol monomers and not sugars. It typically accounts for 17 to 33% of a plant's mass.[28] Coumaryl, coniferyl, and sinapyl alcohol are the three monomeric precursors to lignin[28]; the relative portions of each monomer vary by biomass species. Lignin's structure is highly irregular and forms covalent bonds with the surrounding hemicellulose.[28]

Lignin removal during acid hydrolysis in batch reactors is typically low regardless of biomass type or acidifying agent.[14, 22, 29] Liu and Wyman found that pumping 0.05 to 0.1 wt% H_2SO_4 through corn stover at 180°C increased lignin removal from approximately 10% in a batch reactor to about 50%.[30] The removal of lignin is accompanied by the generation of aromatic monomers in the liquid hydrolysate, and the type and amount of phenols varies with both the biomass treated and hydrolysis conditions.[31] For example, salicylic acid was found in higher concentrations in hydrolysates produced from poplar than from corn stover and pine, and its concentration varied with H_2SO_4 concentration.[31] Other researchers who identified aromatics in hydrolysates include Martín and associates and Excoffier and co-workers.[18, 19]

The limited removal of lignin from biomass during acid hydrolysis may be somewhat deceiving as it has been shown that the carbohydrate fractions can react to

form compounds that analysis procedures classify as lignin. For example, Sievers and co-workers' NMR analysis of loblolly pine hydrolyzed at 200°C with sulfuric, phosphoric, or trifluoroacetic acid ($C_2HF_3O_2$) displayed an increase in signal intensities associated with aromatic carbon, an increase that could only result from reaction of carbohydrates to aromatics or "pseudo-lignin".[32] Sannigrahi and associates provided further evidence of pseudo-lignin formation from carbohydrates by subjecting poplar-derived holocellulose to acid hydrolysis[33]. This team recovered holocellulose, the hemicellulose and cellulose portion[34] of *Populus trichocarpa x deltoides* by twice exposing the biomass to $NaClO_2$ and acetic acid twice at 70°C for one hour. After acid hydrolysis of this holocellulose, a lignin-like fraction, "pseudo-lignin", was detected in the resulting solids by wet chemistry, NMR, and FT-IR.[33] However, because the untreated holocellulose contained only 1.6% Klason lignin, the pseudo-lignin was primarily generated through acid-catalyzed reactions of cellulose and hemicellulose.[33] The increased production of pseudo-lignin with increasing hydrolysis severity suggests that researchers should use multiple analytical procedures when determining lignin removal following high severity hydrolysis.

The lignin that remains in solids following acid hydrolysis is modified in several ways. At a chemical level, researchers have found evidence of acid condensation and oxidation through FT-IR.[14, 29] and a drop in selective bromination.[29] Microscopic examination of the solids following pretreatment revealed dramatic changes in the morphology and distribution of lignin. A number of researchers observed deposition of spherical droplets on cell walls. These droplets were observed to cluster near

ultrastructural features such as cell corners[35, 36] and demonstrated to contain lignin with a number of techniques including $KMnO_4$ staining[35, 36], FTIR spectroscopy[36], NMR analysis[36], and antibody labeling[36]. The morphology and localization of these droplets to the natural pores of biomass led to speculation that a cycle of melting and coalescing may be responsible for lignin removal.[35, 36, 37]

2.3.4. Ash

Biomass also contains inorganic material, commonly referred to as ash,[38] and includes both plant structural components and materials such as in soil picked up in harvesting operations. In woody species, the structural mineral content ranges from 0.3 to 2 wt%, while in herbaceous species and agricultural residues, the structural mineral content may account for as high as 16 wt%.[4] The composition of this inorganic fraction varies by biomass species. Biomass cations include potassium, calcium, magnesium, sodium, manganese, and ammonium; possible anions are sulfates, phosphates, chloride and nitrate.[22, 39, 40, 41] When combined with biomass, mineral acids such as H_2SO_4 are neutralized through an ion-exchange reaction between inorganic cations and hydronium ions.[39] It is difficult to determine the neutralizing capacity of biomass, but the mineral content provides an adequate estimate.[39] Due to their higher mineral content, the neutralizing capacity of herbaceous biomass and agricultural residues is generally higher than that of woody materials.[42, 43] In order to simplify reaction kinetic models, it is frequently assumed that neutralization is instantaneous upon mixing of biomass and acid.[22, 42, 43] However, Springer and Harris demonstrated that neutralization is in fact a complex phenomenon in that the exchange of cations with hydronium ions varies with

temperature and applied acid concentration and is incomplete even under severe hydrolysis.[39]

2.3.5. Ultrastructure

The ultrastructure of biomass undergoes several changes during acid hydrolysis as well. It has been shown that biomass particle sizes decrease during acid hydrolysis and that as the severity of the treatment increases, the percentage of small particles and fines increases.[44] Additionally, it has been shown that the size of intraparticle pores changes as a result of acid hydrolysis. When Grethlein hydrolyzed birch, maple, poplar, white pine, and steam extracted southern pine with 1% H_2SO_4 at 180 to 220^{o}C for 7.8 seconds, he found that the pore volume increased with increasing pretreatment temperature[45] and attributed these changes hemicellulose to removal during pretreatment.[45] Wong and coworkers and Excoffier and associates saw a similar increase in pore volume with increasing hemicellulose removal.[19, 46] However, both groups also indicated that partial removal of cellulose or lignin redistribution might also contribute to changes in pore volume.[19, 43]

2.3.6. Summary of effects of low pH on biomass

The effects of aqueous, low pH conditions on biomass ultimately depend on the concentration of the acidifying agent, temperature, and time of the reactions. In general low pH aqueous treatments produce biomass solids enriched in cellulose and lignin. Some pseudo-lignin formed from hemicellulose may also be included. The acidic liquid stream, or hydrolysate, produced contains hemicellulose derived sugars such as xylose and xylooligomers and associated degradation products such as furfural. Some aromatic

monomers derived from lignin may also be present. Although glucose concentrations are generally low for typically favored pretreatment conditions, the amounts of glucose and cellulose degradation products in the hydrolysate will increase as the severity of the reaction conditions is increased.

2.4. Low pH hydrolysis for biological conversion

2.4.1. Hydrolysis of cellulose to fermentable glucose

Braconnot discovered cellulose hydrolysis to glucose by concentrated acid in 1819.[47] Much of the early wood hydrolysis work focused on using concentrated acids, such as 40 to 42% HCl[47] at atmospheric pressure, to produce glucose for fermentation to ethanol. In the late nineteenth century Simonsen erected an experimental plant in which cellulose hydrolysis was conducted with 0.5% H_2SO_4 at a pressure of 9 atm (T_{sat}= 176^{o}C) for 15 minutes.[47] Work was also conducted using sulfurous acid, H_2SO_3, as the hydrolyzing agent. Although a number of similar facilities were constructed during the early twentieth century, these facilities did not operate for long due to numerous technical and commercial difficulties, and ultimately alcohol production from wood was abandoned.

During World War II the demand for ethanol skyrocketed. As the traditional feedstock, molasses, was scarce, producers began using feedstocks such as wheat flour, corn, sorghum grain, and barley. However, by approximately 1943, these feedstocks became increasingly difficult to obtain, so the War Production Board recommended that ethanol production from wood be investigated resulting in some of the earliest pretreatment research. These early pretreatments were directed at hemicellulose removal

prior to further acid hydrolysis of cellulose to recover six-carbon sugars for fermentation to ethanol by *Sacchromocyes cerevisiae.*[4] Many of the conditions were selected for complete hydrolysis of cellulose to glucose while allowing pentose degradation because pentoses were non-fermentable by the available organisms and considered waste.[5]

One of the first commercial processes for conversion of cellulosic biomass to ethanol was the Scholler process. Sawdust and wood chips were loaded into brick-lined steel percolators and preheated to 129^{o}C by steam injection; batches of 0.5% H_2SO_4 were forced through at 1.14 to 1.24 MPa.[48] Each batch reaction took approximately 45 minutes.[48] In the Madison wood sugar process, a modification of the Scholler process, Douglas fir wood waste first treated with 0.5 to 0.6% H_2SO_4 at 150^{o}C for 20 minutes.[49] Additional dilute acid was added as the temperature was increased to 185^{o}C,[49] and the reactor was maintained at this temperature until the completion of the run, typically 2.3 to 3.0 hours.[49] The resulting sugar solution was continuously removed, and the reducing sugar yields ranged from 35.0% to 49.0% of the theoretical possible maximum.[49]

Sulfuric acid was used in both of these commercial examples, but other catalysts were investigated for the complete conversion of cellulose to glucose. Table 1 outlines some of the conditions tested. The catalysts were evaluated based on the rate of hydrolysis of cellulose relative to the rate of decomposition of hexose. Phosphoric acid was determined to be a poor catalyst due to the slow rate of hydrolysis and the increase in the rate of glucose degradation.[50] Sulfur dioxide was also found to be a poor catalyst for cellulose hydrolysis due to its relatively slow hydrolysis rate[51]. Sulfuric acid and hydrochloric acid catalysts increased the yields of reducing sugars.[51] Hydrofluoric acid,

in both the liquid and vapor phase, was also considered as a catalyst for the production of glucose from lignocellulose.[52, 53] However, although high yields of glucose were achieved at ambient temperatures and pressures, the hazards and costs of working with hydrofluoric acid on a commercial scale limited interest and research.[54]

Table 2.1. Sample pretreatment conditions for the hydrolysis of cellulose to glucose.

Agent	Concentration (wt%)	Temperature (^{o}C)	Time (min)
HCl (Harris and Kline[51])	0.2-3.2	160-190	10-320
H_3PO_4 (Harris and Lang[50])	0.2-3.2	180-195	10-180
SO_2 (Harris and Kline[51])	0.75-3.00	150-180	Various
H_2SO_4 (Harris and Kline[51])	0.04-0.16	170-190	Various
H_2SO_4 (Saeman[86])	0.4-1.6	170-190	0-90

2.4.2. Pretreatment for improved enzymatic digestibility

Concerns about military equipment rotting in the South Pacific during World War II led to the discovery of cellulase, enzymes capable of hydrolyzing cellulose to glucooligomers and glucose.[55] Up until the late 1960's, cellulase was studied in order to avoid degradation.[56] However, the combined pressures of municipal waste disposal and need for alternate fuel sources due to the 1970s energy crisis[57] led researchers to investigate the possibility of producing fermentable glucose from cellulose. The immediate advantages of enzymatic hydrolysis of cellulose to glucose were that only glucose was produced[58] and that its mild hydrolysis conditions required no expensive

construction materials; however, it was also immediately clear that enzymatic hydrolysis of native cellulosic feedstocks was slow with low yields[58]. These disadvantages prompted researchers to search for pretreatments such as with acid to increase cellulose accessibility.

Han and Callihan suggested one of the first pretreatments a two-stage process for sugarcane bagasse.[59] In this system, bagasse was exposed to 10 to 50% H_2SO_4 for 15 minutes at 121^oC in the first stage, after which, the reaction mixture was diluted to 0.5 to 2% H_2SO_4 and reheated to 121^oC for 15 minutes to 2 hours.[59] This treatment improved performance of subsequent enzymatic hydrolysis, but because the digestibility of acid treated bagasse by *Cellulomonas* and *Alcaligenes* was much lower than that of alkali treated material, they concluded that acid pretreatment was not feasible.[59] Nesse and co-workers showed that pretreatment of fiber from feedlot manure using 0.01-3.5% peracetic acid for one hour at room temperature increased its digestibility.[60] The pretreatment used by Han and Callihan[59] was relatively severe while that by Nesse and co-workers[60] was more mild. Researchers at the Lawrence Berkeley Laboratory (LBL) found that batch pretreatment with 0.9 w/w% H_2SO_4 at 100^oC lasting up to 5.5 hours significantly improved yields from enzymatic hydrolysis of several agricultural residues including wheat straw, barley straw, rice straw, sorghum straw, and corn stover.[61] Combined glucose and xylose yields, defined as grams of monomer per gram of monomer equivalent in the raw biomass, from the enzymatic hydrolysis of pretreated material were 10 to 41% higher than yields from the enzymatic hydrolysis of the raw biomass.[61] The

LBL team also showed that very little acid was consumed during the pretreatment step for most of the tested substrates, which would be commercially beneficial.

Grethlein, Converse, and coworkers[58, 62, 63] used a continuous plug flow reactor to pretreat a wide variety of materials including newsprint[57], corn stover[62], oak[62], white pine[58], poplar[63], and mixed hardwood[58]. The concentration of H_2SO_4 was varied from 0.4 to 1.2% at 160°C to 220°C with reactor retention times of 6.6 to 13.2 seconds. Some of these pretreatment conditions were very effective at increasing susceptibility of native materials such as corn stover and oak to enzymatic hydrolysis. It was found that different substrates required different pretreatments in order to achieve high enzymatic hydrolysis yields, with the improvements tentatively attributed to an increase in pore size and surface area. Many processes to increase the accessibility of cellulose to enzymes using acids were patented; for example Foody patented a process to treat lignocellulosic material with 0.15 to 1 w/w% H_2SO_4 at 1.8 MPa to 7.0 MPa.[64]

2.4.3. Pretreatment for improved enzymatic digestibility and hemicellulose sugar recovery

The development of microorganisms capable of converting both pentoses and hexoses to ethanol over the past two decades has made it possible to derive value from all the sugars in hemicellulose and cellulose.[65] Consequently, the current paradigm for ethanol production from cellulosic biomass is to recover as much sugar as possible from cellulose and hemicellulose in the combined operations of pretreatment and enzymatic hydrolysis.[66] In line with this objective, successful pretreatments must not sacrifice sugars from hemicellulose while still modifying the remaining solids so that they are

susceptible to enzymatic hydrolysis with high yields. It is also critical to limit formation of degradation products that inhibit enzymatic hydrolysis or fermentation.[66] Formation of degradation products also comes at the expense of fermentable sugars and thus ethanol. The goal to maximize sugar recovery is just important for pretreatment applications to microbes now being developed to convert biomass to fuels other than ethanol such as hydrogen.[67, 68] Despite the changing goals of pretreatment, SO_2 and H_2SO_4 are still utilized because they are readily available at comparatively low prices and lower pH effectively. Although SO_2 can be recovered and recycled following pretreatment it is more hazardous to work with, and the recovery operations would increase capital and operating costs of a commercial operation. Nitric, hydrochloric, or phosphoric acids to prepare biomass for biological conversion,[66] but the work is limited because their higher costs could present economic challenges. Attempts have been made to use carbon dioxide as an acidifying agent[69, 70, 71, 72] since it is produced during fermentation[73] and would be less corrosive than mineral acids[74]. However, yields from hydrolysis with carbon dioxide fall short of those from H_2SO_4 hydrolysis.[74] Furthermore, Jayawardhana and van Walsum[74] estimated that high pressure carbon dioxide pretreatment reactors would be more expensive than for dilute acid pretreatment.

Since space considerations prevent inclusion of the complete body of research on low pH pretreatments, some results are summarized for thoroughly studied and commercially promising processes based on SO_2 and H_2SO_4 pretreatments, with representative works by leading investigators, both individual and institutional, noted so that the reader can easily locate material for more in-depth information.

2.4.3.a. Pretreatment with sulfur dioxide

Sulfur dioxide has been used to treat a wide variety of biomass including softwoods such as Douglas fir[44], agricultural residues such as corn stover[75] and bagasse[18], and hardwoods such as poplar[75]. In most laboratory studies, biomass solids were impregnated with SO_2 at room temperature. After impregnation, the biomass was transferred to a pretreatment reactor, typically a steam explosion device, and injected with steam until the target reaction time was reached. At that point, a blow-down valve was opened to discharge the pretreated solid material and liquid hydrolysate to atmospheric pressure, cooling the materials almost instantly to 100^{o}C. A flow diagram of a sample experimental procedure and apparatus for SO_2 pretreatment was presented by Stenberg et al.[76] Schell and co-workers provided a detailed process flow diagram of a potential commercial ethanol facility using SO_2 pretreatment.[77]

The length of impregnations varied. For example, the Galbe group[18] performed impregnations lasting 15 to 20 minutes while the Saddler group[44, 75] allowed impregnations to continue overnight. Although most impregnations were performed without wetting the biomass, Öhgren et al.[17] and De Bari et al.[78] presteamed it prior to impregnation. As De Bari et al.[78] noted, when impregnated biomass is transferred from the adsorption vessel to the pretreatment reactor, some SO_2 is lost, making it difficult to compare results among researchers. Consequently, De Bari et al.[78] examined impregnation of aspen chips with SO_2 and the influence of moisture content using a custom-designed adsorption chamber. The chamber was placed on a high resolution industrial weighing platform, and after chips were loaded, sufficient SO_2 was added to

increase the weight by 4 to 5% of the aspen mass. The chamber pressure was monitored to estimate adsorption from the compressibility factor equation of state. After impregnation was complete, the biomass was removed from the reactor, and the decrease in mass was monitored as excess SO_2 desorbed from the biomass. Once a constant mass was reached, the biomass was pretreated. De Bari et al.[78] found that even after extended impregnation times, only 50% of the available gas was adsorbed, with most of it being adsorbed during the first 15 minutes. It was also found that approximately half of the adsorbed gas was lost during outgassing, leaving an adsorbed concentration of 0.6 to 0.9% SO_2 w/w raw, dry biomass. Increasing the biomass moisture content slightly increased the final amount of SO_2 adsorbed. This study[78] aptly illustrated the challenges of controlling SO_2 impregnation and accurately determining the effective SO_2 concentration during pretreatment.

Two stage pretreatment systems have been used in an attempt to increase total sugar recovery.[79] The first stage was optimized for recovery of hemicellulosic sugars, while the second step was optimized for enzymatic digestibility of biomass. Although it was possible to increase final ethanol yields and decrease enzyme usage through such two-stage pretreatments, it is unclear whether these improvements justify the additional costs and technical challenges.

Table 2.2 reveals that although SO_2 has been applied to a diverse range of biomass types, the pretreatment conditions were quite similar: SO_2 concentration ranged from 1.1 to 4.5%, temperatures between 170 and 220^{o}C, and times from 2 to 10 minutes.

However, as De Bari et al.[78] demonstrated, the concentration of SO_2 used for impregnation does not accurately reflect the amount of SO_2 adsorbed.

Table 2.2. Selected conditions for pretreatment with sulfur dioxide prior to biological conversion. Yield is defined as gram carbohydrate equivalent in the liquid hydrolysate following pretreatment per gram of carbohydrate equivalent in the raw biomass.

Substrate (Author)	SO_2 Concentration (%)	Temperature (^oC)	Time (min)	Yield (wt%)	Concentration (g/L)
Douglas fir (Boussaid et al.[44])	2.38-4.5	175-215	2.38-7.5	Mannose yield: 22-49%	
Corn stover, poplar (Bura et al.[75])	3	170-215	5-9		11.2-23.7 g xylose/L hydrolysate
Sugarcane bagasse (Martin et al.[18])	1.1	205	10	Xylan yield: 27%	
Corn stover (Öhgren et al.[17])	3	200	5		35.8 g xylose/L hydrolysate
Picea abies (Söderström et al.[79])	3	180-220	2-10	2-stage mannan yield: 91-96%	

Pretreatment with SO_2 results in the release of hemicellulose sugars and some lignin as well as degradation products at high severities. There are conflicting reports as to the effects of steam explosion with SO_2 on the degree of polymerization of the sugar products. When Boussaid et al.[44] and Söderström et al.[79] pretreated softwoods such as Douglas fir and *Picea abies* with SO_2, mannose, the primary hemicellulose sugar in softwood, was recovered as a monomer. In contrast, Bura et al.[75] found that SO_2 pretreatment of corn stover and poplar produced a lot of oligomers from hemicellulose, and especially xylooligomers. These differences may be due to differences in biomass or in pretreatment conditions. Biomass differences seem the more likely cause as the

pretreatment conditions used by Bura et al.[75] overlap those used by Boussaid et al.[44] and Söderström et al.[79]

Several studies observed that little lignin was removed by SO_2 pretreatment.[44, 75, 78] De Bari et al.[78] found that the amount of lignin increased slightly for high severity pretreatments and attributed this to formation of pseudo-lignin. A number of phenolic compounds such as *p*-coumaric acid, ferulic acid, and 4-hydroxybenzaldehyde were also released by SO_2 pretreatment.[18]

As the severity of pretreatment was increased, sugars were degraded to 5-HMF, furfural, and other non-sugar compounds.[18, 44, 75, 78, 79] Interestingly, Martin et al.[18] found that the concentrations of furfural, 5-HMF, levulinic acid, and formic acid in the hydrolysate from SO_2 catalyzed steam explosion were similar to concentrations found in the hydrolysate from uncatalyzed steam explosion, and the xylose yields from SO_2 pretreatment were only slightly higher than from steam explosion. This outcome may be because the effective SO_2 concentration decreased as biomass was transferred to the reactor or because SO_2 does not significantly accelerate degradation reactions.

2.4.3.b. Pretreatment with sulfuric acid

Dilute sulfuric acid is by far the most common acid catalyst used for biomass pretreatment prior to biological conversion. Like SO_2, it has also been used to pretreat a wide variety of biomass types. Biomass is frequently soaked in dilute acid prior to pretreatment, and the reactors used for pretreatment with H_2SO_4 are almost as diverse as the types of biomass tested. Various possible commercial processes based on dilute sulfuric acid pretreatment have been designed over the years, with a recent design by

Humbird and coworkers being one example.[80] In the case of biological conversion of the cellulose in biomass to glucose, a key research goal has been to reduce the amount of H_2SO_4 used for pretreatment.

Batch reactors are commonly applied for dilute acid pretreatments, and both stirred and unstirred reactors have been used. Lloyd and Wyman employed both reactor types to pretreat corn stover.[26] Small tube reactors typically have an inner diameter of about 10.8 mm to reduce temperature nonuniformity[81, 82] and a length of about 100 mm so reasonable biomass quantities can be processed. A larger stirred reactor with a volume of 1.0 L and an 88.9 mm helical impeller provided agitation was also used by Lloyd and Wyman.[26] The reactors were loaded with a corn stover slurry at 5% solids with 0.22 to 0.98% H_2SO_4 by weight in the water. Pretreatment temperatures varied from 140 to 180^{o}C for times up to 80 minutes. After pretreatment, the solids were subjected to enzymatic hydrolysis with cellulase supplemented with beta-glucosidase. Lloyd and Wyman[26] observed significant production of xylooligomers, during pretreatment especially for short reaction times, and the fraction of xylooligomers relative to total xylose release decreased as the concentration of acid increased. This paper illustrated the classic conundrum of dilute acid pretreatment: how to maximize sugar yields from enzymatic hydrolysis favored by long reaction times while minimizing degradation reactions during pretreatment that occur at long reaction times. In this application, Lloyd and Wyman[26] showed that the maximum yields of glucose, xylose, and combined glucose plus xylose in pretreatment and enzymatic hydrolysis did not occur for the same pretreatment conditions. Therefore, when selecting pretreatment conditions, it is

important to maximize release of all relevant sugars from pretreatment, enzymatic hydrolysis, and subsequent operations.

Dilute sulfuric acid has also been used in steam explosion systems. Sassner et al.[83] used such reactors to pretreat wood chips from a *Salix* hybrid that were presoaked in 0.25 to 0.5% H_2SO_4 for at least 90 minutes. The solids were recovered by filtration and then transferred to a 10 L steam explosion unit; pretreatment temperatures were varied from 180 to 210^{o}C for 4 to 12 minutes. The liquids and solids from pretreatment were subjected to fermentation and enzymatic hydrolysis, respectively. One unique feature of this work was that collection and analysis of the exhaust gases and hydrolysate from pretreatment revealed high concentrations of furfural and acetic acid. Sassner et al. found that xylose degradation decreased when the initial moisture content of the chips was increased.[83] A high initial moisture content increased steam condensation and appeared to improve fermentations by diluting potential inhibitors.[83] The pretreated solids were easily digested during enzymatic hydrolysis despite retaining 74 to 95% of the lignin in the raw biomass.[83]

Cahela et al.[84] pretreated Southern red oak in a percolation reactor with 0.2% H_2SO_4. The reactor had an inner diameter of 25.4 mm and a length of 627 mm and could be loaded with 120 to 140 g of red oak sawdust. As described in greater detail later in this chapter, they also developed a model of hemicellulose hydrolysis for a packed bed that accounted for diffusion of products from the interior of the biomass particle to the bulk liquid. In general, their experimental results and model predictions agreed within

10%, with discrepancies attributed primarily to difficulties in determining the true H_2SO_4 concentration due to the buffering effects of ash in the wood.

Mok et al.'s [85] work provided a second example of percolation pretreatment with H_2SO_4; however, in this work the objective was glucose recovery. The reactor consisted of two chambers: the primary chamber with a diameter of 4.6 mm and a length of 76 mm used to hold the solid substrate and a secondary chamber with variable volume to study the influence of liquid phase reactions. Whatman no.1 and no. 4 filter papers were used as substrates. The flow rate of 0.05% H_2SO_4 was varied from 2 to 4 mL/min, and the pretreatments lasted from 0 to 60 minutes at 190 to 225^{o}C. Although the classic Saeman model of cellulose hydrolysis[86] (see section 2.6.1.a) predicted that decreasing the volume of the secondary reaction chamber would increase the yield of glucose by limiting degradation reactions, Mok et al. found that the glucose yield decreased which led them to propose that cellulose hydrolysis generates oligomers first that are then further hydrolyzed to glucose.[85] Mok et al. also suggested that the increase in glucose yield with increasing flow rate was due to the removal of soluble products prior to degradation.[85]

As with the use of SO_2, the conundrum of minimizing xylose degradation during pretreatment while achieving high digestibility of cellulose in the pretreated solids can be addressed by two stage pretreatments with dilute sulfuric acid. Nguyen et al.[87] tested one such configuration using a mixture of White fir (*Abies concolor*) and Ponderosa pine (*Pinus ponderosa*). The chips were soaked in 0.6 to 2.4 % H_2SO_4 for 4 hours at 60^{o}C and then added to a 4 L steam explosion reactor. During the first pretreatment, the temperature was varied from 180 to 215^{o}C for 1.6 to 4 minutes, giving a combined

severity for the first stage pretreatment ranging from 2.18 to 3.26. At the completion of this time, the solids were washed to remove solubilized hemicellulose sugars and then soaked in 2.5% H_2SO_4 for 3 hours at ambient temperature before being treated at 210^oC for 1.6 to 2 minutes. The solids from this two stage approach were employed in both enzymatic hydrolysis and simultaneous saccharification and fermentation (SSF). The total sugar yields from two stage pretreatment followed by enzymatic hydrolysis was slightly higher than the total sugar yields from single stage pretreatment followed by enzymatic hydrolysis. In addition, two-stage pretreatment could potentially reduce enzyme usage as the cellulose content in the solids from the second pretreatment stage was lower than for one stage pretreatment. However, as with the two-stage SO_2 pretreatment, it is unclear that the performance gains from two-stage pretreatment justify the additional costs.

Pretreatment conditions reviewed in this section are summarized in Table 2.3.

Table 2.3. Selected conditions for pretreatment with sulfuric acid prior to biological conversion. Yield is defined as gram carbohydrate equivalent in the liquid hydrolysate following pretreatment per gram of carbohydrate equivalent in the raw biomass.

Substrate (Author)	Concentration	Temperature (^{o}C)	Time (min)	Yields
Southern red oak (Cahela et al[84])	0.037-0.056 w/v%	140-160	~14-115	Xylan yield: ~8.8-88%
Whatman paper no. 1 and 42 (Mok et al.[85])	5 mM	190-225	0-60	Glucose yield: ~35-85%
Corn stover (Lloyd and Wyman[26])	0.22-0.98 %	140-200	0-80	Maximum xylose yields of 71-85%
White fir and Ponderosa pine (Nguyen et al.[87])	0.6-2.5 %	180-215	1.7-4	2 stage mannose+ galactose+ xylose+ arabinose yield: 84%
Salix hybrid (Sassner et al.[83])	0.25-0.5 w/w%	180-210	4-12	Xylose yield: ~55-75%

2.5. Low pH reactions for chemical conversion

There has been growing interest in producing "drop-in" hydrocarbon fuels from biomass, that is to say, hydrocarbons that can be easily integrated with today's motor vehicles and airplanes. Additionally, since many of today's chemical feedstocks are derived from petroleum, there is a need to generate alternative chemical feedstocks from biomass. Although pretreatment traditionally refers to the preparation of biomass for biological conversion, researchers are now also applying low pH reactions to produce reactive intermediates for catalytic chemical conversion to fuels and chemicals; in a sense, these reactions are also "pretreatments" and certainly share similar features to

historical pretreatment technologies. However, the pretreatment conditions to support catalytic conversion tend to be much more varied due to the wider range of downstream processing objectives.

2.5.1. Furfural production

One of the oldest examples of industrial chemical production from biomass is furfural manufacture from the xylan and arabinan in hemicellulose. Furfural is currently used for applications such as resins, linking foundry sand, lubrication oil extraction, and nematicides[88] but could be used to produce a wide variety of other chemicals. The first industrial production of furfural used oat hulls as a feedstock to take advantage of its high xylan content,[88] and major industrial feedstocks today are corncobs and bagasse.[24]

Furfural can be produced by a one or two stage process.[89] In the one stage process, biomass is combined with about 3% H_2SO_4 by weight in a slurry,[90] and steam is introduced to bring the reactor to the desired temperature. The hemicellulose is hydrolyzed to xylose and arabinose, which in turn are dehydrated to furfural.[91] Furfural is continuously removed from the reactor in the vapor phase to limit decomposition and recondensation reactions.[89] The reactor is typically held at 170 to 185^{o}C for 3 hours, and the process results in furfural yields of approximately 40 to 50% of the theoretical maximum. One of the challenges in this process is the rapid recovery of furfural, but the efficiency of recovery by steam injection is limited due to the boiling point elevation in the reactor as biomass components are solubilized. The two-stage process attempts to separate hemicellulose hydrolysis and xylose cyclodehydration reactions, with hemicellulose hydrolysis conducted at milder conditions to generate a pentose rich liquid

stream for dehydration. By separating the two reactions, it is also possible to produce a cellulose-lignin substrate that can also be converted to chemicals or fuel. A review by Mamman et al.[90] identified a number pretreatments resulting in high xylose yields, some of which are summarized in Table 2.4.

Table 2.4. Pretreatment conditions for high xylose yields in support of furfural production.[90]

Biomass	wt% H_2SO_4	Temperature(^oC)	Time (minutes)
Oil palm empty fruit bunch	4	115	60
Corn fiber	0.75	121	30
Switchgrass	0.5	140-160	10-60

A new field of study in the production of furfural is the use of chloride salts to increase the xylose production rate.[92] Marcotullio and De Jong[92] showed that furfural yields and selectivity increased when chloride salts such as NaCl and $FeCl_3 \bullet 6H_2O$ were added to the cyclodehydration of xylose with dilute hydrochloric acid, and addition of salts increased the reaction rate even for low acid concentrations. Of the salts tested, $FeCl_3 \bullet 6H_2O$ seemed particularly promising due to a dramatic increase in xylose reaction rates. Although details of the mechanism for the conversion of xylose to furfural are unresolved, Marcotullio and De Jong[92] hypothesized that chloride ions promote formation of 1,2-enediol that may be an important intermediate to furfural production.

2.5.2. Levulinic acid

Levulinic acid can be made from cellulose and used to make diesel and gasoline additives. Rackemann and Doherty recently provided a thorough review of the uses and production of levulinic acid from biomass.[93] The Biofine process was developed to produce levulinic acid from cellulosic biomass,[8] and a number of different substrates

were tested including waste paper, waste wood, and agricultural residues. In this case, solids were combined with 2 to 5% H_2SO_4 at ambient temperature and then pumped into a short continuous plug flow reactor at held 215^oC and 3.1 MPa(g) with a residence time of only about 15 seconds to release glucose. The slurry was then pumped to a continuous stirred tank reactor at 193^oC and 1.4 MPa(g) with a residence time of 12 minutes. Slow conversion of sugars to levulinic acid occurred during this stage; the process generated approximately 0.5 kg levulinic acid/kg cellulose. Furfural and formic acid were also produced.

2.5.3. Drop-in hydrocarbons

An emerging processing paradigm is to pretreat biomass in order to release reactive intermediates that can be catalytically converted to drop-in hydrocarbons. The objectives of pretreatment in support of these catalytic processes are to maximize intermediate yields and avoid use or generation of catalyst poisons.[94] One example of pretreatment for this type of process was presented by Li et al[95] in which maple wood was pretreated in 0.5% H_2SO_4 in a steam gun at temperatures between 160 and 180^oC for 10 to 30 minutes.[95] They then subjected the resulting carbohydrate rich liquid stream to low temperature hydrogenation to produce sorbitol and xylitol, which were then converted to gasoline range hydrocarbons. Both of these steps used heterogeneous catalysts. The cellulose and lignin rich solids from pretreatment could then be used in other processes such as ethanol production.[95]

Because mineral acids could deactivate downstream metallic catalysts,[95] two possible solutions have been employed to address this challenge. In the first, the

pretreatment liquor is neutralized prior to catalysis, but as discussed in the section 2.2, this approach is not ideal. The second alternative is to pretreat biomass with an organic acid such as oxalic acid ($C_2H_2O_4$).[94] For example, Zhang and Wyman[94] applied pretreatments lasting 5 to 60 minutes at 160°C using H_2SO_4, HCl, and $C_2H_2O_4$ at concentrations from 0.5 to 2% and found that oxalic acid pretreatments resulted in slightly higher carbon recoveries than pretreatment with mineral acids.[94, 95] In general, the highest xylose monomer recovery was achieved at low acid concentrations. For example, Li et al.[95] reached their maximum xylose recovery using 0.5% $C_2H_2O_4$ at 180°C for 10 minutes. At 160°C, Zhang and Wyman's maximum total xylose recoveries, defined as the xylose equivalent of monomers and oligomers in the hydrolysate as a percentage of xylose equivalents available in the raw biomass, were 84.4%, 73.8%, and 87.5% with 0.5% H_2SO_4 for 30 min, 0.5% HCl for 10 min, and 0.5% $C_2H_2O_4$ for 30 min, respectively.[94] However, the higher cost of $C_2H_2O_4$ relative to mineral acids could limit its use as a catalyst, but no process designs have yet been applied to estimate the tradeoffs for use of oxalic vs. mineral acids. Furthermore, the impact of pretreatment acid type on downstream operations has not been fully investigated.

Recycling $C_2H_2O_4$ will be a key to its use on a commercial scale. Vom Stein and co-workers fractionated beechwood using a biphasic system of an aqueous phase containing wood and oxalic acid in contact with 2-methyltetrahydrofuran (2-MTHF) at temperatures from 125°C to 150°C.[96] Part of this study evaluated the recyclability of $C_2H_2O_4$. Little $C_2H_2O_4$ reacted at temperatures between 125°C and 140°C, but only 70% of $C_2H_2O_4$ was recovered after reaction at 150°C, suggesting side reactions may be

significant at this temperature. They also found that $C_2H_2O_4$ could be recovered by crystallization after reaction and re-used.[96] However, further work is required to fully evaluate the advantages and disadvantages of using $C_2H_2O_4$ with and without recycle relative to mineral acids.

Another biomass conversion system based on dilute acid pretreatment is production of gasoline compatible hydrocarbons via simultaneous hydrolysis and hydrogenation. In this configuration, a metallic catalyst in an acidic aqueous solution with a hydrogen headspace promotes biomass reactions. The reactor is heated to initiate biomass hydrolysis to monomeric sugars, which are then immediately converted to sugar alcohols such as sorbitol over the metallic catalyst for conversion into hydrocarbons in downstream operations. In a study by Robinson et al,[97] idealized substrates and native biomasses such as switchgrass were treated in stirred batch reactors with ruthenium catalyst on a carbon support.[97] Solutions with 0.7% H_2SO_4 and 0.35 to 1.5% H_3PO_4 were tested at temperatures ranging from 160 to 193^oC over a time period of 3 to 17 hours. A recent example of simultaneous hydrolysis and hydrogenation was reported by Palkovits et al[98] in which they tested idealized substrates such as α-cellulose and native spruce. The catalysts Pt-C, Pd-C, and Ru-C were applied in 0.5 to 2.5% H_3PO_4 and H_2SO_4 at 160^oC for 1 to 5 hours to produce five and six carbon alcohols as well as glucose and xylose. Higher conversion of cellulose was obtained using H_2SO_4 compared to H_3PO_4, likely due to H_2SO_4's higher pKa value.[98] Interestingly, this study showed that although overall conversion using the Ru-C catalyst was low in comparison to Pt and Pd catalysts, the Ru-C catalyst gave higher yields of desired products. Additionally, production of

xylose and glucose were greater in the presence of the heterogeneous catalysts than traditional acid hydrolysis.

2.6. Models of low pH biomass reactions

For almost as long as biomass hydrolysis has been studied, there have been efforts to develop kinetic models of the system. Such models have been difficult to develop due to the complexity of the system: the solid/liquid interactions of the biomass and the aqueous phase; the challenges of determining the effective acid concentration during reaction; interactions among cellulose, hemicellulose, and lignin; and the complexity of the composition of these fractions. In addition to the complex reactions, there are also the challenges in assessing and modeling mass and heat transfer within the reactor and biomass. Finally, the diversity and range of biomass and associated chemical bonds within hemicellulose and with lignin limits the extent to which models can be accurately applied. However, it is vital to address these challenges because of the utility of kinetic models in research and industrial production. Models provide a framework to test hypotheses in an efficient and targeted manner. Reliable kinetic models are also vital to scale-up of pretreatment from the lab to commercial production. Finally models assist in determining optimum biomass feedstock and processing configurations.

2.6.1. Cellulose hydrolysis

2.6.1.a. Glucose production

As the early goal of low pH biomass reactions was cellulose hydrolysis to glucose, much of the kinetic modeling literature from that time focused on acid catalyzed hydrolysis of cellulose via the proton catalyzed cleavage of the glycosidic bond.[99] One of

the first models was based on the following series of first order pseudo-homogeneous reactions by Saeman[86]:

$$cellulose \xrightarrow{k_1} glu\cos e \xrightarrow{k_2} 5-HMF \tag{2}$$

Where:

$$k_i = H_i C_a^M exp\left(\frac{-E_{act,i}}{RT}\right) \tag{3}$$

In equation 3, k_i is the reaction rate constant (min^{-1}) for reaction i, H_i is a constant, C_a is the concentration of H_2SO_4 (%), ΔH_{ai} is the activation energy, R is the universal gas constant, and T is the absolute temperature. This model has been the basis of almost every cellulose and hemicellulose hydrolysis model since. Saeman[86] applied his model to a variety of substrates including red oak, Douglas fir, hard maple, and aspen and found that hydrolysis rates did not differ by more than 20%. These differences could be partially explained by differences in buffering capacity of the wood: substrates with the lowest ash content were found to have the highest hydrolysis rates. Saeman[86] also studied hydrolysis of Douglas fir at a variety of temperatures and acid concentrations and found the activation energy was independent of acid concentration while the rate constant increased by 153% for a 100% increase in acid concentration. Definition of acid concentration C_a has been challenging in part due to the neutralizing capacity of biomass. In the past, C_a has been expressed in terms of mass, molarity, and pH at room temperature,[100] and variations in definition partially explains the wide variation in kinetic rate constants for hydrolysis. Lloyd and Wyman[100] demonstrated that the neutralizing capacity of biomass and the temperature have a significant influence on the pH of a system, a fact well worth considering in future modeling.

One of the first modifications to Saeman's model was adjustment of his assumption that the initial glucose concentration was zero. In particular, amorphous cellulose hydrolyzed quickly enough to be included as an initial glucose concentration.[101] Most subsequent modifications have added decomposition reactions and parallel reactions. For example, Conner et al.[102] added reversible formation of levoglucosan from glucose and disaccharides, and Bouchard et al.[103] found evidence for a parallel pathway that modifies cellulose to an unhydrolyzable structure. Abatzoglou et al.[104] added formation of glucooligomer intermediates as a sequential step to Saeman's model. Mok et al.[85] searched for additional evidence of these phenomena, and after eliminating the possibilities that chemical alteration of residual solid cellulose or glucose degradation reactions were responsible for limiting glucose yield, they concluded that unknown products that could not be hydrolyzed to glucose were produced during pretreatment.

2.6.1.b. 5-HMF and levulinic acid production

Levulinic acid is produced from the dehydration of hexose sugars, and production from biomass is based on cellulose first being hydrolyzed to glucose, which then undergoes dehydration to 5-hydroxymethylfurfural (5-HMF) and its reaction to levulinic acid. However, many significant side reactions also occur, lowering the final yield of levulinic acid. Several models have been developed to describe formation of levulinic acid from glucose.[105, 106, 107] Chang and colleagues modeled glucose conversion to 5-hydroxymethyl furfural and subsequently levulinic acid as a series of first order unimolecular reactions and incorporated a parallel reaction for conversion of glucose to humic solids:[105]

$$biomass \overset{k_1}{\rightarrow} glucose \overset{k_2}{\rightarrow} 5-HMF \overset{k_3}{\rightarrow} LA \quad (4)$$

$$glucose \overset{k_4}{\rightarrow} humic\ \&\ unidentified\ products \quad (5)$$

$$glucose \overset{k_5}{\rightarrow} humic\ \&\ unidentified\ products \quad (6)$$

Girisuta applied a similar mechanism but included parallel pathways for decomposition of glucose and 5-hydroxymethyl furfural to humins.[106] Assary and co-workers developed quantum mechanic models for glucose conversion to levulinic acid.[107] They also showed that the first two steps, tautomerization of α-D-glucose to β-D-fructose and dehydration of β-D-fructose to an intermediate, were endothermic and indicated that initial dehydration of β-D-fructose was the rate-limiting step.[107] After developing models for glucose conversion to levulinic acid[106], Girisuta developed a kinetic model for conversion of purified, crystalline cellulose to levulinic acid.[108] This model was then adapted to conversion of biomass such as water hyacinth leaves by including conversion of galactose released from hemicellulose and adding correction factors to account for differences in cellulose properties.[109] The correction factor for conversion of hexoses to levulinic acid was found to be less than one, indicating that the conversion of cellulose in biomass is lower than that of pure cellulose while the correction factor for humin formation from hyacinth leaves was approximately two, indicating that the rate of humin production from hyacinth leaves was greater than the rate of production from pure cellulose. Chang and co-workers developed a model for levulinic acid production from wheat straw based on first order unimolecular reactions with a power law dependence for

acid concentration.[110] It was found that the reaction order of the acid concentration ranged from 0.620 to 1.434.

2.6.2. Hemicellulose hydrolysis

2.6.2.a. Xylose production

In general, hemicellulose hydrolysis models are less well-developed than for cellulose because hemicellulose hydrolysis has been of interest for a shorter period of time and composition and the structure of hemicellulose is more complex than that of cellulose. Although many hemicellulose hydrolysis models were simply adaptations of Saeman's approach to describe cellulose deconstruction, Kobayashi and Sakai[111] assumed that xylose was released from fast and slow reacting fractions, as shown in equation (7):

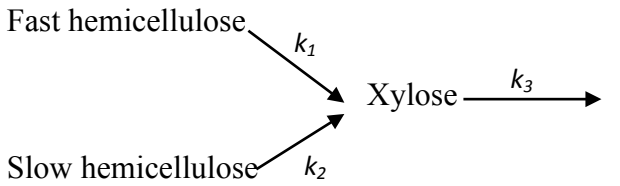

(7)

However, each reaction was still modeled as the first order pseudo-homogeneous system employed by Saeman. Jacobsen and Wyman[101] reported seven examples of this model. Hemicellulose hydrolysis models have also incorporated production of xylooligomer intermediates,[101] and parallel reactions of other hemicellulose constituents such as acetyl groups have also been included.[16]

The combined severity factor, equation (1), was an important development by Abatzoglou et al.[2] and Chum et al.[3] This parameter facilitates comparison of the combined effects of temperature, time, and acid concentration and tradeoffs among them with reaction conditions. It is important to acknowledge that although the combined

severity parameter can be useful in comparing data sets collected at different temperatures and acid concentrations, it cannot reliably predict specific performance as Lloyd and Wyman[26] demonstrated with their study of dilute acid pretreatment of corn stover.

Several studies have attempted to include the effects of diffusion in biomass particles on hemicellulose hydrolysis.[42, 112] Tillman and co-workers experimentally determined the diffusivity of H_2SO_4 in the longitudinal and radial directions of hardwood and showed that the diffusivity in the radial direction was much larger.[112] The diffusivity coefficient they determined was then combined with a biphasic hemicellulose hydrolysis model to predict the spatial dependence of xylose production within hardwood particles of increasing size. The results showed that as the reaction temperature increased, xylose yields dropped due to incomplete acid diffusion.[112] Kim and Lee expanded this work to study the transport properties of H_2SO_4 in sugar cane bagasse, corn stover, rice straw, and yellow poplar.[42] Their results showed that diffusivities in agricultural residues were significantly larger than in yellow poplar and that the diffusion of acid into biomass could significantly impact hemicellulose hydrolysis results depending on particle size, reaction temperature and reaction time.

As stated in section 2.4.3.b, Cahela et al.[84] developed a model to account for diffusion of reaction products out of biomass particles. Hemicellulose was assumed to hydrolyze to xylose and xylooligomers, which then degrade to furfural via first order homogeneous reactions. They refined their model differentiated between the xylose concentration within the pores of the biomass particles and the xylose concentration in

the bulk liquid. From this model, they predicted the maximum xylose yields and associated concentrations as well as operating conditions required to achieve these results. They also found that the intraparticle diffusion of xylose oligomers was significant if the longitudinal chip dimension was greater than 4.2 mm. Because this represents a relatively small particle, mass transfer effects will likely be significant for industrial operations with large biomass particles. Hosseini and Shah[113] took this analysis even further with a more detailed kinetic-mass transfer model that attempted to account for differences in xylooligomer reactivity by assuming that bond breakage is a function of position in the xylooligomer chain. Predictions from this approach strongly correlated with experimental data for hydrolysis of xylooligomers with a degree of polymerization equal to or less than five. Consideration of diffusion of individual oligomer products out of biomass particles showed that the concentrations of xylooligomers within the chip predicted by the model were very sensitive to the assumed value of the diffusion coefficient. This work, as well as others, demonstrated the importance of considering xylooligomer intermediates and mass transfer in kinetic modeling.

The effect of temperature gradients within biomass particles or reactors has also been incorporated into some models. Abasaeed and associates provided two examples of the effects of temperature gradients within biomass particles on the results of cellulose hydrolysis.[114, 115] With the help of Lee and Watson, Abasaeed[114] applied a Saeman type for model to the hydrolysis of cellulose in southern red oak, determined the thermal diffusivities of southern red oak chips saturated with water, and then simultaneously

solved the mass and energy balances of a wood chip. Their models showed that increasing the particle size reduced the maximum achievable glucose yield relative to that predicted based on assumed isothermal conditions and that it took longer to reach this maximum. Increasing the recreation temperature or acid concentration exacerbated the effects of nonisothermal operation. Abasaeed's study with Mansour[115] nonisothermal cellulose hydrolysis in wood chips and came to similar conclusions.

Stuhler and Wyman[82] examined the effects of temperature gradients within tubular batch reactors and applied a parameter, β, to represent the rate of xylan hydrolysis relative to the rate of heat conduction in the radial direction in a batch tubular reactor. They found that when a radial temperature gradient developed within the reactor, there was a substantial reduction in xylan hydrolysis and that the erroneous assumption of isothermal conditions introduced significant errors in predicting xylan conversion. From these studies, it is clear that thermal gradients within biomass particles and reactors can have considerable impact on product yields, and therefore heat transfer must be carefully considered for experimentation, modeling, and commercialization.

2.6.2.b. Furfural production

In the section 2.3.2, researchers were primarily focused on models that could be used to optimize xylose recovery whereas in this section the target was primarily to maximize furfural production. However, as noted earlier, cyclodehydration of xylose to furfural is accompanied by numerous side reactions making it complex reaction to model, and as a result, greater emphasis on furfural consuming reactions is needed to predict furfural concentrations.

The simplest kinetic models of furfural destruction assumed that furfural degrades to decomposition products according to a pseudounimolecular reaction[116,117]:

$$\text{furfural} \xrightarrow{k_1} \text{D} \tag{8}$$

In these studies, the rate of disappearance of furfural was found to be first order with respect to furfural concentration. Williams and Dunlop[116] applied a rate law for furfural disappearance at 150 to 210°C in 0.1 N H_2SO_4 to show that the rate of furfural disappearance at 160°C in 0.05 N HCl and 0.1 N H_2SO_4 were very close, leading them to postulate that the rate of destruction of furfural was first order with respect to hydrogen ion concentration. However, because the hydrogen ion concentration was high, it remained essentially constant during a run.

Weingarten and co-workers[25] developed a slightly more detailed reaction scheme for furfural production from xylose:

$$xylose \xrightarrow{k_1} furfural + 3H_2O \tag{9}$$

$$xylose + furfural \xrightarrow{k_2} D_1 \tag{10}$$

$$furfural \xrightarrow{k_3} D_2 \tag{11}$$

Each reaction was modeled as first order with respect to the reactants and hydrogen ion concentration. One of the most detailed models of furfural production from xylose was developed by Antal and colleagues in which they tracked production and destruction of 11 different compounds.[23] Through experimentation and modeling, they determined the open-chain xylose isomer rapidly converts to undesirable products such as formic acid while the xylopyranose ring underwent dehydration to furfural and undesirable products.

Although the xylopyranose form of xylose is present in greater quantities, the activation energy for the formation of furfural intermediates is larger and thus the reaction proceeded more slowly.[23]

Nimlos and coworkers[118] subsequently developed quantum mechanic models to estimate transition states and energy barriers associated with three different reaction schemes for xylose decomposition to furfural. Based on energy barriers, Nimlos and colleagues[118] concluded that Antal and associates'[23] model for the protonation of xylopyranose followed by dehydration to furfural was the most likely furfural production mechanism.

2.6.3. Summary of kinetic models

Given the highly empirical nature of the kinetic models that have been developed to date, anyone planning to apply kinetic models to biomass deconstruction with dilute acids would be well advised to employ one developed for similar biomass and hydrolysis conditions. In this regard, Table 2.5 summarizes some of the biomass types, hydrolysis conditions, and general model types that have been applied. Although an exhaustive table is beyond the scope of this chapter, it serves merely as a starting point for the interested reader. In addition, in light of their empirical nature, it is vital to confirm models with data collected at relevant conditions to validate their accuracy.

Table 2.5. Summary of kinetic models of acid hydrolysis for biomass types and hydrolysis conditions.

Source	Biomass	Temperature (^oC)	Acidifying Agent	Model Comments
Abasaeed et al.[114]	Southern red oak	198-215	1-3% H_2SO_4	Sequential hydrolysis of cellulose with intraparticle heat transfer
Abasaeed and Mansour[115]	Cellulose			Sequential hydrolysis of cellulose with intraparticle heat transfer
Abatzoglou et al.[104]	Cellulose	200-240	0.2-1.0 wt% H_2SO_4	Sequential hydrolysis of cellulose with oligomer intermediates
Abatzoglou et al.[2]	Corn stalk, alfalfa, *Populus tremuloides, Betula papyrifera*	100-240	0-1.8% H_2SO_4	Severity parameter to predict xylan conversion
Aguilar et al.[16]	Sugar cane bagasse	100-128	2-6% H_2SO_4	Sequential hydrolysis of glucan and xylan. Models for acetic acid and furfural.
Antal et al.[23]	Xylose	250	0-20 mM H_2SO_4	Detailed model of xylose dehydration
Assary et al.[107]	Glucose			Quantum mechanics modeling of glucose decomposition to levulinic acid
Brennan and Wyman[119]	Corn stover	180	0.5-1.0 wt% H_2SO_4	Mass transfer only models.

Table 2.5. continued

Source	Biomass	Temperature (°C)	Acidifying Agent	Model Comments
Cahela et al.[84]	Southern red oak	140-160	0.037-0.056 w/v% H_2SO_4	Sequential hydrolysis of xylan with mass transfer effects.
Canettieri et al.[22]	*Eucalyptus grandis*	130-160	0.65% H_2SO_4	Biphasic, sequential hydrolysis of xylan.
Carrasco and Roy[120]	Corn stover, poplar, wheat straw, bagasse, paper birch	80-260	0.5-4 wt% H_2SO_4	Biphasic, sequential hydrolysis of xylan with oligomer intermediates.
Chang et al.[105]	Glucose	170-210	1-5% H_2SO_4	Sequential destruction of glucose to levulinic acid
Chang et al.[110]	Wheat straw	190-230	1-5 wt% H_2SO_4	Sequential destruction of cellulose to levulinic acid with parallel degradation path.
Chum et al.[3]	*Populus tremuloides*	125-145	0.2-1.7 wt% SO_2	Severity parameter to predict xylan conversion
Converse et al.[121]	90% Birch, 10% Maple	160-265	0.2-2.4 wt% H_2SO_4	Sequential hydrolysis of glucan and xylan
Esteghlalian et al.[43]	Corn stover, poplar, switchgrass	140-180	0.6-1.2 w/w% H_2SO_4	Biphasic, sequential hydrolysis of xylan.
Girisuta et al.[106]	Glucose	140-200	0.05-1 M H_2SO_4	Sequential decomposition of glucose to levulinic acid
Girisuta et al.[108]	Microcrystalline cellulose	150-200	0.05-1 M H_2SO_4	Sequential decomposition of cellulose to levulinic acid

Table 2.5. continued

Source	Biomass	Temperature (°C)	Acidifying Agent	Model Comments
Girisuta et al.[109]	Water hyacinth	150-175	0.1-1 M H_2SO_4	Sequential decomposition of cellulose to levulinic acid. Correction factor for biomass matrix.
Hosseini et al.[113]	Hemicellulose			Xylooligomer depolymerization.
Jacobsen and Wyman[101]	Review of cellulose and hemicellulose hydrolysis models			
Jensen et al.[27]	Mixtures of switchgrass, balsam, red maple, aspen, basswood	175	0.5 wt% H_2SO_4	Biphasic, sequential hydrolysis of xylan.
Kobayashi and Sakai[111]	*Fagus crenata* Blume	74-147	1-16 % H_2SO_4	Biphasic, sequential hydrolysis of xylan.
Lloyd and Wyman[122]	Corn stover	140	0.68-1.0% H_2SO_4	Depolymerization of xylan. Includes oligomer intermediates.
Lu and Mosier[123]	Corn stover	150-170	0.05-0.2 M $C_4H_4O_4$	Saeman sequential hydrolysis of xylan. Biphasic, sequential hydrolysis of xylan.
Maloney et al.[21]	Paper birch	100-170	0.04-0.18 M H_2SO_4	Biphasic, sequential hydrolysis of xylan. Release of acetyl groups.
Mok et al.[85]	Whatman paper no. 1 and 42	190-225	5 mM H_2SO_4	Sequential hydrolysis of cellulose.
Morinelly et al.[124]	Aspen, balsam, switchgrass	150-175	0.25-0.75 wt% H_2SO_4	Sequential hydrolysis of xylan. Includes oligomer intermediates.

Table 2.5. continued

Source	Biomass	Temperature (^oC)	Acidifying Agent	Model Comments
Nimlos et al.[118]	Xylose	160	0.2 N H_2SO_4	Quantum mechanic model of xylose dehydration
Rose et al.[102]	Furfural	150-169	0.1 N HCl	Pseudounimolecular destruction of furfural
Saeman[86]	Cellulose	170-190	0.4-1.6 % H_2SO_4	Sequential hydrolysis of cellulose and monomers
Tillman et al.[112]	Aspen	95-169		Biphasic, sequential hydrolysis of xylan with mass transfer of acid.
Weingarten et al.[25]	Xylose	150-170	0.1 M HCl	Parallel dehydration of xylose
Williams and Dunlop[116]	Furfural	50-300	0.05-0.10 N H_2SO_4	Pseudounimolecular destruction of furfural

2.7. Conclusions

Biomass hydrolysis at low pH is an important role of biomass conversion to fuels and chemicals. Low pH reactions have been used to prepare a wide variety of biomass types including agricultural residues, grasses, hardwoods, and softwoods for subsequent conversion by biological and chemical routes as well as to make sugars, furfural, and other products directly. Acidifying agents and concentrations as well as reactor types, temperatures, and times can be adjusted to accommodate differences in biomass and downstream operations and objectives. Although downstream operations vary considerably, the primary pretreatment goals are to maximize product yields, generate

reactive intermediates such as enzymatically digestible solids, sugars, or furfural, and avoid generation of compounds that would negatively influence downstream operations.

As the emphasis in biomass hydrolysis evolved from recovery of sugars from cellulose to removal of hemicellulose to prepare biomass for subsequent acid catalyzed cellulose hydrolysis and later enzymatic hydrolysis of cellulose, pretreatment objectives have shifted from recovery of glucose for fermentation to the recovery of hemicelluloses-based sugars and modification of cellulose for enzymatic hydrolysis. Sulfur dioxide and sulfuric acid have been the most studied catalysts for biomass pretreatment prior to biological conversion. Most SO_2 systems used batch reactors and steam explosion. Sulfuric acid has been used in batch, percolation, steam explosion, and two-stage batch pretreatments. Other acids such as nitric, phosphoric, hydrochloric, hydrofluoric, and carbonic have been occasionally studied.

Recent interest in producing chemicals and "drop-in" hydrocarbon fuels has brought renewed attention to the hydrolysis of hemicellulose and cellulose to sugars and subsequent reaction to organic aldehydes and acids that can be catalytically converted to hydrocarbons. Although not traditionally referred to as pretreatment, the purpose of these acidic reactions is the same as traditional pretreatments, i.e., production of reactive intermediates for subsequent conversion. Possible goals of these non-traditional pretreatments include maximizing production of furfural, levulinic acid, or carbohydrate rich liquids. Another approach to fuels production is to combine hydrolysis with hydrogenation over a metallic catalyst to produce sugar alcohols.

Most models of cellulose and hemicellulose hydrolysis have been developed assuming a series of first order homogeneous reactions in which the carbohydrate polymer is converted to monomers and then to degradation products. These models have been modified to account for parallel degradation pathways, the formation of oligomer intermediates, and differences in substrate reactivity. There are also several novel models describing hydrolysis including the severity parameter and mass transfer models. However, due to the empirical nature of existing models, their predictions must be validated if they are to be used with confidence.

As the interest in biomass hydrolysis evolved from generation of sugars from cellulose to removal of hemicellulose to prepare biomass for subsequent acid catalyzed cellulose hydrolysis and later enzymatic hydrolysis of cellulose, pretreatment objectives have changed from recovery of glucose for fermentation to the recovery of hemicelluloses-based sugars and modification of cellulose for enzymatic hydrolysis. Sulfur dioxide and sulfuric acid have been the most studied catalysts for biomass pretreatment prior to biological conversion. Most SO_2 systems used batch reactors and steam explosion. Sulfuric acid has been used in batch, percolation, steam explosion, and two-stage batch pretreatments. Other acids such as nitric, phosphoric, and hydrochloric have been occasionally studied.

Recent interest in producing chemicals or "drop-in" hydrocarbon fuels has brought renewed attention to the complete hydrolysis of hemicellulose and cellulose to sugars and their subsequent dehydration to organic aldehydes and acids that can be catalytically converted to hydrocarbons. Although not traditionally referred to as

pretreatment, these acidic reactions function in the same manner as traditional pretreatments, i.e., production of reactive intermediates for subsequent conversion. Possible goals of these non-traditional pretreatments include the maximizing the production of furfural, levulinic acid, or carbohydrate rich liquids. Another approach to fuels production is to combine hydrolysis with hydrogenation over a metallic catalyst to produce sugar alcohols.

Most models of cellulose and hemicellulose hydrolysis have been developed assuming a series of first order homogeneous reactions in which the carbohydrate polymer is converted to monomers and then to degradation products. These models have been modified to account for parallel degradation pathways, the formation of oligomer intermediates, and differences in substrate reactivity. There are also several novel models describing hydrolysis including the severity parameter and mass transfer models.

2.8. Nomenclature

C_a	Concentration of H_2SO_4
D	Degradation product
$E_{act,i}$	Activation energy of reaction i
H_i	Pre-exponential factor for reaction i
k_i	Reaction rate constant for reaction i
log(CS)	Combined severity factor, Equation (1)
LA	levulinic acid
M	Empirically determined exponent for C_a
R	Universal gas constant, 8.314 J/K/mol
t	Pretreatment time, min
T	Pretreatment temperature, ^oC

2.9. References

(1) Martinez A, Rodriguez ME, Wells ML, York SW, Preston JF, Ingram LO. Detoxification of dilute acid hydrolyzates of lignocelluloses with lime. *Biotechnol. Prog*. **2001**; *17*:287-293.

(2) Abatzoglou NJ, Chornet E, Belkacemi K, Overend RP. Phenomenological kinetics of complex systems: the development of a generalized severity parameter and its application to lignocellulosic fractionation. *Chem. Eng. Sci*. **1992**; *47*: 1109-1122.

(3) Chum HL, Johnson DK, Black SK, Overend RP. Pretreatment-catalyst effects and the combined severity parameter. *Appl. Biochem. Biotech*. **1990**; *24/25*: 1-14.

(4) Wyman CE, editors. *Handbook on bioethanol: production and utilization*. United States of America: Taylor and Francis; 1996.

(5) Hallac BB, Ragauskas AJ. Analyzing cellulose degree of polymerization and its relevancy to cellulosic ethanol. *Biofuel. Bioprod. Bior*. **2011**; *5*: 215- 225.

(6) Ding SY, Himmel ME. The maize primary cell wall microfibril: a new model derived from direct visualization. *J. Agric. Food Chem*. **2006**; *54*: 597-606.

(7) Krässig H, Schurz J, Steadman RG, Schliefer K, Albrecht W, Mohring M, Schlosser H. Cellulose. In *Ullmann's Encyclopedia of Industrial Chemistry*, Bohnet M, Bellussi G, Bus J, Cornils B, Drauz K, Greim H et al., Eds. Wiley Online Library: New York: Wiley; 2007. [Internet].

(8) Fitzpatrick SW. *Final technical report commercialization of the Biofine technology for levulinic acid production from paper sludge*; Report No DOE/CE/41178; US Department of Energy: MA, 2002 Apr. 271 p.

(9) Battista OA. Hydrolysis and crystallization of cellulose. *Ind. Eng. Chem*. **1950**; *42*: 502-507.

(10) Battista OA, Coppick S. Hydrolysis of native versus regenerated cellulose structures. *Test. Res. J*. **1947**; *17*: 419-422.

(11) Nickerson RF, Habrle JA. Cellulose intercrystalline structure: study by hydrolytic methods. *Ind. Eng. Chem*. **1947**; *39*: 1507-1512.

(12) Bouchard J, Abatzoglou N, Chornet E, Overend RP. Characterization of depolymerized cellulosic residues: Part 1: Residues obtained by acid hydrolysis processes. *Wood Sci. Technol*. **1989**; *23*: 343-355.

(13) Martínez JM, Reguant J, Montero MA, Montané D, Salvado J, Farriol X. Hydrolytic pretreatment of softwood and almond shells: degree of polymerization and enzymatic digestibility of the cellulose fraction. *Ind. Eng. Chem. Res*. **1997**; *36*: 688-696.

(14) Kumar R, Mago G, Balan V, Wyman CE. Physical and chemical characterizations of corn stover and poplar solids resulting from leading pretreatment technologies. *Bioresour. Technol*. **2009**; *100*: 3948-3962.

(15) Foston M, Ragauskas AJ. Changes in lignocellulosic supramolecular and ultrastructure during dilute acid pretreatment of *Populus* and switchgrass. *Biomass Bioenerg*. **2010**; *34*: 1885-1895.

(16) Aguilar R, Ramírez JA, Garrote G, Vázquez M. Kinetic study of the acid hydrolysis of sugar cane bagasse. *J. Food Eng*. **2002**; *55*: 309-318.

(17) Öhgren K, Rudolf A, Galbe M, Zacchi G. Fuel ethanol production from steam-pretreated corn stover using SSF at higher dry matter content. *Biomass Bioenerg*. **2006**; *30*: 863-869.

(18) Martín C, Galbe M, Nilvebrant NO, Jönsson LJ. Comparison of the fermentability of enzymatic hydrolysates of sugarcane bagasse pretreated by steam explosion using different impregnating agents. *Appl. Biochem. Biotech*. **2002**; *98-100*: 699-716.

(19) Excoffier G, Toussaint B, Vignon MR. Saccharification of steam-exploded poplar wood. *Biotechnol. Bioeng*. **1991**; *38*: 1308-1317.

(20) Kumar R, Wyman CE. The impact of dilute sulfuric acid on the selectivity of xylooligomer depolymerization to monomers. *Carbohyd. Res*. **2008**; *343*: 290-300.

(21) Maloney MT, Chapman TW, Baker AJ. Dilute acid hydrolysis of paper birch: kinetics studies of xylan and acetyl-group hydrolysis. *Biotechnol. Bioeng*. **1985**; *27*: 355-361.

(22) Canettieri EV, Rocha GJM, Carvalho JA Jr., Silva JBA. Evaluation of the kinetics of xylose formation from dilute sulfuric acid hydrolysis of forest residues of *Eucalyptus grandis*. *Ind. Eng. Chem. Res*. **2007**; *46*: 1938-1944.

(23) Antal MJ Jr., Leesomboon T, Mok WS, Richards GN. Mechanism of formation of 2-furaldehyde from D-xylose. *Carbohyd. Res*. **1991**; *217*: 71-85.

(24) Hoydonckx HE, Van Rhijn WM, Van Rhijn W, De Vos DE, Jacobs PA. Furfural and derivatives. In *Ullmann's Encyclopedia of Industrial Chemistry*, Bohnet M, Bellussi G, Bus J, Cornils B, Drauz K, Greim H et al., Eds.; Wiley Online Library: New York, 2007. [Internet].

(25) Weingarten R, Cho J, Conner WC Jr., Huer GW. Kinetics of furfural production by dehydration of xylose in a biphasic reactor with microwave heating. *Green Chem*. **2010**; *12*: 1423-1429.

(26) Lloyd TA, Wyman CE. Combined sugar yields for dilute sulfuric acid pretreatment of corn stover followed by enzymatic hydrolysis of the remaining solids. *Bioresource Technol*. **2005**; *96*: 1967-1977.

(27) Jensen J, Morinelly J, Aglan A, Mix A, Shonnard DR. Kinetic characterization of biomass dilute sulfuric acid hydrolysis: Mixtures of hardwoods, softwood, and switchgrass. *AIChE J*. **2008**; *54*: 1637-1645.

(28) Saake B, Lehnen R. Lignin. In *Ullmann's Encyclopedia of Industrial Chemistry*; Bohnet M, Bellussi G, Bus J, Cornils B, Drauz K, Greim H et al., editors. Wiley Online Library: New York, 2007. [Internet].

(29) Shevchenko SM, Beatson RP, Saddler JN. The nature of lignin from steam explosion/enzymatic hydrolysis of softwood: Structural features and possible uses. *Appl. Biochem. Biotech*. **1999**; *79*: 867-876.

(30) Liu C, Wyman CE. The effect of flow rate of very dilute sulfuric acid on xylan, lignin, and total mass removal from corn stover. *Ind. Eng. Chem. Res*. **2004**; *43*: 2781-2788.

(31) Du B, Sharma LN, Becker C, Chen S-F, Mowery RA, van Walsum GP, Chambliss CK. Effect of varying feedstock-pretreatment chemistry combinations on the formation and accumulation of potentially inhibitory degradation products in biomass hydrolysates. *Biotechnol. Bioeng*. **2010**; *107*: 430-440.

(32) Sievers C, Marzialetti T, Hoskins TJC, Olarte MBV, Agrawal PK, Jones CW. Quantitative solid state NMR analysis of residues from acid hydrolysis of loblolly pine wood. *Bioresource Technol*. **2009**; *100*: 4758-4765.

(33) Ritter GJ, Kurth EF. Holocellulose, total carbohydrate fraction of extractive-free maple wood- Its isolation and properties. *Ind. Eng. Chem*. **1933**; *25*: 1250-1253.

(34) Sannigrahi P, Kim DH, Jung S, Ragauskas A. Pseudo-lignin and pretreatment chemistry. *Energy Environ. Sci*. **2011**; *4*: 1306-1310.

(35) Donaldson LA, Wong KKY, Mackie KL. Ultrastructure of steam-exploded wood. *Wood Sci. Technol*. **1988**; *22*: 103-114.

(36) Donohoe BS, Decker SR, Tucker MP, Himmel ME, Vinzant TB. Visualizing lignin coalescence and migration through maize cell walls following thermochemical pretreatment. *Biotechnol. Bioeng*. **2008**; *101*: 913-925.

(37) Selig MJ, Viamajala S, Decker SR, Tucker MP, Himmel ME, Vinzant TB. Deposition of lignin droplets produced from dilute acid pretreatment of maize stems retards enzymatic hydrolysis of cellulose. *Biotechnol. Prog*. **2007**; *23*: 1333-1339.

(38) Sluiter A, Hames B, Ruiz R, Scarlata C, Sluiter J, Templeton D. Determination of ash in biomass: Laboratory Analytical Procedure [Internet]. National Renewable Energy Laboratory; United States of America: 2005 July. Available from http://www.nrel.gov/biomass/pdfs/42622.pdf

(39) Springer EL, Harris JF. Procedures for determining the neutralizing capacity of wood during hydrolysis with mineral acid solutions. *Ind. Eng. Chem. Prod. Res. Dev*. **1985**; *24*: 485-489.

(40) Chen S-F, Mowery RA, Scarlata CJ, Chambliss CK. Compositional analysis of water-soluble materials in corn stover. *J. Agric. Food Chem*. **2007**; *55*: 5912-5918.

(41) Chen S-F, Mowery RA, Sevcik RS, Scarlata CJ, Chambliss CK. Compositional analysis of water-soluble materials in switchgrass. *J. Agric. Food Chem*. **2010**; *58*: 3251-3258.

(42) Kim SB, Lee YY. Diffusion of sulfuric acid within lignocellulosic biomass particles and its impact on dilute-acid pretreatment. *Bioresour. Technol*. **2002**; *83*: 165-171.

(43) Esteghlalian A, Hashimoto AG, Fenske JJ, Penner MH. Modeling and optimization of the dilute sulfuric acid pretreatment of corn stover, poplar, and switchgrass. *Bioresour. Technol*. **1997**; *59*: 129-136.

(44) Boussaid AL, Esteghlalian AR, Gregg DJ, Lee KH, Saddler JN. Steam pretreatment of Douglas fir wood chips- Can conditions for optimum hemicelluloses recovery still provide adequate access for efficient enzymatic hydrolysis? *Appl. Biochem. Biotech*. **2000**; *84*: 693-705.

(45) Grethlein HE. The effect of pore size distribution on the rate of enzymatic hydrolysis of cellulosic substrates. *Nat. Biotechnol*. **1985**; *3*:155-160.

(46) Wong KKY, Deverell KF, Mackie KL, Clark TA, Donaldson LA. The relationship between fiber porosity and cellulose digestibility in steam-exploded *Pinus radiata*. *Biotechnol. Bioeng*. **1988**; *31*: 447-456.

(47) Sherrard EC, Kressman FW. Review of processes in the United States prior to World War II. *Ind. Eng. Chem*. **1945**; *37*: 5-8.

(48) Faith WL. Development of the Scholler process in the United States. *Ind. Eng. Chem*. **1945**; *37*: 9-11.

(49) Harris EE, Beglinger E. Madison wood sugar process. *Ind. Eng. Chem*. **1946**; *38*: 890-895.

(50) Harris EE, Lang BG. Hydrolysis of wood cellulose and decomposition of sugar in dilute phosphoric acid. *J. Phys. Colloid Chem*. **1947**; *51*: 1430-1441.

(51) Harris EE, Kline AA. Hydrolysis of wood cellulose with hydrochloric acid and sulfur dioxide and the decomposition of its hydrolytic products. *J. Phys. Colloid Chem*. **1948**; *53*: 344-351.

(52) Selke SM, Hawley MC, Hardt H, Lamport DTA, Smith G, Smith J. Chemicals from wood via HF. *Ind. Eng. Chem. Prod. RD*. **1982**; *21*: 11-16.

(53) Rorrer GL, Ashour SS, Hawley MC, Lamport DTA. Solvolysis of wood and pure cellulose by anhydrous hydrogen fluoride vapor. *Biomass*. **1987**; *12*: 227-246.

(54) Wright JD, Power AJ. *Comparative technical evaluation of acid hydrolysis processes for conversion of cellulose to alcohol.* Report no SERI/TP-232-2957. Solar Energy Research Institute: United States, 1986 May; 27 p.

(55) Allen F, Andreotti R, Eveleigh DE, Nystrom J. Mary Elizabeth Hickox Mandels, 90, bioenergy leader. *Biotechnol. Biofuels*. **2009**; *2*.

(56) Mandels M, Sternberg D. Recent advances in cellulase technology. *J. Ferment. Technol*. **1976**; *54*: 267-286.

(57) Grethlein HE. Comparison of economics of acid and enzymatic hydrolysis of newsprint. *Biotechnol. Bioeng*. **1978**; *20*: 503-525.

(58) Grethlein HE, Allen DC, Converse AO. A comparative study of the enzymatic hydrolysis of acid-pretreated white-pine and mixed hardwood. *Biotechnol. Bioeng*. **1984**; *26*: 1498-1505.

(59) Han YW, Callihan CD. Cellulose fermentation: effect of substrate pretreatment on microbial growth. *Appl. Microbiol*. **1974**; *27*: 159-165.

(60) Nesse N, Wallick J, Harper JM. Pretreatment of cellulosic wastes to increase enzyme reactivity. *Biotechnol. Bioeng*. **1977**; *19*: 323-336.

(61) Sciamanna AF, Freitas RP, Wilke CR. *Composition and utilization of cellulose for chemicals from agricultural residues*. Report LBL-5966; United States, 1977 Dec.

(62) Knappert D, Grethlein H, Converse A. Partial acid hydrolysis of cellulosic materials as a pretreatment for enzymatic hydrolysis. *Biotechnol. Bioeng*. **1980**; *22*: 1449-1463.

(63) Grethlein HE, Converse AO. Common aspects of acid prehydrolysis and steam explosion for pretreating wood. *Bioresour. Technol*. **1991**; *36*: 77-82.

(64) Foody P. Method for increasing the accessibility of cellulose in lignocellulosic materials, particularly hardwoods, agricultural residues and the like. US Patent 4461648. 1984 July.

(65) Wyman, CE. Twenty years of trials, tribulations, and research progress in bioethanol technology. *Appl. Biochem. Biotech*. **2001**; *91-93*: 5-21.

(66) Mosier N, Wyman C, Dale B, Elander R, Lee YY, Holtzapple M, Ladisch M. Features of promising technologies for pretreatment of lignocellulosic biomass. *Bioresource Technol*. **2005**; *96*: 673-686.

(67) Almarsdottir AR, Tarazewicz A, Gunnarsson I, Orlygsson J. Hydrogen production from sugars and complex biomass by *Clostridium* species AK_{14} isolated from Icelandic hot spring. *Icel. Agric. Sci*. **2010**; *23*: 61-71.

(68) Cao GL, Ren NQ, Wang AJ, Guo WQ, Xu JF, Liu BF. Effect of lignocelluloses-derived inhibitors on growth and hydrogen production by Thermoanaerobacterium thermosaccharolyticum W16. *Int. J. Hydrogen Energ*. **2010**; *35*: 13475-13480.

(69) Puri VP, Mamers H. Explosive pretreatment of lignocellulosic residues with high-pressure carbon dioxide for the production of fermentation substrates. *Biotechnol. Bioeng*. **1983**; *25*: 3149-3161.

(70) McWilliams RC, van Walsum GP. Comparison of aspen wood hydrolysates produced by pretreatment with liquid hot water and carbonic acid. *Appl. Biochem. Biotech*. **2002**; *98-100*: 109-121.

(71) van Walsum GP, Shi H. Carbonic acid enhancement of hydrolysis in aqueous pretreatment of corn stover. *Bioresource Technol*. **2004**; *93*: 217-225.

(72) Luterbacher JS, Tester JW, Walker LP. High-solids biphasic CO_2-H_2O pretreatment of lignocellulosic biomass. *Biotechnol. Bioeng*. **2010**; *107*: 451-460.

(73) Yang B, Wyman CE. Pretreatment: the key to unlocking low-cost cellulosic ethanol. *Biofuel. Bioprod. Bioref*. **2008**; *2*: 26-40.

(74) Jayawardhana K, van Walsum GP. Modeling of carbonic acid pretreatment process using ASPEN-Plus®. *Appl. Biochem. Biotech*. **2004**; *115*: 1087-1102.

(75) Bura R, Chandra R, Saddler J. Influence of xylan on enzymatic hydrolysis of steam-pretreated corn stover and hybrid poplar. *Biotechnol. Prog*. **2009**; *25*: 315-322.

(76) Stenberg K, Tengborg C, Galbe M, Zacchi G. Optimisation of steam pretreatment of SO_2-impregnated mixed softwoods for ethanol production. *J. Chem. Technol. Biotechnol*. **1998**; *71*: 299-308.

(77) Schell DJ, Torget R, Power A, Walkter PJ, Grohmann K, Hinman ND. A technical and economic analysis of acid-catalyzed steam explosion and dilute sulfuric acid pretreatments using wheat sraw or aspen wood chips. *Appl. Biochem. Biotech*. **1991**; *28/29*: 87-97.

(78) De Bari I, Nanna F, Braccio G. SO_2-catalyzed steam fractionation of aspen chips for bioethanol production: optimization of the catalyst impregnation. *Ind. Eng. Chem. Res*. **2007**; *46*: 7711-7720.

(79) Söderström J; Pilcher L, Galbe M, Zacchi G. Two-step steam pretreatment of softwood with SO_2 impregnation for ethanol production. *Appl. Biochem. Biotech*. **2002**; *98-100*: 5-21.

(80) Humbird D, Davis R, Tao L, Kinchin C, Hsu D, Aden A, Schoen P, Lukas J, Olthof R, Worley M, Sexton D, Dudgeon D. *Process design and economics for biochemical conversion of lignocellulosic biomass to ethanol: dilute acid pretreatment and enzymatic hydrolysis of corn stover*. Report No. NREL/TP-5100-47764; National Renewable Energy Laboratory: CO, 2011. 147 p.

(81) Jacobsen SE, Wyman CE. Heat transfer considerations in design of a batch tube reactor for biomass hydrolysis. *Appl. Biochem. Biotech*. **2001**; *92*: 377-386.

(82) Stuhler SL, Wyman CE. Estimation of temperature transients for biomass pretreatment in tubular batch reactors and impact on xylan hydrolysis kinetics. *Appl. Biochem. Biotech*. **2003**; *105*: 101-114.

(83) Sassner P, Mårtensson CG, Galbe M, Zacchi G. Steam pretreatment of H_2SO_4-impregnated *Salix* for the production of bioethanol. *Bioresource Technol*. **2008**; *99*: 137-145.

(84) Cahela DR, Lee YY, Chambers RP. Modeling of percolation process in hemicellulose hydrolysis. *Biotechnol. Bioeng*. **1983**; *25*: 3-17.

(85) Mok WS, Antal MJ Jr, Varhegyi G. Productive and parasitic pathways in dilute acid catalyzed hydrolysis of cellulose. *Ind. Eng. Chem. Res*. **1992**; *31*: 94-100.

(86) Saeman JF. Kinetics of wood saccharification- Hydrolysis of cellulose and decomposition of sugars in dilute acid at high temperature. *Ind. Eng. Chem*. **1945**; *37*: 43-52.

(87) Nguyen QA, Tucker MP, Keller FA, Eddy FP. Two-stage dilute-acid pretreatment of softwoods. *Appl. Biochem. Biotech*. **2000**; *84-86*: 561-576.

(88) De Jong W, Marcotullio G. Overview of biorefineries based on co-production of furfural- existing concepts and novel developments. *Int. J. Chem. React. Eng*. **2010**; *8*: 1-24.

(89) Mansilla HD, Baeza J, Urzúa S, Maturana G, Villaseñor J, Durán N. Acid-catalysed hydrolysis of rice hull: evaluation of furfural production. *Bioresource Technol*. **1998**; *66*: 189-193.

(90) Mamman AS, Lee JM, Kim YC, Hwang IT, Park NJ, Chang JS, Hwang JS. Furfural: Hemicellulose/xylose-derived biochemical. Biofuel. *Bioprod. Bioref*. **2008**; *2*: 438-454.

(91) Kottke RH. Furan derivatives. In *Kirk-Othmer Encyclopedia of Chemical Technology*, Kirk RE, Othmer DF, Eds.; Wiley Online Library : New York, 2000. [Internet].

(92) Marcotullio G, De Jong W. Chloride ions enhance furfural formation from D-xylose in dilute aqueous acidic solutions. *Green Chem*. **2010**; *12*: 1739-1746.

(93) Rackemann DW, Doherty WOS. The conversion of lignocellulosics to levulinic acid. *Biofuel. Bioprod. Bioref*. **2011**; *5*: 198-214.

(94) Zhang T, Wyman CE. Comparison and optimization of the extraction of hemicellulose from maple wood by different acid pretreatments. *2011*. In preparation.

(95) Li N, Tompsett GA, Zhang T, Shi J, Wyman CE, Huber GW. Renewable gasoline from aqueous phase hydrodeoxygenation of aqueous sugar solutions prepared by hydrolysis of maple wood. *Green Chem*. **2011**; *13*: 91-101.

(96) vom Stein T, Grande PM, Kayser H, Sibilla F, Leitner W, de María PD. From biomass to feedstock: one-step fractionation of lignocellulose components by the selective organic acid-catalyzed depolymerization of hemicellulose in a biphasic system. *Green Chem*. **2011**; *13*: 1772-1777.

(97) Robinson JM, Burgess CE, Bently MA, Brasher CD, Horne BO, Lillard DM, Macias JM, Mandal HD, Mills SC, O'Hara KD, Pon JT, Raigoza AF, Sanchez EH, Villarreal JS. The use of catalytic hydrogenation to intercept carbohydrates in a

dilute acid hydrolysis of biomass to effect a clean separation from lignin. *Biomass Bioenerg*. **2004**; *26*: 473-483.

(98) Palkovits R, Tajvidi K, Procelewska J, Rinaldi R, Ruppert A. Hydrogenolysis of cellulose combining mineral acids and hydrogenation catalysts. *Green Chem*. **2010**; *12*: 972-978.

(99) Fengel D, Wegener G. *Wood- Chemistry, ultrastructure and reactions*. New York, NY: Walter de Gruyter; 1984.

(100) Lloyd TA, Wyman CE. Predicted effects of minerals on pretreatment. *Appl. Biochem. Biotech*. **2004**; *113-116*: 1013-1022.

(101) Jacobsen SE, Wyman CE. Cellulose and hemicellulose hydrolysis models for application to current and novel pretreatment processes. *Appl. Biochem. Biotech.* **2000**; *84-86*: 81-96.

(102) Conner AH, Wood BF, Hill CG, Harris JF. Kinetic modeling of the saccharification of prehydrolyzed Southern Red Oak. In *Cellulose: structure, modification and hydrolysis;* Young RA, Rowell RM, Eds.; John Wiley and Sons: New York, 1986.

(103) Bouchard J, Abatzoglou N, Chornet E, Overend RP. Characterization of depolymerized cellulosic residues. 1. Residues obtained by acid-hydrolysis processes. *Wood Sci. Technol*. **1989**; *23*: 333-355.

(104) Abatzoglou N, Bouchard J, Chornet E. Dilute acid depolymerization of cellulose in aqueous phase: experimental evidence of the significant presence of soluble oligomeric intermediates. *Can. J. Chem. Eng*. **1986**; *64*: 781-786.

(105) Chang C, Ma X, Cen P. Kinetics of levulinic acid formation from glucose decomposition at high temperature. *Chinese J. Chem. Eng*. **2006**; *14*: 708-712.

(106) Girisuta B, Janssen PBM, Heeres HJ. Green chemicals: A kinetic study on the conversion of glucose to levulinic acid. *Chem. Eng. Res. Des*. **2006**; *84*: 339-349.

(107) Assary RS, Redfern PC, Hammond JR, Greeley J, Curtiss LA. Computational studies of the thermochemistry for conversion of glucose to levulinic acid. *J. Phys. Chem*. **2010**; *114*: 9002-9009.

(108) Girisuta B, Janssen PBM, Heeres HJ. Kinetic study on the acid-catalyzed hydrolysis of cellulose to levulinic acid. *Ind. Eng. Chem. Res*. **2007**; *46*: 1696-1708.

(109) Girisuta B, Danon B, Manurung R, Janssen PBM, Heeres HJ. Experimental and kinetic modeling studies on the acid-catalysed hydrolysis of the water hyacinth plant to levulinic acid. *Bioresource Technol*. **2008**; *99*: 8367-8375.

(110) Chang C, Ma X, Cen P. Kinetic studies on wheat straw hydrolysis to levulinic acid. *Chinese J. Chem. Eng*. **2009**; *17*: 835-839.

(111) Kobayashi T, Sakai Y. Hydrolysis rate of pentosan of hardwood in dilute sulfuric acid. *Agr. Biol. Chem. Tokyo*, **1956**; *20*: 1-7.

(112) Tillman LM, Lee YY, Torget R. Effect of transient acid diffusion on pretreatment/hydrolysis of hardwood hemicellulose. *Appl. Biochem. Biotech*. **1990**; *24/25*: 103-113.

(113) Hosseini SA, Shah N. Multiscale modeling of biomass pretreatment for biofuels production. *Chem. Eng. Res. Des*. **2009**; *87*: 1251-1260.

(114) Abasaeed AE, Lee YY, Watson JR. Effect of transient heat transfer and particle size on acid hydrolysis of hardwood cellulose. *Bioresour. Technol*. **1991**; *35*: 15-21.

(115) Abasaeed AE, Mansour ME. Thermal effects on acid hydrolysis of cellulose. *Bioresour. Technol*. **1992**; *40*: 221-224.

(116) Williams DL, Dunlop AP. Kinetics of furfural destruction in acidic aqueous media. *Ind. Eng. Chem*. **1948**; *40*: 239-241.

(117) Rose IC, Epstein N, Watkinson AP. Acid-catalyzed 2-furaldehyde (furfural) decomposition kinetics. *Ind. Eng. Chem. Res*. **2000**; *39*: 843-845.

(118) Nimlos MR, Qian X, Davis M, Himmel ME, Johnson DK. Energetic of xylose decomposition as determined using quantum mechanics modeling. *J. Phys. Chem*. **2006**; *110*: 11824-11838.

(119) Brennan MA, Wyman CE. Initial evaluation of simple mass transfer models to describe hemicellulose hydrolysis in corn stover. *Appl. Biochem. Biotech*. **2004**; *115*: 965-976.

(120) Carrasco F, Roy C. Kinetic study of dilute-acid prehydrolysis of xylan-containing biomass. *Wood Sci. Technol*. **1992**; *26*: 189-207.

(121) Converse AO, Kwarteng IK, Grethlein HE, Ooshima H. Kinetics of thermochemical pretreatment of lignocellulosic materials. *Appl. Biochem. Biotech*. **1989**; *20/21*: 63-78.

(122) Lloyd TA, Wyman CE. Application of a depolymerization model for predicting thermochemical hydrolysis of hemicellulose. *Appl. Biochem. Biotech*. **2003**; *105*: 53-67.

(123) Lu Y, Mosier NS. Kinetic modeling analysis of maleic acid-catalyzed hemicellulose hydrolysis in corn stover. *Biotechnol. Bioeng*. **2008**; *101*: 1170-1179.

(124) Morinelly JE, Jensen JR, Browne M, Co TB, Shonnard DR. Kinetic characterization of xylose monomer and oligomer concentrations during dilute acid pretreatment of lignocellulosic biomass from forests and switchgrass. *Ind. Eng. Chem. Res*. **2009**; *48*: 9877-9884.

Chapter 3.

Evaluation of options for a high throughput pretreatment and hydrolysis system for screening biomass.[*]

[*] This work was done in collaboration with Dr. Jaclyn DeMartini with guidance from Dr. Michael Studer. Their contributions have been noted as appropriate.

3.1. Abstract

One of the greatest obstacles to the production of ethanol from cellulosic biomass is the reducing the cost of releasing sugars from the biomass. This challenge could be meet with less recalcitrant biomass feedstocks and improved enzymes. Since biomass recalcitrance cannot be predicted a priori, thousands of combinations of plants, pretreatments, and enzyme formulations must be tested through trial and error; therefore a high throughput pretreatment and hydrolysis system was needed. The steps of such a process were identified and then possible solutions for each step were considered. Four systems were designed using the identified unit operations and evaluated using a Kepner-Tregoe type decision matrix. The matrix identified a custom-built metal 96 well plate for pretreatment and enzymatic hydrolysis as the most viable solution.

3.2. Introduction

Improving sugar yields while reducing costs has the greatest potential to lower the cost of cellulosic ethanol.[1] The conversion of biomass into sugars is the most expensive steps in the production of ethanol from cellulosic biomass and also the one most susceptible to improvement[2] through the development of less recalcitrant biomass feedstocks and improved pretreatments and enzymes. However, because the factors determining biomass recalcitrance have not been conclusively identified,[3] a trial and error approach must be used to identify superior feedstocks. New feedstocks result from genetic modification and surveys of natural variants while simultaneously, new enzyme formulations are in development. Consequently, the number of tests to identify favorable combinations of biomass, pretreatment and enzymes increases rapidly. One of the first objectives of the BioEnergy Science Center was develop a high throughput pretreatment system for hundreds of biomass samples that would be compatible with enzymatic hydrolysis in a 96 well plate. First the process steps required for such a system were identified and a set of evaluation criteria was established. Possible options for each unit operation were considered before developing and evaluating four complete systems.

3.3. Fundamental system concepts and unit operations

The process steps for pretreatment and enzymatic hydrolysis are summarized in Figure 3.1.

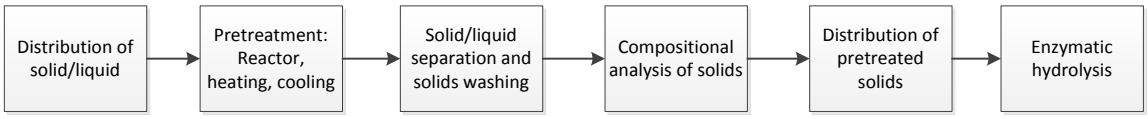

Figure 3.1. Flow diagram of pretreatment and enzymatic hydrolysis. Adapted from Studer et al.[4]

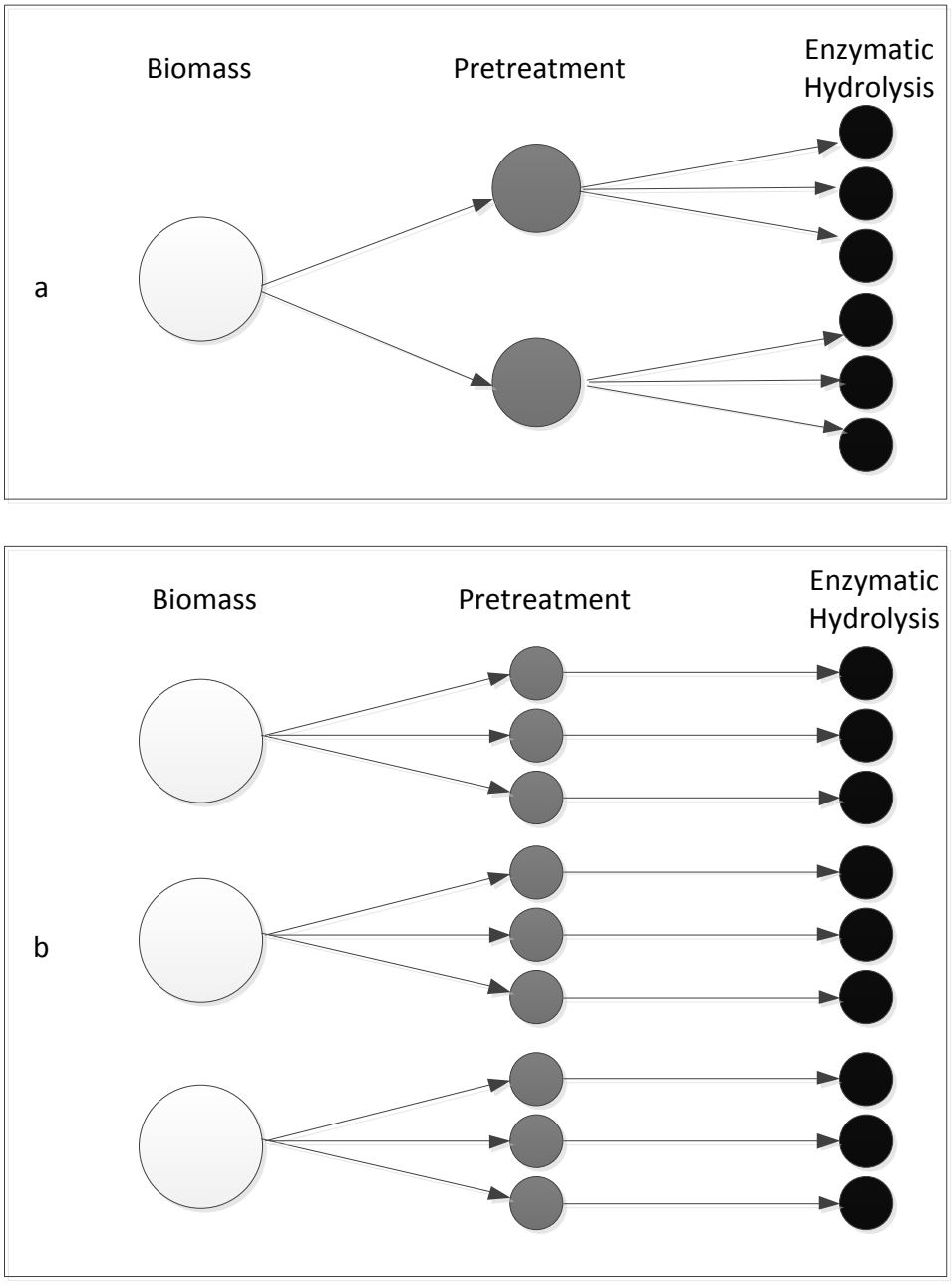

Figure 3.2. Comparison of possible approaches for high throughput pretreatment and hydrolysis systems. (a) A single pretreatment reactor feeding many wells for enzymatic hydrolysis. (b) Many pretreatment reactors feeding the same number of wells for enzymatic hydrolysis. Adapted from Studer et al.4

These process steps could be accomplished through two approaches: 1) one pretreatment reactor, whether a batch or a continuous microchannel feeding many wells for enzymatic hydrolysis, and 2) many pretreatment reactors to many wells for enzymatic hydrolysis. These concepts are illustrated in Figure 3.2 (previous page). At the outset, both approaches appeared viable.

3.4. Evaluation criteria

The Kepner-Tregoe[5] type decision matrix of critical and non-critical criteria, was used as a framework for evaluation. Failure to meet critical criteria, listed in Table 3.1, would disqualify the system from further consideration. Non-critical criteria, listed in Table 3.2, are "bonus" specifications that a system's ability to match boosted its final score. The total system score was determined by multiplying each non-critical criterion's weighting by its score and then summing the products. A score of one indicated that it would be impossible for the system to achieve the criterion while a score of ten indicated that there was no doubt that the system would achieve the criterion. The criteria were considered for both short-term implementation (less than one year) and long-term implementation.

Table 3.1. Critical evaluation criteria for high throughput pretreatment and hydrolysis system.

Criteria Description
Operating temperature range of 100°C to 180°C
Uniform temperature distribution
Accurate temperature control
Reproducible heating and cooling
Maximum operating pressure of 20 bar
Accurate distribution of pretreatment reactants, esp. solids
Compatible with sulfuric acid concentrations up to 1.0 wt%
Variable reaction time
Biomass slurry can be pumped/stirred/distributed/etc.
Accurate distribution of pretreated biomass to enzyme assay
Daily process rate of 20 biomass samples with 2 pretreatment conditions and 6 enzyme conditions
Prototype by Oct 2008

Table 3.2. Non-critical evaluation criteria for high throughput pretreatment and hydrolysis system.

Criteria Description	Weight
Separation of liquid and solid fractions after pretreatment	10
Washing of biomass after pretreatment	10
Reactor core operational in 2-3 months	9
Daily process rate of 4 pretreatments	8
Rapid heating and cooling: $(t_{heat} + t_{cool}) < t_{reaction}$	6
Automated solids distribution at the front end	4
Minimal manual operation	4

3.5. Options for process steps

The options for the reactor, heating system, and cooling system are examined below. Dr. Jaclyn DeMartini examined possible solids distribution and separation systems (not presented here). Two of the systems developed from these unit operations are described in section 3.6.

3.5.1. Reactor

From Tables 3.1 and 3.2, the reactor needed to be compatible with sulfuric acid concentrations up to 1.0 wt% and with variable reaction times, be capable of maintaining slurry homogeneity during pretreatment, allow for easy recovery of solids after pretreatment and facilitate solids distribution to a 96 well plate for enzymatic hydrolysis.

One reactor design considered was a column reactor packed with biomass operated under batch conditions. Loading water and sulfuric acid would be simple, however, experience has shown that adding dry biomass to and recovering wet, pretreated biomass from such a system is challenging.

The second design considered was a large stirred tank. Sufficient biomass for multiple enzyme tests would be pretreated and then distributed to a 96 well plate for enzymatic hydrolysis. A stirred tank would have the advantages of easy loading and unloading of material and uniform heating and cooling. However, accurate distribution of pretreated biomass to a 96 well plate would be challenging.

The possibility of developing a miniature reactor to pretreat only enough biomass for a single enzymatic hydrolysis test was also considered. It was envisioned that biomass, water, and acid would be added to each reactor and pretreatment conducted. Liquid and solid separation would be performed and the solids washed. After the biomass had been washed, enzymes would be added in order to perform enzymatic hydrolysis. The greatest challenge foreseen for such a system was distributing biomass.

The final reactor type considered was a microchannel reactor. Slugs of biomass slurry would be pumped through a microchannel reactor alternating with slugs of an

insoluble solution. Each slug of pretreated slurry would perform as a batch reactor. The biomass slurry would then be collected in sample vials or a well plate for separation, washing, and enzymatic hydrolysis. The primary concern with this system was if a biomass slurry could be effectively pumped through a microchannel without solids settling or plugging.

3.5.2. Heating and cooling systems

From Tables 3.1 and 3.2, the heating system needed to provide uniform and rapid heat up from ambient temperatures to 180^{o}C, maintenance of isothermal conditions for up to 1.5 hours and rapid cool-down. Indirect, direct heating, and microwaves were considered.

Indirect heating options included the use of a reactor jacket or internal coil. Heating could be provided by a heating fluid such as steam or by an electric resistance heater. One disadvantage of using a heating fluid was the reduction of reactor mobility due to piping connections.

Injection of steam to initiate pretreatment and cold water to quench the reaction was also considered. However, such injections would make it challenging to seal a reactor and develop a reliable mass balance.

Microwave heating was the third option considered but quickly discarded because the associated cooling system suing air was deemed too slow.

The cooling system needed to provide rapid and uniform cool-down. This could be achieved with a cooling fluid such as water or by convection cooling with air.

3.6. Proposed HTP systems and evaluation

The unit operations were assembled into four HTP systems and evaluated in detail with Dr. Jaclyn DeMartini. The Syrris Africa system and custom 96 well plate system are evaluated below. Dr. DeMartini evaluated systems developed by Chemspeed and Symyx.

3.6.1. Syrris Africa

The Africa system, developed by Syrris, is built around a microchannel reactor. The microchannel reactor is shown in Figure 3.3a. It is a glass chip with a total volume of 250 μL. An organic carrier solution is continuously pumped through the microchannel and volumes of biomass slurry are injected from a large feed tank into the carrier solution via the Syrris injection loop, shown in Figure 3.3b. The microchip is heated and cooled by a Peltier device, a heat pump that consumes electricity to transfer heat from one side of the device depending upon the direction of the current[6]. The heart of each biomass slug is automatically collected and dispensed into a 96 well filtration plate, which consists of four layers. The upper layer is a deep well microplate with a filter screen bottom. The screen is sufficiently fine that liquid does not flow out until a vacuum is applied. This plate is stacked on a closed bottom plate, and a vacuum applied to draw the pretreatment hydrolysate into the lower plate. The pretreatment hydrolysate is retained for analysis. The pretreated biomass could then be washed in the filter plate before the addition of enzymes and fresh water.

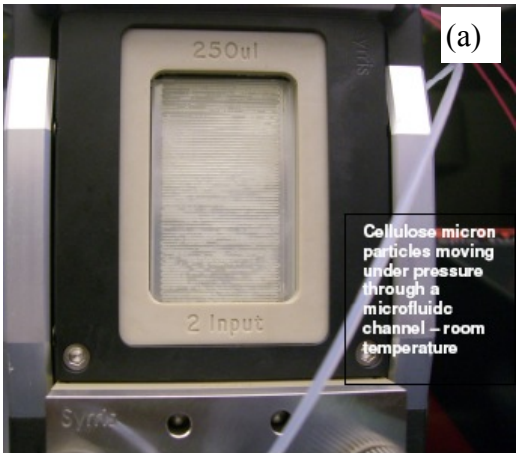

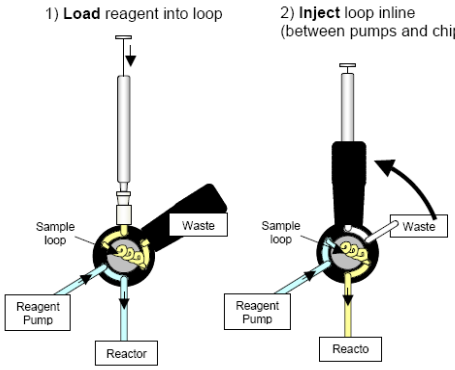

Figure 3.3a. Syrris glass microreactor as cellulose micron particles are pumped through the reactor.
Figure 3.3b. Illustration of Syrris injection loop.

After detailed consultation with Dr. Martin Peacock, a Syrris representative[7], it was determined that all of the critical criteria could be met except for an operating reactor pressure of 20 bar. Dr. Peacock reported that when a *Populus trichocarpa*-water slurry was pumped through the reactor at 180°C the system pressure was 0.7 MPa. This observation raised significant concern, as the steam pressure of water at 180°C is 1.0 MPa, and represented a potential immediate debarment from further consideration. Table 3.3 lists the non-critical criteria, weighting, and the short term and long-term scores for the Syrris system. In the short term, the system scores 81% on the non-critical criteria due to concern about the homogeneity of the biomass slurry feed tank and the efficiency of the filtration plates. It was felt that these issues could be resolved in the long term and thus the system's non-critical score rose to 93% for long-term implementation. The system was estimated to cost $500, 000.

Table 3.3. Syrris Africa system scores for non-critical criteria.

Description of criteria	Weight	Short Term Score	Long Term Score
Separation of liquid and solid fractions after pretreatment	10	8	10
Washing of biomass after pretreatment	10	6	8
Reactor core is operational in 2-3 months	9	9	n/a
Daily process rate of 4 pretreatments	8	10	10
Rapid heating and cooling: $(t_{heat} + t_{cool}) < t_{reaction}$	6	10	10
Automated solids distribution at the front end	4	4	9
Minimal manual operation	4	9	9
Score on Non-Critical *Perfect Score Short Term- 510* *Perfect Score Long Term- 420*		413	392

3.6.2. In-house 96 well plate

The second system considered was a custom metal 96 well plate. In the initial design, it was proposed that the 96 well plate would be made by drilling wells in an aluminum block and sealed with a rubber gasket and aluminum lid so that the plate could withstand pretreatment temperatures and pressures. In this system, biomass and water would be added to each well. Once the plate was sealed, it would be heated using indirect steam. After the reaction was completed, the steam would be flashed and the chamber flooded with water to quench the reaction. The pretreated biomass would be separated from the hydrolyzate by centrifugation and pipetting of the supernatant. The biomass would then be resuspended in fresh water with enzymes. Significant concerns about the technical feasibility and time requirements for solids separation following pretreatment led to the proposal that this step be omitted and enzymes be directly added

to the pretreatment slurry. The direct addition of enzymes to the pretreated biomass slurry was named co-hydrolysis.

Comparison of the well plate performance against the critical performance criteria revealed that primary point of concern was even temperature distribution across the plate. Initial calculations suggested that the temperature distribution within a solid aluminum block heated by steam would be even. Testing would be required for confirmation. Table 3.4 presents the 96 well plate system's scores for the non-critical criteria. The co-hydrolysis scores were determined by excluding the solid-liquid separation and biomass washing scores from the summation. The greatest concerns with this system was the number of man-hours that would be required to operate the system and thus the daily processing rate as well.

Table 3.4. In-house 96 well plate system with co-hydrolysis scores for non-critical criteria.

Description of criteria	Weight	Short Term	Long Term
Separation of liquid and solid fractions after pretreatment	10	10	10
Washing of biomass after pretreatment	10	10	10
Reactor core is operational in 2-3 months	9	10	n/a
Daily process rate of 4 pretreatments	8	5	5
Rapid heating and cooling: $(t_{heat} + t_{cool}) < t_{reaction}$	6	10	10
Automated solids distribution at the front end	4	8	8
Minimal manual operation	4	5	9
Score on Non-Critical *Perfect Score Short Term- 510* *Perfect Score Long Term- 420*		442	368
Score on Non-Critical, co-hydrolysis *Perfect Score Short Term- 310* *Perfect Score Long Term-220*		242	168

3.6.3. Comparison of results of HTP system evaluations

Table 3.5 compares the final scores for each system as percentages of perfect scores. From this table, it can be seen that despite its low non-critical scores, only the 96 well plate system can satisfactorily meet all of the critical criteria and at the lowest estimated price. Based on this score, it was decided that the 96 well plate system represented the best design for a HTP system and would be further developed.

Table 3.5. Comparison of criteria score and cost of proposed HTP systems.

System	Critical Criteria Score (%)	Non-critical Criteria, Washed Hydrolysis (%)	Non-critical Criteria, Co-Hydrolysis (%)	Cost (US $)
Chemspeed	84.6	71.4	72.2	400,000
Symyx	92.3	72.3	73.9	590,000
Syrris, Short term	92.3	80.9	88.1	265,000
Syrris, Long term	92.3	93.3	96.3	265,000
96 well plate, Short term	100	86.7	78.1	40,000
96 well plate, Long term	100	87.6	76.3	40,000

3.7. Closing thoughts

In order to harness the potential of improved biomass feedstocks and enzymes for the production of inexpensive sugars for fermentation to ethanol a high throughput pretreatment and enzymatic hydrolysis system was needed. The development of such a system began with the identification of the process steps and possible methods of accomplishing those steps. An evaluation system based on the Kepner-Tregoe decision-making system[5] was used to evaluate four potential systems. From this analysis it was

determined that a custom-built metal 96 well plate that both pretreatment and enzymatic hydrolysis could be performed in was the most promising system. The system required a major process modification to conventional biomass processing: the addition of enzymes directly to the pretreatment hydrolysate. Studer and co-workers proved the viability of co-hydrolysis.[8] A new well plate design consisting of individual steel wells pegged to a base was developed and its performance evaluated.[4]

3.8. References

(1) Wyman CE. What is (and is not) vital to advancing cellulosic ethanol. *Trends Biotechnol*. **2007**; *25*(4): 153-157.

(2) Lynd LR, Laser MS, Bransby D, Dale BE, Davison B, Hamilton R, Himmel M, Keller M, McMillan JD, Sheehan J, Wyman CE. How biotech can transform biofuels. *Nat. Biotechnol*. **2008**; *26*(2): 169-172.

(3) DeMartini JD. Chemical and structural features of plants that contribute to biomass recalcitrance. Ph.D., University of California Riverside, Riverside California, December 2011.

(4) Studer MH, DeMartini JD, Brethauer S, McKenzie HL, Wyman CE. Engineering of a high-throughput screening sysetm to identify cellulosic biomass, pretreatments, and enzyme formulations that enhance sugar release. *Biotechnol. Bioeng*. **2010**; *105*(2): 231-238.

(5) Kepner Tregoe decision making: the steps, the pros and the cons. http://www.decision-making-confidence.com/kepner-tregoe-decision-making.html. Accessed March 2012.

(6) Thermoelectric cooling. http://en.wikipedia.org/wiki/Peltier_device (accessed May 2012).

(7) Peacock M. Syrris Inc. Private communication, 2007.

(8) Studer MH, Brethauer S, DeMartini JD, McKenzie HL, Wyman CE. Co-hydrolysis of dilute pretreated Populus slurries to support development of a high throughput pretreatment system. *Biotechnol. Biofuels*. **2011**; *4*: 231-238.

Chapter 4.

A comparison of the heating performance of a fluidized sand bath and a steam chamber and their effects on the results of pretreatment and enzymatic hydrolysis.

4.1. Abstract

Both fluidized sand baths and steam chambers have been used for heating transfer during biomass pretreatment. It was found that the use of a sand bath or a steam chamber did not influence glucan or xylan yields from pretreatment and enzymatic hydrolysis. Several aspects of the heating performance of these devices were compared: time to heat reactors to reaction temperature, the stability of reactor temperature, the consistency of reactor temperature from run to run, and the convection coefficient. The convection coefficient was determined using correlations and multiple analyses of empirical data. The steam chamber heats reactors to 178^{o}C in a tenth of the time sand baths can, maintains a more stable temperature during pretreatment, results in more reproducible temperature profiles, and has a convection coefficient one to two magnitudes greater than that of the sand bath. Therefore if heat transfer is critical to an experiment, a steam chamber is advantageous.

4.2. Introduction

Ethanol, a ready alternative to petroleum based fuels, can be produced from the fermentation of sugars stored as the polymers cellulose and hemicellulose in biomass such as *Populus*. In order to efficiently recover the sugars by enzymatic hydrolysis in high yields, pretreatment which alters the composition and structure of the biomass is required[1]. Pretreatment with water at elevated temperatures, or hydrothermal pretreatment, has been shown to be an effective pretreatment[2, 3, 4, 5, 6, 7, 8, 9, 10, 11]. Fluidized sand baths are commonly used to heat pretreatment reactors[7, 9] but the development of a 96 well plate for pretreatment led to the introduction of a steam chamber[12] for heating reactors. Consequently, the objectives of this study were to determine 1) if the heating device used for pretreatment affects glucan and xylan yields from the pretreatment and enzymatic hydrolysis of *Populus trichocarpa*, 2) the time for reactors to reach reaction temperature in each device, 3) the temperature stability of the reactors during pretreatment, and 4) the convection coefficients that describe heat transfer in each device.

4.3. Calculations for the determination of convection coefficients

The convection coefficient, h, depends on fluid properties, surface geometry and flow conditions[13]. It can be calculated with an appropriate correlation or from experimental data. In this study both approaches were used.

4.3.1. Calculation of convection coefficient from literature correlations

4.3.1.a. For the fluidized sand bath

The convection coefficient from a gas-fluidized bed to a solid rod can be calculated as the sum of: a gas convective component, h_g, a particle convective component, h_p, and a radiative component, h_r[14,15,16].

$$h_{SB} = h_r + h_g + h_p \tag{1}$$

Since h_r is only significant at temperatures greater than 600°C, it was considered negligible in this study. The Martin correlation for h_g is[14, 15, 16]:

$$Nu_g = \frac{h_g d_p}{k_g} = 0.009 Ar^{0.5} \Pr^{0.33} \tag{2}$$

Where *Ar*, the Archimedes number, is given by:

$$Ar = \frac{\rho_p \rho_g d_p^3 g}{\mu_g^2} \tag{3}$$

and *Pr*, the Prandtl number, is given by:

$$\Pr = \frac{\mu_g c_{p,g}}{k_g} \tag{4}$$

The Martin particle convective component is defined as[14, 15, 16]:

$$Nu_p = \frac{h_p d_p}{k_g} = (1-\varepsilon) * z * (1 - e^{-N}) \tag{5}$$

where ε is the bed voidage. The characteristic group for particle convection, *z,* and the non-dimensional contact time, *N,* are[14, 15, 16]:

$$z = \sqrt{\frac{g d_p^3 (\varepsilon - \varepsilon_{mf})}{5(1-\varepsilon)(1-\varepsilon_{mf})}} \frac{\rho_p c_{p,p}}{6 k_g} \tag{6}$$

$$N = \frac{Nu_{wp}}{Cz} \tag{7}$$

The constant C[15] was experimentally determined to be 2.6. The heat transfer coefficient between the rod surface and a single particle in the bed is described by Nu_{wp}:

$$\frac{1}{Nu_{wp}} = \frac{1}{(Nu_{wp})_{\max}} + \frac{k_g / k_p}{4\left[1 + \left(\frac{3}{2}\frac{C}{\pi}\frac{k_g}{k_p} z\right)^{1/2}\right]} \tag{8}$$

Where:

$$(Nu_{wp})_{\max} = 4\left[(1+Kn)\ln\left(1+\frac{1}{Kn}\right) - 1\right] \tag{9}$$

The Knudsen number, Kn, is defined as:

$$Kn = \frac{4}{d_p}\left(\frac{2}{\gamma} - 1\right)\frac{\sqrt{2\pi R T^{\#}/M}\, k_g}{p(2c_{p,g} - R/M)} \tag{10}$$

The accommodation coefficient of the gas, γ, is equal to:

$$\gamma = \left[1 + 10^{(0.6-(1000/T^{\#}+1)/2.8)}\right]^{-1} \tag{11}$$

An alternative prediction of the average heat transfer coefficient in a fluidized bed developed by Molerus is[17, 18]:

$$Nu = \frac{h_{SB} l'}{k_g} = \frac{0.125(1-\varepsilon_{mf})\left\{1 + 33.3\left(\sqrt[3]{\beta_1}\beta_2\right)^{-1}\right\}^{-1}}{1 + \beta_3\left\{1 + 0.28\left(1-\varepsilon_{mf}\right)^2 \beta_1^{-1}\beta_2^2\beta_4^{1.5}\right\}} + 0.165\,\mathrm{Pr}^{1/3}\,\beta_4\left(1 + 0.05\beta_1^{-1}\right)^{-1} \tag{12}$$

Where:

$$l' = \left[\frac{\mu_g}{\sqrt{g}\left(\rho_p - \rho_g\right)} \right]^{2/3} \tag{13}$$

$$\beta_1 = \frac{u - u_{mf}}{u_{mf}} \tag{14}$$

$$\beta_2 = \sqrt[3]{\frac{\rho_p c_p}{k_g g}}\left(u - u_{mf}\right) \tag{15}$$

$$\beta_3 = \frac{k_g}{2 c_p \mu_g} \tag{16}$$

$$\beta_4 = \sqrt[3]{\frac{\rho_g}{\rho_p - \rho_g}} \tag{17}$$

Zabrodsky's prediction of the maximum heat transfer coefficient in a fluidized bed is[18, 19]:

$$h_{SB,\max} = 35.7 \rho_p^{0.2} k_g^{0.6} d_p^{-0.36} \tag{18}$$

4.3.1.b. For the steam chamber

The convection coefficient associated with the laminar film condensation of steam on the outer surface of a horizontal tube can be estimated as[13]:

$$h_{SC} = 0.729 \left[\frac{g \rho_l (\rho_l - \rho_v) k_l^3 h_{fg}^{'}}{\mu_l (T_{sat} - T_{surf}) d_{rod}} \right]^{1/4} \tag{19}$$

Where:

$$h_{fg}^{'} = h_{fg} + 0.68 c_{p,l} (T_{sat} - T_{surf}) \tag{20}$$

4.3.2 Experimental determination of convection coefficients

4.3.2.a. The energy balance

To describe the temperature gradient in a metal rod with radius r_o that develops as the rod is heated from a uniform temperature T_i an energy balance on a differential volume of the rod is applied[13]:

$$\frac{1}{r}\frac{\partial}{\partial r}\left(k_{rod} r \frac{\partial T}{\partial r}\right) + \frac{1}{r^2}\frac{\partial}{\partial \vartheta}\left(k_{rod}\frac{\partial T}{\partial \vartheta}\right) + \frac{\partial}{\partial x}\left(k_{rod}\frac{\partial T}{\partial x}\right) + \dot{q} = \rho_{rod} c_{p,rod}\frac{\partial T}{\partial t} \tag{21}$$

If $L/r_o \geq 10$, the cylinder can be treated as an infinite cylinder ($\partial T/\partial x = 0$). Assuming that the temperature profile is symmetric ($\partial T/\partial \vartheta = 0$), k_{rod}, ρ_{rod}, and $c_{p,rod}$ are constant and no energy is generated within the rod ($\dot{q} = 0$), equation (21) simplifies to:

$$\frac{1}{r}\frac{\partial}{\partial r}\left(k_{rod} r \frac{\partial T}{\partial r}\right) = \rho_{rod} c_{p,rod}\frac{\partial T}{\partial t} \tag{22}$$

The initial value and boundary conditions for a rod in the sand bath at T_∞ are:

$$T(r, t=0) = T_i \tag{23}$$

$$\left.\frac{\partial T}{\partial r}\right|_{r=0} = 0 \tag{24}$$

$$-k_{rod}\left.\frac{\partial T}{\partial r}\right|_{r=r_o} = h * (T(r=r_o, t) - T_\infty) \tag{25}$$

By transforming to the following non-dimensional variables:

$$\theta^* = \frac{\theta}{\theta_i} = \frac{T - T_\infty}{T_i - T_\infty} \tag{26}$$

$$t^* = Fo = \frac{\alpha_{rod} t}{r_o^2} \tag{27}$$

$$r^* = \frac{r}{r_o} \tag{28}$$

Thus the sand bath initial value problem, equations (22) to (25), can be rewritten as:

$$\frac{1}{r*}\frac{\partial}{\partial r*}\left(r*\frac{\partial \theta*}{\partial r*}\right)=\frac{\partial \theta*}{\partial t*} \tag{29}$$

$$\theta*(r*,0)=1 \tag{30}$$

$$\left.\frac{\partial \theta*}{\partial r*}\right|_{r*=0}=0 \tag{31}$$

$$\left.\frac{\partial \theta*}{\partial r*}\right|_{r*=1}=-\frac{hr_o}{k_{rod}}\theta*(1,t*) \tag{32}$$

Equations (22), (23), and (24) also apply to a rod in the steam chamber. However, since steam is injected into the steam chamber as the rod is heated, the temperature of the surroundings, T_∞, is a function of time; therefore the boundary condition at $r=r_o$ must be modified to:

$$-k_{rod}\left.\frac{\partial T}{\partial r}\right|_{r=r_o}=h*(T(r=r_o,t)-T_\infty(t)) \tag{33}$$

And two additional dimensionless temperature variables are defined:

$$\tau*=\frac{\tau}{\tau_i}=\frac{T-T_i}{T_{\infty,ss}-T_i} \tag{34}$$

$$\tau_\infty*=\frac{\tau_\infty}{\tau_i}=\frac{T_\infty(t)-T_i}{T_{\infty,ss}-T_i} \tag{35}$$

Where $T_{\infty,ss}$ is the steady state temperature of the steam chamber. Rewriting equations (22) to (24) and (33) with $\tau*$ and $\tau_\infty*$:

$$\frac{1}{r*}\frac{\partial}{\partial r*}\left(r*\frac{\partial \tau*}{\partial r*}\right)=\frac{\partial \tau*}{\partial t*} \tag{36}$$

$$\tau^*(r^*,0) = 0 \tag{37}$$

$$\left.\frac{\partial \tau^*}{\partial r^*}\right|_{r^*=0} = 0 \tag{38}$$

$$\left.\frac{\partial \tau^*}{\partial r^*}\right|_{r^*=1} = -\frac{hr_o}{k_s}(\tau^*(1,t^*) - \tau_\infty{}^*(t^*)) \tag{39}$$

These initial value problems can be solved several different ways as described in the following sections.

4.3.2.b. The lumped capacitance method

If the conduction rate is significantly larger than the convection rate, the rod's radial temperature gradient will be negligible. In this case, the energy balance on the entire rod is[13]:

$$-hA_s(T - T_\infty) = \rho_{rod} V c_{p,rod} \frac{\partial T}{\partial t} \tag{40}$$

Using the dimensionless temperature, equation (26), and substituting $A=2\pi r_o L$, for an infinite cylinder, and $V=\pi r_o{}^2 L$, equation (40) is integrated to:

$$\ln\theta^* = -\frac{2h}{\rho_{rod} r_o c_{p,rod}} t \tag{41}$$

The convection coefficient can be determined from the slope of a plot of $\ln\theta^*$ as a function of time. This method is known as the lumped capacitance model, and the error associated with neglecting the radial temperature gradient is generally small if[13]:

$$Bi = \frac{hr_o}{k_{rod}} < 0.1 \tag{42}$$

4.3.2.c. The instantaneous lumped capacitance method

Equation (40) can also be rearranged to solve for an instantaneous value of the convection coefficient as a function of time. In order to use this approach, it is necessary to fit functions to the empirical temperature-time profiles.

4.3.2.d. The analytical solution

The initial value problem of heating a rod in the sand bath defined by equations (29) to (32) can be solved analytically[13]:

$$\theta^* = \sum_{n=1}^{\infty} K_n \exp(-\zeta_n^2 Fo) J_o(\zeta_n r^*) \tag{43}$$

Where:

$$K_n = \frac{2}{\zeta_n} \frac{J_1(\zeta_n)}{J_o^2(\zeta_n) + J_1^2(\zeta_n)} \tag{44}$$

$$\zeta_n \frac{J_1(\zeta_n)}{J_o(\zeta_n)} = Bi = \frac{hr}{k_s} \tag{45}$$

If the Fourier number, *Fo* (equation (27)), is greater than 0.2, equation (43) can be approximated by the first term. Thus, assuming that *Fo*>0.2, the time dependence of the centerline (r^*=0) temperature is approximately:

$$\theta^* = K_1 \exp(-\zeta_1^2 Fo) \tag{46}$$

Equation (46) can be re-arranged to:

$$\ln \theta^* = -\zeta_1^2 \frac{\alpha}{r_o^2} t + \ln K_1 \tag{47}$$

Inspection of equations (45) and (47) reveals that the convection coefficient can be determined from the slope of the plot of natural logarithm of the non-dimensional

temperature as a function of time. Some iteration is required in order to reach agreement between the slope and intercept of equation (47). Due to the more complex boundary conditions for the initial value problem of the steam chamber, equations (36) to (39) cannot be easily solved analytically.

4.3.2.e. Finite difference methods

The initial value problems can also be solved using finite difference methods and non-linear fitting. By using a non-linear least squares solver, such as Matlab[20]'s *lsqcurvefit*, and a finite differences solver, such as Matlab[20]'s *pdepe*, the convection coefficient can be determined. An initial guess of the convection coefficient is used in the finite differences solution to equations (29) to (32) and equations (36) to (39) to calculate a centerline temperature-time profile. This result is compared to the experimental data, and the convection coefficient is then adjusted to reduce the sum of the squares of the residuals between the calculated and experimental temperature profiles. This approach is repeated until the residuals cannot be reduced further. The initial guess for the convection coefficient can be obtained using the approaches described in sections 4.3.1, 4.3.2.b, and 4.3.2.d.

4.4. Experimental apparatus and procedures

4.4.1. Experimental apparatus

4.4.1.a. Substrate

Populus trichocarpa was provided by Oak Ridge National Laboratory for this study. Logs were debarked, split with an axe, chipped (Yard Machines 10HP, MTD Products Inc., Cleveland, OH), and knife milled (Model 4 Wiley Mill, Thomas Scientific,

Swedesboro, NJ) through a 1 mm screen size; all of these operations were performed at the National Renewable Energy Laboratory (NREL). After one month of air-drying at NREL, the chips had a moisture content of approximately 5 wt%. The material was further milled through a 20-80 mesh screen to produce particles with diameters of 0.18 mm to 0.85 mm (Thomas-Wiley Laboratory Mill Model 4, Arthur H. Thomas Company, Philadelphia, PA) before being shipped to UCR.

4.4.1.b. Pretreatment reactors

Custom-built 10 mL reactors were used for pretreatment. The reactors were constructed from stainless steel tubing with an outer diameter of 12.7 mm and a length of 150 mm. The reactors were sealed using threaded caps (SS-810-C, Swagelok, San Diego, CA). One reactor was prepared with a thermocouple (.062-K-U-4"-T3-10 ft TF/TF-MP, Wilcon Industries, Lake Elsinore, CA) inserted along the centerline to record the reactor temperature as a function of time using a Digi-Sense DualLogR Thermocouple Meter (15-176-96, Fisher Scientific, Pittsburgh, PA). Data was transferred from the meter to a computer using an infrared adapter (EW-91100-85, Cole Parmer**,** Vernon Hills, IL).

4.4.1.c. Thermocouple rod

Two thermocouple rods were used to determine the convection coefficients. Each rod had a diameter of 12.7 mm and a length of 150 mm. A 3.17 mm K-type thermocouple (.125-K-316-U-10”-T3-6 ft, Wilcon Industries, Lake Elsinore, CA) was inserted 76.2 mm into each rod along the centerline. The external portion of the thermocouple was insulated with Teflon tape. One rod was made of copper alloy 145

(9100K143, McMaster Carr, Santa Fe Springs, CA) and the other of stainless steel 316 (1305T171, McMaster Carr, Santa Fe Springs, CA). The physical properties of the two metals are listed in Table 4.1.

Table 4.1. Physical properties of copper and stainless steel thermocouple rods.

Physical properties	Copper alloy 145	Stainless steel 316
k (W/m*K)	382	13.4
ρ (kg/m^3)	8940	8238
$c_{p,rod}$ (J/kg*K)	385	468
α (m^2/s)	$1.11*10^{-4}$	$3.48*10^{-6}$

4.4.1.d. Heating apparatuses

The first heating apparatus was a 4-kW model SBL-2D fluidized sand bath (Techne, Princeton, NJ). The diameter of the bed of sand was 0.23 m; at rest the height of the bed was 0.33 m. Air was provided to the base of the bed at a rate of 5.2 m^3/hr at 20^{o}C in order to fluidize the bed. The density, thermal conductivity and heat capacity of sand were assumed to be 1515 kg/m^3, 0.27 W/m*K, and 800 J/kg*K, respectively[13]. The average particle size of the sand was assumed to be 0.18 mm.

The second heating apparatus was a custom-built steam chamber. Studer et al provide a detailed description of this chamber.[12] The chamber was constructed from off-the-shelf 1 MPa rated fittings. The central chamber has an outer diameter of 102 mm and a length of 0.61 m and is accessed through a ball valve. The chamber is connected to a steam boiler (FB-075-L, Fulton Companies, Pulaski, NY) and cooling water. The temperature of the chamber is measured by a K-type thermocouple (Wilcon Industries, Lake Elsinore, CA).

4.4.2. Experimental procedure

4.4.2.a. Pretreatment

A representative pretreatment run is described. Nine tube reactors were used for each pretreatment condition. Each tube reactor was loaded with 8.34 mL of *Populus trichocarpa*-deionized water slurry containing 5 wt% dry *Populus trichocarpa*. Once the reactor was loaded, it was sealed, shaken, and left overnight. The thermocouple reactor was loaded with 8.34 mL deionized water. The sand bath was heated to 182^{o}C. Nine tube reactors and the thermocouple reactor were loaded into a wire basket and the temperature was recorded every five seconds by the Digi-Sense DualLogR Thermocouple Meter. The basket and reactors were lowered into the sand bath; the start of the reaction was taken as the time when the reactors reached 178^{o}C, at which point the sand bath temperature control set point was reset to 180^{o}C. The reaction was allowed to proceed for 17.6 minutes. The wire basket and reactors were then submerged in a water bath and cooled to 80^{o}C. The thermocouple meter was stopped, and the data was transferred to a computer. This procedure was repeated for reactions lasting 27.8, 44.1, 55.5, and 69.9 minutes. The runs lasting 17.6, 44.1, and 69.9 minutes were performed in triplicate.

This series of experiments was also performed using the steam chamber. The boiler was preheated to an output pressure of 889 kPag. Before the reactors were placed in the steam chamber, the chamber walls were preheated by introducing steam to the chamber for approximately one minute. The flow of steam to the chamber was then stopped, and the steam in the chamber was released to atmosphere. The chamber was then flooded with cooling water for approximately one minute and then drained. Nine

tube reactors were then loaded into the chamber for pretreatment. The boiler pressure was reduced to 861 kPag, and steam was introduced to the chamber. Once the temperature reached 178^{o}C, the boiler pressure was increased to 889 kPag for the duration of the run. At the end of pretreatment, the steam inlet valve was closed, and reactors were cooled by flashing the steam and flooding the chamber with water.

Following pretreatment, the reactors from each run were processed in batches of three. The contents of three tube reactors were filtered using a pre-weighed crucible, with the filtrate retained for analysis. The pretreated solids were washed with three volumes of 500 mL of deionized water. The solids and crucible were then transferred to a 45^{o}C oven for 24 hours of drying. The dried crucible and solids were then massed. The solids were stored at room temperature until compositional analysis was performed.

The contents of the second and third reactor trios were used for enzymatic hydrolysis. The contents of three tube reactors were transferred to a massed 50 mL centrifuge tube, and the mass of the centrifuge tube and pretreated slurry were then recorded. The slurries were then separated by centrifugation. The supernatant was removed and the solids were washed by resuspension in approximately 40 mL of deionized water and centrifuged, with this procedure repeated three times. After the third centrifugation, deionized water was used to adjust the mass of centrifuge tube and solids to the weight of the initial pretreated slurry. This slurry of washed, pretreated solids and deionized water was transferred to a 125 mL screw top flask for enzymatic hydrolysis.

4.4.2.b. Enzymatic hydrolysis

Citrate buffer and sodium azide were added at concentrations of 0.05 M and $1.54*10^{-4}$ M, respectively in the enzymatic hydrolysis flasks. Xylanase (Multifect Xylanase, protein content 56.6 mg/ml, lot number 4900667792; Genencor, Palo Alto, CA) and cellulase (Spezyme CP, protein content 116.0 mg/ml, lot number 3016295230; Genencor, Palo Alto, CA) were mixed at a ratio of 1:3 based on their protein content, and diluted 1:3 with HPLC-grade water. This mixture was added to achieve a final concentration of 15 mg xylanase protein and 45 mg cellulase protein per gram glucan plus xylan in the raw *Populus trichocarpa*. The flasks were then incubated at 50°C for 72 hours while being shaken a 150 rpm. After enzymatic hydrolysis, a 2 mL liquid sample was taken for analysis.

4.4.2.c. Analytical techniques

The hydrolyzate liquid from pretreatment was processed by the strong acid hydrolysis procedure described by Sluiter et al.[21] to convert sugar oligomers to monomers that could be measured by HPLC at the conditions described below. The glucose and xylose contents of the raw and pretreated biomass solids were measured in triplicate using the procedure described by Sluiter et al.[22] However, the procedure was modified slightly in that no extraction was performed prior to the two-step acid hydrolysis because of the low extractives content of *Populus trichocarpa*. After hydrolysis, a 20 mL aliquot of the liquor was withdrawn and neutralized with calcium carbonate (Sigma-Aldrich, St. Louis, MO). A 2 mL sample of the neutralized liquor was centrifuged in order to separate the neutralization salts. The composition of the supernatant of the centrifuged

sample was measured by HPLC at conditions described below. The glucose and xylose content of biomass from the National Institute of Standards and Technology (NIST) were measured in parallel to authenticate the results of the solids compositional analysis. Glucose and xylose concentrations were converted to glucan and xylan equivalents by dividing by 1.1111 and 1.3622, respectively, to account for the mass gain during hydrolysis.

The enzymatic hydrolysis liquid sample was centrifuged to prevent any solid material from being injected into the HPLC. The glucose and xylose concentrations in a 450 μL volume of the supernatant of the centrifuged sample was measured by HPLC at the conditions described below.

Sugars were detected by HPLC using an Aminex HPX-87H column (BioRad, Hercules, CA) heated to 65^{o}C with a separation module (Alliance 2695, Waters, Milford, MA) equipped with a refractive index detector (2414, Waters, Milford, MA). The eluent was 0.005 M sulfuric acid in the isocratic mode.

4.4.2.d. Determination of convection coefficients

The copper thermocouple rod was attached to the Digi-Sense DualLogR Thermocouple Meter and placed in a wire basket. The sampling interval of the Digi-Sense DualLogR Thermocouple Meter was set to one second. The sand bath was heated to 182^{o}C. Data collection was initiated before the basket and thermocouple rod were submerged in the sand bath. The rod was left in the sand bath until the centerline temperature of the rod was constant for 40 to 120 seconds; the rod was then transferred to a water bath and data collection was stopped. The time/temperature data was transferred

to the computer. This procedure was repeated for each run. In total, three runs with each rod were performed in the sand bath, alternating between the copper and steel thermocouple rods.

The rods were then inserted in the steam chamber by threading the wires through an open pipe, which was then filled with J-B Weld epoxy (J-B Weld Co., Sulphur Springs, TX). The boiler was preheated to an output pressure of 861 kPag. In order to mimic the heating of pretreatment reactors, the chamber was preheated as described in section 4.4.2.a. After cooling the chamber, the steel thermocouple rod and steam chamber thermocouple were attached to the Digi-Sense DualLogR Thermocouple Meter, and the data sampling interval was set to one second. Data collection was initiated, and steam was introduced to the steam chamber. The temperature of the rod and steam were recorded as a function of time. Once the centerline temperature of the rod had been constant for 50 to 140 seconds, the flow of steam to the chamber was stopped, and cooling water was introduced into the chamber. The time/temperature data was transferred to a computer. The copper thermocouple rod malfunctioned in the steam chamber data in that once the temperature of the rod reached approximately 100^{o}C: the temperatures recorded by the data logger jumped erratically but due to the J-B Weld it was not possible to remove the copper thermocouple rod for repairs; therefore only three runs were performed in the steam chamber, all with the steel thermocouple rod.

4.5. Results and discussion

4.5.1. Comparison of pretreatment and enzymatic hydrolysis yields

In this thesis, yield is defined as the glucan or xylan equivalent of glucose or xylose, respectively, recovered in the liquid phase from pretreatment, enzymatic hydrolysis, or the two combined as a percentage of the glucan or xylan initially available in the raw solids. The percent yields of xylan and glucan from hydrothermal pretreatment and enzymatic hydrolysis are plotted in Figures 4.1a to 4.1f as functions of pretreatment time. Stage 1 refers to pretreatment, and Stage 2 refers to enzymatic hydrolysis. From top to bottom are the combined glucan-xylan, xylan, and glucan yields. Figures 4.1a to 4.1c, and 4.1d to 4.1f present results from pretreatment in the sand bath and steam chamber, respectively. The yields after 17.6, 44.4, and 69.9 minutes are the averages of triplicate runs and the bars represent the standard deviation of triplicates. Several trends can be seen in these figures. Xylan was the primary pretreatment product and glucan was the primary enzymatic hydrolysis product. As is typical, xylan yields from pretreatment increased with pretreatment time as xylose and xylooligomers were released from *Populus trichocarpa* to a maximum and then decreased due to degradation reactions[23]. As previously shown for corn stover, the maximum xylan, glucan and total yields do not coincide, emphasizing the importance of optimizing the system as a whole[24]. Comparison of the plots shows that the yields from hydrothermal pretreatment and enzymatic hydrolysis were not influenced by the method of heating used for pretreatment. Since sand baths are less expensive and less dangerous to operate, laboratory scale pretreatments can still be performed in the fluidized sand bath.

However, this study also demonstrated that the results from pretreatment performed using an indirect steam chamber can be compared to pretreatment work performed with fluidized sand baths.

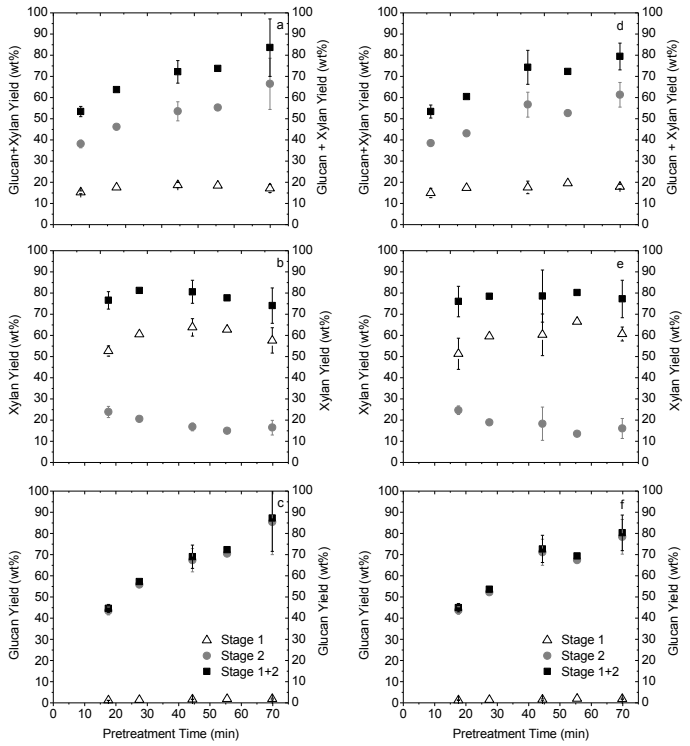

Figure 4.1. Percent yield of glucan and xylan from hydrothermal pretreatment at 180^{o}C (Stage 1) and enzymatic hydrolysis (Stage 2) of *Populus trichocarpa* as a function of pretreatment time. Figures a/b/c are for pretreatment using the sand bath. Figures d/e/f are for pretreatment conducted in the steam chamber. Figures a/d present the recovery of glucan and xylan combined. Figures b/e present the recovery of xylan. Figures c/f present the recovery of glucan.

4.5.2. Reactor heating

An important measure of the heating performance of the sand bath and steam chamber is the time for the nine pretreatment reactors to reach 180^{o}C. The reactor heating time was recorded for each run; the results are presented in Figure 4.2. From Figure 4.2, it can be seen that the average heat-up time in the sand bath was 3.10$\pm$0.35

min while the average heat-up time in the steam chamber was 0.39±0.10 min. This reduced heating time is a reflection of the better heat transfer properties of steam relative to fluidized sand. The reduced standard deviation of the steam chamber is a reflection of the immutable physical properties of steam. In contrast, the standard deviation of the sand bath reflects the variability of sand bath conditions: variables influencing heat transfer such as the flow rate of air were not precisely controlled and could have varied.

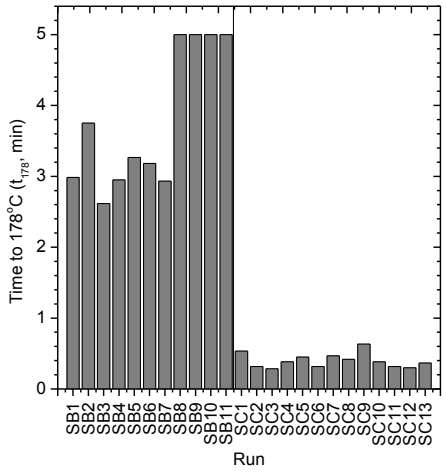

Figure 4.2. Comparison of the time for nine tube reactors to reach 178°C in the fluidized sand bath (SB) and the steam chamber (SC).

4.5.3. Stability and consistency of reactor temperature

Another important aspect of heating during pretreatment is the stability of the temperature during the reaction. Sample temperature profiles from a pretreatment in the sand bath and in the steam chamber are shown in Figure 4.3. In Figure 4.4, the minimum, average, and maximum reactor temperatures during each pretreatment run are shown. Both of these figures demonstrate that there was less variation in the temperature of the reactors during a run when the steam chamber was used which reflects the temperature stability of the surroundings. A TC-8D controller (Techne, Princeton, NJ)

of the reactors during a run when the steam chamber was used which reflects the temperature stability of the surroundings. A TC-8D controller (Techne, Princeton, NJ) cycles the sand bath heating elements on and off in response to changes in the bed temperature while the steam chamber temperature is dictated by the boiler pressure controller which adjusts power to the heating elements. Figure 4.3 indicates that the boiler pressure was more stable than the sand bath temperature indicating that the boiler pressure was subject to fewer disturbances or that the boiler pressure controller was better tuned than the sand bath temperature controller. Figure 4.4 also illustrates the run to run consistency of the heating devices. Like the heating times, this consistency is a reflection of the variability of the heating devices.

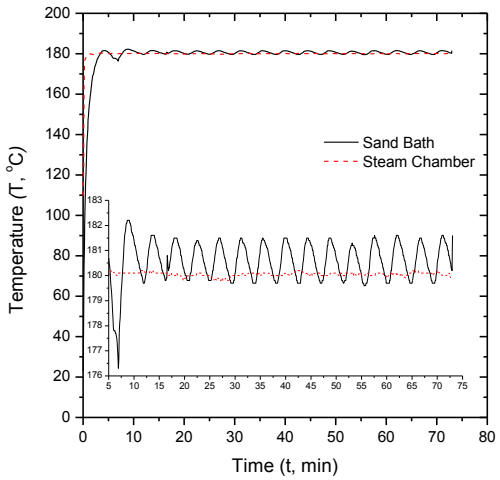

Figure 4.3. Temperature profiles of nine tube reactors during pretreatment at 180°C for 69.9 minutes in the fluidized sand bath (black, solid) and steam chamber (red, dotted).

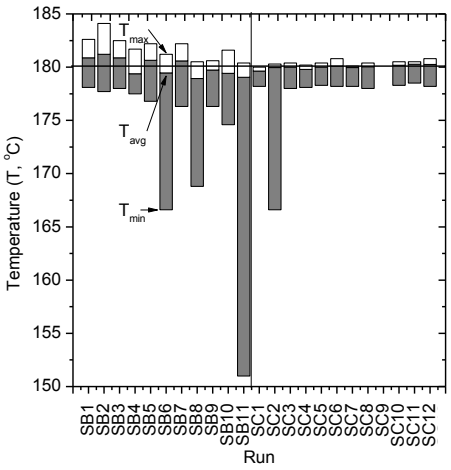

Figure 4.4. Minimum, average, and maximum temperatures observed during pretreatment of biomass in nine tube reactors at 180°C in the sand bath (SB) and steam chamber (SC). Runs lasted 17.6 to 69.9 minutes.

4.5.4. Convection coefficients

4.5.4.a. Sand bath convection coefficient

4.5.4.a.i. Calculated by correlation

The sand bath convection coefficient was predicted with the correlations developed by Martin, Molerus, and Zabrodsky[14, 15, 17, 19]. The physical properties of air were evaluated at atmospheric pressure at 182°C. The bed voidage at minimum fluidization and operating conditions was estimated to be 0.38 and 0.51, respectively, from force balances on the bed[14, 25]. Sensitivity analyses in which relevant variables were changed by ±25% were conducted for each correlation.

The convection coefficient of the sand bath at 182°C was calculated to be 436 W/m^2K using the Martin correlation, equations (1) to (11)[14, 15]. The results of Martin correlation[14, 15] sensitivity analysis in Figure 4.5 show that the experimental constant *C* has the greatest influence on the convection coefficient followed closely by the bed

voidage, ε. The constant C is the one fitting parameter in Martin's model and was validated under numerous operating conditions[15]. Therefore, although varying C results in convection coefficients ranging from 315 W/m^{2}K to 526 W/m^{2}K, it is unlikely that Martin's recommended value of 2.6 is invalid. A second sensitivity analysis of the variables influencing the calculation of ε was conducted, with the results shown in Figures 4.6a and 4.6b. As seen in Figure 4.6a, 25% changes in the sand and air density, particle size, air viscosity, and superficial velocity resulted in 0.13 to 14% changes in the bed voidage, which in turn led to a mere 0.40 to 7.8% change in the convection coefficient (Figure 4.6b). Therefore, the dramatic changes in the convection coefficient in Figure 4.5 are physically unlikely. Finally, from Figure 4.5 it can be seen that inaccuracies in the particle size, bed voidage at minimum fluidization, sand density, accommodation coefficient, sand heat capacity, or conductivity do not result in a significantly larger or smaller predictions of the sand bath convection coefficient.

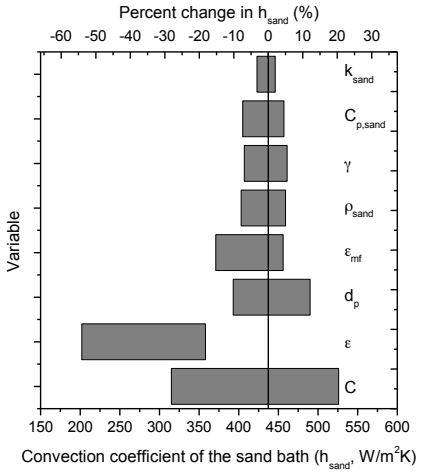

Figure 4.5. Response in predicted convection coefficient to a +/-25% sensitivity analysis of the Martin correlation, equations (1) to (11)[14, 15].

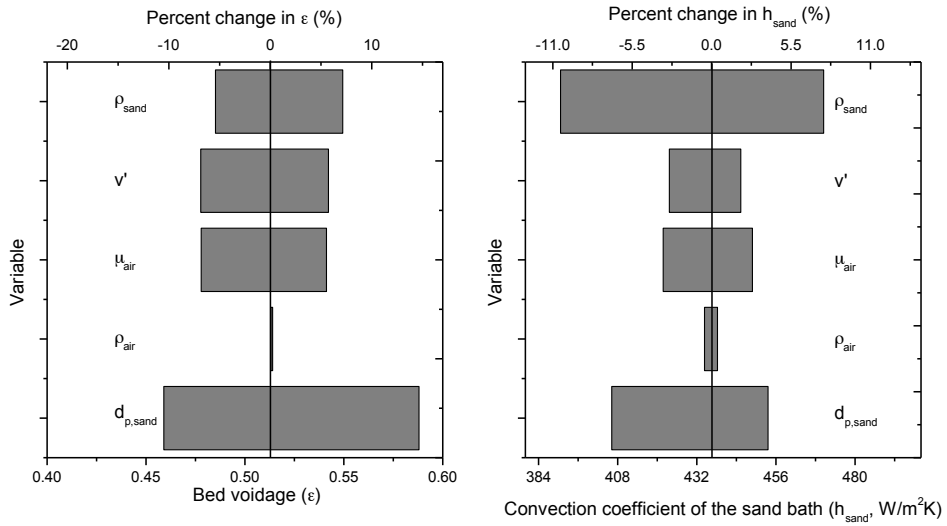

Figure 4.6a. Response in bed voidage to +/-25% sensitivity analysis of bed voidage determining parameters.
Figure 4.6b. Response in convection coefficient calculated from the Martin correlations equations (1) to (11) to a +/-25% sensitivity analysis[14, 15].

The convection coefficient of the fluidized sand bath at 182^{o}C was estimated to be 198 W/m^{2}K based on the Molerus correlation[17]. The +/-25% sensitivity analysis presented in Figure 4.7 shows that changes in sand properties, bed voidage, and bed voidage at minimum fluidization do not significantly alter the predictions of the convection coefficient of the sand bath. This value is approximately half the convection coefficient predicted using Martin's equations[14, 15]. The Molerus correlation[17] was developed in order to address some of the deficiencies in the Martin equation[14, 15]. However, as will be shown in section 4.5.4.a.vi, the Martin correlation[14, 15] more closely matches the convection coefficients predicted empirically; therefore, in this study, it appears that the Martin correlation[14, 15] is the better choice.

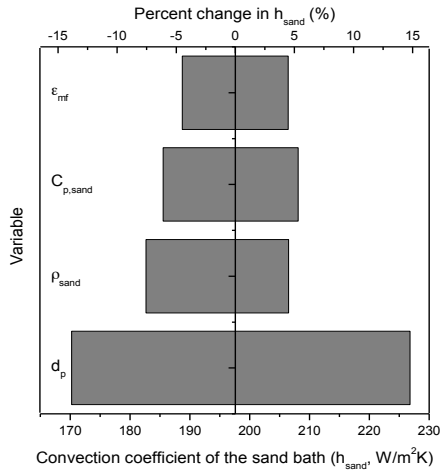

Figure 4.7. Response in predicted convection coefficient to a +/-25% sensitivity analysis of the Molerus correlation, equation (12). [17]

The maximum convection coefficient of the fluidized sand bath at 182^{o}C was determined to be 481 W/m^{2}K using the Zabrodsky correlation[19]; this is comparable to the prediction using the Martin correlation[14, 15]. As shown by the +/-25% sensitivity analysis presented in Figure 4.8, inaccuracies in the particle size, particle density, or gas conductivity do not significantly change the estimate of the maximum possible convection coefficient.

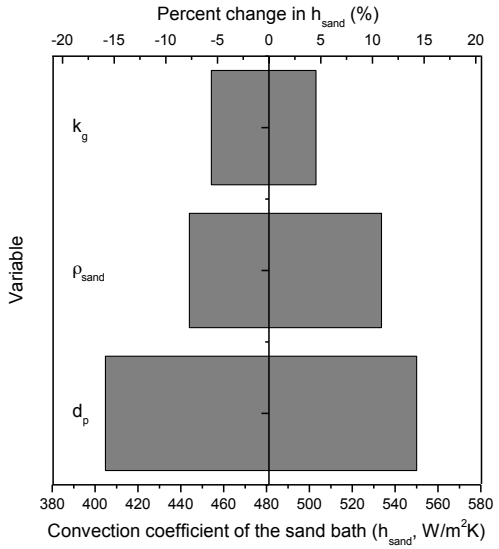

Figure 4.8. Response in predicted convection coefficient to a +/-25% sensitivity analysis of the Zabrodsky correlation, equation (18) [19].

4.5.4.a.ii. Calculated by lumped capacitance

The first estimate of the convection coefficient from sand bath experimental data was made using the lumped capacitance method. In this case, the convection coefficient was calculated by fitting a linear regression line to the plot of the natural logarithm of the non-dimensional temperature as a function of time multiplied by $-2/(\rho_{rod} r_o c_{p,rod})$; from equation (41) the slope of this line is equal to the convection coefficient. A sample plot using data collected with the copper thermocouple rod is shown in Figure 4.9. The average convection coefficient from the three runs with the copper thermocouple rod was 381 ± 18 W/m^{2}K while the average convection coefficient from the three steel thermocouple rods was 365 ± 4 W/m^{2}K. Because the associated Biot numbers were 0.0063 and 0.17, respectively, the lumped capacitance assumption would be appropriate

for the copper thermocouple rod but not the steel one. Despite this, the convection coefficients from the two rods are in close agreement.

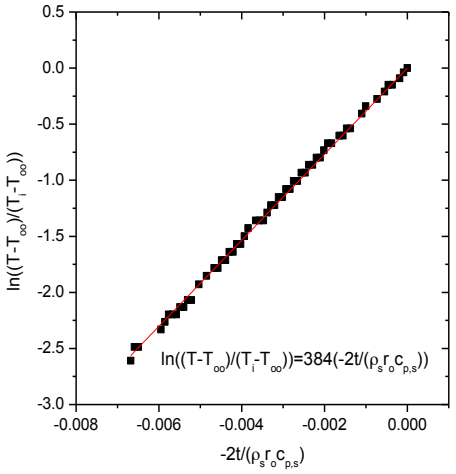

Figure 4.9. Dimensionless centerline temperature of the copper thermocouple rod (run 2) in the sand bath as a function of modified time.

4.5.4.a.iii. Instantaneous lumped capacitance convection coefficient

To determine the instantaneous convection coefficient of a sand bath with equation (40), it was necessary to develop a function for temperature as a function of time with the following properties:

$$f(0) = T_i \tag{48}$$

$$\lim_{t\to\infty} f(t) = T_{ss} \tag{49}$$

$$\lim_{t\to\infty} f'(t) = 0 \tag{50}$$

Based on these conditions, it was decided to model T as:

$$T = f(t) = a + b \times \exp(-t/c) \tag{51}$$

The experimental thermocouple rod temperature for each run is plotted as a function of time in Figure 4.10 along with the fitted equations. Thus, equation (51) can be used to accurately predict the thermocouple temperature as a function of time.

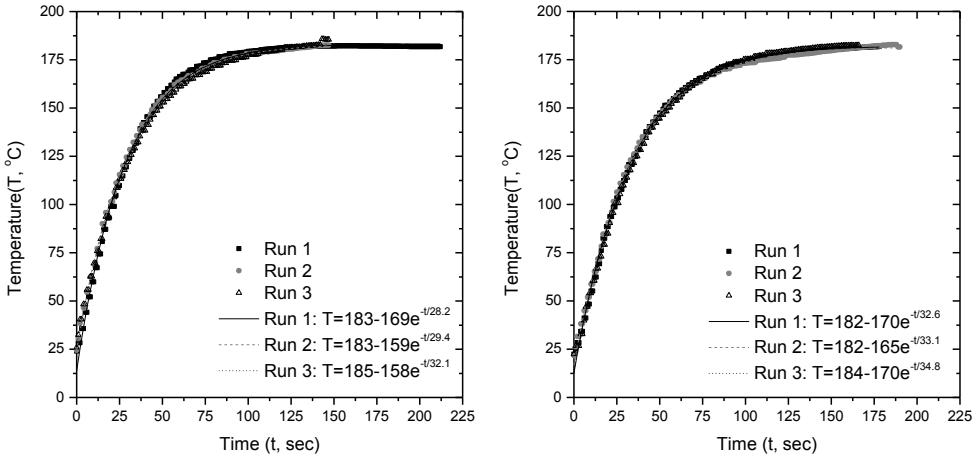

Figure 4.10. Experimental and predicted temperature of the copper (a) and steel (b) thermocouple rods in the sand bath as a function of time for each run.

In Figure 4.11, the instantaneous lumped capacitance convection coefficient of the sand bath is plotted as a function of time for each run for the copper and steel thermocouple rods, with the coefficients ranging from 347 to 430 W/m^{2}K and from 355 to 406 W/m^{2}K, respectively. Thus, convection coefficients predicted for the copper and steel thermocouple rod are again in close agreement. As time increased, both the differential of rod temperature with respect to time and the difference in the thermocouple rod and sand bath temperatures decreased. From equation (40), it can be seen that these factors decrease and increase the convection coefficient, respectively. However, since the convection coefficient gradually increases as time increases, the difference in the thermocouple rod and sand bath temperature had the greatest influence on the convection coefficient.

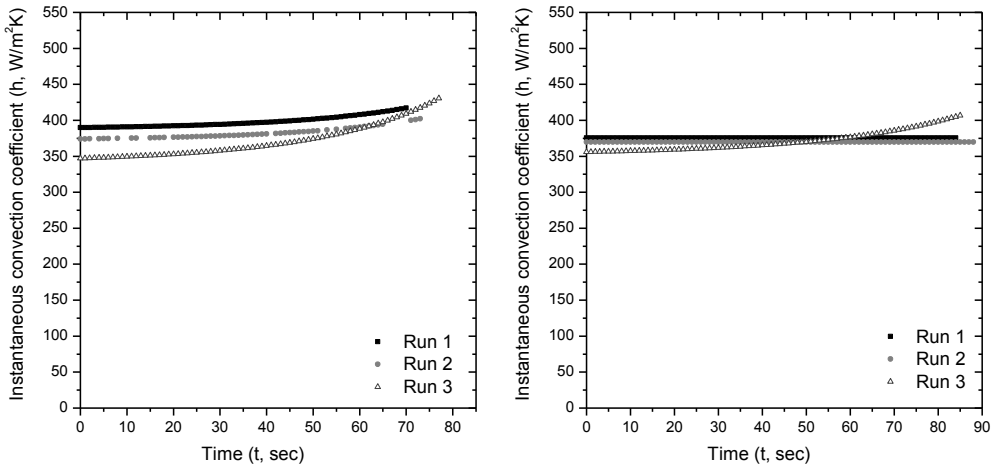

Figure 4.11a. Instantaneous convection coefficient as a function of time for copper (a) and steel (b) thermocouple rods in the sand bath.

4.5.4.a.iv. Analytical solution

As shown in section 4.5.4.a.ii, the lumped capacitance assumption proved invalid for the steel thermocouple rod; therefore, equation (47) should be used to account for the rod's radial temperature gradient. The natural logarithm of the dimensionless temperature was plotted as a function of dimensionless time and the linear regression model was fit to the data; a sample is shown in Figure 4.12a. Since the slope and intercept of this model both depend on ξ_1, as defined by equations (44) and (45), several iterations were required to reach agreement between equations (44), (45), and (47). Once this was achieved, as shown in Figure 4.12b, the convection coefficient was calculated from equations (45) and (47). Using this approach, the average convection coefficient from the three runs with the copper and steel thermocouple rods were 374 ± 23 W/m^{2}K and 392 ± 4.7 W/m^{2}K, respectively. As with the lumped capacitance approach, the results from the copper and steel thermocouple rod are in close agreement.

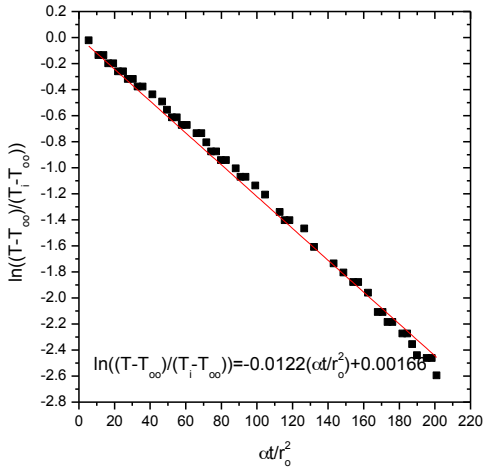

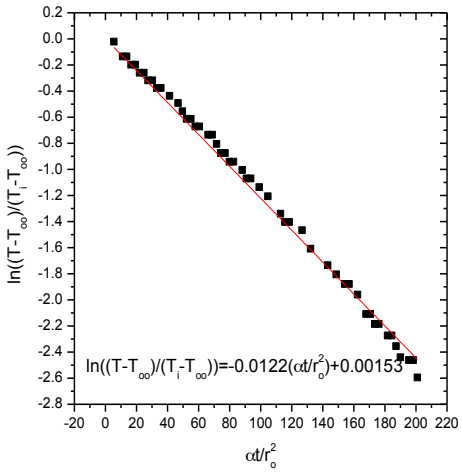

Figure 4.12a. Initial linear fit of equation (47) to the data from copper thermocouple rod (run 2) in the sand bath.
Figure 4.12b. Linear fit of equation (47) to the data from copper thermocouple rod (run 2) in the sand bath after reaching agreement with equations (44) and (45).

4.5.4.a.v. Finite elements approach

The initial value problem posed by equations (22) to (25) was also solved numerically as outlined in 4.3.2.e. The solutions obtained in sections 4.5.4.a.i, 4.5.4.a.ii, and 4.5.4.a.iv were used as initial guesses for the convection coefficient; initial guesses bracketing these values were also used.

Table 4.2 summarizes the convections coefficients for run 1 with the copper thermocouple rod for each initial guess using three different radial meshes. It can be seen that the calculated convection coefficient changed by only 0.66% as the radial mesh size was decreased from 0.1 to 0.001 thus there is little benefit in further refining the radial mesh. The convection coefficient for the remaining runs was calculated using a mesh size of 0.001. It can also be seen in Table 4.2, that the initial guess does not influence the final convection coefficient. However, using a poorly selected initial guess significantly increased the simulation processing time; therefore the convection coefficient for

subsequent runs was calculated using the solutions from sections 4.5.4.a.i, 4.5.4.a.ii, and 4.5.4.a.iv.

Table 4.2. Convection coefficients from the finite differences approximation solution for copper rod run 1.

Source of initial guess	Initial guess, h_o (W/m^2K)	h for $\Delta r=0.1$ (W/m^2K)	h for $\Delta r=0.01$ (W/m^2K)	h for $\Delta r=0.001$ (W/m^2K)	h_{avg} (W/m^2K)
	1	369	368	367	368±1.1
Molerus correlation[17]	198	369	368	367	368±1.1
Section 4.3.1.b	389	369	368	367	368±1.1
Section 4.3.1.d	398	369	368	367	368±1.1
Martin correlation[14, 15]	436	369	368	367	368±1.1
Zabrodsky correlation[19]	481	369	368	367	368±1.1
	1000	369	368	367	368±1.1

The average convection coefficients from three runs using the copper and steel thermocouple rods were determined to be 366±8.6 W/m^2K and 375±6.7 W/m^2K, respectively. There was a 2.3% difference in these values.

4.5.4.a.vi. Comparison of results

The convection coefficients of the sand bath calculated by the different approaches are summarized in Table 4.3. With the exception of the Molerus correlation[17], the convection coefficients have a relatively narrow range of 347 W/m^2K to 481 W/m^2K, giving us confidence that the true convection coefficient of the sand bath is within this range. It can also be seen in Table 4.3 that the convection coefficients calculated using data from the copper thermocouple rod agree with the convection coefficients calculated using the steel thermocouple rod. This is expected because the

convection coefficient represents heat transfer from the sand bath and should only be influenced by the rod geometry and bed conditions. It can also be seen that the standard deviations associated with the copper thermocouple rod are consistently larger than those associated with the steel thermocouple rod. This may reflect construction issues or a malfunction of the copper thermocouple rod.

Table 4.3. Convection coefficient of the sand bath as determined by the methods outlined in sections 4.3.1, 4.3.2.b, 4.3.2.c, 4.3.2.d, and 4.3.2.e.

Approach	Convection coefficient (h, W/m^2K) For Copper Thermocouple Rod	For Steel Thermocouple Rod
Martin correlation[14, 15]	436	
Molerus correlation[17]	198	
Zabrodsky correlation[19]	481	
Lumped capacitance (4.3.2.b)	381±18	365±4
Instantaneous lumped capacitance (4.3.2.c)	347 to 430	355 to 406
Analytical (4.3.2.d)	379±14	392±4.9
Finite elements (4.3.2.e)	366±8.6	375±6.7

4.5.4.b. Steam chamber convection coefficient

4.5.4.b.i. Calculated by correlation

Equation (19) depends upon on the properties of steam and thus on the steam temperature, which is increasing as the rod is heated. Consequently, the convection coefficient for the steam chamber as estimated by equation (19) is plotted as a function of time in Figure 4.13. The properties of the vapor and the enthalpy of vaporization were evaluated at the steam temperature, and the properties of the saturated liquid were evaluated at the film temperature, which was assumed to be the average of the steam and

surface temperatures. The convection coefficients estimated in this manner had a large range: 10,428 W/m^{2}K to 26,576 W/m^{2}K. The correlation predicted an increase in the convection coefficient with increasing time due to the increase in the enthalpy of vaporization with increasing steam temperature and a decrease in the difference between the steam chamber temperature and thermocouple rod temperature.

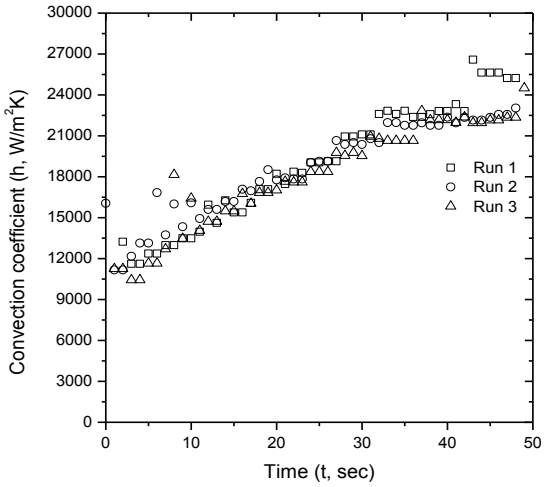

Figure 4.13. Convection coefficient of steam chamber predicted with equation (19) as a function of time.

4.5.4.b.ii. Calculated by lumped capacitance

The first attempt to estimate the convection coefficient used the lumped capacitance approach described in section 4.3.2.b. For this approach, the Biot number should be less than 0.1, and surrounding temperature should be constant. Since the steam chamber temperature was not constant, the lumped capacitance method could not be accurately applied, but the result provides an initial guess for the numerical methods approach described in section 4.5.4.b.v. Using the steady state steam chamber temperature, 180^{o}C, the convection coefficient was calculated to be 1508$\pm$288 W/m^{2}K, and the corresponding Biot number was determined to be 0.71. This large Biot number

indicated there is a radial temperature gradient within the thermocouple rod therefore the lumped capacitance approach is invalid.

4.5.4.b.iii. Instantaneous lumped capacitance convection coefficient

The instantaneous convection coefficient for the steel thermocouple rod in the steam chamber was calculated using the approach described in section 4.3.2.c. The temperature profiles of the steel thermocouple and steam chamber were fit using equation (51). The instantaneous steam chamber convection coefficients plotted in Figure 4.14 ranged from 137 to 83, 908 W/m^2K. A negative convection coefficient was calculated during run 1 due to preheating, which resulted in the thermocouple rod temperature being slightly higher than that of the steam chamber at the start of the run. As in the sand bath, as time increased, the rate of change in thermocouple rod temperature with respect to time and the difference in the temperature of the rod and the temperature of the steam chamber decreased. However, in the steam chamber, the decrease in the temperature-time differential was greater, resulting in a decreasing convection coefficient with increasing time.

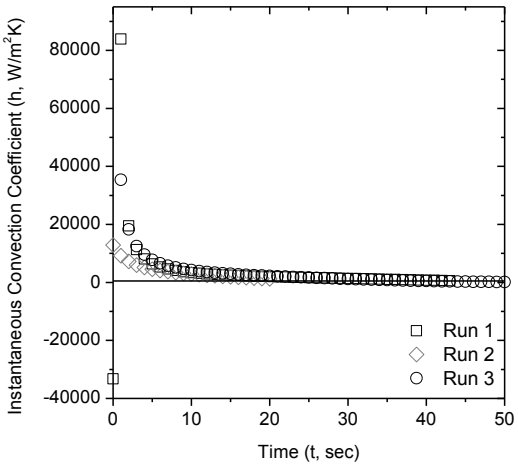

Figure 4.14. Instantaneous convection coefficient as a function of time for the steel thermocouple rod in the steam chamber.

4.5.4.b.iv. Analytical solution

As an approximation, the convection coefficient of the steam chamber was calculated using the analytical solution outlined in section 4.3.2.d. Because this approach required the assumption of a constant steam chamber temperature, as for 4.5.4.b.ii, the temperature was assumed to be constant at 180^{o}C. The iterative method described in section 4.5.4.a.iv was used to reach agreement between equations (44), (45), and (47). The average convection coefficient was found to be 2097$\pm$583 W/m^{2}K.

4.5.4.b.v. Finite elements approach

In order to apply the approach described in section 4.3.2.e equation (51) was used to model the steam chamber temperature's change with time in terms of the dimensionless variables in equations (27) and (25). The sum of the squares of the residuals is shown to be an asymptotic function of the convection coefficient in Figure 4.15. Thus, no convection coefficient can be found to minimize the difference between

the predicted and experimental centerline temperature profile. To address this, the approach in 3.2.5 was modified to determine a convection coefficient using Matlab's *fzero* function that would match the predicted time to reach 178°C, $t_{pred,178}$, with the experimental time, $t_{exp,178}$. Plotting the difference in $t_{pred,178}$ and $t_{exp,178}$ as a function of convection coefficient in Figure 4.16 shows there were two possible roots for run 1, and the experimental and predicted temperature profiles for each root are plotted in Figure 4.17. Neither root adequately described the experimental profile therefore the finite differences method provides no estimates of the steam chamber convection coefficient.

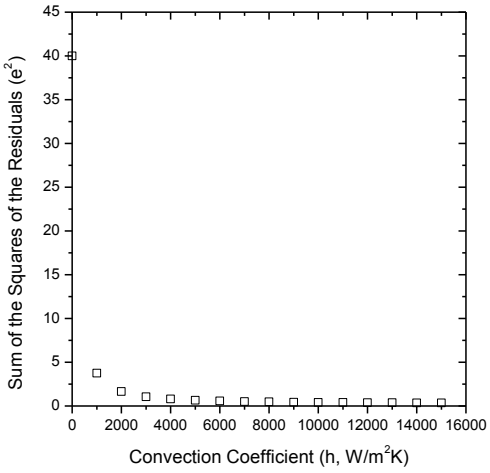

Figure 4.15. Plot of the sum of the square of the residuals for the differences between the calculated and experimental centerline thermocouple temperatures as a function of steam chamber convection coefficient for an assumed convection coefficient for the steam chamber.

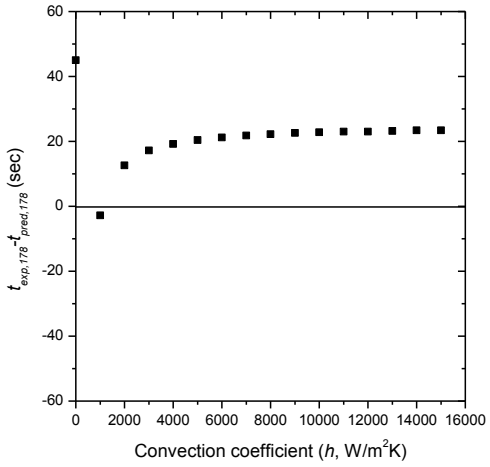

Figure 4.16. Plot of the difference in predicted, $t_{pred,\ 178}$, and experimental, $t_{exp,178}$, times to reach 178^{o}C as a function of steam chamber convection coefficient for an assumed convection coefficient for the steam chamber.

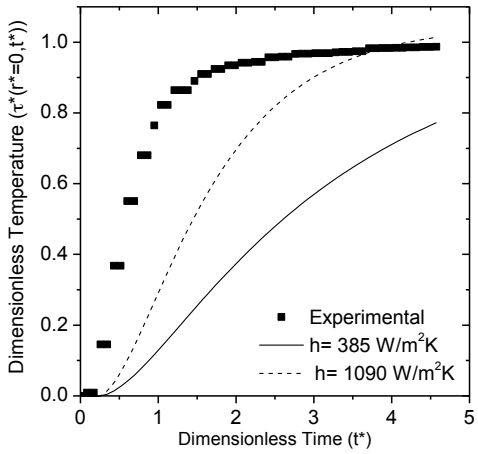

Figure 4.17. Comparison of dimensionless experimental centerline temperature of steel thermocouple rod in the steam chamber to those predicted for convection coefficients of 385 W/m^{2}K and 1090 W/m^{2}K as a function of dimensionless time.

4.5.4.b.vi. Comparison of results

The summary in Table 4.4 of the steam chamber convection coefficients calculated above shows significant variation in the results. However, the convection coefficients calculated using lumped capacitance and analytical solution are in agreement, although both approaches rely upon the erroneous assumption of a constant

steam chamber temperature. Furthermore, the range of convection coefficients calculated using the instantaneous lumped capacitance approach spanned the values calculated by the alternate approaches. The results could be improved if the design of the steam chamber were modified so that the chamber could reach a steady state temperature prior to the heating of the steel thermocouple rod. This would create a steady state boundary condition and simplify the initial value problem of equations (36) to (39) to that of equations (29) to (32).

Table 4.4. Convection coefficients of the steam chamber as determined by the methods outlined in sections 4.3.1, 4.3.2.b, 4.3.2.c, and 4.3.2.d.

Approach	Convection coefficient (h, W/m^2K) For Steel Thermocouple Rod
Incropera and DeWitt correlation	10,428 to 16,148
Lumped capacitance (4.3.2.b)	1,508±288
Instantaneous lumped capacitance (4.3.2.c)	137 to 83,771
Analytical (4.3.2.d)	2,097±583
Finite elements (4.3.2.e)	n/a

4.5.4.c. Comparison of the convection coefficients of the sand bath and steam chamber

Both the sand bath and steam chamber use a fluid to transfer heat from resistance heaters to thermocouple rods or pretreatment reactors; the convection coefficient of each system reflects the efficiency of this transfer. The convection coefficient of the sand bath was determined to be between 365 W/m^2K to 436 W/m^2K. The convection coefficient of the steam chamber was more difficult to determine and values ranged from 137 to

83, 908 W/m^{2}K. However, with the exception of the instantaneous lumped capacitance method, the convection coefficient of the steam chamber was at least one order of magnitude greater than that of the sand bath. Inspection of the Martin correlation, equations (1) to (6), and equations (19) and (20) reveals that the sand bath convection coefficient increase with the heat capacity and thermal conductivity of the transfer fluids. From Table 4.5 it is clear that the thermal conductivity and heat capacity of saturated liquid water in the steam chamber is 2.5 to 17.7 times higher than that of air and sand. Additionally, the steam chamber convection coefficient depends on the enthalpy of vaporization of water, which is, of course very high. Thus the high thermal conductivity, heat capacity and enthalpy of vaporization of steam all contribute to the high steam chamber convection coefficient.

Table 4.5. Comparison of thermal conductivities and heat capacities of sand, air, and saturated water at 180^{o}C.

Material	Thermal conductivity (k, W/m^2/K)	Heat capacity (C_p, kJ/kg/K)
Sand	0.27	0.80
Air, P_{atm}, 180^{o}C	0.038	1.02
Water, saturated liquid, 180^{o}C	0.67	4.39

4.6. Conclusions

Differences between two heating systems, a fluidized sand bath and a steam chamber, were investigated as part of the Wyman lab's pretreatment research. It was found that the type of heating device used during pretreatment did not influence the glucan and xylan yields from the pretreatment and enzymatic hydrolysis of *Populus trichocarpa*. However, there were significant differences in the heating performances of

the two systems. The steam chamber heated pretreatment tube reactors to 178^{o}C in approximately a tenth of the time it took the sand bath. This reduced heating time is a reflection of the improved heat transfer from the heat transfer medium to the reactors. The temperature of the pretreatment reactors in the steam chamber was also more stable than the temperature of the pretreatment reactors in the sand bath, likely due to better temperature control and a more even medium temperature. The run to run consistency in the reactor temperature in the steam chamber was also better than that of the sand bath. More consistent sand bath performance might be possible by more precisely controlling bed conditions, such as mass of sand and air flow rate.

The convection coefficient of each device was determined from data collected using custom-designed thermocouple rods. Analysis of the data by multiple approaches indicated that the convection coefficient of the steam chamber was one to two orders of magnitude greater than that of the sand bath.

Overall, because the heat transfer performance of the steam chamber was superior to that of the sand bath in all aspects, a steam chamber should be utilized for experiments with critical heat transfer requirements. However, yield data from pretreatment and enzymatic hydrolysis was comparable for both the sand bath and steam chamber, indicating that the reaction kinetics were quite forgiving for the reaction times applied in pretreatment. Thus, sand baths still provide a viable heat source for pretreatment studies, at least for the longer times reported here.

4.7. Nomenclature

a	Fitting parameter, equation (51)
Ar	Archimedes number, equation (3)

A_s	Surface area (m^2)
b	Fitting parameter, equation (51)
Bi	Biot number, equation (42)
c	Fitting parameter, equation (51)
c_p	Heat capacity (J/kgK)
C	Empirical constant, 2.6
d	Diameter (m)
Fo	Fourier number, equation (27)
g	Acceleration due to gravity, 9.81 m/s^2
h	Convection coefficient (W/m^2K)
h_{fg}	Enthalpy of vaporization (J/kg)
J_0	Zero order Bessel function of the first kind
J_1	First order Bessel function of the first kind
k	Thermal conductivity (W/mK)
K	Coefficient
Kn	Knudsen number, equation (10)
l'	Molerus correlation parameter, equation (13)
L	Total length of rod (m)
M	Molar mass (kg/kmol)
N	Non-dimensional contact time
Nu	Nusselt number
p	Pressure (Pa)
Pr	Prandtl number, equation (4)
r	Radius (m)
R	Universal gas constant, 8314 J/kmolK
$\dot{q}$	Heat generation (W/m^3)
t	Time (s)
T	Temperature of the rod unless otherwise indicated (^oC)
u	Superficial bed velocity (m/s)
V	Volume (m^3)
x	Vertical axis
z	Characteristic group, equation (6)

Greek

α	Thermal diffusivity, $k/\rho c_p$ (m^2/s)
β_{1-4}	Molerus correlation parameters, equations (14) to (17)
ε	Bed voidage
γ	Accommodation coefficient of gas, by equation (11)
μ	Viscosity (Pa*s)
θ	Temperature difference, by equation (26)
ρ	Density (kg/m^3)
τ	Temperature difference, equation (34)

ϑ	Angular axis
ξ	Eigenvalue, equation (45)

Subscripts

fg	Of vaporization
g	Gas
i	Initial conditions at t=0
l	Liquid
mf	At minimum fluidization
n	n^{th} solution
o	Outer radius of rod
p	Particle
r	Radiative
rod	Of the rod
sat	Saturated conditions
ss	Steady state
surf	At the surface of the rod
SB	For the sand bath
SC	For the steam chamber
v	vapor
wp	Single particle to surface
∞	Of the surroundings

Superscripts

#	Film temperature, $0.5(T_{surf} + T_{\infty})$
*	Dimensionless

4.8. References

(1) Mosier N, Wyman CE, Dale B, Elander R, Lee YY, Holtzapple M, Ladisch M. Features of promising technologies for pretreatment of lignocellulosic biomass. *Bioresour. Technol.* **2005**; *96*: 673-686.

(2) Allen SG, Schulman D, Lichwa J, Antal MJ Jr., Jennings E, Elander R. A comparison of aqueous and dilute acid single temperature pretreatment of yellow poplar sawdust. *Ind. Eng. Chem. Res.* **2001**; *40*: 2352-2361.

(3) Heitz M, Capek-Menard E, Koerberle PG, Gagne J, Chornet E, Overend RP, Taylor JD, Yu E. Fractionation of *Populus tremuloides* at the pilot plant scale: Optimization of steam pretreatment conditions using the STAKE II technology. *Bioresour. Technol.* **1991,** *35*, 23-32.

(4) Negro MJ, Manzanares SP, Ballesteros I, Oliva JM, Cabanas A, Ballesteros M. Hydrothermal pretreatment conditions to enhance ethanol production from poplar biomass. *Appl. Biochem. Biotechnol.* **2003**; *105*: 87-100.

(5) Tucker MP, Farmer JD, Keller FA, School DJ, Nguyen QA. Comparison of yellow poplar pretreatment between NREL digester and Sunds hydrolyzer. *Appl. Biochem. Biotechnol.* **1998**; *70-72*: 25-35.

(6) Bobleter O. Hydrothermal degradation of polymers derived from plants. *Prog. Polym. Sci.* **1994**; *19*: 797-841.

(7) Kim Y, Mosier NS, Ladisch MR. Enzymatic digestion of liquid hot water pretreated hybrid poplar. *Biotechnol. Prog.* **2009**; *25*: 340-348.

(8) Bonn G, Concin R, Bobleter O. Hydrothermolysis- A new process for the utilization of biomass. *Wood Sci. Technol.* **1983**; *17*: 195-202.

(9) Lloyd T, Wyman CE. Combined sugar yields for dilute sulfuric acid pretreatment of corn stover followed by enzymatic hydrolysis of the remaining solids. *Bioresour. Technol.* **2005**, *96*, 1967-1977.

(10) Grous WR, Converse AO, Grethlein HE. Effect of steam explosion pretreatment on pore size and enzymatic hydrolysis of poplar. *Enzyme Microb. Technol.* **1986**; *8*: 274-280.

(11) Brownell HH, Saddler JN. Steam pretreatment of lignocellulosic material for enhanced enzymatic hydrolysis. *Biotechnol. Bioeng.* **1987**; *25*: 228-235.

(12) Studer MH, DeMartini JD, Brethauer S, McKenzie HL, Wyman CE. Engineering of a high-throughput screening system to identify cellulosic biomass, pretreatments, and enzyme formulations that enhance sugar release. *Biotechnol. Bioeng.* **2010**; *105*: 231-238.

(13) Incropera FP, DeWitt DP. *Introduction to heat transfer*, 4th ed.; John Wiley and Sons: New York, 2002.

(14) Martin H. Heat transfer between gas fluidized beds of solid particles and the surfaces of immersed heat exchanger elements, Part I. *Chem. Eng. Proces.* **1984**; *18*: 157-169.

(15) Martin H. Heat transfer between gas fluidized beds of solid particles and the surfaces of immersed heat exchanger elements, Part II. *Chem. Eng. Proces.* **1984**; *18*: 199-223.

(16) Ackeskog HBR, Almstedt AE, Zakkay V. An investigation of fluidized bed scaling: Heat transfer measurements in a pressurized fluidized-bed combustor and a cold model bed. *Chem. Eng. Sci.* **1993**; *48*: 1459-1473.

(17) Molerus O, Burschka A, Dietz S. Particle migration at solid surfaces and heat transfer in bubbling fluidized beds- II. Prediction of heat transfer in bubbling fluidized beds. *Chem. Eng. Sci.* **1995**; *50*: 879-885.

(18) Pisters K, Prakash A. Investigations of axial and radial variations of heat transfer coefficient in bubbling fluidized bed with fast response probe. *Powder Technol*. **2011**; *207*: 224-231.

(19) Zabrodsky SS. *Hydrodynamics and heat transfer in fluidized beds*. M.I.T. Press: Cambridge, MT, 1966.

(20) MatLab, ver. 7.11.0.584; MathWorks: MA, 2010.

(21) Sluiter A, Hames B, Ruiz R, Scarlata C, Sluiter J, Templeton D. *Determination of sugars, byproducts, and degradation products in liquid fraction process samples laboratory analytical procedure;* NREL/TP-510-42623. National Renewable Energy Laboratory: Golden, CO, 2006;14 p.

(22) Sluiter A, Hames B, Ruiz R, Scarlata C, Sluiter J, Templeton D, Crocker D. *Determination of structural carbohydrates and lignin in biomass laboratory analytical procedure*; NREL/TP-510-42618; National Renewable Energy Laboratory; Golden CO, 2011; 18 p.

(23) Saeman JF. Kinetics of wood saccharification: Hydrolysis of cellulose and decomposition of sugars in dilute acid at high temperature. *Ind. Eng. Chem*. **1945**; *37*(1): 43-52.

(24) Lloyd TA, Wyman CE. Combined sugar yields for dilute sulfuric acid pretreatment of corn stover followed by enzymatic hydrolysis of the remaining solids. *Bioresour. Technol*. **2005**; *96*(18): 1967-1977.

(25) Geankoplis CJ. *Transport processes and separation process principles,* 4th ed.; Prentice Hall PTR: Upper Saddle River, NJ, 2003.

Chapter 5.

Data development and modeling to define operating strategies and baseline performance for the study of biomass deconstruction during hydrothermal pretreatment.

5.1. Abstract

Flowthrough pretreatment offers a number of advantages over traditional batch pretreatment systems including: the monitoring of the evolution of pretreatment products as a function of time, the limitation of side and degradation reactions, and the removal of pretreatment products prior to reaction quenching thus avoiding precipitation of products. In subsequent chapters, flowthrough pretreatment will be used to study xylan and lignin removal from biomass during pretreatment therefore it was necessary to first determine operating conditions. The temperatures 140 and 180^{o}C were selected as key temperatures of interest. The reactor outlet pressure was equal to saturation pressure thus ensuring that the reactor pressure was above the saturation pressure. It was determined that the flow rate could be reduced to 20 mL/min without introducing mass transfer limitations. Triplicate runs of flowthrough and batch pretreatments were performed at 140^{o}C and 180^{o}C. It was found that the standard deviations for glucan, xylan yields and lignin removal were less than 5% therefore the procedures are readily reproducible. This chapter serves as a baseline for subsequent chapters.

5.2. Introduction

One of the challenges when using batch reactors for hydrothermal pretreatment is tracking product evolution as a function of time. Side and degradation reactions that generate products such as furfural, humins, and pseudo-lignin become significant for extended batch pretreatment times[1, 2] The quenching of batch reactors to stop a reaction potentially creates artifacts. For example, oligomers that are soluble at reaction temperatures are insoluble at lower temperatures and precipitate.[3] This artificially skews removal calculations. A fixed bed flowthrough reactor offers the opportunity to avoid these problems. In this system, solubilized products are removed from the reactor quickly therefore hydrolysis products can be tracked as a function of time and the potential for side and degradation reactions is limited. Additionally, the evolution of hydrolysis products reflects the relative recalcitrance of the biomass fraction. Finally, few solubilized products are present in the reactor during the reaction quench thereby lowering the possibility of precipitates.

Bobleter et al.[4] pioneered the use of flowthrough reactors. Flowthrough pretreatment has been shown produce highly digestible cellulose, increase hemicellulose recovery and lignin removal. Liu and Wyman[5] found that flowthrough pretreatment removed more hemicellulose and lignin from corn stover than batch pretreatment. A later study by Yang and Wyman[6] found that flowthrough pretreated corn stover was also more digestible than the batch pretreated material. Allen et al.[7], Bobleter et al.[4], Mok and Antal[8], Liu and Wyman[9], Torget et al. [10], and van Walsum et al.[11] made similar observations.

In subsequent chapters, the flowthrough reactor system will be applied to understand the interaction of the cellulose, hemicellulose, and lignin during pretreatment. These studies require careful selection of the operating temperature, pressure, time, and flow rate. The interplay of these variables will be investigated in this chapter in order to identify experimental conditions for subsequent studies. Table 5.1 summarizes the biomass and operating conditions used in previous studies.

5.2.1. Temperature considerations

Zhang et al.[12] found that xylan and lignin removal from *Miscanthus sinensis /Miscanthus sacchariflorus IV* exceeded 90 wt% and 70 wt% respectively after 10 minutes of pretreatment at 200^{o}C and higher while approximately 80 wt% and 60 wt% of the xylan and lignin were removed after 10 minutes of pretreatment at 180^{o}C. The rapid release of xylan and lignin at temperatures greater than 180^{o}C results in a narrow window of opportunity for observation. Additionally, lowering the pretreatment temperature reduces heat and pressure requirements, which is important to minimizing capital and operating costs at the commercial scale. With these issues in mind, it was decided that the maximum flowthrough pretreatment temperature would be 180^{o}C.

It has been proposed that lignin may melt, coalesce, and migrate through the cell walls during pretreatment at temperatures above the glass transition temperature[13]. In order to examine the influence of such a phase change, the effects of pretreatment near the glass transition temperature will be studied in chapter 7. For now, it is sufficient to identify the range of potential glass transition temperatures. The glass transition of water-saturated lignin was found to fall between 80 and 100^{o}C.[14] Dynamic mechanical

Table 5.1. Summary of operating conditions reported in the literature for flowthrough pretreatment. *Biomass had a moisture content of 8-50%. **Not reported if the loaded biomass was oven dried or not.

Source	Biomass			Operating Conditions				
	Type	m_{sub} (g)	d_{part} (mm)	T_{op} (^oC)	P_{op} (MPa)	Q (mL/min)	C_{acid} (wt%)	t_{rxn} (min)
Allen et al.[7]	Sugar cane bagasse and leaves	15-25*		190-230	5.00	400-500	0	4
Bobleter et al.[4]	Filter paper and natural straw	0.15**		203-275	P_{max}=8.59	0.91-1.23	0	22-45
Kim and Lee[15]	Corn stover	10	9-35 mesh	170-220	2.50	1.0-7.5	0	10-75
Kumar et al.[16]	Switchgrass and corn stover	11	20/60 mesh	150-190		2.5	0	50
Mok and Antal[8]	6 woody, 4 herbaceous	0.3**	1	200-230	34.5	1.00	0	0-15
Torget et al.[10]	*Liriodendron tulipifera L.*	114.7	4	150-204	0.547-1.83	70.5-141	0.0735-0.735	10-20
van Walsum et al.[11]	Aspen and bagasse	10-15	3	220	5.00	500	0	2
Yang and Wyman[6]	Corn stover	2		180-215	2.50-2.85	2-25	0-0.1	0-300
Yu et al.[17]	Sweet sorghum bagasse	20	18-40 mesh	180-200		15-30	0	6-14
Zhang et al.[12]	*Miscanthus sp.*	1	0.25-0.85	160-220	0.689-2.34	25	0	3-70

thermal analysis has shown the glass transition temperature of lignin in hardwoods to range between 65 to 85°C and in softwoods from 90 to 105°C.[18] Irvine predicted the glass transition to occur over the temperature interval 100 to 170°C.[19] The glass transition temperature of isolated lignin was reported to be 110 to 174°C[18] depending on experimental procedure while another found that the glass transition temperature of isolated lignin ranged from 127°C to 193°C[20] depending on biomass source and method of isolation. Shao et al.[21] reported the glass transition temperatures of lignin in raw and steam exploded bamboo meal as 162°C and 136°C. Computer simulations of lignin polymers in aqueous solution suggest that lignin transitions from a compact conformation to an extended conformation between 147°C and 207°C[22]. Fang et al.[23] observed the reaction chemistry and phase behavior of organosolv lignin in a diamond anvil cell as it was heated; melting began at 174°C. In summary, observed glass transition temperatures range from 80°C to 193°C and this range reflects differences in biomass, sample moisture content[18], isolation procedures[18], and analytical techniques[18, 19]. Given this vast range of temperatures, a trial and error approach beginning at 100°C will be used to find a comparatively low pretreatment temperature where moderate lignin and xylan removal are achieved. The severity parameter will be used to guide the selection of temperature-time combinations for testing. The parameter is defined as[24, 25]:

$$log(R_o) = t_{rxn} exp\left(\frac{T_{rxn} - 100}{14.75}\right) \quad (1)$$

5.2.2. Pressure considerations

Torget et al.[10] used operating pressures 69.0 to 138 kPa above the saturation pressure associated with the reaction temperature in order to maintain water in the liquid

phase within the reactor. This was unnecessary for this reactor system as the pressure is set at the outlet of the system thus the back pressure regulator is the lowest pressure in the system upstream of the sampling point. The pressure in the reactor must be greater than the pressure at the valve therefore if the pressure at the valve is at saturation pressure the water within the reactor must be a compressed liquid.

5.2.3. Flow rate considerations

Liu and Wyman[5] found that increasing the flow rate from 1 mL/min to 10 mL/min enhanced the removal of total mass, xylan, and lignin, and also increased the yield of xylooligomers. Their initial testing found there was little difference in results at flow rates above 10 mL/min[5]. The use of high flow rates reduces the possibility of mass transfer limitations but high flow rates also reduce product concentrations making detection and measurement difficult. Zhang et al.[12] used a flow rate of 25 mL/min in order to avoid mass transfer limitations. A simple model is used to predict if this flow rate can be reduced to improve product detection without introducing mass transfer limitations. The pretreatment reactor containing *Populus trichocarpa* is modeled as a bed of xylose spheres with constant diameter. Figure 5.1 is a schematic of the model with definitions of the variables.

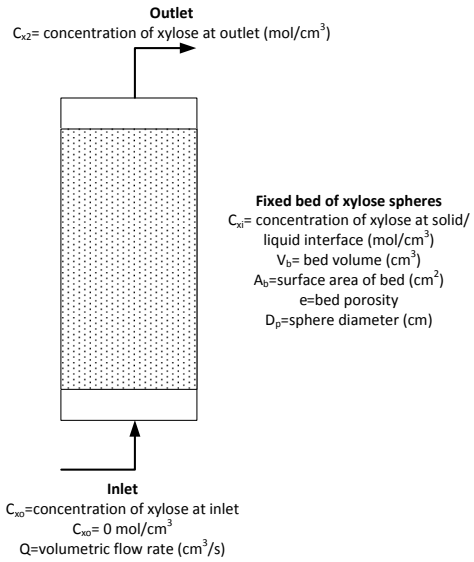

Figure 5.1. Diagram of mass transfer model of flowthrough pretreatment and definition of variables. The biomass within the pretreatment reactor is modeled as xylose spheres with constant diameter.

For such a system, the outlet concentration of the solute, xylose, is defined by[26]:

$$C_{x2} = C_{xi}\left[1 - exp\left(-\frac{A_b k_c}{Q}\right)\right] \tag{2}$$

Where the surface area and mass transfer coefficient are defined as[26]:

$$A_b = \frac{6(1-\varepsilon)}{D_p} V_b \tag{3}$$

$$k_c = \frac{1.1068 v'}{\varepsilon} Re^{-0.72} Sc^{-2/3} = \frac{1.1068 v'}{\varepsilon}\left(\frac{\rho_w D_p v'}{\mu_w}\right)^{-0.72}\left(\frac{\mu_w D_{AB}}{\rho_w}\right)^{-2/3} \tag{4}$$

The model can be applied at any operating temperature using the relevant density and viscosity of water. The diameter of the xylose spheres is equal to the largest diameter of the biomass particles, 0.85 mm. The bed porosity, ε, is assumed equal to the porosity determined by Torget and coworkers[10], 0.762. The equilibrium concentration of xylose in water at the operating temperature is used as the xylose concentration at the solid

liquid interface and was estimated using the equilibrium xylose concentration at 25°C[27] and the equation of solubility for an ideal solution[28]:

$$ln(x_x\gamma_x) = -\frac{\Delta H_x^{fus}}{RT_{mx}}\left(\frac{T_{mx}}{T} - 1\right) \quad (5)$$

The diffusivity at the desired temperature, D_{AB}, was determined from the diffusivity at 25°C reported by Sjöman et al.[29] and the Wilke-Chang correlation[26]:

$$D_{AB} = 1.173 * 10^{-16}(\phi M_B)^{1/2}\frac{T}{\mu_B V_A^{0.6}} \quad (6)$$

5.3. Experimental apparatus and procedures

5.3.1. Experimental apparatus

The biomass, *Populus trichocarpa*, used in chapter 4 was also used for this study. The material was bark-free, milled to a particle diameter of 0.18 mm to 0.85 mm, and had a moisture content of approximately 5 wt%.

A schematic of the flowthrough reactor system is shown in Figure 5.2. A 2 L feed tank is used to hold the desired pretreatment solvent, water. A positive displacement pump (Prep100, LabAlliance, State College, PA) delivers water to the reactor and the pressure of the system is set using the backpressure regulator (GO, Spartanburg, SC). The system pressure is monitored by pressure gauges P1 (US Gauge, max P 20.6 MPag), P2, and P3 (Ashcroft, max P 4.2 MPag). The heating coil and reactor are heated using a fluidized sand bath (SBL-2D, Techne, Princeton, NJ). The heating coil is a 2.6 m length of 3.18 mm stainless steel tubing and the coil diameter is 50.9 mm. The reactor is constructed of 12.7 mm stainless steel tube. Swagelok fittings (SS-8-VCR-1, SS-8-VCR-3-8TA, SS-8VCR-6-810, SS-200-R-8, Swagelok, San Diego, CA) are added to this tube

so that the reactor can be connected to the inlet and outlet piping. The total reactor length is 152 mm. The biomass is held in the reactor by 5 micron gaskets (SS-8-VCR-2-5M, Swagelok, San Diego, CA). The system temperature is monitored with K-type thermocouple T1 at the reactor outlet and recorded as a function of time using a Digi-Sense DualLogR Thermocouple Meter (15-176-96, Fisher Scientific, Pittsburgh, PA). Data is transferred from the meter to a computer using an infrared adapter (EW-91100-85, Cole Parmer**,** Vernon Hills, IL). The cooling coil, a 5.3 m length of 3.18 mm stainless steel tubing with a coil diameter of 44.5 mm is submerged in a 19 L water bath so that the hydrolysate is cooled prior to sampling.

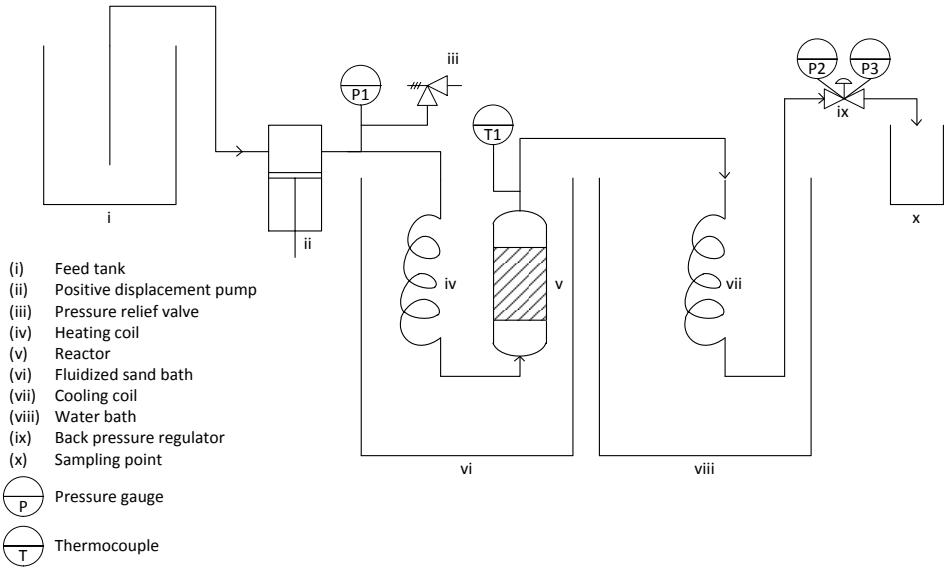

Figure 5.2. Schematic of flowthrough system.

The 10 mL tube reactors described in chapter 4 are also used. One of the batch reactors contains a thermocouple (.062-K-U-4"-T3-10 ft TF/TF-MP, Wilcon Industries, Lake Elsinore, CA) inserted along the centerline for monitoring batch reactor temperature.

5.3.2. Experimental procedure

5.3.2.a. Pretreatment

A representative flowthrough pretreatment is described. The pump was primed and the sand bath was heated to 190^{o}C. The reactor was loaded with 1.0 g dry biomas and attached the piping system. The pump was started at a flow rate of 25 mL/min and the back pressure gauge was adjusted to 1.1 MPag. The system was pressurized at room temperature and all connections were then inspected for leaks. Once the system was leak free, the reactor and heating coil were lowered into the sand bath and the cooling coil was lowered into the water bath. The hydrolysate produced as the reactor was heated was collected in a pre-massed flask. The time to reach 178^{o}C (T_{rxn}-2^{o}C) was recorded and was taken as the start of the reaction. Samples were collected in five minute intervals using premassed flasks. The mass and pH of the samples was recorded. After 30 minutes, the reactor and heating coil were submerged in the water bath and the pump was stopped once the system reached 70^{o}C. The residual solids in the reactor were collected by filtration, washed, and dried. The operating conditions for the other runs are summarized in Table 5.2.

A representative batch pretreatment run is described. Two tube reactors, each loaded with 8.34 mL of *Populus trichocarpa*-deionized water slurry containing 5 wt% dry solids, were used for each pretreatment condition. Once the reactor was loaded, it was sealed, shaken, and left overnight. The thermocouple reactor was loaded with 8.34 mL deionized water. The sand bath was heated to 182^{o}C. The Digi-Sense DualLogR Thermocouple Meter was set to record the temperature every five seconds and started. A

wire basket containing two tube reactors and the thermocouple reactor was lowered into the sand bath; the time it took the reactors to reach 178°C was recorded; this was taken as the start of the reaction and the sand bath temperature was reset to 180°C. The reaction was allowed to proceed for 12 minutes before cooling the reactors to 70°C in a water bath. The thermocouple meter was stopped and the data was transferred to a computer. This procedure was repeated for the other runs described in Table 5.2. Following pretreatment, the contents of the two reactors were combined and filtered using a pre-weighed crucible. The filtrate was retained for analysis. The pretreated solids were washed with three volumes of 100 mL of deionized water before being dried for 24 hours in a 45°C oven. The dried crucible and solids were massed prior to compositional analysis.

Table 5.2. Summary of pretreatment conditions.

Run	Set Pressure (MPag)	Reactor Temperature (°C)	Sand Bath Temperature (°C)	Time (min)	Flow rate (mL/min)	Number of runs
1	0	100	106	120	25	1
2	0.17	130	139	120	25	1
3	0.17	130	139	320	25	1
4	0.28	140	149	60	25	1
5	0.28	140	149	160	25	1
6	0.28	140	149	160	20	1
7-9	0.28	140	149	192	20	3
10-12	n/a	140	142	192	0/batch	3
13	1.10	180	194	30	25	1
14	1.10	180	194	10	25	1
15-17	1.10	180	194	10	20	3
18	1.10	180	194	10	15	1
19	1.10	180	194	12	20	1
20-22	n/a	180	182/180	12	0/batch	3

5.3.2.b. Analytical techniques

By converting oligomers to monomers using Sluiter et al.'s[30] strong acid hydrolysis procedure the total sugar content of the pretreatment hydrolysate was determined. The monomers were detected by HPLC under the conditions described below. The glucose, xylose, and Klason lignin content of the pretreated biomass solids were measured using the procedure described by Sluiter et al.[31] However, no extraction was performed prior to the two-step acid hydrolysis because of the low extractives content of *P. trichocarpa*. A 2 mL liquid sample was withdrawn after hydrolysis and centrifuged to ensure no solids were injected into the HPLC at the conditions described below. The sample was not neutralized prior to injection on the HPLC. Glucose and xylose concentrations were converted to glucan and xylan equivalents by dividing by 1.1111 and 1.3622, respectively, to account for the mass gain during hydrolysis.

Sugars were detected by HPLC using an Aminex HPX-87H column (BioRad, Hercules, CA) heated to 65^{o}C with a separation module (Alliance 2695, Waters, Milford, MA) equipped with a refractive index detector (2414, Waters, Milford, MA). The eluent was 0.005 M sulfuric acid in the isocratic mode.

5.4. Results and discussion

The glucan yield is the glucan equivalent of the glucose and glucooligomers detected in the liquid hydrolysate as a percentage of the glucan initially available in the raw *Populus trichocarpa*. The xylan yield is similarly defined. Lignin removal is the difference between the lignin initially available in the raw biomass and the lignin in the residual solids as a percentage of the lignin initially available in the raw biomass.

5.4.1. Temperature considerations

Figure 5.3a shows the glucan and xylan yields and lignin removal after the pretreatment of *Populus trichocarpa* at 180°C at 25 mL/min for 30 minutes. Very little glucan was removed by pretreatment but 87% and 71% of the total xylan and lignin, removed, respectively, was removed within the first 10 minutes of pretreatment. In order, to develop more detailed time course data the pretreatment time and sampling interval were shortened to ten and two minutes, respectively. The results are plotted in Figure 5.3b.

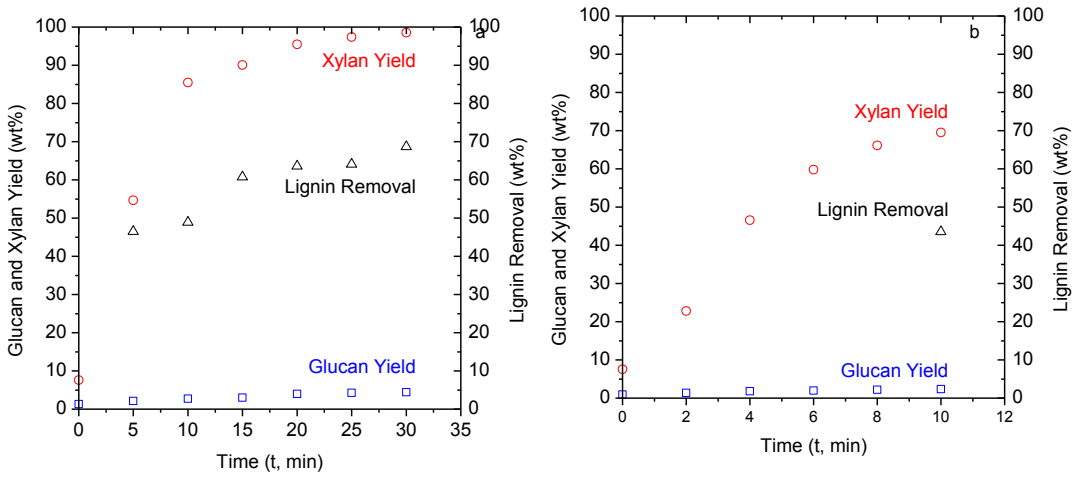

Figure 5.3. Glucan (blue) and xylan (red) yields and lignin removal (black) from the pretreatment of *Populus trichocarpa* at 180°C for 30 minutes (a) and 10 minutes (b) with a flow rate of 25 mL/min.

In order to test the influence of the glass transition temperature, pretreatment was also conducted at low temperatures. The first low temperature run was conducted at 100°C for 120 minutes. The total solubilization of *Populus trichocarpa* was 3.3% therefore the pretreatment temperature was increased to 130°C and 140°C. The pretreatment times at these temperatures, 320 and 160 minutes, respectively, were

selected to match the severity of 10 minutes at 180°C (Equation (1)). The glucan and xylan yields from these runs are plotted in Figure 5.4a as a function of pretreatment time and as a function of severity in Figure 5.4b. In Figure 5.4b it can be seen that when xylan yields are plotted as a function of severity the differences in the yields from pretreatment at 130°C and 140°C are up to 9.9% which is greater than the standard deviation in xylan pretreatment yield at 140°C (Figure 5.7b) indicating slightly greater xylan hydrolysis at 140°C. The total lignin removal from *Populus trichocarpa* by these pretreatments is shown in Figure 5.4c. Pretreatment at 140°C for 160 minutes removed 5.5% more lignin than pretreatment at 130°C for 320 minutes. As will be shown in Figure 5.7b this is only slightly higher than the standard deviation for lignin removal, 5.0%, so the difference is negligible. Comparison of Figure 5.3b with Figure 5.4c reveals that 7 to 12% less lignin is removed during these low temperature pretreatments in comparison to pretreatment at 180°C. All three runs have the same severity parameter, therefore Arrhenius kinetics do not fully describe the system and it may be that a mechanism for lignin removal at high temperature, such as melting, migration, and extrusion[13], is less effective at lower temperatures. These differences will be explored in greater detail in chapter 7. Low temperature pretreatments will be conducted at 140°C as it results in moderate lignin removal within a practical time frame.

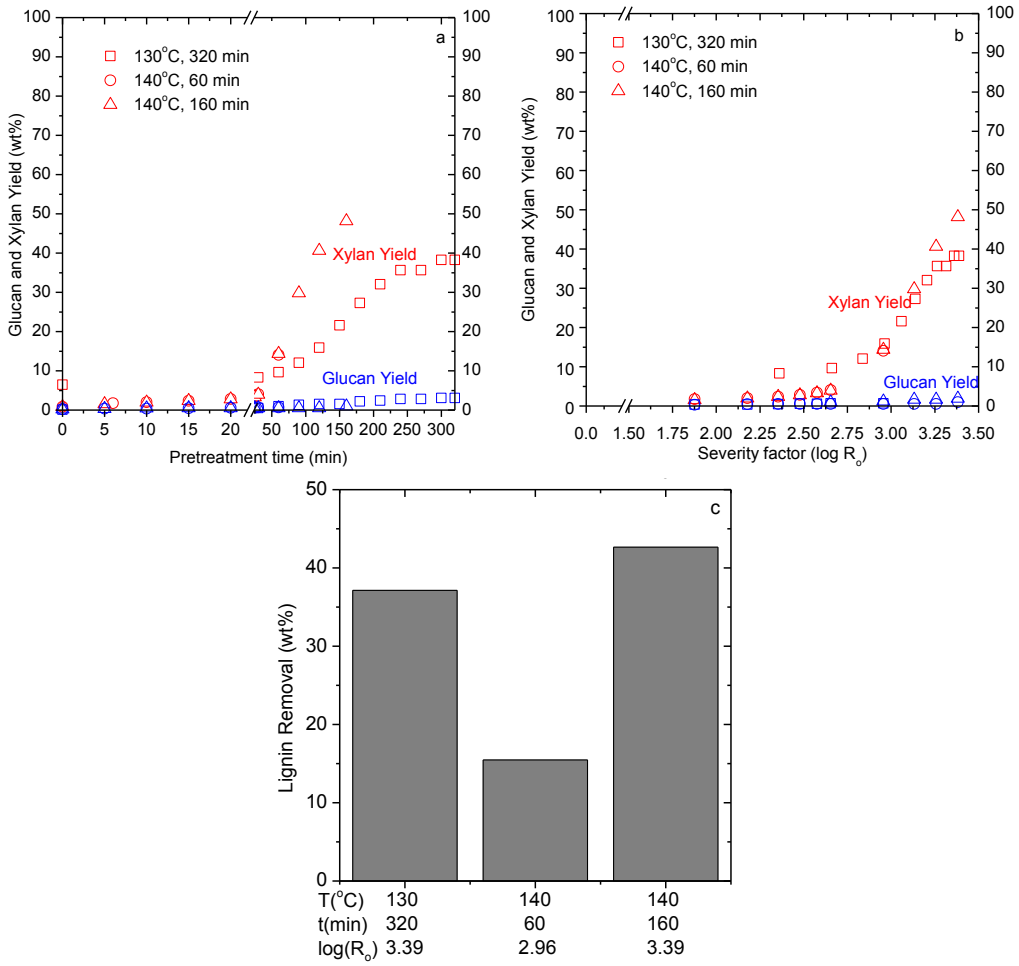

Figure 5.4. Glucan and xylan yields from flowthrough pretreatment of *Populus trichocarpa* at 130 and 140°C as a function of pretreatment time (a) and as a function of severity, Equation (1) (b). Lignin removal from *Populus trichocarpa* during pretreatment at 130 and 140°C (c). The flow rate was 25 mL/min.

5.4.2. Flow rate considerations

Flowthrough pretreatment of biomass was modeled as a bed of xylose spheres with constant diameter exposed to a flow of water at pretreatment temperature. Equation (2) was used to predict the concentration of xylose exiting the reactor as the flow rate was varied from 25 to 15 mL/min. The predicted concentrations were normalized against the outlet concentration predicted when the flow rate was 25 mL/min and plotted in Figure

5.5. It is clear from Figure 5.5 that the model does not predict a decrease in the outlet concentration of xylose when the flow rate is decreased for either temperature. Based on these results, lower flow rates were tested to increase product concentration and thus improve detection and quantification.

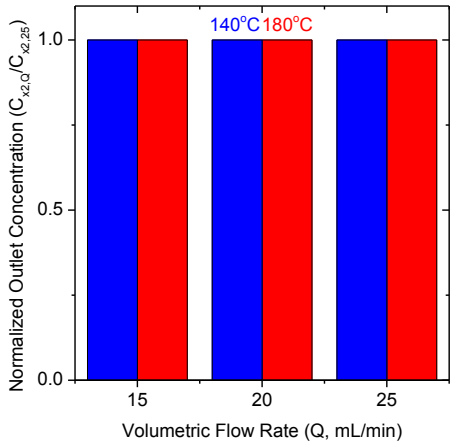

Figure 5.5. Normalized outlet concentration of xylose after water at 140°C (blue) and 180°C (red) passes over a bed of xylose spheres at varying flow rates as predicted by Equation (2). The calculated outlet concentration was normalized to the outlet concentration when the flow rate is equal to 25 mL/min.

Figure 5.6a shows the glucan and xylan yields and lignin removal after 10 minutes of pretreatment at 180°C for flow rates of 15, 20, and 25 mL/min. The differences in xylan yields at 20 and 25 mL/min range from 1.1 to 8% while the differences in xylan yields at 15 and 25 mL/min range from 0.1 to 20%. The initial lag in xylan release at 15 mL/min compared to xylan release at 25 mL/min was of particular concern as it suggested a change in the mass transfer regime. Although Liu and Wyman[5] reported no differences in the results of pretreatment of corn stover at flow rates above 10 mL/min, they did not provide detailed data for flow rates above 10 mL/min therefore a comparison cannot be made with the current work. The difference in lignin removal at

20 and 25 mL/min was only 1.5%. Therefore, the flow rate of 20 mL/min was tentatively selected for future runs. Before 20 mL/min could be selected for all future work, it was necessary to verify that reducing the flow rate from 25 mL/min to 20 mL/min during pretreatment at 140°C did not change the xylan or lignin removal patterns. From Figure 5.6b it can be seen that the difference in xylan yields at 20 mL/min and 25 mL/min range from 0.2 to 8.7%. Reducing the flow rate caused a mere 10% difference in the lignin removal. Therefore it was concluded that subsequent runs could be conducted at a flow rate of 20 mL/min.

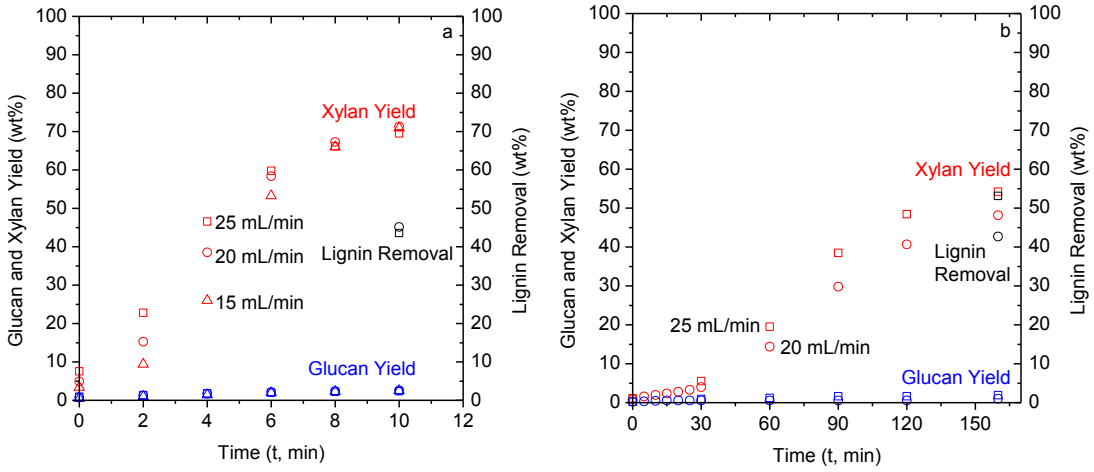

Figure 5.6. The effect of flow rate on glucan (blue) and xylan (red) yield and lignin removal (black) from *Populus trichocarpa* during pretreatment at 180°C (a) and at 140°C (b) as a function of time. Flow rates are represented by shape: square- 25 mL/min, circle- 20 mL/min, triangle- 15 mL/min.

5.4.3. Establishment of standard deviations

Based on the results from the exploratory runs, the following pretreatment conditions were selected for subsequent studies: a flow rate of 20 mL/min, pretreatment temperatures of 140 and 180°C for 12 to 192 minutes. Batch and flowthrough triplicate runs were performed.

From Figure 5.7a it can be seen that the maximum standard deviations associated with glucan and xylan yield under flow conditions at 180°C are 0.03 wt% and 2.0 wt%, respectively. The glucan and xylan yield standard deviations following batch pretreatment at 180°C were 0.1 wt% and 1.9 wt%, respectively. The standard deviation of lignin removal under flow and batch conditions at 180°C were 4.2 wt% and 1.0 wt%, respectively. From Figure 5.7b it can be seen that the maximum standard deviations associated with glucan and xylan yield from flowthrough pretreatment at 140°C were 0.6 wt% and 3.2 wt%. The standard deviation of lignin removal was 5.0 wt%. The standard deviations of glucan and xylan yield, and lignin removal after batch pretreatment at 140°C were 0.1, 0.5, and 2.6%. These results indicate that despite biomass heterogeneity, the procedures are readily reproducible.

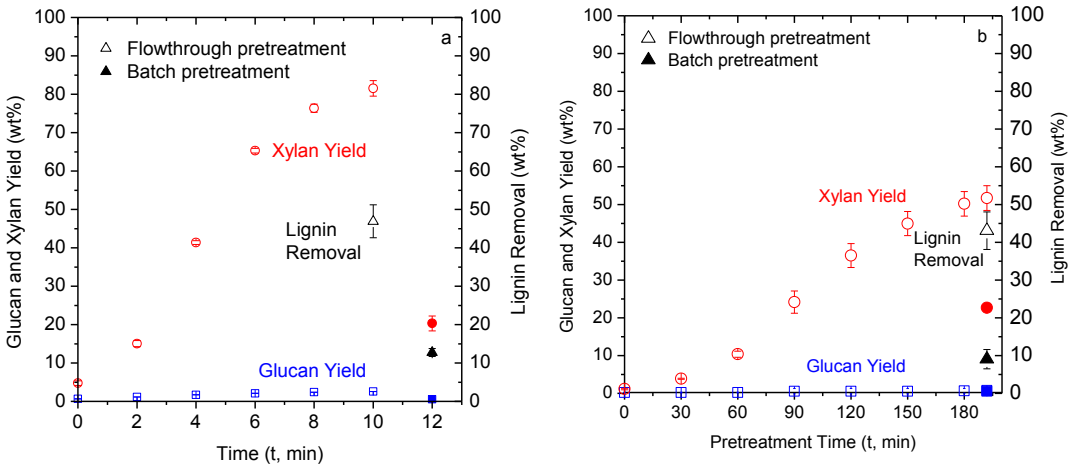

Figure 5.7a. Glucan (blue) and xylan (red) yields and lignin removal (black) from flowthrough (open symbols) and batch (solid symbols) pretreatment. Pretreatment was conducted at 180°C for 10 to 12 minutes (a) and at 140°C for 192 minutes (b). A flow rate of 20 mL/min was used for flowthrough pretreatment. Results are the average of triplicates and error bars are the standard deviation of triplicates.

5.5. Conclusions

The objectives of this chapter were to identify operating temperature, pressure, flow rate, and times for subsequent pretreatment studies and establish the reproducibility of the procedures. Temperatures of 140 and 180°C were selected; the operating pressure was equivalent to the associated saturation pressure. It was found that the majority of xylan and lignin removal occurred in 10 minutes. In subsequent studies, a pretreatment time of 12 minutes was used in order to collect sufficient liquid samples for analysis. Based on the severity parameter, 12 minutes of pretreatment at 180°C is equivalent to 192 minutes of pretreatment at 140°C. After modeling flowthrough pretreatment as a bed of xylose spheres and some experimental trial and error, a flow rate of 20 mL/min was selected for subsequent studies. Triplicate pretreatments were performed at the identified conditions. Standard deviations of glucan and xylan yields and lignin removal were less than 5% indicating the procedures are reproducible.

5.6. Nomenclature

A	Area, cm^2
C	Concentration, mol/cm^3
D_{AB}	Diffusivity of xylose in water, cm^2/sec
D_p	Particle diameter, cm
ΔH^{fus}	Enthalpy of fusion, J/mol
k_c	Mass transfer coefficient, Equation (4), cm/sec
$log(R_o)$	Logarithm of severity parameter, Equation (1)
M_B	molecular weight of water, g/mol
Q	Volumetric flow rate, cm^3/sec
R	Universal gas constant, 8.314 J/K/mol
Re	Reynolds number, $\rho_w D_p v' / \mu_w$
Sc	Schmidt's number, $\mu_w D_{AB} / \rho_w$
t_{rxn}	Duration of reaction/pretreatment, min
T	Temperature, K
T_{rxn}	Temperature of reaction/pretreatment, °C

x	Mole fraction
v'	Superficial fluid velocity, Q/A_{cross}, cm/s
V_A	Xylose molar volume at the boiling point, cm^3/mol
V	Volume, cm^3

Greek

ε	Bed porosity
ϕ	Association parameter of water, 2.6
γ	Activity coefficient
μ	Viscosity, g/cm/sec
ρ	Density, g/cm^3

Subscripts

0	At inlet
2	At outlet
b	Of reactor bed
cross	Cross-sectional
i	At solid/liquid interface
m	Melting
w	Of water
x	Of xylose

5.7. References

(1) Saeman JF. Kinetics of wood saccharification: Hydrolysis of cellulose and decomposition of sugars in dilute acid at high temperature. *Ind. Eng. Chem*. **1945**; *37*(1): 43-52.

(2) Sannigrahi P, Kim DH, Jung S, Ragauskas A. Pseudo-lignin and pretreatment chemistry. *Energy Environ. Sci*. **2011**; *4*(4): 1306-1310.

(3) Gray MC, Converse AO, Wyman CE. Solubilities of oligomer mixtures produced by the hydrolysis of xylans and corn stover in water at 180°C. *Ind. Eng. Chem. Res*. **2007**; *46*(8): 2383-2391.

(4) Bobleter O, Niesner R, Rohr M. The hydrothermal degradation of cellulosic matter to sugars and their fermentative conversion to protein. *J. Appl. Polym. Sci*. **1976**; *20*(8): 2083-2093.

(5) Liu C, Wyman CE. The effect of flow rate of compressed hot water on xylan, lignin, and total mass removal from corn stover. *Ind. Eng. Chem. Res*. **2003**; *42*(21): 5409-5416.

(6) Yang B, Wyman CE. Effect of xylan and lignin removal by batch and flowthrough pretreatment on the enzymatic digestibility of corn stover cellulose. *Biotechnol. Bioeng*. **2004**; *86*(1): 88-95.

(7) Allen SG, Kam LC, Zemann AJ, Antal MJ Jr. Fractionation of sugar cane with hot, compressed liquid water. *Ind. Eng. Chem. Res*. **1996**; *35*(8): 2709-2715.

(8) Mok WS, Antal MJ Jr. Uncatalyzed solvolysis of whole biomass hemicellulose by hot compressed liquid water. *Ind. Eng. Chem. Res*. **1992**; *31*(4): 1157-1161.

(9) Liu C, Wyman CE. Impact of fluid velocity on hot water only pretreatment of corn stover in a flowthrough reactor. *Appl. Biochem. Biotech*. **2004**; *113*(1-3): 977-987.

(10) Torget R, Hatzis C, Hayward TK, Hsu T, Philippidis GP. Optimization of reverse-flow, two-temperature, dilute-acid pretreatment to enhance biomass conversion to ethanol. *Appl. Biochem. Biotech*. **1996**; *57-58*: 85-101.

(11) van Walsum GP, Allen SG, Spencer MJ, Laser MS, Antal MJ Jr., Lynd LR. Conversion of lignocellulosics pretreated with liquid hot water to ethanol. *Appl. Biochem. Biotech*. **1996**; *57-58*: 157-170.

(12) Zhang T, Wyman CE, Yang B, Zhang J. Identification of desirable traits in Miscanthus to enhance total sugar yields in biological conversion. Presented at 31st Symposium on Biotechnology for Fuels and Chemicals, San Francisco CA, May 3-6, 2009.

(13) Donohoe BS, Decker SR, Tucker MP, Himmel ME, Vinzant TB. Visualizing lignin coalescence and migration through maize cell walls following thermochemical pretreatment. *Biotechnol. Bioeng*. **2008**; *101*(5): 913-925.

(14) Salmén L. Viscoelastic properties of *in situ* lignin under water-saturated conditions. *J. Mater. Sci*. **1984**; *19*(9): 3090-3096.

(15) Kim TH, Lee YY. Fractionation of corn stover by hot water and aqueous ammonia treatment. *Bioresource Technol*. **2006;** 97(2): 224-232.

(16) Kumar S, Kothari U, Kong L, Lee YY, Gupta RB. Hydrothermal pretreatment of switchgrass and corn stover for production of ethanol and carbon microspheres. *Biomass Bioenerg*. **2011**; *35*(2): 956-968.

(17) Yu Q, Zhuang X, Yuan Z, Wang W, Qi W, Wang Q, Tan X. Step-change flow rate liquid hot water pretreatment of sweet sorghum bagasse for enhancement of total sugars recovery. *Appl. Energ*. **2011**; *88*(7): 2472-2479.

(18) Saake B, Lehnen R. Lignin in *Ullmann's Encyclopedia of Industrial Chemistry*; Bohnet M, Bellussi G, Bus J, Cornils B, Drauz K, Greim H et al., Eds. Wiley Online Library: New York; 2007. [Internet].

(19) Irvine GM. The significance of the glass transition of lignin in thermochemical pulping. *Wood Sci. Technol*. **1985**; *19*(2): 139-149.

(20) Sarkanen KV, Ludwig CH, Eds. *Lignins- Occurence, formation, structure, and reactions*. Canada: John Wiley & Sons Inc.; 1971.

(21) Shao S, Jin Z, Wen G, Iiyama K. Thermocharacteristics of steam-exploded bamboo (*Phyllostachys pubescens*) lignin. *Wood Sci. Technol*. **2009**; *43*(7-8): 643-652.

(22) Petridis L, Schulz R, Smith JC. Simulation analysis of the temperature dependence of lignin structure and dynamics. *J. Am. Chem. Soc*. **2011**; *133*(51): 20277-20287.

(23) Fang Z, Sato T, Smith RL Jr., Inomata H, Arai K, Kozinski JA. Reaction chemistry and phase behavior of lignin in high temperature and supercritical water. *Bioresource Technol*. **2008**; *99*(9): 3424-3430.

(24) Abatzoglou NJ, Chornet E, Belkacemi K, Overend RP. Phenomenological kinetics of complex systems: the development of a generalized severity parameter and its application to lignocellulosic fractionation. *Chem. Eng. Sci*. **1992**; *47*(5): 1109-1122.

(25) Chum HL, Johnson DK, Black SK, Overend RP. Pretreatment-catalyst effects and the combined severity parameter. *Appl. Biochem. Biotech*. **1990**; *24/25*: 1-14.

(26) Geankoplis CJ. *Transport processes and separation process principles (Includes unit operations)*, 4th ed.; Prentice Hall PTR: Upper Saddle River, NJ, 2003.

(27) Liley PE, Thomson GH, Friend DG, Daubert TE, Buck E. Physical and Chemical Data. In *Perry's Chemical Engineers' Handbook 7th ed.* Perry RH, Green DW, Ed.; McGraw-Hill: New York, 1997; p 2-47.

(28) Elliot JR, Lira CT. *Introductory chemical engineering thermodynamics*; Prentice Hall PTR: Upper Saddle River, NJ, 1999.

(29) Sjöman E, Mänttäri M, Nyström M, Koivikko H, Heikkilä H. Separation of xylose from glucose by nanofiltration from concentrated monosaccharide solutions. *J. Membrane Sci*. **2007**; *292*: 106-115.

(30) Sluiter A, Hames B, Ruiz R, Scarlata C, Sluiter J, Templeton D. *Determination of sugars, byproducts, and degradation products in liquid fraction process samples laboratory analytical procedure*; NREL/TP-510-42623; National Renewable Energy Laboratory: Golden, CO, 2006; 14 p.

(31) Sluiter A, Hames B, Ruiz R, Scarlata C, Sluiter J, Templeton D, Crocker D. *Determination of structural carbohydrates and lignin in biomass laboratory analytical procedure*; NREL/TP-510-42618; National Renewable Energy Laboratory: Golden, CO, 2011; 18 p.

Chapter 6.

Deconstruction of xylan in *Populus trichocarpa* and model substrates during hydrothermal pretreatment.[*]

[*] Seokwon Jung, Georgia Institute of Technology, prepared holocellulose from *Populus trichocarpa* for this study. Glucooligomers and xylooligomers were measured by ultra high pressure liquid chromatography-mass spectrometry (UPLC-MS) by Drs. Bruce Tomkins, Timothy Tschaplinski, and Gary Van Berkel at Oak Ridge National Laboratory.

6.1. Abstract

Within the plant cell wall, hemicellulose shares hydrogen bonds with cellulose and covalent bonds with lignin. During hydrothermal pretreatment hemicellulose is hydrolyzed to monomers and oligomers; in a hardwood such as *Populus trichocarpa* xylose and xylooligomers are the primary products. In order to determine the influence of cell wall cross-linking on hemicellulose hydrolysis, *P. trichocarpa*, holocellulose derived from *P. trichocarpa*, and birchwood xylan were subjected to flowthrough pretreatment at 180^{o}C for up to 12 minutes. Differences in the hydrolysate and residual solids from these pretreatments indicate that lignin-hemicellulose bonds limit the production of xylooligomers and increase the proportion of xylooligomers with a degree of polymerization less than seven. Cellulose-hemicellulose bonds have a similar effect of xylan hydrolysis but to a lesser degree.

6.2. Introduction

Cellulose and hemicellulose are the primary carbohydrates that make up plant cell walls. Cellulose is a linear glucose-based polymer while hemicellulose contains many sugar monomers and has a complex, branched structure. In the primary cell wall, hemicellulose is primarily composed of xyloglucan, which has a cellulose-like backbone with short side chains of xylosyl and other monosaccharides.[1] Glucuronoxylans are the primary hemicellulose in secondary cell walls and have a xylan backbone with 4-O-methyl α-D-glucosyluronic acid residues and *O*-acetyl groups.[1] Hydrogen bonds between hemicellulose and cellulose readily form. The hemicellulose bound to cellulose serves as an indirect bridge to the other cell wall components, such as lignin. Hemicellulose is covalently bound to lignin through ester linkages, ether linkages, and indirect ester-ether bridges.[1, 2]

The commercial success of a cellulosic ethanol facility is closely tied to its ability to achieve high ethanol yields from hemicellulose and cellulose in the biomass. During pretreatment, hemicellulose is hydrolyzed to oligomers and monomers which can then degrade to products such as furfural.[3] Furfural and other degradation products are undesirable because they represent a loss of fermentable sugars and are inhibitory to downstream biological operations. Some studies have found that hemicellulose removal is key to increasing the enzymatic digestibility of biomass while others have found that hemicellulose removal has limited or negligible impact of cellulose digestibility.[4, 5] Even if hemicellulose removal does not affect cellulose digestibility, the importance of recovering high yields of oligomers and monomers from hemicellulose without

degradation products requires a thorough understanding of hemicellulose hydrolysis during pretreatment in order to optimize the process.

The principal mechanism of polysaccharide hydrolysis during hydrothermal pretreatment is the proton-catalyzed cleavage of the glycosidic bonds.[2] As temperature increases, the dissociation of water increases leading to an increase in the concentration of catalytic hydronium ions.[6] These ions coupled with the greater kinetic energy available at high temperatures catalyze hydrolysis during hydrothermal pretreatment.[6] Since the mechanism of hydrothermal pretreatment is very similar to that of dilute acid pretreatment, the kinetic principles and models are very similar.[7] The first model of biomass hydrolysis was Saeman's[3] model of cellulose hydrolysis by acid as a series of sequential reactions:

$$cellulose_{(s)} \overset{k_1}{\rightarrow} glucose_{(aq)} \overset{k_2}{\rightarrow} decomposition\ product_{(aq)} \quad (1)$$

Each step was modeled as a first order pseudohomogeneous reaction and the reaction rate constants follow the Arrhenius rate law with an additional power law dependence on acid concentration.[3] Saeman's paper has been the basis of almost every subsequent model of dilute acid and hydrothermal pretreatment. When this model is used, hemicellulose is frequently treated as xylan with furfural as the primary degradation product[8]:

$$xylan_{(s)} \overset{k_1}{\rightarrow} xylose_{(aq)} \overset{k_2}{\rightarrow} furfural_{(aq)} \quad (2)$$

The first major modification of Saeman's[3] model was made by Kobayashi and Sakai[9] who observed that the initial rates of pentosan hydrolysis were much faster than those observed later in the reaction leading them to propose the existence of two fractions of

pentosan, an easily hydrolyzed, fast reacting fraction and another more difficult to hydrolyze fraction. The proposed reactions are:

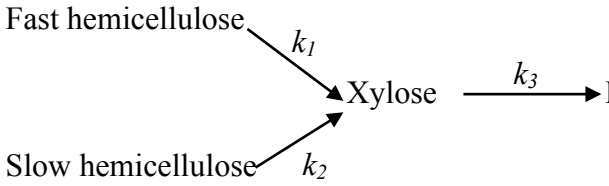

(3)

Each reaction was assumed to be a first order pseudohomogeneous reaction with Arrhenius type reaction rate constants. The three most commonly proposed causes for the biphasic behavior are[10]: heat or mass transfer limitations within the biomass resulting in local concentrations, different intrinsic reactivities, or changes in the interfacial surface area. The second explanation, different reactivities, is most frequently cited and has since been attributed to aspects of cell wall structure such as lignin-carbohydrate bonds[11, 12, 13] and hemicellulose-cellulose interactions[13] as well as the number and types of hemicellulose side chain substituents[11, 13]. Acetyl groups, arabinose, and uronic acid typically increase the solubility of xylan.[11]

The reaction schemes described by Equations (2) and (3) have been further amended to include the formation of oligomers prior to the formation of the xylose monomer. These and similar models have been used to describe the hydrolysis of hardwoods[12, 14, 15, 16], agricultural and industrial residues [17, 18, 19], and energy crops such as *Arundo donax* L.[20] Models including parallel reactions of other hemicellulose constituents such as arabinan, acetyl groups and uronic acid[18, 20] have also been developed.

Given the hundreds of potential reactions in both the solid and liquid phase during pretreatment, the anisotropy of biomass, especially wood, and the structural changes in biomass, modeling pretreatment is extremely complex[21]. Generalizations in biomass composition and assumption of homogeneous conditions have historically been used to meet these challenges.[10] The resulting models fit the data from which they were developed reasonably well but the variation in the models indicates that none truly describe the underlying mechanisms. For example, eleven hemicellulose models examined by Jacobsen and Wyman[8] predicted maximum theoretical xylose yields ranging from 77% to 97%. The differences in models and model predictions reflect differences in experimental conditions such as the liquid-solid ratio, the length of the heating period, differences in analytical techniques, and the natural variation of biomass composition.[22] The inclusion of xylooligomer intermediates was an improvement but further work is required since authors such as Kabel et al.[23] and Montane et al.[24] have shown that hydrothermal pretreatment results in a range of diverse xylooligomers. The next important advance in studying pretreatment kinetics should be the inclusion of the previously identified cell wall polymer interactions[25, 26, 27, 28] during pretreatment. Although the biphasic models assume such interactions are important[11, 12, 13] there has been little study of such interactions. Until there are well-developed models to predict the results of pretreatment, a time and labor intensive trial and error approach will continue to dominate lignocellulosic ethanol research and the scale-up and commercialization of pretreatment will be limited.

Using batch reactors to study biomass pretreatment, particularly the progress of hemicellulose hydrolysis is challenging. Xylose and xylooligomers react to generate products such as furfural, humins, and pseudo-lignin[3, 29] and cooling batch reactors may lead to the precipitation of oligomers.[28] In a fixed bed flowthrough reactor soluble products are removed from the reactor quickly limiting side and degradation reactions as reducing the possibility of product precipitation at the end of the reaction therefore hydrolysis products can be better tracked as a function of time. A previous study by Liu and Wyman[27] found that fixed bed flowthrough pretreatment enhances xylan removal from biomass and increases hemicellulose sugar recoveries indicating the removal of products prior to degradation. Liu and Wyman[27] also found that more xylooligomers were produced by flowthrough pretreatment than by batch pretreatment revealing the importance of xylooligomers as intermediates during hemicellulose hydrolysis.

Given the inherent advantages of fixed bed flowthrough pretreatment, as demonstrated by Liu and Wyman's study, such a reactor will be used to examine the role of hemicellulose-cellulose bonds and hemicellulose-lignin bonds in hemicellulose hydrolysis during the hydrothermal pretreatment of *Populus trichocarpa*, holocellulose isolated from *P. trichocarpa*, and birchwood xylan. The differences in the extraction of xylan, the rate of xylan removal, and oligomer release between *P. trichocarpa* and holocellulose should reflect the influence of hemicellulose-lignin bonds while the differences between holocellulose and birchwood xylan should reflect the influence of hemicellulose-cellulose bonds.

6.3. Experimental apparatus and procedures

6.3.1. Experimental apparatus

The first substrate used in this study was *Populus trichocarpa*; the source and preparation of the material is described in chapter 4. The first model substrate was holocellulose, the cellulose and hemicellulose fractions isolated from *P. trichocarpa,* prepared by Seokwon Jung (Georgia Institute of Technology). First, extractives were removed from *P. trichocarpa* with sequential five hour Soxhlet extractions according to the procedure described by Sluiter and coworkers[30]. The extraction flask was filled with CH_2Cl_2 and then refluxed at a boiling rate of five solvent cycles per hour. The extractive-free solids were air dried overnight and then lignin was removed by an oxidative treatment similar to that outlined by Zhang et al.[31] and Wickholm et al.[32] In brief, extractive-free poplar was dispersed into deionized (DI) water (100mL/g sample) with sodium chlorite (40% by dry weight of sample) and glacial acetic acid (10% by dry weight of sample) in a sealed plastic pouch (Kapak Corporation, Minneapolis, MN). The pouch was then placed in a reciprocating water bath at 70 °C for one hour. The oxidative treatment was repeated three more times to produce holocellulose. The holocellulose was recovered by filtration and washed thoroughly with DI water. The second model substrate, birchwood xylan, was purchased from Sigma-Aldrich (Lot 010M0169). The composition of three substrates is provided in Table 6.1. Acid insoluble residue (AcIR) is the sum of Klason lignin and ash in a substrate. Given the low ash content of these three materials, AcIR is approximately equivalent to the Klason lignin content.

Table 6.1. Composition (wt%) of *Populus trichocarpa*, holocellulose isolated from *Populus trichocarpa*, and birchwood xylan (Sigma-Aldrich, Lot 010M0169).

Substrate	Glucan (wt%)	Xylan (wt%)	AcIR (wt%)
Populus trichocarpa	40.5	11.5	22.7
Holocellulose	58.0	21.2	n/a
Birchwood xylan	1.6	67.3	n/a

These substrates were pretreated in the flowthrough pretreatment reactor system described in chapter 5.

6.3.2. Experimental procedure

6.3.2.a. Pretreatment

P. trichocarpa was subjected to flowthrough pretreatment at 180^{o}C using the methods described in chapter 5. In brief, the reactor was loaded with 1 g moisture free biomass and then installed in the piping system. The pump was set to a flow rate of 20 mL/min and started. The back pressure valve was adjusted to 1.1 MPag. Once the system was verified to be leak free, the reactor and heating coil were lowered into the sand bath, heated to 190^{o}C. The hydrolysate produced as the reactor was heated to 178^{o}C was collected. Once this temperature was attained the reaction was said to have started. Hydrolysate was collected in three minute intervals until the desired reaction time was reached. Reactions lasted 3 to 12 minutes. The reactor and heating coil were then transferred to a water bath in order to stop the reactions. A run was also performed in which the reactor was cooled immediately after reaching 178^{o}C; this was taken as "zero minutes". The residual solids were collected from the reactor by filtration, washed, and retained for analysis. These pretreatments were repeated using holocellulose and birchwood xylan.

6.3.2.b. Analytical techniques

6.3.2.b.i. Monomer and oligomer hydrolysate analysis

Sluiter et al.'s[33] strong acid hydrolysis procedure was used to determine the total sugar content of the liquid pretreatment hydrolysate by converting oligomers to monomers. Untreated hydrolysate was also injected on the HPLC in order to measure the monomer content. The sugars were detected by HPLC using an Aminex HPX-87H column (BioRad, Hercules, CA) heated to 65^{o}C with a separation module (Alliance 2695, Waters Associates, Milford, MA) equipped with a refractive index detector (2414, Waters Associates, Milford, MA). The eluent was 0.005 M sulphuric acid in the isocratic mode. Glucose and xylose concentrations were converted to glucan and xylan equivalents by dividing by 1.1111 and 1.3622, respectively, to account for the mass gain during hydrolysis.

6.3.2.b.ii. Ultra high performance liquid chromatographic separations with mass spectrometric detection

Drs. Tomkins, Tschaplinski, and Van Berkel (Oak Ridge National Laboratory) analyzed the hydrolysates using ultra high performance liquid chromatography (UPLC) with mass spectrometric detection to identify and quantify glucooligomers and xylooligomers with a degree of polymerization (DP) up to and including six. The standard analytes were purchased from Sigma-Aldrich (St. Louis, MO), Toronto Research Chemicals, Inc. (North York, Ontario, Canada), or Megazyme International Ireland, Bray, County Wicklow, Ireland), with purity >95%, and were used as received. Standards were prepared in 80/20 (v/v) acetonitrile/water using Fisher Optima® LC/MS

grade solvents (Fisher Scientific, Fair Lawn, NJ). The acetonitrile and water eluents were both prepared using Optima® grade solvent and contained 10 μM reagent-grade sodium acetate as a modifier.

All samples were filtered through a 0.2 μm porosity nylon filter (Cat. 24137, Grace Davison Discovery Sciences, Deerfield, IL) prior to analysis. Each sample was diluted from fifty- to five-hundred-fold using 80/20 (v/v) acetonitrile/water.

The oligomers were separated using an ACQUITY™ Ultra Performance Liquid Chromatograph equipped with a sample manager, binary solvent manager, and a BEH® HILIC UPLC column (2.1 mm i.d. x 100 mm length, packed with 1.7 μm diameter particles), all from Waters Associates (Milford, MA). The injection volume was 0.5 μL. The column oven and sample manager temperatures were maintained at 35 and 4 °C, respectively. The linear gradient separation employing acetonitrile/10 μM sodium acetate (Solvent A) and water/10 μM sodium acetate (Solvent B), described in Table 6.2, was used. The eluent flow rate was maintained at 0.5 mL/min. Sample-to-sample analysis time was approximately 6 min. All samples were analyzed in at least triplicate.

Table 6.2. Concentration profiles of acetonitrile with 10 μM sodium acetate (Solvent A) and water with 10 μM sodium acetate (Solvent B) during ultra-high pressure liquid chromatography-mass spectrometry (UPLC-MS) analysis of hydrolysate from the pretreatment of *Populus trichocarpa*, holocellulose, and birchwood xylan.

Time (min)	Concentration of Solvent A (v/v%)	Concentration of Solvent B (v/v%)	Flow rate (mL/min)
0	80	20	0.5
1.0	80	20	0.5
2.0	70	30	0.5
2.1	5	95	0.5
3.0	5	95	0.5
3.1	80	20	0.5

The oligomers were detected as their sodiated analogs in the single-ion monitoring (SIM) mode using an AB/SCIEX 4000 QTrap® System (AB/Sciex, Foster City, CA) employing electrospray ionization in the positive ionization mode. Cellodextrins were detected at *m/z* 365.1, 527.2, 689.2, and 851.3, corresponding to cellobiose, -triose, -tetraose, and –pentaose, respectively. Xylodextrins and arabinodextrins were detected at *m/z* 305.1, 437.2, 569.2, 701.3, and 833.3, corresponding to the respective biose, triose, tetraose, pentaose, and hexaose, respectively. The instrument was optimized for detection of each target *m/z* value.

6.3.2.b.iii. Structural carbohydrate and Klason lignin analysis

The glucan, xylan, and Klason lignin content of the raw and pretreated *P. trichocarpa,* holocellulose, and birchwood xylan were determined using the two-step acid hydrolysis procedure outlined by Sluiter et al.[34] No extraction was performed prior to the two-step acid hydrolysis because the substrates contain few extractives. After hydrolysis, a 2 mL liquid sample was withdrawn and centrifuged. The sample supernatant was not neutralized prior to injection on the HPLC. HPLC conditions were as described in section 6.3.2.b.i. The measured glucose and xylose concentrations were converted to glucan and xylan equivalents by dividing by 1.1111 and 1.3622, respectively, to account for mass gain during hydrolysis.

6.4. Results and discussion

6.4.1. Glucan release from *Populus trichocarpa* and model substrates during hydrothermal pretreatment

The glucan released from *P. trichocarpa*, holocellulose, and birchwood xylan is shown as a function of pretreatment time in Figure 6.1. Very little of the available glucan is removed from *Populus* and holocellulose. This is expected as hydrothermal pretreatment has little effect on cellulose, the largest source of glucan. However, almost all of the available glucan is removed from birchwood xylan. This could be because the glucan remaining in birchwood xylan is derived from hemicellulose as opposed to cellulose.

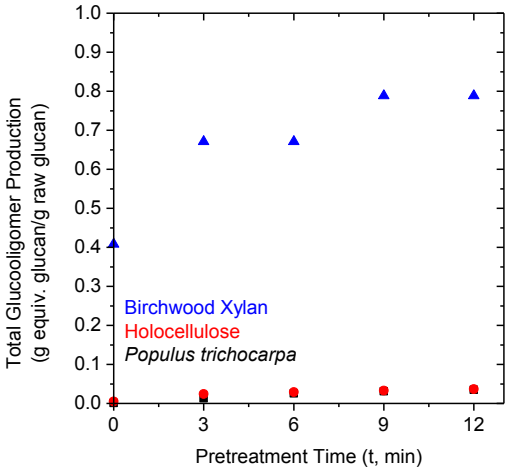

Figure 6.1. Glucan release from *Populus trichocarpa* (black squares), holocellulose (red circles), and birchwood xylan (blue triangles) by flowthrough pretreatment at 180°C as a function of pretreatment time.

6.4.2. Xylooligomer production from *Populus trichocarpa* and model substrates during hydrothermal pretreatment

The total xylooligomer production or xylan yield from the three substrates is shown as a function of pretreatment time in Figure 6.2a. The instantaneous derivative, i.e. the instantaneous rate of production, was calculated and is plotted as a function of pretreatment time in Figure 6.2b. Figure 6.3 shows the production of individual xylooligomers as measured by HPLC and UPLC-MS as a function of pretreatment time; each is expressed in grams per gram xylan in the raw solids. Xylooligomers with a degree of polymerization greater than or equal to seven were determined from the difference in the total xylose content of the hydrolysate as determined by post-hydrolysis and HPLC and the sum of xylooligomers with a degree of polymerization less than or equal to six; the calculation was performed on a gram xylose equivalent basis.

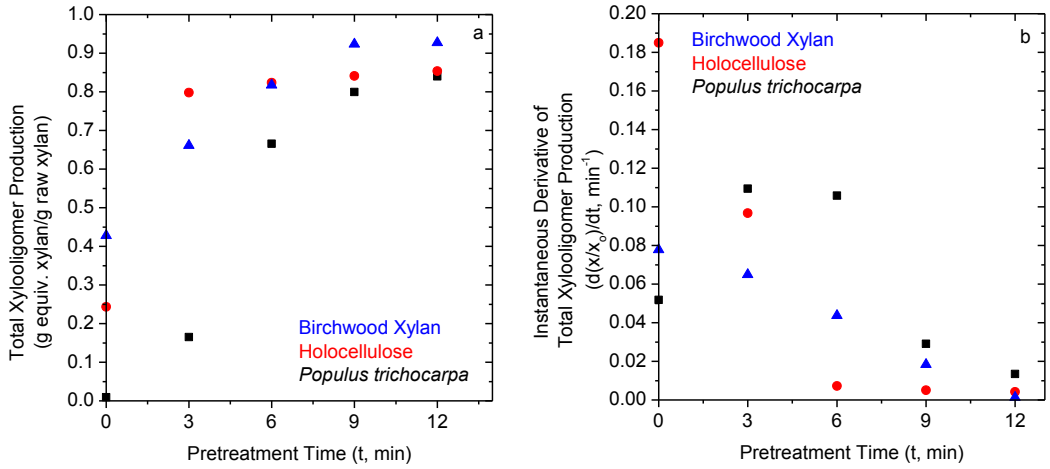

Figure 6.2. (a) Xylooligomer production (gram xylan equivalent per gram of xylan in untreated substrate) from *Populus trichocarpa* (black square), holocellulose (red circle), and birchwood xylan (blue triangle) by flowthrough pretreatment at 180°C as a function of pretreatment time. (b) Instantaneous derivative of xylooligomer production from *Populus trichocarpa* (black square), holocellulose (red circle), and birchwood xylan (blue triangle) by flowthrough pretreatment at 180°C as a function of pretreatment time.

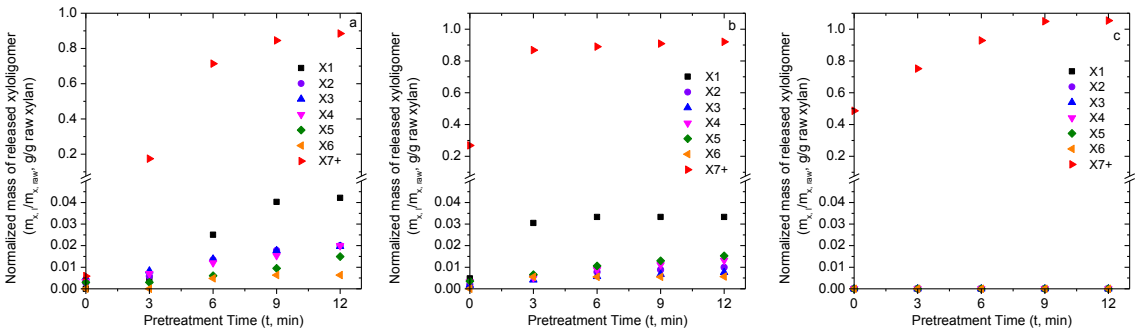

Figure 6.3. Cumulative production of xylooligomers in the hydrolysate from the flowthrough hydrothermal pretreatment of *Populus trichocarpa* (a), holocellulose (b) and birchwood xylan (c) at 180°C as a function of time. The mass of each xylooligomer was normalized against the mass of xylan initially present in the substrate.

In Figure 6.2a, it can be seen that xylan yields from all three substrates begin to plateau after approximately 9 minutes of pretreatment; this is paralleled by the approach of the instantaneous rates of production to zero in Figure 6.2b. *P. trichocarpa* was pretreated for 192 minutes at 180°C in the flowthrough reactor and the total xylooligomer production from this pretreatment was 0.92 g xylan equivalent per gram xylan in the raw biomass, only 9.5% greater than the total xylooligomer production after 12 minutes of pretreatment. This plateau in xylan removal is in agreement with previous studies[9-20] that observed that a portion of hemicellulose is more resistant to hydrolysis.

Comparison of the xylan yield from *P. trichocarpa* and holocellulose in Figure 6.2a reveals that 79% to 96% more xylan is released from holocellulose as the reactor is heated to 180°C and during the first three minutes. The difference in yield gradually decreases with pretreatment time. The rate of xylooligomer production from holocellulose is initially high but decreases with pretreatment time while the rate of xylooligomer production from *P. trichocarpa* increases to 0.11 min^{-1} at the three minute mark before decreasing to zero. For both substrates, xylooligomers with a degree of

polymerization greater than seven accounted for the majority of the xylooligomers produced (Figures 6.3a and 6.3b). Comparison of Figures 6.3a and 6.3b reveal that more xylose, xylobiose, xylotriose, and xylotetraose are produced from *P. trichocarpa* than from holocellulose after the three minute mark. Previous researchers have suggested that lignin-hemicellulose interactions limit the release of xylooligomers.[11-13] Such bonds are not present in holocellulose. Given the slower release of xylooligomers particularly short xylooligomers (DP≤4) and the ultimately greater quantities of short xylooligomers from *P. trichocarpa* compared to holocellulose, it appears that the lignin-hemicellulose interactions impede xylooligomer production at the outset of pretreatment. The timing may be related to delignification. As *P. trichocarpa* is heated, the lignin may soften, coalesce and migrate leading to fewer lignin-hemicellulose interactions[35, 36]; this will be discussed in greater detail in chapter 7. During the early stages of pretreatment, lignin may not be sufficiently softened which would limit the initial release of xylooligomers. However, lignin's branched structure and shared bonds with hemicellulose likely also limits lignin's coalescence and migration prior the breaking of lignin-hemicellulose bonds.[37] Alternatively, the lignin-hemicellulose bonds could limit xylooligomer solubility. Intra-xylan bonds could break rapidly relative to the lignin-xylan bonds. The lignin-xylan fragments are less soluble and thus unable to enter the bulk liquid phase until the fragments are quite small. Once this threshold is achieved there would be a sudden increase in xylooligomer production. This hypothesis is consistent with the increase in xylooligomer production seen in Figure 6.3a after three minutes of pretreatment.

A comparison of the total xylooligomer production from holocellulose and birchwood xylan in Figure 6.2a reveals that there is 43% difference in the production of xylooligomers during the heating period. Although xylooligomer production from holocellulose temporarily exceeds xylooligomer production from birchwood xylan at the three minute mark, after 12 minutes there is 7.9% more xylooligomers are produced from birchwood xylan than from holocellulose. In Figure 6.3c, it can be seen that negligible amounts of xylooligomers with a degree of polymerization less than seven are produced from birchwood xylan while Figure 6.3b shows that 5 to 38% of the xylooligomers from holocellulose have a degree of polymerization less than 7. Based on the differences in total xylooligomer production, it appears that hydrogen bonding between cellulose and hemicellulose limits xylan extraction from holocellulose relative to birchwood xylan. Furthermore, the presence of short xylooligomers in the holocellulose hydrolysate and their absence in the birchwood xylan hydrolysate indicates that the hemicellulose-cellulose interactions also limit the release of large xylooligomers.

6.4.3. Analysis of residual solids

The composition of *P. trichocarpa* and holocellulose before and after pretreatment are presented in Figure 6.4. The pretreatment of both substrates results in the removal of xylan; lignin is removed from *P. trichocarpa.* No lignin was detected in the holocellulose. The removal of xylan and lignin leads to the enrichment of the solids in glucan. Although the composition of the raw birchwood xylan was measured (Table 6.1), pretreated birchwood xylan solids were insufficient for quantitative saccharification of pretreated birchwood xylan.

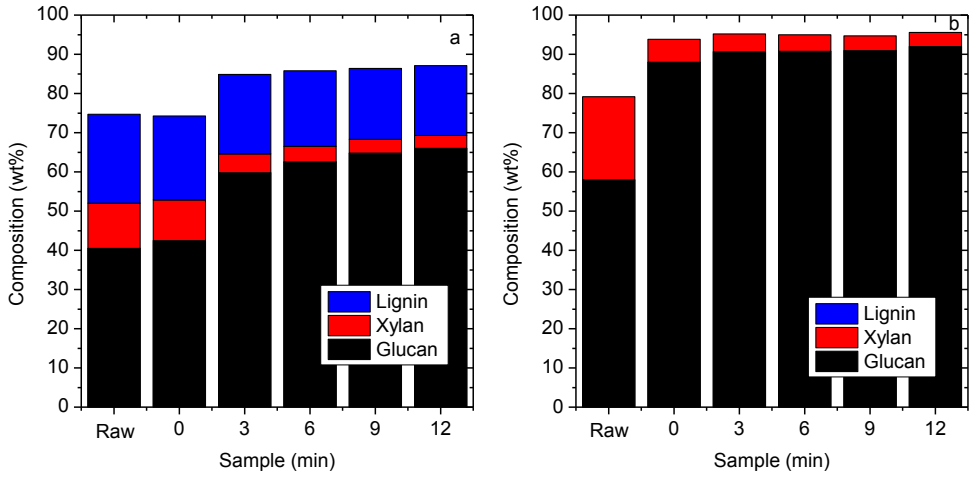

Figure 6.4. Composition of raw and pretreated *Populus trichocarpa* (a) and holocellulose (b).

6.5. Conclusions

Populus trichocarpa, holocellulose prepared from *P. trichocarpa*, and birchwood xylan were subjected to flowthrough pretreatment in order to study the influence of hemicellulose-lignin and hemicellulose-cellulose bonds on the results of xylan hydrolysis. The hydrolysate and pretreated solids were characterized by combination of techniques including strong acid hydrolysis, HPLC, and UPLC. The greatest amount of xylooligomers was produced from birchwood xylan followed by holocellulose, and then *P. trichocarpa*. The xylooligomers produced from birchwood xylan all had a degree of polymerization greater than seven while a fraction of the xylooligomers produced from holocellulose and *P. trichocarpa* had a degree of polymerization less than seven; the greatest amount of xylose was produced from *P. trichocarpa*. These differences indicate that lignin-hemicellulose bonds and to a lesser extent cellulose-hemicellulose bonds limit the hydrolysis of hemicellulose and promote the production of xylose during pretreatment.

6.6. References

(1) Albersheim P, Darvill A, Roberts K, Sederoff R, Staehelin A. *Plant cell walls from chemistry to biology*. Garland Science: New York, 2011.

(2) Fengel D, Wegener G. *Wood: chemistry, ultrastructure, and reactions*; Walter de Gruyter: New York, 1984.

(3) Saeman JF. Kinetics of wood saccharification: hydrolysis of cellulose and decomposition of sugars in dilute acid at high temperatures. *Ind. Eng. Chem*. **1945**; *37*: 43-52.

(4) Yang B, Wyman CE. Effect of xylan and lignin removal by batch and flowthrough pretreatment on the enzymatic digestibility of corn stover cellulose. *Biotechnol. Bioeng*. **2004**; *86*: 88-95.

(5) Kumar R, Wyman CE. Key features of pretreated lignocelluloses biomass solids and their impact on hydrolysis. In: *Bioalcohol production : Biochemical conversion of lignocellulosic biomass*; Waldon K, Ed.; Woodhead Publishing Ltd.: Oxford, 2010; 73-121.

(6) Mosier NS. Fundamentals of Biomass Pretreatment at Neutral pH. In *Aqueous Pretreatment of Plant Biomass for Biological and Chemical Conversion to Fuels and Chemicals*; Wyman CE, Ed.; John Wiley & Sons, in preparation.

(7) Vila C, Garrote G, Dominguez H, Parajó JC. Hydrolytic processing of rice husks in aqueous media: a kinetic assessment. *Collect. Czech. Chem. C*. **2002**; *67*: 509-530.

(8) Jacobsen SE, Wyman CE. Cellulose and hemicellulose hydrolysis models for application to current and novel pretreatment processes. *Appl. Biochem. Biotechnol*. **2000**; *84-86*: 81-96.

(9) Kobayashi T, Sakai Y. Hydrolysis rate of pentosan of hardwood in dilute sulfuric acid. *B. Agr. Chem. Soc. Japan*. **1956**; *20*: 1-7.

(10) Maloney MT, Chapman TW, Baker AJ. Dilute acid hydrolysis of paper birch: kinetics studies of xylan and acetyl group hydrolysis. *Biotechnol. Bioeng*. **1985**; *27*: 355-361.

(11) Chen X, Lawoko M, van Heiningen A. Kinetic and mechanism of autohydrolysis of hardwoods. *Bioresource Technol*. **2010**; *101*: 7812-7819.

(12) Conner AH. Kinetic modeling of hardwood prehydrolysis: Part I. Xylan removal by water prehydrolysis. *Wood Fiber Sci*. **1984**; *16*: 268-277.

(13) Lee YY, Iyer P, Torget RW. Dilute-acid hydrolysis of lignocellulosic biomass. *Adv. Biochem. Eng. Biot*. **1999**; *65*: 93-115.

(14) Conner AH, Lorenz LF. Kinetic modeling of hardwood prehydrolysis: Part III: Water and dilute acetic acid prehydrolysis of southern red oak. *Wood Fiber Sci*. **1986**; *18*: 248-263.

(15) Garrote G, Dominguez H, Parajó JC. Mild autohydrolysis: an environmentally friendly technology for xylooligosaccharide production from wood. *J. Chem. Technol. Biot*. **1999**; *74*: 1101-1109.

(16) Mittal A, Chatterjee SG, Scott GM, Amidon TE. Modeling xylan solubilization during autohydrolysis of sugar maple wood meal: reaction kinetics. *Holzforchung*. **2009**; *63*: 307-314.

(17) Carvalheiro F, Garrote G, Parajó JC, Pereira H, Gírio FM. Kinetic modeling of brewery's spent grain autohydrolysis. *Biotechnol. Progr*. **2005**; *21*: 233-243.

(18) Garrote G, Dominguez H, Parajó JC. Kinetic modeling of corncob autohydrolysis. *Process Biochem*. **2001**; *36*: 571-578.

(19) Garrote G, Dominguez H, Parajó JC. Production of substituted oligosaccharides by hydrolytic processing of barley husks. *Ind. Eng. Chem.* **2004**; *43*: 1608-1614.

(20) Capparrós S, Garrote G, Ariza J, López F. Autohydrolysis of *Arundo donax* L., a kinetic assessment. *Ind. Eng. Chem.* **2006**; *45*: 8909-8920.

(21) Grénman H, Wärna J, Mikkola J-P, Sifontes V, Fardim P, Murzin DY, Salmi T. Modeling the influence of wood anisotropy and internal diffusion on delignification kinetics. *Ind. Eng. Chem. Res*. **2010**; *49*: 9703-9711.

(22) Carrasco F, Roy C. Kinetic study of dilute-acid prehydrolysis of xylan-containing biomass. *Wood Sci. Technol*. **1992**; *26*: 189-208.

(23) Kabel MA, Carvalheiro F, Garrote G, Avgerinos E, Koukios E, Parajó JC, Gírio FM, Schols HA, Voragen AGJ. Hydrothermally treated xylan rich by-products yield different classes of xylo-oligosaccharides. *Carbohyd. Polym*. **2002**; *50*: 47-56.

(24) Montane D, Farrioal X, Salvadó J, Jollez P, Chornet E. Application of steam explosion to the fractionation and rapid vapor-phase alkaline pulping of wheat straw. *Biomass Bioenerg*. **1998**; *14*: 261-276.

(25) Abatzoglou, N.J., E. Chornet, K. Belkacemi, and R.P. Overend, "Phenomenological kinetics of complex systems: the development of a generalized severity parameter and its application to lignocellulosic fractionation," Chemical Engineering Science, **47**, 1109-1122 (1992).

(26) Abatzoglou N, Bouchard J, Chornet E. Dilute acid depolymerization of cellulose in aqueous phase: experimental evidence of the significant presence of soluble oligomeric intermediates. *Can. J. Chem. Eng*. **1986**; *64*: 78-786.

(27) Liu C, Wyman CE. The effect of flow rate of compressed hot water on xylan, lignin, and total mass removal from corn stover. *Ind. Eng. Chem. Res*. **2003**; *42*(21): 5409-5416.

(28) Gray MC, Converse AO, Wyman CE. Solubilities of oligomer mixtures produced by the hydrolysis of xylans and corn stover in water at 180^{o}C. *Ind. Eng. Chem. Res*. **2007**; *46*(8): 2383-2391.

(29) Sannigrahi P, Kim DH, Jung S, Ragauskas A. Pseudo-lignin and pretreatment chemistry. *Energy Environ. Sci*. **2011**; *4*(4): 1306-1310.

(30) Sluiter A, Ruiz R, Scarlata C, Sluiter J, Templeton D. *Determination of extractives in biomass*. Report No. NREL/TP-510-42619; National Renewable Energy Laboratory: Golden, CO, 2005 Jul; 12p.

(31) Zhang DC, Pu YQ, Chai XS, Naithani V, Jameel H, Ragauskas AJ. Elucidating carboxylic acid profiles for extended oxygen delignification of high-kappa softwood kraft pulps. *Holzforschung*. **2006**; *60*: 123-129.

(32) Wickholm K, Larsson PT, Iversen T. Assignment of non-crystalline forms in cellulose I by CP/MAS C-13 NMR spectroscopy. *Carbohydr. Res.* **1998**; *312*: 123-129.

(33) Sluiter A, Hames B, Ruiz R, Scarlata C, Sluiter J, Templeton D. *Determination of sugars, byproducts, and degradation products in liquid fraction process samples laboratory analytical procedure*. Report No. NREL/TP-510-42623; National Renewable Energy Laboratory: Golden, CO, 2006 Dec.; 14 p.

(34) Sluiter A, Hames B, Ruiz R, Scarlata C, Sluiter J, Templeton D, Crocker D. *Determination of structural carbohydrates and lignin in biomass laboratory analytical procedure.* Report No. NREL/TP-510-42618; National Renewable Energy Laboratory: Golden, CO, 2011 Jul; 18 p.

(35) Donohoe BS, Decker SR, Tucker MP, Himmel ME, Vinzant TB. Visualizing lignin coalescence and migration through maize cell walls following thermochemical pretreatment. *Biotechnol. Bioeng*. **2008**; *101*(5): 913-925.

(36) Selig MJ, Viamajala S, Decker SR, Tucker MP, Himmel ME, Vinzant TB. Deposition of lignin droplets produced during dilute acid pretreatment of maize stems retards enzymatic hydrolysis of cellulose. *Biotechnol. Prog*. **2007**; *23*(6): 1333-1339.

(37) Irvine GM. The significance of the glass transition of lignin in thermochemical pulping. *Wood Sci. Technol*. **1985**; *19*(2): 139-149.

Chapter 7.

Deconstruction of lignin during hydrothermal pretreatment*

* Dr. Shilin Cao at the Georgia Institute of Technology prepared cellulolytic enzyme lignin for this study. Molecular weight was measured by gel permeation chromatography by Dr. Marcus Foston and Dr. Arthur Ragauskas at the Georgia Institute of Technology. Dr. Marcus Foston and Dr. Arthur Ragauskas also used heteronuclear single quantum coherence nuclear magnetic resonance to analyze raw and pretreated cellulolytic lignin. Additional thanks to Dr. Foston for his edits to section 7.4.1.d. Phenols in the pretreatment hydrolysates were measured by gas chromatography-mass spectrometry by Nancy Engle and Dr. Timothy Tschaplinski at Oak Ridge National Laboratory.

7.1. Abstract

In order to investigate lignin behavior during pretreatment, *Populus trichocarpa* and cellulolytic enzyme lignin (CEL) isolated from *P. trichocarpa* were subjected to batch and flowthrough hydrothermal pretreatment at 140 and 180^{o}C for 12 to 192 minutes. The residual solids and liquid hydrolysate were characterized by a wide range of techniques. Changes in the structure of the solids recovered after the pretreatment of CEL and the production of phenol monomers point strongly to depolymerization and condensation being the primary mechanism of lignin extraction and redeposition. Limiting the residence time of products in the bulk liquid phase limits condensation reactions. However, there was also evidence of lignin undergoing phase transitions. Given the branched nature of lignin it would seem that bond hydrolysis enables the coalescence and migration of lignin. The differences in lignin removal from native *P. trichocarpa* and CEL suggest that the hemicellulose-lignin interactions increase lignin extraction and increase the extractability of syringyl groups relative to guaiacyl groups.

7.2. Introduction

Lignin is a polyphenol compound found in the cell walls of vascular plants. It strengthens plants to keep them vertical and its hydrophobic character reduces water loss from the cell.[1] Although the mechanism of lignin biosynthesis is still debated[2], *p*-coumaryl, coniferyl, and sinapyl alcohols[3] are the primary structural units, and the final polymer structure is amorphous and three-dimensional[2]. Hardwoods such as *Populus* typically contain syringyl lignin and guaiacyl lignin synthesized from sinapyl and coniferyl alcohol, respectively[2]. Select monomers are shown in Figure 7.1. In hardwoods, β-O-4 (β aryl ether) linkages account for approximately 80% of the linkages involving syringyl units[4]. Other linkages such as β -5/α-*O*-4 phenyl-coumararan and spirodienone linkages are also present. The chemical structures are shown in Figure 7.2.

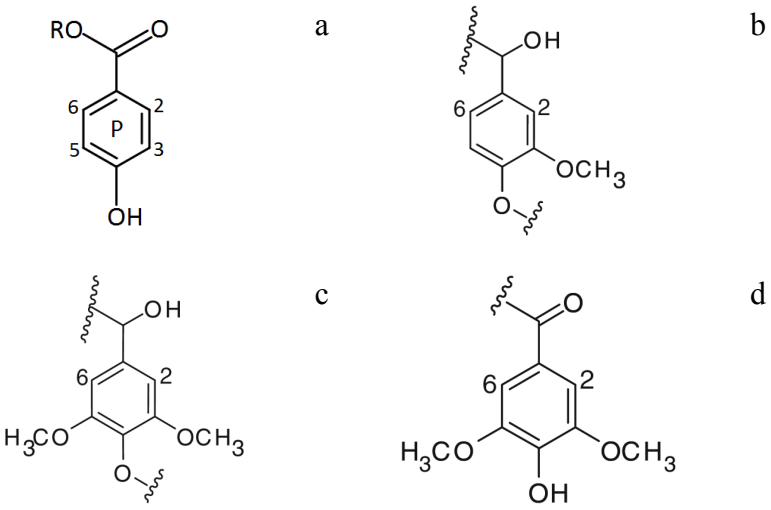

Figure 7.1. Select lignin monomers found in hardwoods: *p*-hydroxybenzoate (a), guaiacyl unit (b), syringyl unit (c), and oxidized syringyl unit (d).

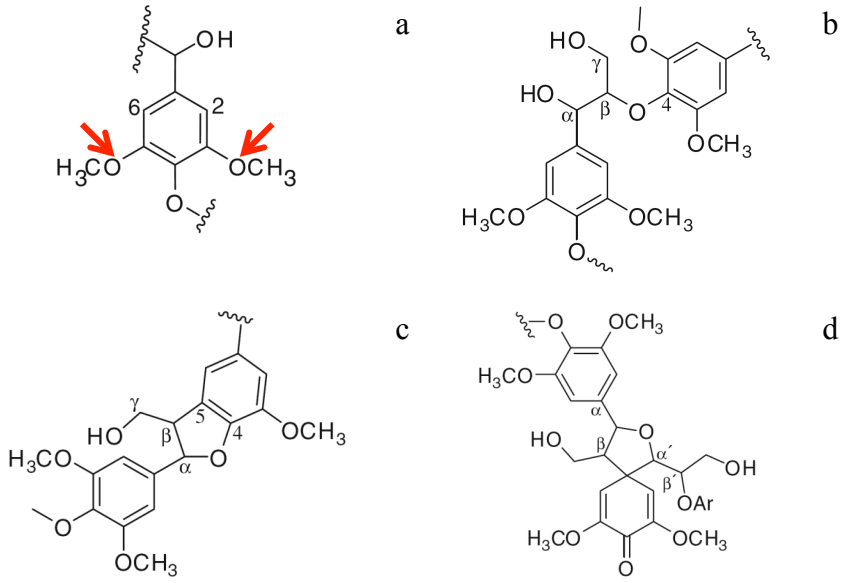

Figure 7.2. Select lignin structures found in hardwoods: methoxy group (a), β-*O*-4 ether (b), β-5/α-*O*-4 phenyl-coumararan (c), spirodienone (d).

As the cell wall is lignified, lignin forms ester, ether, and glycosidic bonds between lignin and polysaccharides have been identified[3, 4] generating lignin-carbohydrate complexes (LCC)[3]. There may also be noncovalent interactions between lignin and hemicellulose but there are few interactions between lignin and cellulose.

Generally delignification improves enzymatic hydrolysis of polysaccharides although some reports have found the opposite.[5] Lignin's negative impact on enzymatic hydrolysis occurs through a number of mechanisms: by physically shielding carbohydrates from enzymes, slowing the adsorption of enzyme on carbohydrates, and irreversibly binding enzymes, thus reducing the effective enzyme concentration.[5] Finally lignin breakdown products may be inhibitory to enzymes.[5] For these reasons, lignin removal is an oft-cited goal for pretreatment, and a better understanding the mechanisms of lignin removal during pretreatment may lead to insight for new pretreatment or plant modification strategies.

Lignin appears to cycle between the solid and liquid phase during pretreatment through a complex mechanism. Lignin enters the liquid phase in a soluble or mobile form generated by phase transition, reaction, or solubilization during pretreatment. However, it may be redeposited on the solids due to reactions producing insoluble compounds and/or precipitation when the system is cooled. Lignin morphology and distribution changes during pretreatment, possibly through phase change. Many researchers[6, 7, 8, 9, 10] have observed droplets on a wide variety of biomass including corn stover, switchgrass, wheat straw, and *Tamarix ramosissima* following hydrothermal or dilute acid pretreatment and these droplets have been identified as lignin[6]. Kristenson et al. [7] and Xiao et al.[10] both observed a very large increase in the lignin signal in ATR-FTIR spectra, which may reflect an absolute increase in lignin content on the surface. It has been proposed that these droplets form as a result of lignin melting and then coalescing, migrating and extruding from the cell wall.[6] Once the system is cooled these droplets harden. This view is somewhat simplified since the effects of increasing the temperature of an amorphous solid are complex. The melt of a crystalline solid is associated with the release of latent heat at single temperature[11]; the same does not occur when an amorphous polymer is heated. When an amorphous solid is heated it passes through a stage known as the glass transition, which occurs over a range of temperatures.[12]. A number of physical changes ensue including a decrease in stiffness[12], a decrease in viscosity[11], and an abrupt increase in heat capacity[11]. Rubbery flow of uncross-linked material will occur if no thermal degradation occurs; a cross-linked polymer such as lignin can only undergo rubbery flow after bonds break.[12] A review of

the literature indicates the glass transition of lignin occurs somewhere in the range between 80°C and 193°C[12, 13, 14, 15, 16, 17, 18]; the breadth of this range reflects differences in biomass, sample moisture content[15], lignin isolation procedures[15], and analytical techniques[12, 15].

In addition to these morphological changes, lignin reacts during pretreatment. In the presence of protons, carbonium intermediates with a high affinity for nucleophiles form within the lignin structure.[3] Hydrolysis leads to depolymerization while reactions between these carbonium ions and nucleophiles leads to repolymerization or condensation.[19] There are many sources of nucleophiles during pretreatment including unsaturated aromatic and aliphatic lignin fragments, lignin degradation products, and carbohydrate degradation products such as furfural.[19] The addition of a nucleophile that undergoes a single electrophilic substitution, such as *p*-hydroxybenzoic acid or 2-naphthol, has been shown to limit repolymerization.[19, 20, 21] Evidence of depolymerization during pretreatment includes the loss of β-O-4 bonds[21, 22] and a decrease in the molecular weight of lignin at extended pretreatment times[23, 24]. Steam hydrolysis of *Populus tremuloides* by Bardet et al.[25] resulted in the extensive cleavage of β-O-4 bonds but this evidence of depolymerization was not accompanied by high yields of lignin monomers, leading Bardet et al. to suggest that reactions counteracting monomer formation occur. Additional evidence of repolymerization includes an increase in molecular weight during shortened pretreatments[21, 23, 24], an increase in carbon-carbon bonds based on changes in the substitution patterns of the aromatic rings as detected by infrared spectroscopy[24], and a decrease in the yield of aromatic aldehyde from alkaline

nitrobenzene oxidation of pretreated lignin[26]. The relative rates of depolymerization and repolymerization during the course of pretreatment are uncertain. A previous comparison of the batch pretreatment of isolated lignin and wood found that condensation reactions occur more rapidly in isolated lignin.[24] The slower reaction rate in wood was attributed to the diffusional effects and the reaction of carbohydrate degradation products in condensation.[24] Previous work has shown that the conversion of xylan could be correlated to a general reaction ordinate or severity parameter[27]:

$$\log R_o = \log\left(t_{rxn} \exp\left(\frac{T_{rxn} - 100^o C}{14.75} \right) \right) \quad (1)$$

where t_{rxn} is the reaction time in minutes and T_{rxn} is the reaction temperature in ^oC. The parameter is useful for comparing the combined effects of temperature and time on the extent of reaction.

In addition to these carbohydrate-lignin reactions, there is evidence to suggest that the presence of carbohydrates influences the solubility of lignin during pretreatment. The addition of carbohydrates such as pectin or arabinoxylan during the *in vitro* synthesis of artificial lignin (dehydrogenation polymer, DHP) resulted in an increase in the molecular weight of the lignin produced.[28, 29] This was likely the result of the formation of hydrophobic complexes between the DHP and carbohydrates that prevented the precipitation DHP as monomer units were added to the polymer chain.[28, 29, 30] Barakat and coworkers[28] also found that the structure of the artificial lignin produced in the presence of arabinoxylan more closely resembles that of native lignin. The covalent bonds between lignin and hemicellulose or the formation of hydrophobic aggregates may

also improve lignin solubility during lignin deconstruction. When corn stover was subjected to flowthrough pretreatment there was a linear relationship between xylan and lignin removal, leading to the hypothesis that lignin is released to solution as part of a LCC and once in solution the bonds within the LCC break, producing lignin and carbohydrate fragments.[31, 32, 33] The lignin fragments could be soluble at reaction temperature or when connected to more soluble carbohydrate oligomers but they are insoluble once the LCC decomposes or once the reactor is cooled.[32, 34].

The objectives of this chapter are to examine the importance of phase transition, reaction, and solubility to the deconstruction of lignin during pretreatment by pretreating cellulolytic enzyme lignin isolated from *P. trichocarpa* (CEL) in batch and flowthrough systems. Lignin removal and changes in molecular weight, chemical bonds and functional groups, and soluble phenol products will be examined. *P. trichocarpa* will be pretreated under the same conditions in order to study the extent of lignin removal and production of phenols in the presence of polysaccharides. Differences in the results of the pretreatment of CEL and *P. trichocarpa* may reflect the interactions between lignin and polysaccharides.

7.3. Experimental apparatus and procedure

7.3.1. Experimental apparatus

Two substrates were used in this study: *Populus trichocarpa*, which was described in chapter 4, and cellulolytic enzyme lignin (CEL) isolated from *Populus trichocarpa*. The CEL isolation procedure, performed by Dr. Shilin Cao (Georgia Institute of Technology), was based on methods described by Chang et al.[35] and

Björkman[36]. The first step in isolating CEL was to perform an extraction using a 2:1 v:v solution of benzene/ethanol for twenty-four hours, followed by a second twenty-four hour extraction with water at 60°C. The extractive free solids were dried for seventy-two hours in a vacuum oven in the presence of P_2O_5, a desiccant. *P. trichocarpa* was ball-milled for 7 days in a 1 L vibratory porcelain jar under a nitrogen atmosphere; the porcelain ball to biomass weight ratio was 30:1. The ball-milled powder was then subjected to enzymatic hydrolysis with 500 IU cellulase/g *P. trichocarpa* (Novozym 188, Sigma-Aldrich, St. Louis, MO) and 200 IU β-glucosidase/g *P. trichocarpa* (Celluclast 1.5L, Sigma-Aldrich, St. Louis, MO) for seventy-two hours at 50°C shaken at a frequency of 150 rpm. The residual solids were washed three times with HCl (pH=2) followed by distilled water. Lignin was solubilized by two applications of dioxane/water (96 wt%, 1 g:10 mL) in a dark, coned beaker for twenty-four hours. Centrifugation was used to separate the lignin solution from the insoluble residue, and the lignin solution was concentrated by rotary evaporation. The concentrate was added drop-wise to distilled water causing lignin to precipitate; the final volume ratio was 1 mL lignin concentrate to 250 mL distilled water. The lignin precipitate was recovered by centrifugation and then freeze dried. This crude lignin was dissolved in an acetic acid solution (1 g acetic acid:20 mL distilled water) and then reprecipitated by drop wise addition to water. The precipitate was recovered by centrifugation and freeze-drying.

Pretreatment was conducted in the flowthrough and batch reactor systems described in chapter 5.

7.3.2. Experimental procedures

7.3.2.a. Pretreatment

A representative flowthrough pretreatment run is described. Prior to flowthrough pretreatment at 140°C, the pump was primed, and the sand bath was heated to 149°C. The reactor was loaded with 0.71 g dry CEL and attached to the flowthrough piping system. The pump was set to 20 mL/min and started, and the back pressure gauge was adjusted to 0.28 MPag. The pressurized system was inspected for leaks at room temperature. After fixing any leaks, the reactor and heating coil were lowered into the sand bath, and the cooling coil was lowered into the water bath. A Digi-Sense DualLogR Thermocouple Meter was used to monitor the reactor temperature during the run. The hydrolysate produced as the reactor was heated was collected in a pre-massed flask. The time at which the temperature reached 138°C (T_{rxn}-2°C) was recorded as the start of the reaction. Samples were collected in three minute intervals using pre-massed flasks, massed, and retained for analysis. After twelve minutes, the reactor and heating coil were transferred to a water bath and cooled to 70°C, at which point the pump was stopped and the reactor was removed from the piping. The residual solids in the reactor were collected by filtration, washed with three 100 mL volumes of deionized water, and dried at 45°C for twenty four hours. As the solids had fused to the reactor, vigorous scraping was required to recover them.

For a typical batch pretreatment run, the sand bath was heated to 142°C. A batch reactor loaded with 0.70 g lignin and 7.6 mL of deionized water was sealed, shaken, and allowed to soak for 3.5 hours. A separate reactor equipped with a thermocouple was

loaded with 8.34 mL deionized water. Both the tube reactor and thermocouple reactor were placed into a wire basket before being were lowered into the sand bath, and the temperature was monitored with a Digi-Sense DualLogR Thermocouple Meter. The time at which the reactors reached 138^{o}C was taken as the start of the reaction, and the sand bath temperature was reset to 140^{o}C. After 192 minutes, the wire basket and reactors were transferred to a water bath and cooled to 70^{o}C, and the temperature data was transferred to a computer. Following pretreatment, the residual solids were recovered by filtration using a pre-weighed crucible, and the filtrate was retained for analysis. Once again, the solids had fused to the reactor and vigorous scraping was required. The pretreated solids were washed and dried as described above. The solids were stored at room temperature until the analyses was performed.

Table 7.1 summarizes the pretreatment conditions for all runs with both CEL and *Populus trichocarpa*. Flowthrough pretreatment of *P. trichocarpa* employed 1.05 g of biomass, and batch pretreatment of *P. trichocarpa* was conducted in two tube reactors, each loaded with 0.46 g biomass and 7.88 mL of deionized water. Runs with CEL will be referred to as CEL*j* where *j* is the run number. Similarly, pretreatment experiments with *P. trichocarpa* will be referred to as Pt*j*.

Table 7.1. Summary of flowthrough and batch pretreatment conditions for *Populus trichocarpa* and cellulolytic enzyme lignin derived from *P. trichocarpa*. Runs with a flow rate of 0 mL/min are batch pretreatments.

Run (*j*)	Flow rate (Q, mL/min)	Temperature, Sand Bath (T_{sand}, ^oC)	Temperature, Reactor (T_{rxtr}, ^oC)	Set Pressure (P, MPag)	Time (t_{rxn}, min)	Severity (log R_o)	Sample Interval (Δt, min)
1	20	149	140	0.28	12	2.26	3
2	20	149	140	0.28	192	3.46	15
3	0	142	140	n/a	192	3.46	n/a
4	20	194	180	1.10	12	3.43	3
5	20	194	180	1.10	192	4.64	15
6	0	182/180	180	n/a	12	3.43	n/a

7.3.2.b Analytical techniques

7.3.2.b.i. Gel permeation chromatography

Dr. Marcus Foston (Georgia Institute of Technology) determined the number average and weight average molecular weights of CEL before and after pretreatment by gel permeation chromatography using the procedure described by Samuel et al.[37] To prepare acetylated lignin for analysis, 20 mg of CEL was dissolved in 1 mL of 1:1 pyridine/acetic anhydride for twenty-four hours at room temperature. Adding 5 mg of ethanol quenched the reaction and remaining anhydride. The solvents were removed by overnight evaporation in a vacuum oven. The acetylated lignin was dissolved in tetrahydrofuran injected in an Agilent GPC SECurity 1200 system with a refractive index detector and a UV detector (270 nm) using tetrahydrofuran as an eluent at a flow rate of 1.0 mL/min. Four Waters Styragel columns (HR1, HR2, HR4, HR6) were used to separate the acetylated lignin by molecular weight. The calibration curve was constructed using eight polystyrene standards ranging in molecular weight from 1.5×10^3

to 3.6 x 10^6 g/mol. The data was collected and processed using Polymer Standards Service WinGPC Unity software (Build 6807). The number and weight average molecular weights were calculated as:

$$\overline{M_n} = \frac{\sum_i N_i M_i}{\sum_i N_i} \quad (2)$$

$$\overline{M_w} = \frac{\sum_i N_i M_i^2}{\sum_i N_i M_i} \quad (3)$$

where N_i is equal to number of polymers detected having molecular weight M_i.

7.3.2.b.ii. Heteronuclear single quantum coherence nuclear magnetic resonance

Dr. Marcus Foston used Heteronuclear Single Quantum Coherence Nuclear Magnetic Resonance (HSQC NMR) to analyze the functional groups and intra-lignin bonds of CEL. CEL was prepared for HSQC by dissolving 60 mg solids in 1 mL of dimethyl sulfoxide. However, because complete dissolution of the pretreated CEL was not achieved, the results can only be interpreted qualitatively. 2D ^{13}C-^{1}H HSQC correlation NMR spectra were recorded on Bruker DRX 500 spectrometer with a 5 mm z-gradient triple resonance probe with inverse geometry at 60 °C. Analysis was performed with a Bruker phase-sensitive gradient-edited HSQC pulse sequence using 1024 data points for a 0.11 s acquisition time, a 1.5 s recycle delay, a $^{1}J_{C\text{-}H}$ coupling constant of 145 Hz, and acquisition of 256 data points in the F1 dimension. The data was processed using zero-filling to 2048 points and a typical squared sine-bell apodization in both F2 and F1 dimensions. Cross peaks were assigned according to Samuel et al.[37] as listed in Table 7.2.

Table 7.2. Assignment of ^{13}C-^{1}H correlation signals in the HSQC spectrum of cellulolytic enzyme lignin isolated from *Populus trichocarpa.*[37]

δ_C/δ_H (ppm)	Assignment
53.2/3.5	C_β/H_β in phenylcoumarin substructure (B)
53.6/3.1	C_β/H_β in resinol (β-β) substructure
55.7/3.8	C/H in methoxyl group
60.2/3.6	C_γ/H_γ in β-O-4 substructure (A)
62.8/3.8	C_β/H_β in phenylcoumarin substructure (B)
71.5/4.8	C_α/H_α in β-O-4 linkage
84.8/4.3	C_β/H_β in β-O-4 linkage
81.4/5.1	C_β/H_β in spirodienone substructure (C)
84.7/4.7	C_α/H_α in spirodienone substructure (C)
87.1/5.5	C_α/H_α in phenylcoumarin substructure (B)
104.3/6.7	$C_{2,6}/H_{2,6}$ in etherified syringyl units (S)
105.5/7.3	$C_{2,6}/H_{2,6}$ in oxidized C_α=O (S')
113.7/6.3	C_β/H_β in cinnamate unit (E)
111.4/7.0	C_2/H_2 in guaiacyl units (G)
115.4/6.77	C_5/H_5 in guaiacyl units (G)
119.3/6.82	C_6/H_6 in guaiacyl units (G)
130.0/7.5	$C_{2,6}/H_{2,6}$ in p-hydroxyphenyl units
144.7/7.5	C_α/H_α in cinnamate unit (E)

7.3.2.b.iii. Gas chromatography-mass spectrometry

The phenols in the hydrolysates from the pretreatment of CEL and *P. trichocarpa* were determined by Ms. Nancy Engle and Dr. Tim Tschaplinski (Oak Ridge National Laboratory) using trimethylsilyl (TMS) derivatization and analysis by gas chromatography-mass spectrometry (GCMS)[38, 39] (Jung et al. 2009, Li et al. 2011). The samples were first filtered through a 0.45 μm nylon membrane, and 0.5 ml aliquots were dried in a helium stream. Sorbitol (15 μL of a 1 mg/mL aqueous solution) was added as

an internal standard to correct for differences in derivatization efficiency and changes in sample volume during heating. The dried extracts were dissolved in 500 μL of silylation–grade acetonitrile followed by the addition of 500 μL N-methyl-N-trimethylsilyltrifluoroacetamide with 1% trimethylchlorosilane. To generate trimethylsilyl derivatives, the samples were heated for one hour at 70°C. After 2 days, 1-μL aliquots were injected into an Agilent Technologies Inc. 5975C inert XL gas chromatograph-mass spectrometer. Key mass/charge (m/z) ratios for identified aromatic metabolites were extracted from the total ion current to quantify metabolites free from co-eluting interference.

7.3.2.b.iv. Structural carbohydrate and Klason lignin analysis

The glucan, xylan, and Klason lignin content of the raw and pretreated *P. trichocarpa* as well as the raw CEL were determined using the two-step acid hydrolysis procedure outlined by Sluiter et al.[40] No extraction was performed prior to the two-step acid hydrolysis because *P. trichocarpa* contains few extractives. After hydrolysis, a 2 mL liquid sample was withdrawn and centrifuged; the sample supernatant was not neutralized. Sugars in the sample were detected by HPLC using an Aminex HPX-87H column (BioRad, Hercules, CA) heated to 65^{o}C with a separation module (Alliance 2695, Waters, Milford, MA) equipped with a refractive index detector (2414, Waters). The eluent was 0.005 M sulfuric acid in the isocratic mode. The measured glucose and xylose concentrations were converted to glucan and xylan equivalents by dividing by 1.1111 and 1.3622, respectively, to account for mass gain during hydrolysis.

7.4. Results and discussion

7.4.1. Hydrothermal pretreatment of cellulolytic enzyme lignin

7.4.1.a. Changes in the physical appearance of cellulolytic enzyme lignin following hydrothermal pretreatment

Figure 7.3 is photos of the raw and pretreated CEL from batch and flowthrough pretreatments and Figure 7.4 is a photo of the batch reactor containing CEL after pretreatment at 180^{o}C for 12 minutes. All of the photos show that the color and morphology of CEL changed significantly during pretreatment. Although it is difficult to see in CEL1 and CEL2, lignin formed a bead with an outer diameter equal to that of the reactor and an inner channel for the flow of water during flowthrough pretreatment. Figure 7.4 illustrates the molding and fusing of CEL to the reactor. An attempt was made to examine the solids with scanning electron microscopy (SEM). However, this required breaking the large solid samples so the SEM images reflected the shattering of the solids as opposed to features resulting from pretreatment, making the images of little value. The molding of CEL to the reactor suggests that the solids underwent a phase transition even at 140^{o}C.

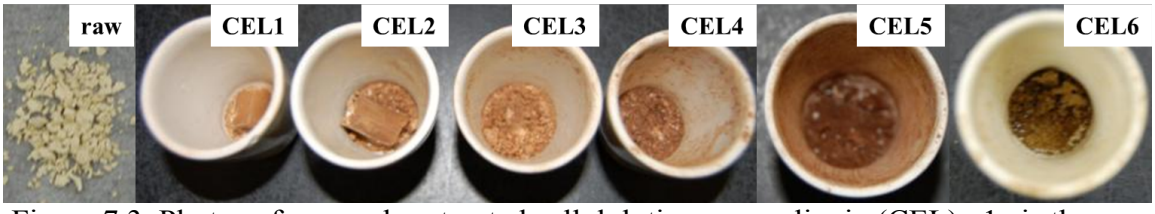

Figure 7.3. Photos of raw and pretreated cellulolytic enzyme lignin (CEL). 1a is the raw, untreated CEL. CEL1, 2, and 3 were pretreated at 140^{o}C while samples CEL4, 5, and 6 were pretreated at 180^{o}C. Samples CEL1, 4, and 6 were pretreated for 12 minutes while samples CEL2, 3, and 5 were pretreated for 192 minutes. Samples CEL1, 2, 4, and 5 were subjected to flowthrough pretreatment. Samples CEL3 and 6 were subjected to batch pretreatment.

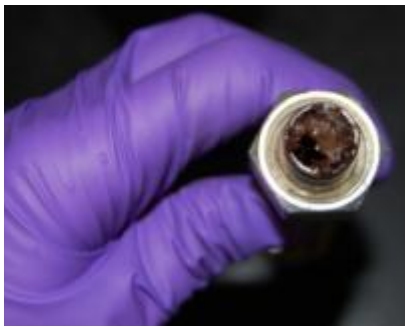

Figure 7.4. Cellulolytic enzyme lignin (CEL) after batch pretreatment at 180^{o}C for 12 minutes (CEL6) prior to removal from the reactor.

7.4.1.b. Lignin removal during hydrothermal pretreatment of cellulolytic enzyme lignin

The percent lignin removal from CEL by pretreatment shown in Figure 7.5 was determined from the difference in the mass of solids loaded in the reactor and the mass of solids recovered after pretreatment. Comparison of runs CEL2 and CEL3, and CEL4 and CEL 6 show that at equal temperature and time, more lignin is removed during flowthrough pretreatment. Therefore, the flow of water removes lignin fragments redeposited. The lignin removal in run CEL1 was approximately equal to the lignin removal in run CEL3 despite CEL3 lasting sixteen times longer, suggesting that interrupting the lignin cycle can shorten pretreatment times without compromising lignin removal. Another striking result in Figure 7.5 is that although run CEL5 was sixteen times longer than run CEL4, lignin removal increased by only 3%. Since flowing water appears to significantly disrupt lignin redeposition it appears that there is a fraction of lignin resistant to removal. Finally, if phase transition were the key factor in solids loss, one would expect the solids removal during the two batch pretreatments (CEL3 and CEL6) to be approximately equal. However, the solids removal by pretreatment at 180^{o}C

is 7% greater than the solids removal by pretreatments at 140°C suggesting that a temperature dependent mechanism is primarily responsible.

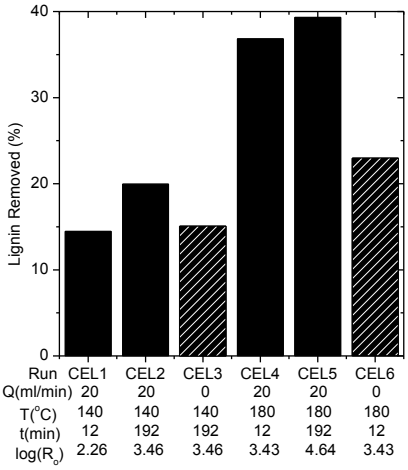

Figure 7.5. Percent lignin removal from CEL during flowthrough and batch pretreatment. Removal was calculated by the mass balance of solids loaded in the reactor before pretreatment and the solids recovered from the reactor after pretreatment.

7.4.1.c. Changes in the molecular weight of cellulolytic enzyme lignin following hydrothermal pretreatment

The number and weight average molecular weights of CEL were determined before and after pretreatment using GPC and Equations (2) and (3). The results shown in Figure 7.6a show that the number average molecular weight of the flow and batch pretreated pairs (CEL2 and CEL3, CEL4 and CEL6) were similar while the weight average molecular weights of the batch pretreated CEL (CEL3 and CEL6) were 16 to 18% higher. Since the weight average molecular weight is more sensitive to the presence of large polymers, there must be more long chain polymers in the batch pretreated CEL than flow pretreated CEL. The solids had equal residence times during batch and flowthrough pretreatment, but compounds in the bulk liquid had a short residence time,

0.15 min, during flowthrough pretreatment. Therefore, while solid phase reactions, such as depolymerization could proceed continuously during pretreatment, reactions in the liquid phase such as repolymerization were cut short by flowthrough pretreatment. The increase in the solids' molecular weight after run CEL1 also suggested repolymerization reactions. Others[21, 23, 24] have also reported increases in the molecular weight of lignin following pretreatment.

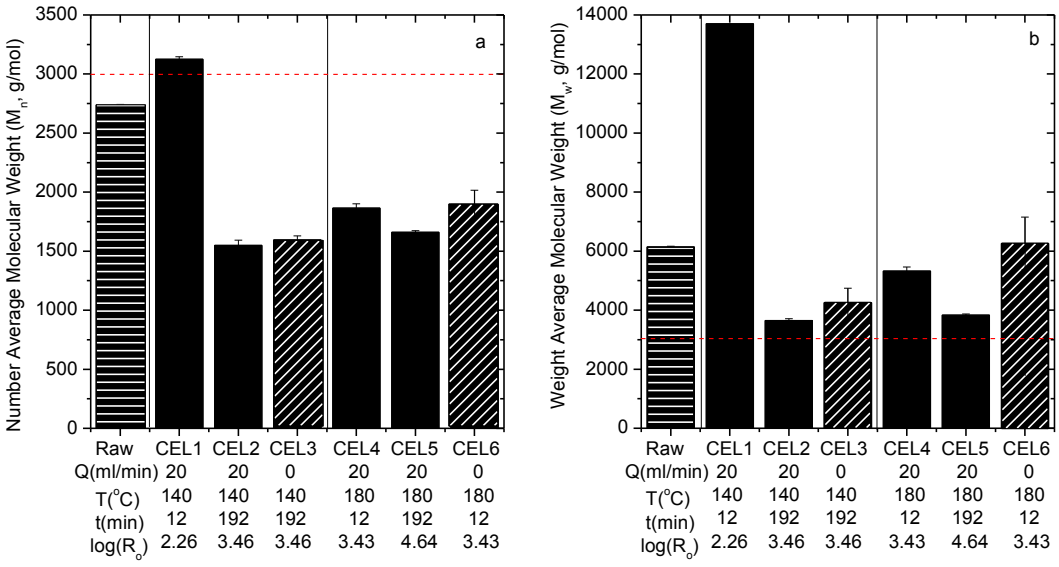

Figure 7.6. Number average (a) and weight average (b) molecular weights of cellulolytic enzyme lignin (CEL) before (horizontal hatching) and after flowthrough (solid) and batch (diagonally hatching) pretreatment as determined by gel permeation chromatography. The red dashed line represents a molecular weight of 3000 on both figures.

7.4.1.d. Changes in the structure and composition of cellulolytic enzyme lignin following hydrothermal pretreatment

HSQC NMR was applied to examine the inter-unit linkages in CEL, but due to difficulties in dissolving pretreated CEL for analysis, the results presented in Figure 7.7 can only be interpreted qualitatively. Three general trends can be observed. The spectra of the raw CEL provide evidence of residual carbohydrates which are not present in the

spectra of the pretreated materials, indicating that all of the residual carbohydrates were removed or reacted to produce pseudo-lignin[41]. Although the morphological changes in CEL prevented compositional analysis of the solids following pretreatment, Sluiter's method[40] would not provide any additional information because it cannot differentiate Klason lignin from pseudo-lignin. Second, the broader, more distorted appearance of aromatic cross-peaks in the spectra (recorded under identical conditions) of the pretreated materials was indicative of a significantly reduced signal to noise ratio with respect to untreated CEL. This was attributed to altered solubility and a modified lignin structure with low local molecular mobility presumably due to condensation reactions. Finally, the relative intensity of signals resulting from the pretreated spectra were less intense in comparison to the signals in the spectra of the raw CEL, indicating a loss of methoxy groups, β-O-4 ether bonds, β-5/α-O-4 phenyl-coumararan bonds and spirodienone bonds. The significance of these observations will be discussed below.

The key aromatic and aliphatic chemical moieties in CEL were also observed using HSQC-NMR and well-established lignin spectral assignments[37]. Again, HSQC-NMR is inherently difficult to quantitate for a polymer system for a variety of reasons as outlined by Zhang et al.[42], although methods for semi-quantification have been proposed[43, 44]. Moreover, because of the difficulties in dissolving CEL for NMR, the results in Figure 7.8 are only discussed qualitatively. Once again, the cross peaks in the spectra of the pretreated CEL were broad and distorted due to a low signal to noise ratio and altered nuclear relaxation. The relative decrease in signal intensity of each cross-peak indicated a reduction in the number of functional groups.

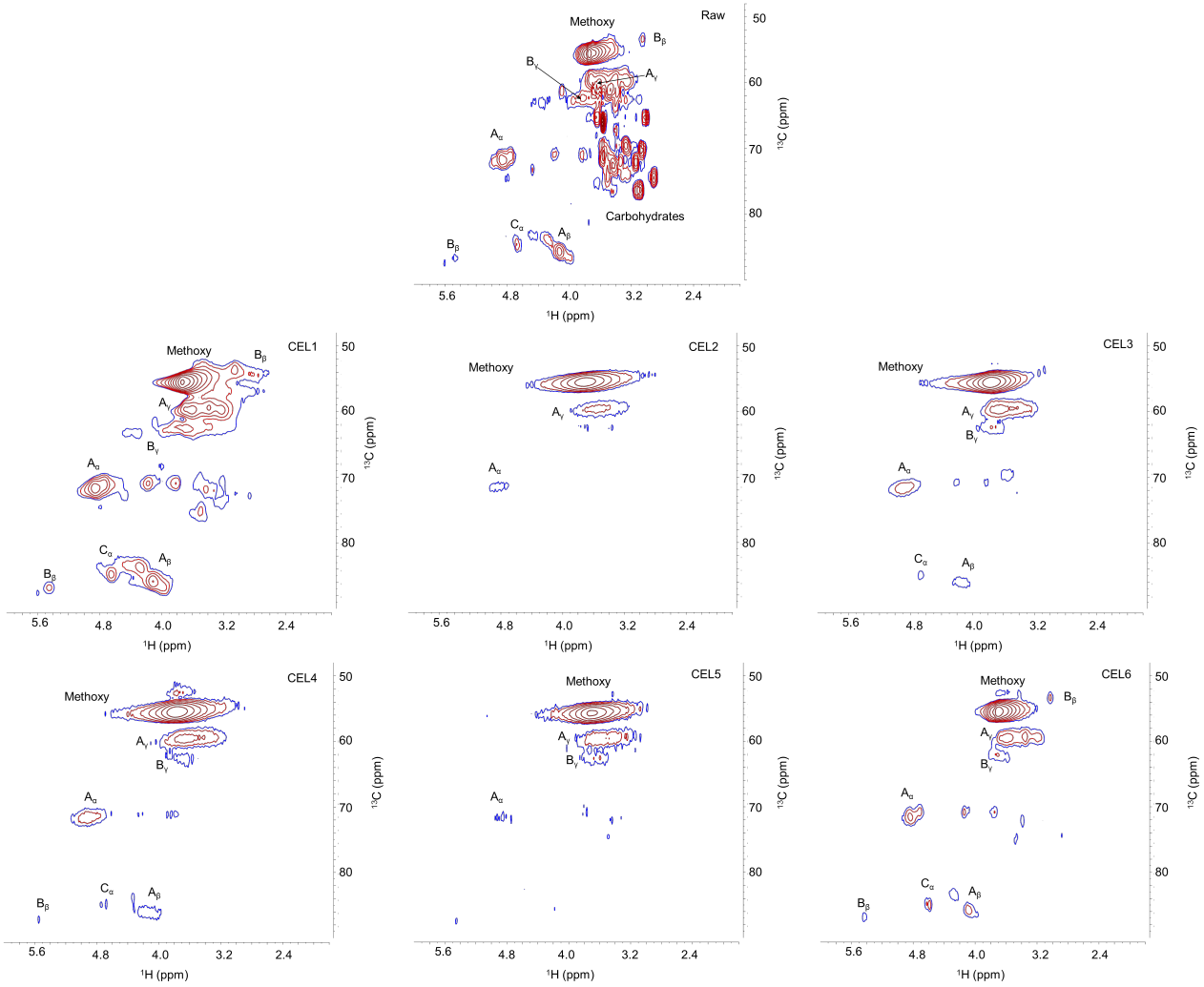

Figure 7.7. HSQC NMR spectra of raw and pretreated cellulolytic enzyme lignin in the aliphatic region. Identified units include methoxy groups, β-*O*-4 ethers (A_α, A_β, A_γ), β-5/α-*O*-4 phenyl-coumararan (B_α, B_β, B_γ), and spirodienone (C_α) units.

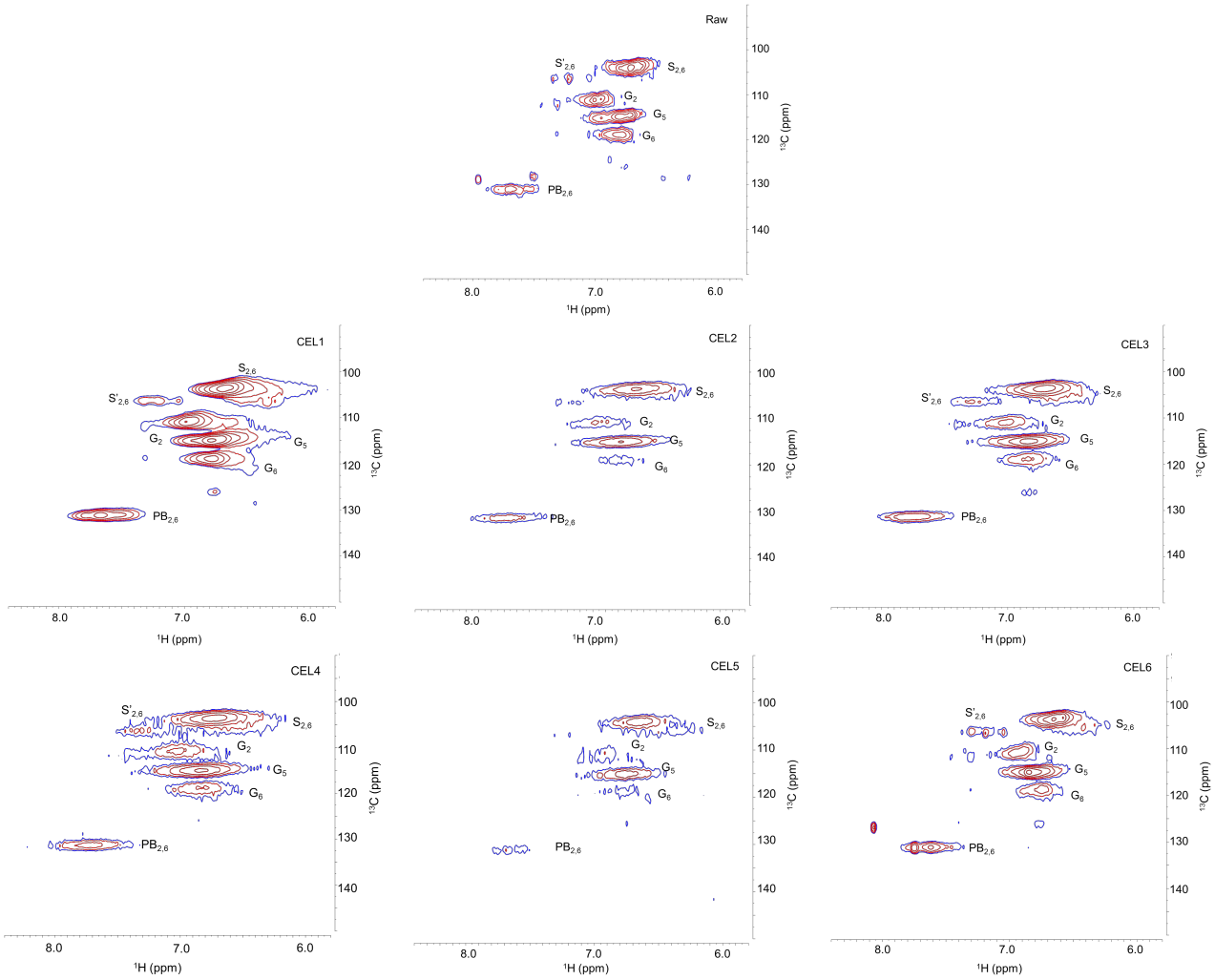

Figure 7.8. HSQC NMR spectra of raw and pretreated cellulolytic enzyme lignin in the aromatic region. Identified units include p-hydroxyphenyl ($PB_{2,6}$), guaiacyl (G_2, G_5, G_6), syringyl ($S_{2,6}$), and oxidized syringyl ($S'_{2,6}$) units.

The poor solubility of the pretreated solids and the low signal to noise ratio of the spectra in Figures 7.7 and 7.8 are typically associated with large polymers. Similarly, the suspected change in nuclear relaxation is also normally related to significant a reduction in local molecular mobility such as systems with increased numbers of fixed carbon centers. However, the loss of aliphatic functionality, typically associated with monolignol inter-unit linkages, suggested depolymerization to an extent that makes the molecular weights reported in Figure 7.6 seem surprisingly high. This was particularly true for run CEL1 where the loss of functional groups was accompanied by an increase in molecular weight. The evidence of large polymers combined with loss of ether bonds and functional groups suggest that the repolymerization of lignin resulted in a condensed polymer with primarily carbon-carbon bonds and little branching, in agreement with results from previous studies.[24, 26]

7.4.1.e. Production of phenols from the hydrothermal pretreatment of cellulolytic enzyme lignin

Gas-chromatography mass-spectrometry was used to detect phenols in the hydrolysate produced by the pretreatment of CEL. The cumulative release of total phenols normalized to the mass of raw solids is plotted as a function of pretreatment time for runs CEL1, CEL2, CEL4, and CEL5 in Figure 7.9, and the cumulative release of key individual phenols is also presented. The distribution of phenols produced by CEL3 and CEL6 are shown as pie charts in the same figure along with the total normalized mass of phenols detected. In total, eighteen phenol monomers including hydroquinone, *p*-hydroxybenzoic acid, coniferyl alcohol, *p*-coumaryl alcohol, 5-hydroxyconiferyl alcohol,

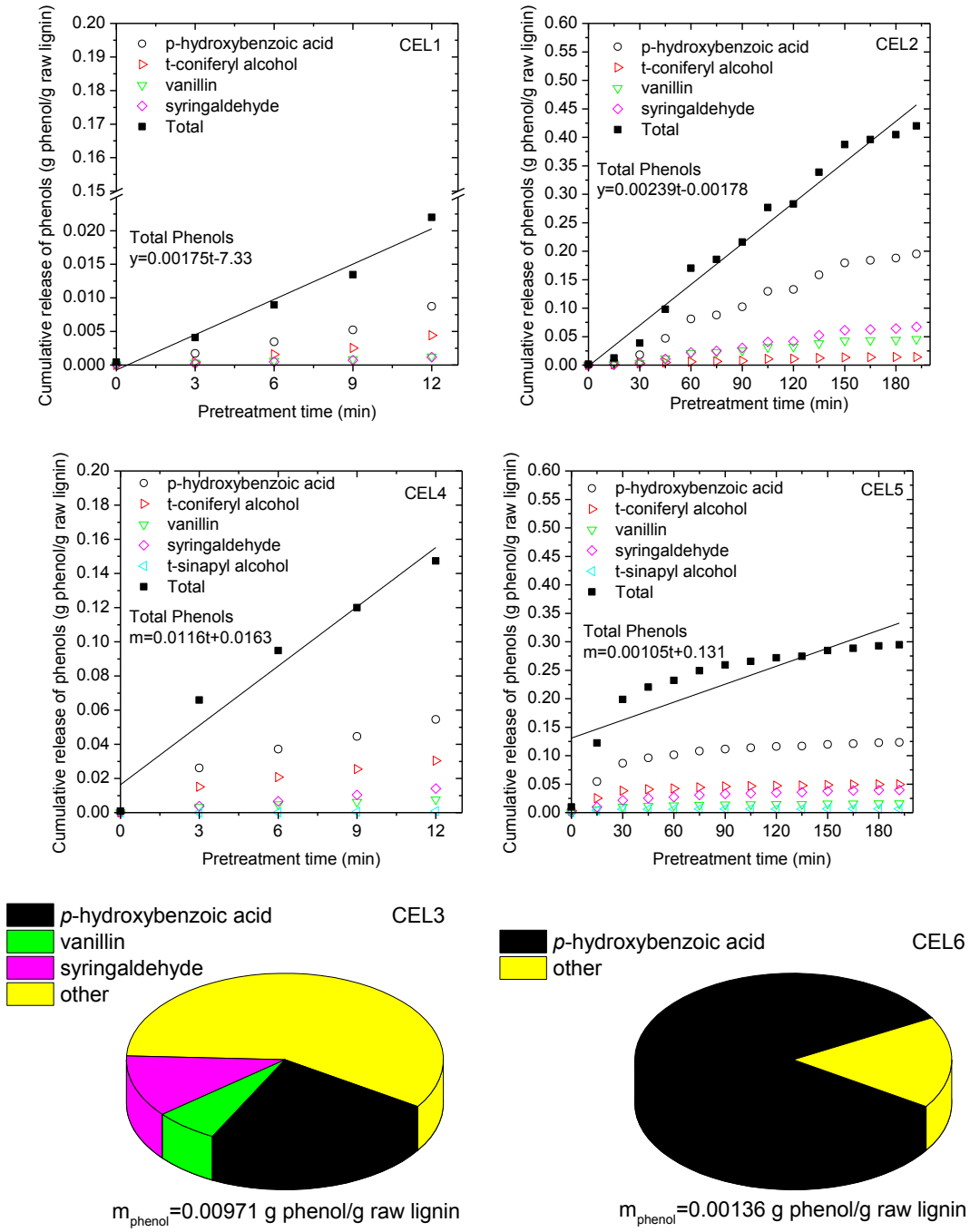

Figure 7.9. Phenols in the hydrolysate generated by the flowthrough and batch pretreatment of cellulolytic enzyme lignin.

vanillic acid, protocatechuic acid, syringic acid, syringylglycerol (erythro and threo), coniferyl aldehyde, sinapyl aldehyde, syringaresinol, vanillin, syringaldehyde, sinapyl alcohol, medioresinol, and pinoresinol were identified. Eighteen other detected compounds could not be identified but were believed to likely also be phenols.

Figure 7.9 shows that there were very few monomers in the hydrolysates from batch pretreatment. When this observation is considered in tandem with the other batch pretreatment results: low solids removal, high weight average molecular weight, and loss of characteristic bonds and side chains, the case for the condensation reactions becomes very strong. The product profile after batch pretreatment at 140^{o}C (run CEL3) was much more diverse than after pretreatment at 180^{o}C (run CEL6); in fact, *p*-hydroxybenzoic acid accounted for 83% of the phenols produced during CEL6. This result suggests that the condensation of phenols, with the exception of *p*-hydroxybenzoic acid, was much greater at 180^{o}C. Greater repolymerization at 180^{o}C was also supported by the fact that the weight average molecular weight of CEL6 was slightly higher than the weight average molecular weight of CEL3, as shown in Figure 7.6b.

Comparison CEL1 with CEL2 and CEL4 with CEL5 shows that the mass of total phenols at the 12 and 15 minute marks are comparable, demonstrating repeatability of pretreatment. However, the relative rates of generation, as represented by the slope of the fitted line, are quite different. During the first 12 minutes of pretreatment at 140^{o}C, the rate of phenol production was slower than the rate of phenol production during run CEL2; the opposite was true at 180^{o}C. In terms of severity (Equation (1)), runs CEL2 and CEL4 were equivalent, while run CEL5 was more severe. Therefore, it is possible

that the decrease in reaction rate from run CEL4 to run CEL5 could occur if a pretreatment longer than 192 minutes was performed at 140°C.

Comparison of the production rate and total mass of phenols at 140°C and 180°C for 12 minutes (CEL1 and CEL4) revealed, unsurprisingly, that phenols were produced more rapidly and in greater amounts at 180°C. However, it is surprising that the production rate and total mass of phenols released after 192 minutes of pretreatment at 140°C (CEL2) was greater than the rate and mass of phenols produced at 180°C (CEL5). Given that the total mass of lignin removed during run CEL5 was greater than the total mass removed by run CEL2 (Figure 7.5) and that the molecular weights of the solids recovered from these runs were similar, it seems unlikely that condensation reactions accelerated relative to the depolymerization reactions at 180°C. The lower mass of phenol monomers at 180°C could be because the higher temperature allowed for production of phenol oligomers that were undetectable by GCMS due to their low volatility.

p-Hydroxybenzoic acid is the primary phenol observed in the hydrolysate for all runs. However, based on the HSQC spectra of raw CEL in Figure 7.8 CEL contains fewer *p*-hydroxybenzoate groups than syringyl and guaiacyl units. Therefore, it appears that *p*-hydroxybenzoate groups were produced more easily from CEL than syringyl or guaiacyl groups. Since *p*-hydroxybenzoic acid could limit condensation reactions, the increase in molecular weight following run CEL1 could be due to a lack of *p*-hydroxybenzoic acid. However, this seems unlikely because the proportions of *p*-

hydroxybenzoic acid found in the CEL1 and CEL4 hydrolysate were similar, and the molecular weight of CEL4 solids was lower than that of the raw CEL.

It has been previously suggested that due to greater propensity for covalent linkages, guaiacyl units are less easy to extract than syringyl units during hydrothermal pretreamtment.[26, 37, 45] It has also been shown that due to the lack of a methoxyl group in the C5 position, guaiacyl units undergo condensation reactions more easily.[26] This hypothesis is supported by the greater coniferyl alcohol production during flowthrough pretreatment at 180°C in comparison to flowthrough pretreatment at 140°C. However, the hypothesis is contradicted by the greater quantity of coniferyl alcohol and vanillin relative to sinapyl alcohol and syringaldehyde in the CEL1, CEL4, CEL5, and CEL6 hydrolysate. Similarly Martin et al.[46] observed approximately double the amount of vanillin as syringaldehyde in the hydrolysate from steam explosion of bagasse. These results are compared with the results of pretreatment of *P. trichocarpa* in section 7.4.2.c.

7.4.2. Hydrothermal pretreatment of *Populus trichocarpa* and comparison to the hydrothermal pretreatment of cellulolytic enzyme lignin

7.4.2.a. Lignin removal during hydrothermal pretreatment of *Populus trichocarpa*

The percent lignin removal from *P. trichocarpa* by pretreatment was determined from the difference in the mass of lignin in the biomass loaded into the reactor initially and the mass of the lignin in the pretreated biomass. These results are shown in Figure 7.10 along with the lignin removal from CEL after the same pretreatments. As with CEL, more lignin was removed during flowthrough pretreatment of *P. trichocarpa* than during batch pretreatment, indicating that flow of water removes lignin fragments from the

reactor before they return to the solid phase. From Figure 7.10, it can be seen that more lignin was removed by batch pretreatment of CEL than was removed from *P. trichocarpa*. This could be due to the formation of pseudo-lignin from carbohydrates.[41] However, because no Klason lignin was detected in holocellulose pretreated at the same conditions (data not shown), pseudo-lignin formation during these batch pretreatments seems unlikely. The difference may be due to the difficulty in recovering pretreated CEL from the reactor. It can also be seen in Figure 7.10 that more lignin was removed from *P. trichocarpa* than from CEL during flowthrough runs 2, 4, and 5. This outcome could be due to differences in surface area or to the presence of polysaccharides.

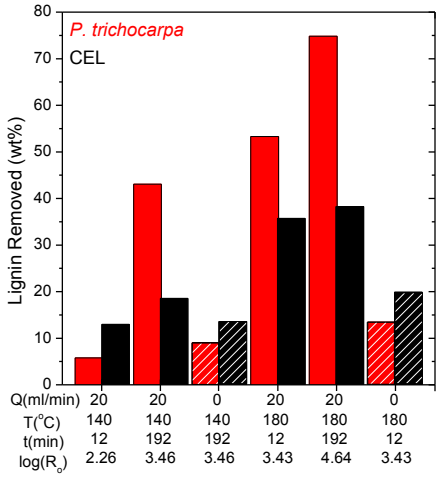

Figure 7.10. Percent lignin removal from *Populus trichocarpa* and cellulolytic enzyme lignin (CEL) during pretreatment as calculated from mass balance of solids loaded in reactor before pretreatment and solids recovered from the reactor after pretreatment.

Unlike CEL, *P. trichocarpa* remained as discrete particulates during pretreatment which could result in substantial differences in reactive surface areas and hence delignification during pretreatment. In order to examine this possibility, a series of simple

models were applied. For a reaction at a solid-liquid interface, the rate of reaction is given by[47]:

$$r = k''\rho_p A_{surf} f(C) \quad (4)$$

where k'' is the rate constant per unit surface area, ρ_p is the particle density, A_{surf} is the surface area, and $f(C)$ is a function of reactant concentration. From Equation (4) it can be seen that the rate and extent of lignin extraction should be proportional to the surface area. To examine surface area effects, it was first assumed that all parameters were constant except the surface area. Based on the appearance of the residual solids, the pretreatment of *P. trichocarpa* was modeled as a bed of nonporous spherical lignin particles with constant diameter; no allowance was made for the presence of polysaccharides. Therefore, the surface area was calculated as[48]:

$$A_{surf,Pt,F} = \frac{6(1-\varepsilon)\pi r_{rxtr}^2 h_{rxtr}}{D_p} \quad (5)$$

where ε is the void fraction of the bed and is assumed to be equal to 0.762 as determined by Torget et al.[49] The particle size, D_p, was assumed to be 0.18 mm, the minimum radius of the sieved *P. trichocarpa* used in this study. From Equation (5), the surface area during flowthrough pretreatment of *P. trichocarpa* was estimated to be 0.15 m^2. Flowthrough pretreatment of CEL was modeled as a tube with an outer radius r_{rxtr} and an inner radius of $0.5r_{rxtr}$ with the surface area calculated by:

$$A_{surf,CEL,F} = \pi r_{rxtr}[0.75r_{rxtr} + h_b] \quad (6)$$

where h_b is the height of the cylinder equal to 15 mm. Therefore, the surface area of CEL during flowthrough pretreatment was estimated to be $4.0*10^{-4}$ m^2. The solid interface

during the batch pretreatment of CEL was modeled as a solid cylinder with only the upper surface available for reaction, the area of which was calculated by:

$$A_{surf,CEL,B} = \pi r_{rxtr}^2 \quad (7)$$

From Equation (7), the surface area of CEL during batch pretreatment was estimated to be $1.2*10^{-4}$ m^2. The ratios of these surface areas are presented in Table 7.3a (left), and the ratios of mass removed by pretreatment at 180°C are presented in Table 7.3b (right). Comparison of these two tables quickly reveals that differences in surface areas were far too great relative to the differences in mass removal to account for the differences in lignin removal from *P. trichocarpa* and CEL. The concentration of lignin during pretreatment of *P. trichocarpa* was lower than the lignin concentration during pretreatment of CEL. If f(C) in Equation (4) is assumed to follow a power law, then:

$$r = k'' \rho_p A_{surf} C^n \quad (8)$$

The ratio of mass removed is proportional to Equation (7) for each system; for example:

$$\frac{m_{Pt,F}}{m_{CEL,B}} \propto \frac{\left(k'' \rho_p A_{surf} C^n\right)_{Pt,F}}{\left(k'' \rho_p A_{surf} C^n\right)_{CEL,B}} \quad (9)$$

Assuming the power law dependence is the same for both systems, Equation (9) can be rearranged to solve for the n required to negate the effects of surface area. In order to compensate for differences in surface areas between flowthrough pretreatment of *P. trichocarpa* and batch pretreatment of CEL required a value of n equal to 4.93, while a value of n equal to 4.42 was needed to adjust for differences in surface areas between flowthrough pretreatment of *P. trichocarpa* and CEL. These large exponents further emphasize that the surface area differences were very large relative to the differences in

mass removal. Consequently, it seems more likely that the presence of carbohydrates influences the extent of lignin extraction during pretreatment.

Table 7.3. Ratio of surface areas (a, left) and mass removed (b, right) during condition *i* to surface area during condition *j* for the flowthrough pretreatment of *P. trichocarpa* (Pt, F) and cellulolytic enzyme lignin in flowthrough and batch pretreatment (CEL, F and CEL, B) at 180°C.

Area j / i	CEL, B	CEL, F
Pt, F	1209	384
CEL, F	3	

Mass Removed j / i	CEL, B	CEL, F
Pt, F	2.5	1.5
CEL, F	1.7	

7.4.2.b. Lignin removal as a function of xylan during hydrothermal pretreatment of *Populus trichocarpa*

Lignin removal from *P. trichocarpa* is plotted as a function of xylan removal in Figure 7.11. An attempt was made to fit a linear model to the data, but the adjusted R^2 value, 0.78, indicates a poor fit. This is in contrast to the linear relationship that Liu and Wyman[32, 33] found between xylan and lignin removal from corn stover during flowthrough pretreatment. The lack of a linear relationship in this study may be due to the differences between *P. trichocarpa* and corn stover.

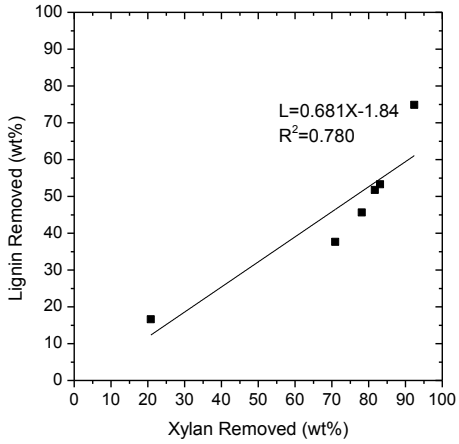

Figure 7.11. Lignin removal from *P. trichocarpa* as a function of xylan removal.

7.4.2.c. Production of phenols from hydrothermal pretreatment of *Populus trichocarpa*

The eighteen phenols identified by gas-chromatography mass-spectrometry in the CEL pretreatment hydrolysates were also identified in the *P. trichocarpa* pretreatment hydrolysates along with the other eighteen unidentifed compounds. In Figure 7.12 the cumulative release of total phenols normalized to the mass of lignin in the biomass loaded in the reactor is plotted as a function of pretreatment time for *Pt*1, *Pt*2, *Pt*4, and *Pt*5. The cumulative release of individual phenols of special interest are also plotted. Figure 7.12 also includes pie charts of the phenols produced by batch pretreatment of *P. trichocarpa* (*Pt*3 and *Pt*6). Comparison of *Pt*1 with *Pt*2 and *Pt*4 with *Pt*5 reveals that the cumulative masses of phenols after twelve and fifteen minutes were comparable, again indicating reproducibility. As with CEL, more phenols were produced during flowthrough pretreatment than batch pretreatment, indicating that flowing water interrupts the repolymerization of lignin.

As with the pretreatment of CEL, *p*-hydroxybenzoic acid was the primary phenol measured for all runs except *Pt*4. Without HSQC analysis of *P. trichocarpa*, the relative content of *p*-hydroxybenzoate units to syringyl and guaiacyl units was unknown. However, given the significant quantities of *p*-hydroxybenzoic acid, it seems likely that these units were released easily.

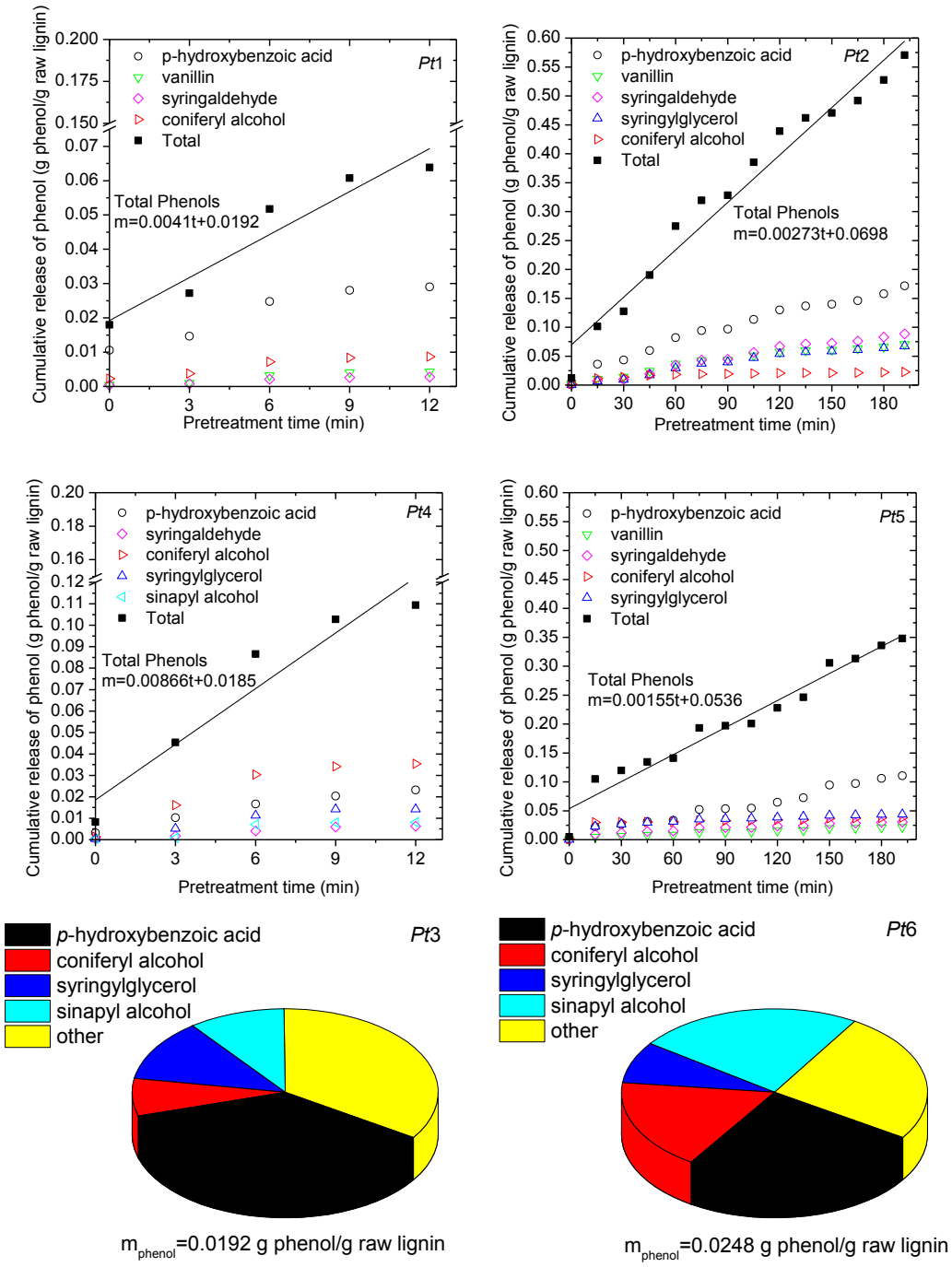

Figure 7.12. Phenols in the hydrolysate from the flowthrough and batch pretreatment of *Populus trichocarpa*.

As with CEL, more coniferyl alcohol was released during runs at 180°C compared to runs at 140°C, suggesting that guaiacyl groups are more difficult to extract from lignin. With the exception of run *Pt*4, syringaldehyde, syringylglycerol, syringylglycerol glycoside, and sinapyl alcohol accounted for a greater percentage of the phenols than coniferyl alcohol and vanillin. This product distribution is in agreement with previous work that found that syringyl units are more reactive.[26, 37] The differences in the relative amounts of guaiacyl type products and syringyl type products from CEL and *P. trichocarpa* suggest that cross-linking between lignin and hemicellulose changes the relative reactivity of guaiacyl and syringyl units.

Similar to CEL, the rate of production and total amount of phenols released from the 12 minute pretreatment at 180°C was greater than the rate of production and total amount of phenols at 140°C but the rate of release and total mass of phenols released after 192 minutes of pretreatment at 140°C were greater than that at 180°C. The mass of lignin removed during run *Pt*5 was higher than the mass of lignin removed during *Pt*2, mirroring the CEL results and reinforcing the hypothesis that condensation reactions do not accelerate relative to depolymerization reactions at higher temperatures. Instead, the comparatively low phenols from run *Pt5* could be due to the formation of soluble, nonvolatile phenol oligomers that were undetectable by GCMS.

Lora and Wayman[24] found that autohydrolysis of aspen proceeded more slowly than autohydrolysis of milled wood lignin and attributed this difference to the reaction of carbohydrate degradation products with lignin products. However in this study, with the exception of *Pt4*, more phenols were produced from *P. trichocarpa* than from CEL.

Differences in results between this study and Lora and Wayman's could be due to a number of factors. The lignin that Lora and Wayman used was produced by ball milling biomass for 18 days followed by a dioxane water extraction, while the CEL used in this study was produced under less severe conditions (7 days ball milling, enzymatic digestion of carbohydrates), thus reducing the possibility of producing an isolated lignin that is more reactive than native lignin. In addition, Lora and Wayman's[24] work was conducted in a batch reactor for which condensation reactions were more significant. As previously noted in this paper, the very short space time of the flowthrough reactor limited production of carbohydrate degradation products and thus carbohydrate dependent condensation reactions. Thus assuming that CEL is representative of native lignin, the greater phenol production from *P. trichocarpa* must be due the presence of carbohydrates increasing lignin solubility, as shown during the *in situ* synthesis of lignin[28, 29, 30], or reactivity.

7.5. Conclusions

Previous studies have shown that during hydrothermal pretreatment, lignin cycles between the solid and liquid phase, but the mechanism was not well understood. In order to investigate the lignin behavior during pretreatment, *Populus trichocarpa* and cellulolytic enzyme lignin (CEL) isolated from *P. trichocarpa* were subjected to batch and flowthrough hydrothermal pretreatment at 140 and 180^{o}C for 12 to 192 minutes. The residual solids and liquid hydrolysate were characterized by a wide range of techniques.

Pretreatment of CEL resulted in loss of characteristic lignin bonds and functional groups from the solids and the production of phenol monomers. However, reductions in

molecular weight were modest. These observations point strongly to depolymerization and condensation being the primary mechanisms for lignin extraction and redeposition. The lack of phenols in the batch pretreatment hydrolysates and presence of larger polymers in batch pretreated solids indicated that condensation reactions were significant during batch pretreatment. However, changes in the appearance of lignin also suggest that phase transition occurred. A possible mechanism, given the branched nature of lignin, is that bond hydrolysis enabled the coalescence and migration of lignin.

There were some similarities in the pretreatment of *P. trichocarpa* and CEL. *p*-Hydroxybenzoic acid was a primary product from both substrates, suggesting that it was more easily removed than the other lignin units and that it was not involved in condensation reactions. Short liquid residence times due to the flow of water limited condensation reactions for both substrates, as evidenced by greater lignin extraction by flowthrough pretreatment. Surprisingly, 192 minutes of pretreatment produced more phenol monomers at 140^{o}C than at 180^{o}C. This unexpected finding could be the result of the generation of larger phenol oligomers at 180^{o}C that cannot be detected by gas chromatography-mass spectrometry at the higher temperature.

More lignin was extracted and more phenols were produced by pretreatment of *P. trichocarpa* than by pretreatment of CEL. The difference in lignin extraction between the two substrates was too small to be due to differences in solid-liquid interfacial area therefore it is likely that hemicellulose-lignin interactions significantly influence lignin deconstruction during pretreatment. Although guaiacyl units are thought to be less easily extracted and more easily condensed due to their greater potential for cross-linking,

guaiacyl based phenols were the dominant type produced from CEL. However, syringyl based phenols were the dominant phenols released from *P. trichocarpa,* suggesting that cross-links between hemicellulose and lignin modify the reactivity of guaiacyl and syringyl groups.

7.6. Nomenclature

A_{surf}	Surface area
C	Reactant concentration
D	Diameter (mm)
h	Length (mm)
k''	Reaction rate constant per unit surface area
$log\ R_o$	Severity parameter for hydrothermal pretreatment, Equation (1)
m	Mass removed
M	Molecular weight
$\overline{M}$	Average molecular weight
N	Number of
r	Radius (mm)
t	Time (min)
T	Temperature (^oC)

Greek

ε	Void fraction of the bed
ρ	Density

Subscripts

b	Of biomass bed
B	For batch pretreatment
CEL	Cellulolytic enzyme lignin
F	For flowthrough pretreatment
n	Number average
p	Particle
Pt	*Populus trichocarpa*
rxn	Reaction condition
$rxtr$	Of reactor
w	Weight average

7.7. References

(1) Raven PH, Evert RF, Eichhorn SE. *Biology of plants,* 7th ed.; W.H. Freeman and Company Publishers: New York, 2005; pp. 31-32.

(2) Sannigrahi P, Ragauskas AJ, Tuskan GA. Poplar as a feedstock for biofuels: A review of compositional characteristics. *Biofuels Bioprod. Bior*. **2010**; *4*(2): 209-226.

(3) Fengel D, Wegener G. *Wood: Chemistry, ultrastructure, reactions.* Walter de Gruyter & Co: Berlin, 1983.

(4) Albersheim P, Darvill A, Roberts K, Sederoff R, Staehelin A. *Plant cell walls from chemistry to biology*. Garland Science: New York, 2011.

(5) Kumar R, Wyman CE. Key features of pretreated lignocelluloses biomass solids and their impact on hydrolysis. In: *Bioalcohol production : Biochemical conversion of lignocellulosic biomass*; Waldon K, Ed.; Woodhead Publishing Ltd.: Oxford, 2010; 73-121.

(6) Donohoe BS, Decker SR, Tucker MP, Himmel ME, Vinzant TB. Visualizing lignin coalescence and migration through maize cell walls following thermochemical pretreatment. *Biotechnol. Bioeng*. **2008**; *101*(5): 913-925.

(7) Kristensen JB, Thygesen LG, Felby C, Jørgensen H, Elder T. Cell-wall structural changes in wheat straw pretreated for bioethanol production. *Biotechnology for Biofuels*. **2008**; *1*(5).

(8) Pingali SV, Urban VS, Heller WT, McGaughey J, O'Neill H, Foston M, Myles DA, Ragauskas A, Evans BR. Breakdown of cell wall nanostructure in dilute acid pretreated biomass. *Biomacromolecules*. **2010**; *11*(9): 2329-2335.

(9) Selig MJ, Viamajala S, Decker SR, Tucker MP, Himmel ME, Vinzant TB. Deposition of lignin droplets produced during dilute acid pretreatment of maize stems retards enzymatic hydrolysis of cellulose. *Biotechnol. Prog*. **2007**; *23*(6): 1333-1339.

(10) Xiao LP, Sun ZJ, Shi ZJ, Xu F, Sun RC. Impact of hot compressed water pretreatment on the structural changes of woody biomass for bioethanol production. *Bioresources*. **2011**; *6*(2): 1576-1598.

(11) Gutzow IS, Schmelzer JWP. Basic properties and the nature of glasses: an overview. In *Glasses and the Glass Transition*, 1st Ed[Online]; Schmelzer JWP, Gutzow IS, eds.; Wiley-VCH: Hoboken, NJ, 2011; 1-89.

(12) Irvine GM. The significance of the glass transition of lignin in thermochemical pulping. *Wood Sci. Technol*. **1985**; *19*(2): 139-149.

(13) Fang Z, Sato T, Smith RL Jr., Inomata H, Arai K, Kozinski JA. Reaction chemistry and phase behavior of lignin in high temperature and supercritical water. *Bioresource Technol*. **2008**; *99*(9): 3424-3430.

(14) Petridis L, Schulz R, Smith JC. Simulation analysis of the temperature dependence of lignin structure and dynamics. *J. Am. Chem. Soc*. **2011**; *133*(51): 20277-20287.

(15) Saake B, Lehnen R. Lignin. In *Ullmann's Encyclopedia of Industrial Chemistry* [Online]. Bohnet M, Bellussi G, Bus J, Cornils B, Drauz K, Greim H et al., ed.; Wiley: New York, 2007. Available from: Wiley Online Library.

(16) Salmén L. Viscoelastic properties of *in situ* lignin under water-saturated conditions. *J. Mater. Sci*. **1984**; *19*(9): 3090-3096.

(17) Sarkanen KV, Ludwig CH, editors. *Lignins- Occurrence, formation, structure, and reactions*; John Wiley & Sons Inc.: Canada, 1971.

(18) Shao S, Jin Z, Wen G, Iiyama K. Thermocharacteristics of steam-exploded bamboo (*Phyllostachys pubescens*) lignin. *Wood Sci. Technol*. **2009**; *43*(7-8): 643-652.

(19) Chua MGS, Wayman M. Characterization of autohydrolysis aspen (*P. tremuloides*) lignins. Part 3. Infrared and ultraviolet studies of extracted autohydrolysis lignin. *Can. J. Chem*. **1979**; *57*(19): 2603-2611.

(20) Lora JH, Wayman M. Simulated autohydrolysis of aspen milled wood lignin in the presence of aromatic additives- Changes in molecular weight distribution. *J. Appl. Polym. Sci*. **1980**; *25*(4): 589-596.

(21) Li J, Henriksson G, Gellerstedt G. Lignin depolymerization/repolymerization and its critical role for delignification of aspen wood by steam explosion. *Bioresource Technology*. **2007**; *98*(16): 3061-3068.

(22) Marchessault RH, Coulombe S, Morikawa H. Characterization of aspen exploded wood lignin. *Can. J. Chem*. **1982**; *60*(18): 2372-2382.

(23) Chua MGS, Wayman M. Characterization of autohydrolysis aspen (*P. tremuloides*) lignins. Part 1. Composition and molecular weight distribution of extracted autohydrolysis lignin. *Can. J. Chem*. **1979**; *57*(10): 1141-1149.

(24) Lora JH, Wayman M. Autohydrolysis of aspen milled wood lignin. *Can. J. Chem*. **1980**; *58*(7): 669-676.

(25) Bardet M, Robert DR, Lundquist K. On the reactions and degradation of the lignin during steam hydrolysis of aspen wood. *Sven. Papperstidn*. **1985**; *88*(6): R61-R67.

(26) Wayman M, Chua MGS. Characterization of autohydrolysis aspen (*P. tremuloides*) lignins. Part 2. Alkaline nitrobenzene oxidation studies of extracted autohydrolysis lignin. *Can. J. Chem*. **1979**; *57*(19): 2599-2602.

(27) Abatzoglou NJ, Chornet E, Belkacemi K, Overend RP. Phenomenological kinetics of complex systems: the development of a generalized severity parameter and its application to lignocellulosic fractionation. *Chem. Eng. Sci*. **1992**; *47*: 1109-1122.

(28) Barakat A, Chabbert B, Cathala B. Effect of reaction media concentration on the solubility and the chemical structure of lignin model compounds. *Phytochemistry*. **2007**; *68*(15): 2118-2125.

(29) Cathala B, Monties B. Influence of pectins on the solubility and molar mass distribution of dehyrogenative polymers (DHPs, lignin model compounds). *Int. J. Biol. Macromol*. **2001**; *29*(1): 45-51.

(30) Barakat A, Winter H, Rondeau C, Saake B, Chabbert B, Cathala B. Studies of xylan interactions and cross-linking to synthetic lignins formed by bulk and end-wise polymerization: a model study of lignin carbohydrate complex formation. *Planta*. **2007**; *226*(1): 267-281.

(31) Foston MB, McKenzie HL, Wyman CE, Ragauskas AJ. Analysis of ^{13}C enriched corn stover by water-only flow-through pretreatment. Presented at 33rd Symposium on Biotechnolgy for Fuels and Chemicals, Seattle, WA, May 3, 2011; 6-05.

(32) Liu C, Wyman CE. The effect of flow rate of compressed hot water on xylan, lignin, and total mass removal from corn stover. *Ind. Eng. Chem. Res*. **2003**; *42*(21): 5409-5416.

(33) Liu C, Wyman CE. The effect of flow rate of very dilute sulfuric acid on xylan, lignin, and total mass removal from corn stover. *Ind. Eng. Chem. Res*. **2004**; *43*(11): 2781-2788.

(34) Gray MC, Converse AO, Wyman CE. Solubilities of oligomer mixtures produced by the hydrolysis of xylans and corn stover in water at 180°C. *Ind. Eng. Chem. Res*. **2007**; *46*(8): 2383-2391.

(35) Chang HM, Cowling EB, Brown W, Adler E, Miksche G. Comparative studies on cellulolytic enzyme lignin and milled wood lignin of sweetgum and spruce. *Holzforschung*. **1975**; *29*(5): 153-159.

(36) Björkman A. Studies on finely divided wood, Part 1 Extract of lignin with neutral solvents. *Svensk Papperstidn*. **1956**, *59*(13): 477-485.

(37) Samuel R, Pu YQ, Raman B, Ragauskas AJ. Structural characterization and comparison of switchgrass ball-milled lignin before and after dilute acid pretreatment. *Appl. Biochem. Biotechnol*. **2010**; *162*(1): 62-74.

(38) Jung HW, Tschaplinski TJ, Wang L, Glazebrook J, Greenberg JT. Priming in systemic plant immunity. *Science*. **2009**; *324*(5923): 89-91.

(39) Li Y, Tschaplinski TJ, Engle NL, Hamilton CY, Rodriguez M. Jr., Liao JC, Schadt CW, Guss AM, Yang Y, Graham DE. Combined inactivation of the *Clostridium cellulolyticum* lactate and malate dehydrogenase genes substantially increases ethanol yield from cellulose and switchgrass fermentations. *Biotechnology for Biofuels*. **2012** Jan; *5*(2). doi:10.1186/1754-6834-5-2

(40) Sluiter A, Hames B, Ruiz R, Scarlata C, Sluiter J, Templeton D, Crocker D. Determination of structural carbohydrates and lignin in biomass laboratory analytical procedure. CO: National Renewable Energy Laboratory; 2011 Jul. 18 p. Report No. NREL/TP-510-42618.

(41) Sannigrahi P, Kim DH, Jung S, Ragauskas AJ. Pseudo-lignin and pretreatment chemistry. *Energ. Environm. Sci*. **2011**; *4*(4): 1306-1310.

(42) Zhang L, Gellerstedt G. Quantitative 2D HSQC NMR determination of polymer structures by selecting suitable internal standard references. *Mag. Res. Chem.* **2007**; *47*: 37-45.

(43) Samuel R, Foston M, Jaing N, Cao S, Ragauskas AJ, et al. HSQC (heteronuclear single quantum coherence) $^{13}C–^{1}H$ correlation spectra of whole biomass in perdeuterated pyridinium chloride–DMSO system: An effective tool for evaluating pretreatment. *Fuel* **2011**; *90*: 2836-2842.

(44) Samuel R, Foston M, Jaing N, Allison L, Ragauskas AJ,. Structural changes in switchgrass lignin and hemicelluloses during pretreatments by NMR analysis. *Polym. Degrad. Stabil.***2011**; *96*: 2002-2009.

(45) Chiang VL, Funaoka M. The differences between guaiacyl and guaiacyl-syringyl lignins in their responses to Kraft delignification. *Holzforschung*. **1990**: *44*: 309-313.

(46) Martín C, Galbe M, Nilvebrant NO, Jönsson LJ. Comparison of the fermentability of enzymatic hydrolysates of sugarcane bagasse pretreated by steam explosion using different impregnating agents. *Appl. Biochem. Biotech*. **2002**; *98-100*(1): 699-716.

(47) Fogler HS. *Elements of Chemical Reaction Engineering*, 4th ed.; Prentice Hall Professional Technical Reference: Upper Saddle River, NJ, 2006; Chapters 10-12.

(48) Geankoplis CJ. *Transport processes and separation process principles (Includes unit operations)*, 4th ed.; Prentice Hall PTR: Upper Saddle River, NJ: 2003, p.485.

(49) Torget R, Hatzis C, Hayward TK, Hsu T, Philippidis GP. Optimization of reverse-flow, two-temperature, dilute-acid pretreatment to enhance biomass conversion to ethanol. *Appl. Biochem. Biotech*. **1996**; *57-58*(1): 85-101.

Chapter 8.

Cellulosic ethanol and gasoline for 100 years: A comparison of carbon dioxide fluxes associated with production and use of ethanol from cellulosic energy crops grown in different regions of North America to the production and use of gasoline from various fossil fuel feedstocks over 100 years.[*]

[*] This work was done in partnership with Drs. Jaclyn DeMartini and Qing Qing. All three authors contributed equally to this work.

8.1. Introduction

There are significant concerns about the effects of global warming, which is caused by anthropogenic emissions of greenhouse gases such as carbon dioxide. Consequently, efforts are being made to reduce greenhouse gas emissions. In 2006, direct CO_2 emissions from the transportation sector were the largest single fraction, of the United States' total emissions[1]. If the emissions associated with petroleum fuel production were included, transportation emissions would account for 38.2% of the United States' 2006 emissions[1]. Historically, gasoline has been produced from conventional petroleum but a combination of "geologic, economic, environmental, [and] political difficulties"[2] will likely result in increased gasoline production from nonconventional hydrocarbons such as oil sands, oil shale, methane or coal. The use of these feedstocks results in higher greenhouse gas emissions. Therefore, alternatives to petroleum transportation fuels such as cellulosic ethanol are vital to reducing overall emissions.

A possible way to cut soaring carbon dioxide emissions and reduce global warming is sequestration of carbon dioxide and has in fact already been implemented on a commercial scale[3]. The primary options for underground carbon dioxide storage are depleted oil and gas reservoirs, deep saline reservoirs and unminable coal seams[4]. However, the cost of separating carbon dioxide from dilute gas streams such as flue gas from a fossil fuel power plant is considerable using current technology[5]. In the case of ethanol production, major carbon dioxide sources are fermentation of plant-derived sugars, lignin combustion, and the end-use combustion of ethanol. If the carbon dioxide

from fermentation and lignin combustion could be collected and sequestered, the net release of carbon dioxide would be significantly lower.

Although ethanol produced from cellulosic biomass is a frequently proposed solution questions have been raised about the balance between the carbon dioxide sequestered in the biomass and soil and the carbon dioxide emitted from farming, conversion to ethanol, and the distribution and combustion of ethanol. The objective of this chapter is to develop detailed carbon fluxes for the production and use of ethanol derived from an energy crop grown on a 50-mile radius for 100 years. Mixed prairie grass and poplar were selected as sample energy crops. Marginal land and cropland in the United States and Canadian temperate forests were selected as possible locations for an energy crop plantation and biorefinery. In addition, the carbon dioxide flux for the production and consumption of gasoline produced from a variety of hydrocarbons was developed for comparison. A sensitivity analysis was conducted to verify the models' robustness. The impact of sequestering carbon dioxide from fermentation and lignin combustion on the carbon dioxide flux associated with cellulosic ethanol production and use will also be examined in this paper. The purpose of this study is to provide hypothetical scenarios, whose inputs can be easily adjusted to examine various circumstances.

8.2. Development of carbon dioxide emissions from ethanol production

Ethanol production from poplar or mixed prairie grass, grown in a 50-mile radius on three different types of land over 100 years was studied. The three types of land studied were degraded land and cropland in the United States, and temperate forest in

Canada. In each case, the annual ethanol production goal was equal to the amount of ethanol that could be produced if the entire 50-mile radius were planted with an energy crop under assumed crop and ethanol yields.

In the case of energy crop production on forested land, it was assumed that native biomass would be harvested and used to produce the annual ethanol quota in the first year. The cleared land would then be replanted with energy crops. In the following years, the entire available energy crop is harvested along with enough native biomass to meet the annual ethanol quota. Poplar was assumed to be harvested on a 4-year rotation. In the case of production on American marginal and croplands, mixed grasses are planted on the entire plot in year 1 and then harvested in full in each of the following years. For poplar, due to the selected 4-year crop rotation, it was assumed that a quarter of the study plot was planted in each of the first four years and harvested accordingly.

The processing of the cellulosic feedstock to ethanol was assumed to yield a lignin residue that would be burned to provide process steam and electricity as well as a small amount of electricity for export to the grid. System carbon dioxide emissions were also determined for the sequestration of carbon dioxide from fermentation and lignin combustion. The factors used to determine carbon dioxide emissions are organized by process blocks in Figure 8.1 and summarized in Table 8.1. Based on Wyman[6], the density and energy content of ethanol were assumed to be 6.56 lb/gal and 83,957 BTU/gal respectively.

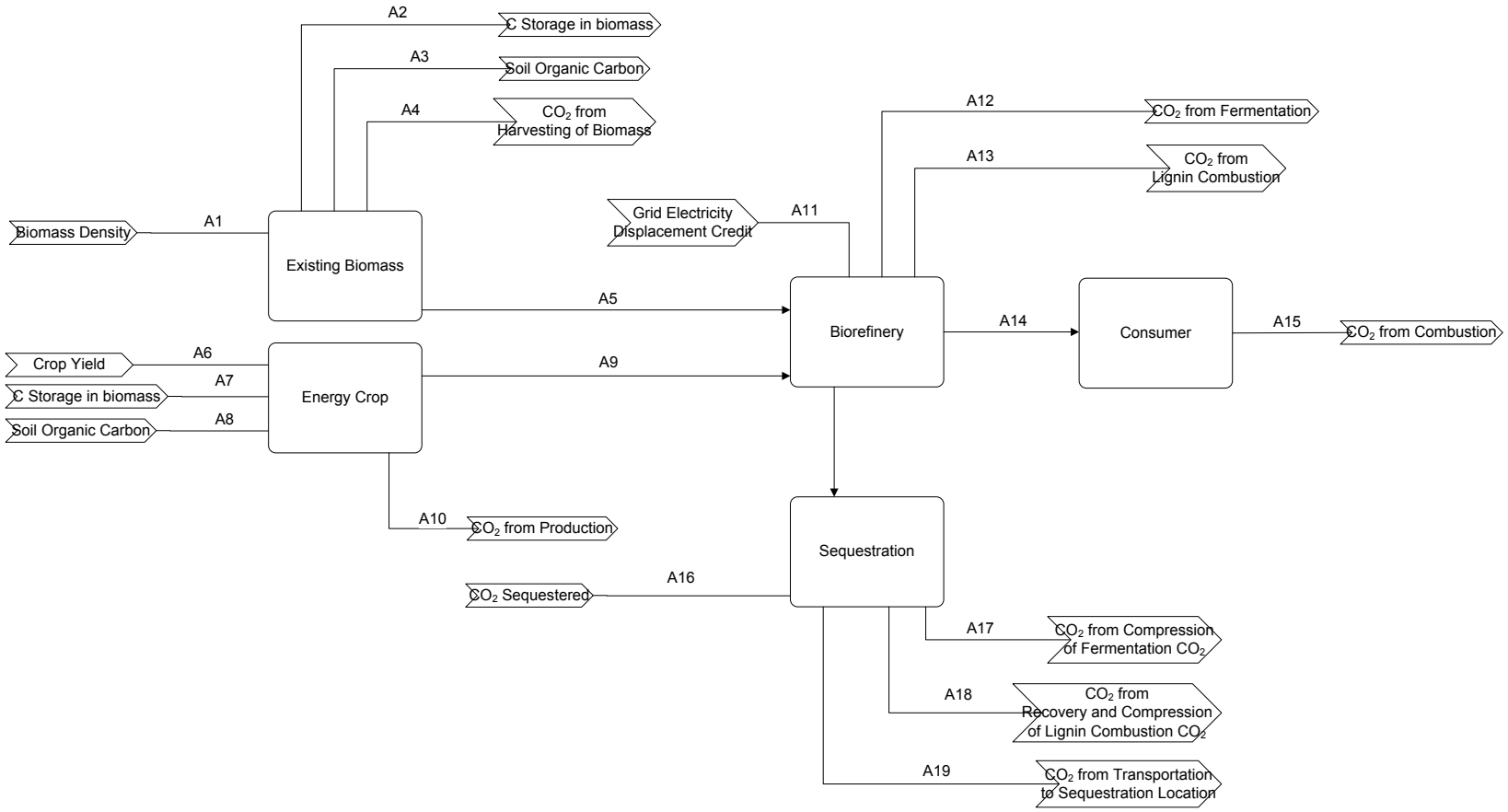

Figure 8.1. Illustration of factors used to determine mass flows of CO_2 during the production of cellulosic ethanol.

Table 8.1. Factors used to determine mass flows of CO_2 for 6 cellulosic ethanol cases.

Stream	Stream Description	Units	Mixed Prairie Grass			Poplar		
			US Marginal Lands	US Cropland	Canadian Temperate Forest	US Marginal Lands	US Cropland	Canadian Temperate Forest
Existing Biomass								
A1	Density of Pre-existing Biomass	ton biomass/acre	0	0	35.7[7]	0	0	35.7[13]
A2	Carbon Stored in the Pre-existing Biomass	ton C/acre	0	0	17.8[13]	0	0	17.8[13]
A3	Soil Organic Carbon (SOC) Under Pre-existing Biomass	ton C/acre	N.A.	N.A.	72[8]	N.A.	N.A.	72[14]
A4	CO_2 from Harvesting of Biomass	lb CO_2/acre biomass	0	0	795[9,10]	0	0	795[15,16]
A5	Ethanol Yield from Pre-existing Biomass	gal/ton biomass	N.A.	N.A.	90	N.A.	N.A.	90
Energy Crop								
A6	Energy Crop Yield	ton biomass/acre-yr	3.35[11,15]	6.69[17]	6.69[15,17]	2.52[15,17]	5.04[17]	5.04[17]
A7	Carbon Stored in the Energy Crop	%	46[17]	46[17]	46[17]	50[12]	50[17]	50[17]
A8	Rate of SOC Storage Under Energy Crop	ton C/acre-yr	0.357[17]	0.357[17]	0.357[17]	0.491[17]	0.491[17]	0.491[17]
A9	Ethanol Yield from Energy Crop	gal/ton biomass	100	100	100	100	100	100
A10	CO_2 from Biomass Production	lb CO_2/acre biomass	124[15]	159[15]	159[15]	619[15]	795[15,16]	795[15,16]

Table 8.1. continued

Stream	Stream Description	Units	Mixed Prairie Grass			Poplar		
			US Marginal Lands	US Cropland	Canadian Temperate Forest	US Marginal Lands	US Cropland	Canadian Temperate Forest
Biorefinery								
A11	CO_2 Credit for Displacement of Grid Electricity	lb grid electricity CO2/ton biomass	304[13,14]	304[13,14]	304[13,14]	304[13,14]	304[13,14]	304[13,14]
A12	CO_2 Emitted from Fermentation	lb CO_2/gal EtOH	6.27	6.27	6.27	6.27	6.27	6.27
A13	CO_2 Emitted from the Combustion of Lignin	lb/ton biomass	1565[13,15]	1565[13,15]	1565[13,15]	1745[13,15]	1745[13,15]	1745[13,15]
Consumer								
A14	CO_2 Emitted During Transport of Ethanol to Fueling Station	lb CO_2/lb EtOH	0.0397[14]	0.0397[14]	0.0358[14]	0.0397[14]	0.0397[14]	0.0358[14]
A15	CO_2 Emitted During Combustion of Ethanol	lb CO_2/lb EtOH	1.91	1.91	1.91	1.91	1.91	1.91

Table 8.1. continued

Stream	Stream Description	Units	Mixed Prairie Grass			Poplar		
			US Marginal Lands	US Cropland	Canadian Temperate Forest	US Marginal Lands	US Cropland	Canadian Temperate Forest
Sequestration								
A16	Amount of CO_2 Sequestered	% of available	80	80	80	80	80	80
A17	CO_2 Emitted from Compression of CO_2 from fermentation to 60 bars	lb CO_2/gal EtOH	0.209[5,16]	0.209[5,16]	0.209[5,16]	0.209[5,16]	0.209[5,16]	0.209[5,16]
A18	CO_2 Emitted from Recovery and Compression of CO_2 from lignin combustion to 60 bars	lb CO_2 emitted/ lb CO_2 sequestered	2.13 E-03[5]	2.13 E-03[5]	2.13 E-03[5]	2.13 E-03[5]	2.13 E-03[5]	2.13 E-03[5]
A19	CO_2 Emitted During Transport of CO_2 to Sequestration Location	lb CO_2 emitted/ lb CO_2 sequestered	2.28 E-03[14]	2.28 E-03[14]	2.28 E-03[14]	2.28 E-03[14]	2.28 E-03[14]	2.28 E-03[14]

For stream A2, Canadian forest was assumed to no longer be emitting or sequestering carbon dioxide, i.e. the land was in carbon equilibrium with the environment[12]. It was also assumed that when existing biomass was cleared the carbon dioxide emissions were due to the loss of 60% of the original soil organic carbon (SOC) in Canadian forest during clearing[17].

Streams A4 and A10 account for carbon dioxide emissions from the production of the bioenergy crop. The overall biomass production emission factors are estimated from the values presented for degraded and fertile lands by Tilman and coworkers[9]. American cropland and Canadian forest are treated as fertile land. The factors for streams A4 and A10 include emissions from seed production, planting, fertilizer production and application, harvesting, and biomass transportation from the field to refinery. However, Tilman and co-workers'[9] estimate of the emissions associated with farm capital, machinery, and the sustaining the farm household are not included in this analysis as the emission factors for gasoline production did not consider equivalent carbon dioxide sources. It was also assumed that biomass production emissions from poplar would be 5 times higher than that from mixed grasses. This assumption was based on Zhu's[10] data showing that the size reduction of woody biomass requires between 4 to 14 times more energy than the size reduction of grasses and the assumption that harvesting native woody biomass would require more energy, and therefore have higher emissions compared to grasses. Finally, it is also important to note that the carbon dioxide emissions from farming were based on application of sound agricultural practices such as no till farming.

In stream A6, it was assumed that energy crop yields on degraded land were half of the yields achieved in fertile soil[9]. For stream A7, the carbon content of poplar and mixed prairie grass were assumed to be 50% and 46%, respectively.[11] The SOC storage rate for the bioenergy crops, stream A8, was assumed to remain constant for 50 years[11, 17] on American degraded land, or until 50% of the SOC lost due to clearing had been regained[11], as for Canadian forest. Depending on the biomass crop, this period ranges from 44 to 61 years. For American cropland, it is assumed that the soil can add an additional 4.46 tons C/acre when switched from previous agricultural crops to a perennial bioenergy crop[18]. This is equal to 9 and 13 years of soil sequestration for poplar and mixed grasses, respectively, with the assumed SOC storage rates. The lignin combustion emissions reported in stream A11 were based on the report by Aden and colleagues[13]. Based on Aden's carbon balance[13], the total carbon dioxide emissions from lignin combustion represented 46% of the carbon contained in the biomass used. Consequently, the lignin combustion emission factors are 1565 lb CO_2/ton mixed prairie grass and 1745 lb CO_2/ton poplar. Based on Aden et al.'s[13] work, the combustion of lignin produces $6.91*10^5$ BTU electricity/ton dry biomass and 8.92% of this electricity is available for export to the grid. The export of lignin electricity displaces electricity generated from conventional sources such as coal thus indirectly reducing emissions. The transportation emission factors recorded in stream A14 were based on GREET 1.8[14].

It was assumed that the carbon dioxide emitted from fermentation would be a clean stream, which could be easily collected while the carbon dioxide from lignin combustion would be mixed with other gases such as N_2, O_2, CO, NO_X, SO_2, and

particles. However, it was assumed that the current technology for the separation of carbon technology from hydrocarbon flue gases could also be used to capture and separate the lignin combustion carbon dioxide[1]. A collection efficiency of 80% was assumed in stream A16 due to lack of reference data. It was also assumed that the energy required for the separation and compression of carbon dioxide could be supplied by lignin combustion itself. It was assumed that carbon dioxide is compressed to 60 bars[19] and transported 65 miles[14]. A sensitivity analysis of the capture efficiency and transport emission factor was conducted to clarify their influences on final total emissions.

8.3. Development of carbon dioxide emissions from gasoline production

Data on the carbon dioxide emitted during the production and combustion of gasoline from several feedstocks was gathered for comparison to carbon dioxide emissions from bioethanol. Based on GREET 1.8, 96% of American gasoline is produced in American refineries using a feedstock blend that is 2% Canadian oil sands, 6.86% Alaskan crude, 7.84% conventional Canadian and Mexican crude, 34.3% conventional crude from the continental United States, and 49% crude from offshore countries.[14] The balance of American gasoline is imported from Canadian and Caribbean refineries. The production and transportation emissions associated with crude from Middle East were calculated using GREET 1.8 with the assumption that the crude oil was shipped 8336 nautical miles by tanker to an American refinery.[14]

As discussed previously, gasoline production will likely shift from conventional oil resources to feedstocks such as oil sands and coal. Canadian oil sands were selected as the first representative alternative hydrocarbon feedstock due to the current high levels of

production and importance to the American market. Coal was selected as the second alternative feedstock as it was the largest potential source of liquid fuels reported by Brandt and Farrell[2]. Coal to liquid (CTL) fuel production requires the gasification and reforming of coal to syngas, a mixture of CO and H_2, followed by fuel synthesis by the Fischer-Tropsch process[2]. The carbon dioxide emissions associated with the recovery of feedstock, refining and transportation are presented in Table 8.2.

Avallone and Baumeister[20] reported the density and energy content of gasoline as 6.15 lb/gal and 127, 654 BTU/gal. The average amount of carbon dioxide emitted from combustion of gasoline is $1.52*10^{-4}$ lb CO_2/BTU gasoline[21].

Table 8.2 Carbon dioxide emissions from the production, transportation, and combustion of gasoline produced from varying feedstocks.

Feedstock	CO_2 Emissions from Production and Transportation of Gasoline (lb/BTU)	CO_2 Emissions from Production, Transportation and Combustion of Gasoline (lb/BTU)
Crude from Continental U.S.A.	4.77 E-05[i]	2.00 E-04[ii]
Crude from Middle East	4.30 E-05[i]	1.95 E-04[ii]
Current Feedstock Blend	4.41 E-05[i]	1.96 E-04[ii]
Canadian Oil Sands	9.50 E-05[i]	2.47 E-04[ii]
Coal to Liquid	2.10 E-04[i]	3.62 E-04[ii]

[i]Values listed are the average of those provided by Brandt and Farrell[2] and GREET 1.8[14].
[ii]Carbon dioxide emissions from the combustion of gasoline[21] is $1.52*10^{-4}$ lb CO_2/BTU.

8.4. Results and discussion

In order to examine the long term impact of the six cellulosic ethanol scenarios, Figure 8.2 shows the annual carbon dioxide emissions normalized by the energy content

of ethanol produced. For comparison, emissions from conventionally sourced gasoline assuming Brandt and Farrell's[2] emission factor are also shown.

Carbon dioxide emissions from ethanol produced in the Canadian forest are shown to be higher than those of gasoline for the first four and five years for poplar and mixed grasses, respectively. Emissions are initially high due to the use of pre-existing biomass and the release of soil organic carbon when the native biomass is harvested. As the ratio of pre-existing biomass used to bioenergy crop used decreases, emissions from soil organic carbon also decrease. Additionally, as more bioenergy crop is planted, there is a larger amount of carbon sequestered in the soil beneath the crops. Consequently, as time progresses, carbon dioxide emissions decrease until year 20 for both poplar and mixed grasses. At this point, the soil has regained 50% of the carbon that it lost due to clearing pre- existing biomass and it was assumed that the soil does not sequester any additional carbon. Poplar grown on both U.S. crop and degraded lands exhibits negative carbon dioxide emissions for the first 11 and 23 years, respectively. For both lands, the emissions stepwise increase because the soil has become saturated with organic carbon, and soil sequestration ceases. Emissions from ethanol produced from mixed grasses grown on both U.S. degraded and croplands show similar patterns, but with slightly higher emissions over the 100-year period.

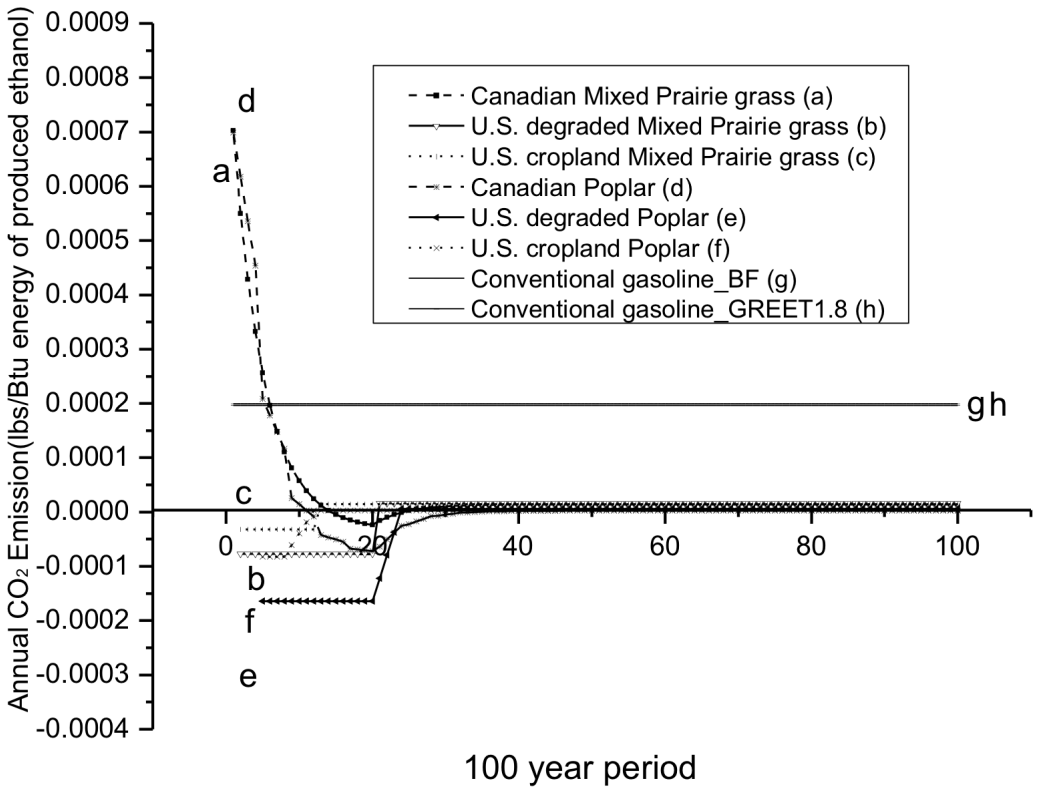

Figure 8.2. Annual emissions of CO_2 per BTU of ethanol produced over 100 years for 6 cellulosic ethanol cases.

Figure 8.3 shows the total 100-year carbon dioxide emissions associated with the production and use of a fuel relative to energy content for the six bioethanol cases and four gasoline cases. For each land type, the use of poplar as an energy crop results in lower carbon dioxide emissions than mixed grasses. This difference can be attributed to higher soil organic carbon storage by poplar; from Table 8.1, it can be seen that poplar's SOC is 37% higher than that of mixed prairie grasses. It can also be observed in Figure 8.3 that the 100-year emissions of cellulosic ethanol are between 161 and 241 lbs CO_2 per MM BTU lower than the 100-year emissions of gasoline from conventional petroleum. However, as stated in the introduction, conventional petroleum will become increasingly

difficult to access[2], therefore alternative transportation fuels such as sustainably sourced bioethanol or gasoline from hydrocarbons such as oil sands and coal will be needed. Figure 8.3 clearly shows that regardless of energy crop or land type utilized, the emissions from bioethanol are much lower than the emissions associated with gasoline from oil sands or coal to liquids.

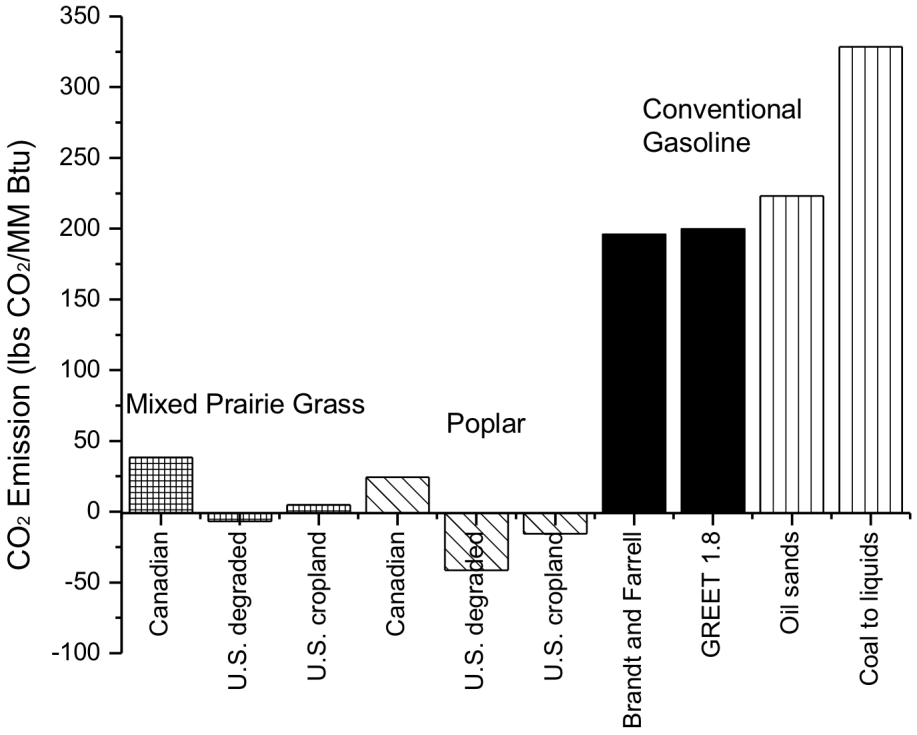

Figure 8.3. 100 year carbon dioxide emissions normalized to energy content of fuel produced (lb CO_2/ MM BTU fuel) for 6 cellulosic ethanol cases and 4 gasoline cases.

Figure 8.4 compares the total carbon dioxide emissions for the six scenarios from this study to that of similar studies by other authors. The study by Tilman et al.[9] examined carbon dioxide emissions for biofuels derived from low-input high-diversity (LIHD) mixtures of native grassland perennials. This study is seen to be quite comparable to the case of mixed prairie grasses grown on U.S. degraded lands. It should be noted that

Tilman et al.'s[9] study was based on a 30 year time frame, which is considerably shorter than this study's 100 year period. Figure 8.2 shows that the annual carbon dioxide emissions for mixed prairie grasses planted on degraded lands is very stable over the 100 year period except for a minor shift up during the 21st year which partially explains why the difference in study period did not greatly affect the comparison.

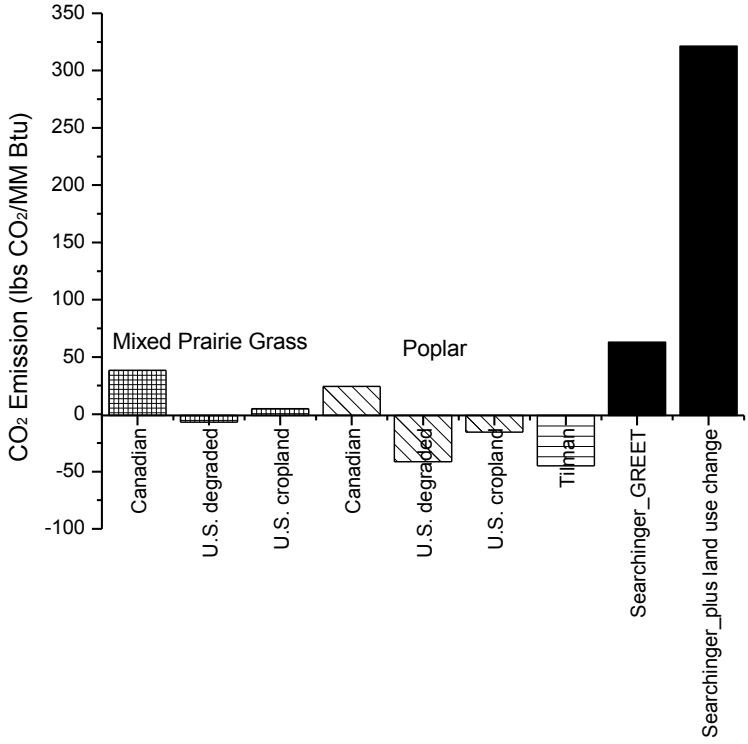

Figure 8.4. Comparison of 100-year carbon dioxide emissions normalized for fuel production (lb CO_2/ MM BTU) as calculated in current study to other authors[9, 22].

Geological sequestration of carbon dioxide emitted from ethanol fermentation and lignin combustion was considered in order to illustrate the potential improvement to the full carbon dioxide emission cycle of bioethanol. The emissions from the separation of carbon dioxide from other gases and compression of carbon dioxide to the preferred transportation pressure were accounted for when determining the effects of sequestration.

Additionally, the effects of exporting excess electricity from lignin combustion to the grid were also considered. The consequences of these activities relative to the base cases scenarios are shown in Figure 8.5. Sequestration of 80% of the carbon dioxide from fermentation, 57.3 lbs CO_2/MM BTU, results in negative 100 year CO_2 emissions per MM BTU for all six bioethanol cases indicating that carbon dioxide is removed from the atmosphere. Sequestration of carbon dioxide from lignin combustion, assuming 80% collection efficiency, further reduces the 100 year carbon dioxide emissions by 148 to 151 lbs CO_2/MM BTU. The exported electricity is assumed to displace electricity generated from fossil fuels or nuclear reactors, which indirectly reduces total carbon dioxide emissions in the proposed scenarios. From Aden et al.[13] it was determined that the electricity exported to the grid is equivalent to 8.92% of the energy content of the lignin burned; therefore 8.92% of the carbon dioxide emitted from lignin combustion should be associated with the exported electricity. As a result, depending on the cellulosic ethanol case and year, lignin-generated electricity has an emission intensity of 202 to 212 lb CO_2/MM BTU electricity. In comparison, GREET 1.8[14] reports that the production of electricity in the United States has an average emission factor of 441 lb CO_2/MM BTU electricity. Accounting for this effect further reduces the 100-year emissions from the production and use of bioethanol as seen in Figure 8.5. The consideration of sequestration and credits for electricity exports reflects the best scenario for cellulosic ethanol fuel production, and speaks to the possible improvements available to reduce carbon dioxide emissions.

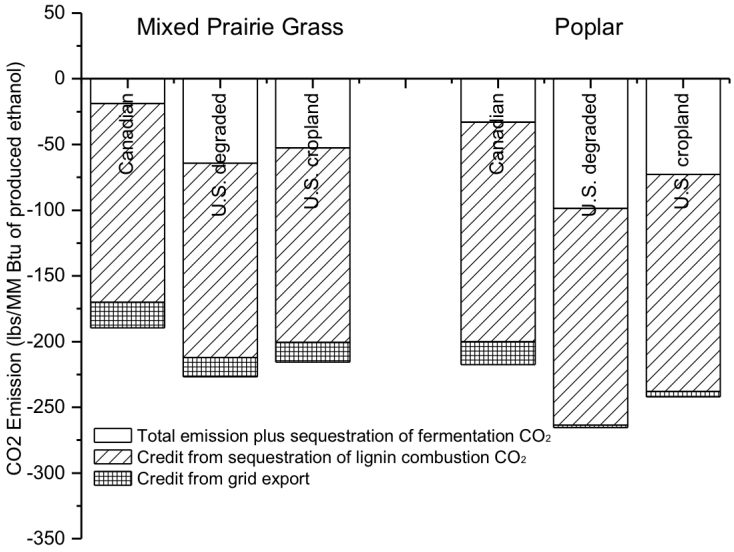

Figure 8.5. 100 year CO_2 emissions from cellulosic ethanol normalized for fuel production (lb CO_2/MM BTU fuel) implementing geologic sequestration of CO_2 from fermentation and lignin combustion.

8.5. Sensitivity analysis

To test both the robustness of the models and the sensitivity of results to the assumed input values, a sensitivity analysis was performed. The x-axis of all sensitivity plots shows the relative percent change in the input value, while the y-axis is the relative percent change in the 100-year total carbon dioxide emissions from ethanol, minus the total 100-year total carbon dioxide emissions avoided from replacing gasoline, all divided by the 100-year total of BTU energy produced. Thus, any value that lies above the x-axis represents a decrease in carbon dioxide emissions for ethanol compared to gasoline, while any value that lies below the x-axis represents an increase in carbon dioxide emissions for ethanol as compared to gasoline.

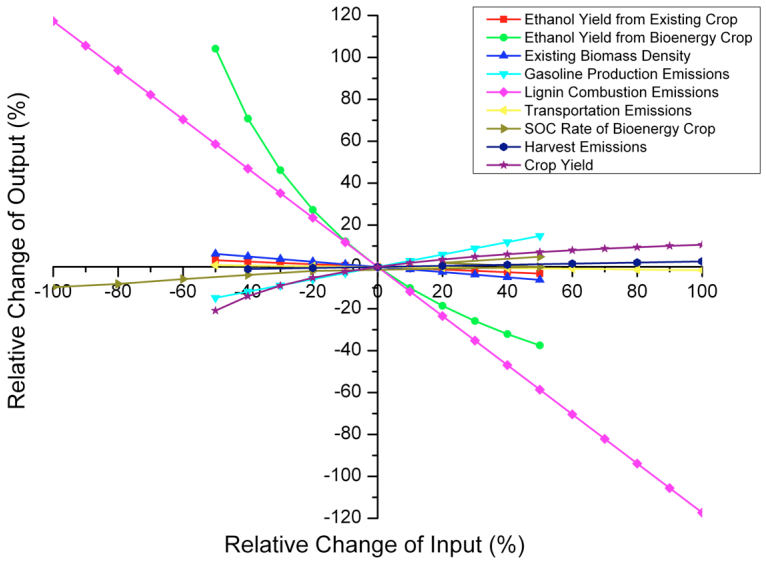

Figure 8.6. Sensitivity analysis for mixed grass grown in the Canadian forest.

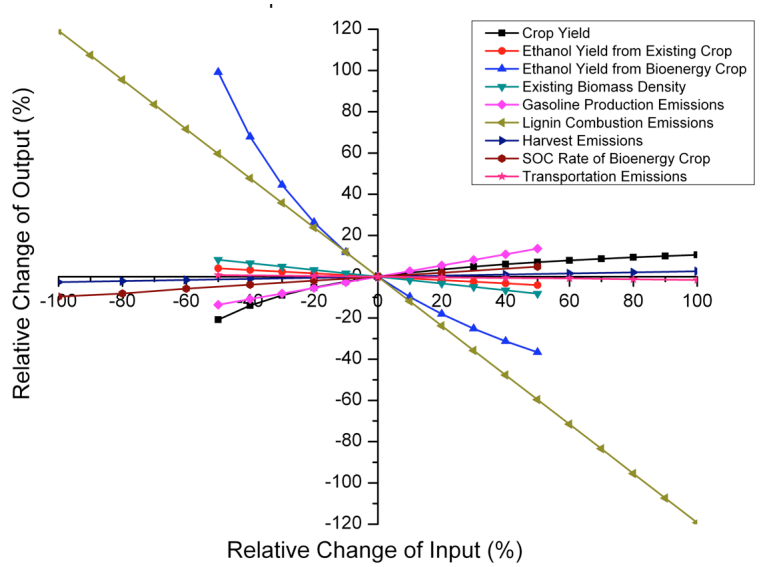

Figure 8.7. Sensitivity analysis for poplar grown in the Canadian forest.

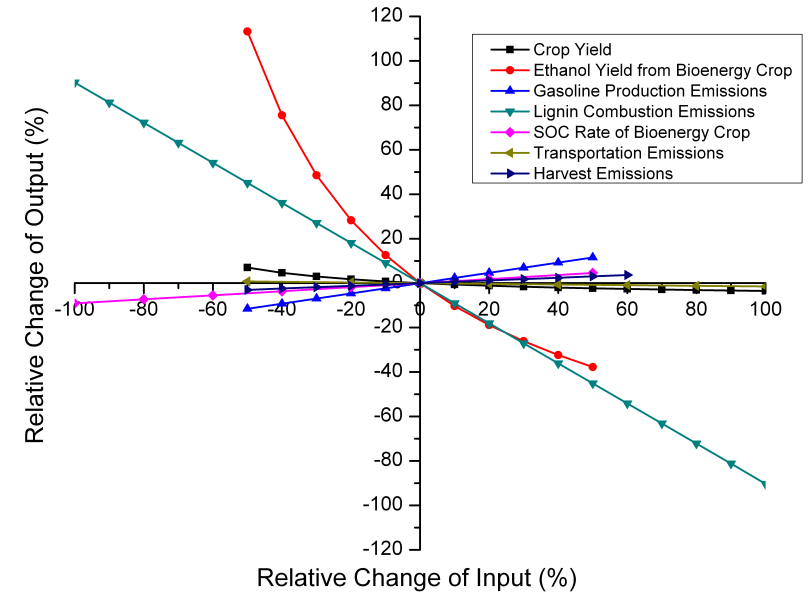

Figure 8.8. Sensitivity analysis for mixed grass grown on American degraded land.

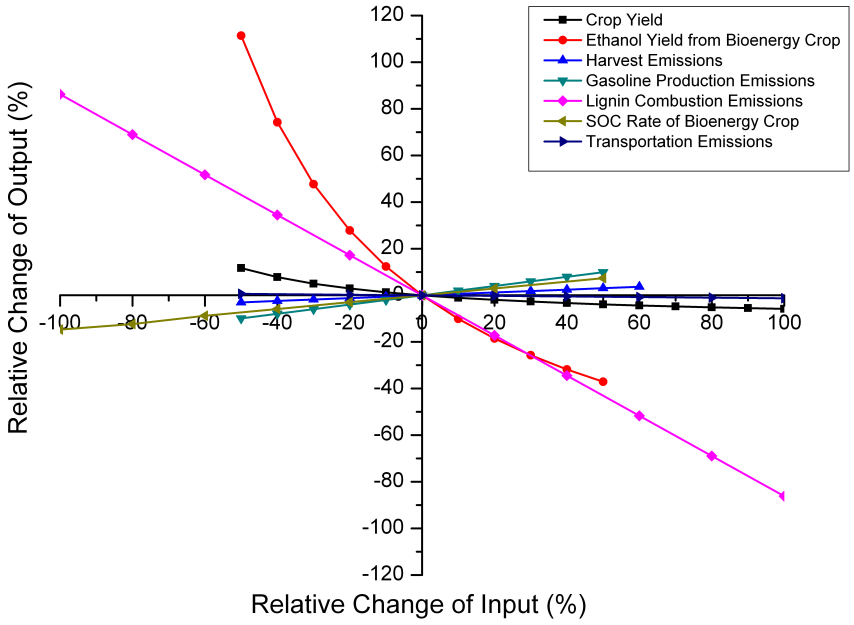

Figure 8.9. Sensitivity for poplar grown on American degraded land.

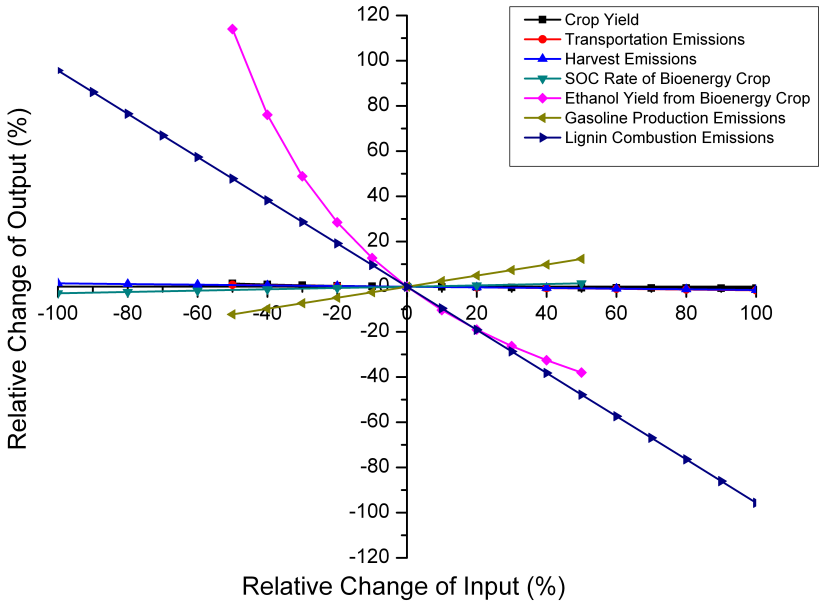

Figure 8.10. Sensitivity analysis for mixed grass grown on American cropland.

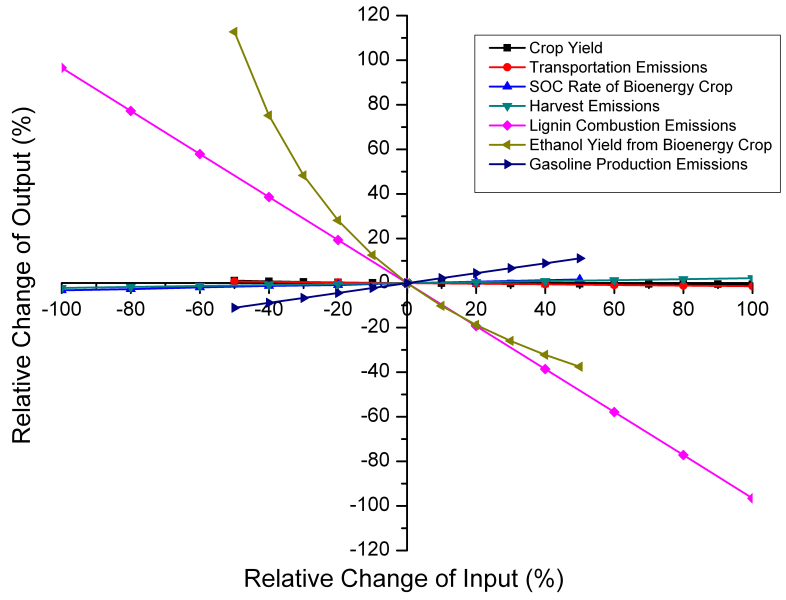

Figure 8.11. Sensitivity analysis for poplar grown on American cropland.

By examining Figures 8.6 through 8.11, it can be observed that for all scenarios, the carbon dioxide emissions are most sensitive to the ethanol yield from the bioenergy crop and the lignin combustion emission factor. When both inputs increase, the resulting

carbon dioxide emissions for ethanol also increase. Larger emissions associated with an increasing lignin combustion emission factor are intuitive. Less apparent however is why ethanol carbon dioxide emissions on a per BTU basis from ethanol increase with a higher ethanol yield. When the ethanol yield from bioenergy crop is changed, four individual carbon dioxide flux outputs change: carbon dioxide absorbed by biomass, excluding soil; carbon dioxide absorbed by bioenergy crop SOC; carbon dioxide released from harvest; and carbon dioxide released from lignin combustion. All four of these outputs increase with decreasing ethanol yield from bioenergy crop; however, the first two represent carbon dioxide sequestration, so they result in decreasing overall emissions for ethanol, while the latter two are emissions, and thus increase overall emissions. The total 100-year process carbon dioxide emissions decrease with decreasing ethanol yield from bioenergy crop because the two emission fluxes change more strongly than the two sequestration fluxes.

A sensitivity analysis was also performed to examine all the inputs used for geological sequestration of ethanol fermentation and lignin combustion carbon dioxide. Grasses grown in a Canadian forest are shown in Figure 8.12 as a representative scenario since all scenarios display similar trends. By examining all of the sequestration related inputs, the collection efficiency is found to be the dominant factor.

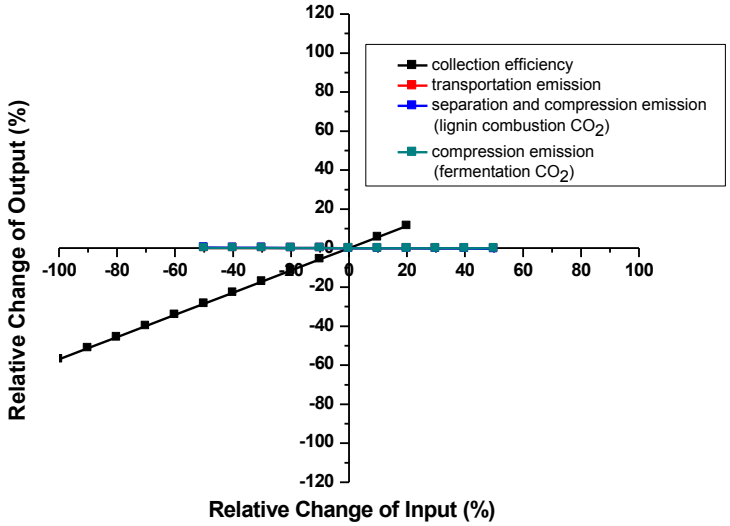

Figure 8.12. Sensitivity analysis of CO_2 sequestration inputs for grasses grown in a Canadian forest.

8.6. Conclusions

Cellulosic ethanol has the potential to be sustainable and lasting alternative to petroleum. This study was developed to examine the carbon dioxide emissions associated with producing ethanol from poplar or mixed grasses grown on American degraded land or cropland, or in Canadian temperate forest for 100 years. Key to the development of this study was the assumption that cellulosic ethanol would be produced intelligently through the successful utilization of pre-existing biomass, the adoption of good farming practices, and energy efficient biorefinery design. To provide perspective, the emissions were compared to the carbon dioxide emissions from gasoline production from conventional and unconventional petroleum sources.

For poplar production on both American land types, carbon dioxide was sequestered each year during the 100-year period, while the growth of mixed grasses on these lands resulted in some years of net sequestration and some years of net emissions

within the study period. Replacing the natural vegetation of the Canadian forest with energy crops resulted in carbon dioxide emissions higher than those from gasoline for the first five years after energy crop establishment. However, after this point ethanol emissions decreased to less than gasoline emissions and ultimately the environment was sequestering carbon dioxide each year.

When comparing among the six different cellulosic ethanol scenarios, poplar results in lower carbon dioxide emissions than for grasses grown on the same land type and creates strong carbon sinks when grown on both type of American land. It was also shown that the net 100-year emissions with the exception of the production of mixed grasses on American cropland or in Canadian forests are negative for the ethanol systems. Emissions from all six ethanol scenarios can be further decreased if sequestration of carbon dioxide from fermentation and lignin combustion were employed. For all ethanol production cases, carbon dioxide emissions over a 100-year period are significantly lower than emissions from the production and use of gasoline from conventional crude oil and alternative fossil fuels such as coal.

There is an urgent need for alternatives to gasoline usage. This study has shown that ethanol can be an effectively reduce carbon dioxide emissions. When ethanol is produced on domestic degraded or crop lands, or in Canadian forest, it has either low or negative carbon dioxide emissions over a 100 year period. However, these benefits will take time to accrue, so the sooner the technology is implemented, the sooner we will see positive results.

8.7. References

(1) Conti J, Sweetnam GE. *Emissions of Greenhouse Gases in the United States 2008*; Report no: DOE/EIA-0573(2008); U.S. Energy Information Administration: Washington, D.C., 2009.

(2) Brandt AR, Farrell AE. Scraping the bottom of the barrel: Greenhouse gas emission consequences of a transition to low-quality and synthetic petroleum resources. *Climatic Change*. **2007**; *84*(3-4): 241-263.

(3) Lake LW. *Enhanced Oil Recovery*. Prentice-Hall: Englewood Cliffs, New Jersey, 1989.

(4) Davison J, Freund P, Smith A. (Eds.), 2001. Putting Carbon Back Into the Ground. IEA Greenhouse Gas R&D Programme.

(5) Kheshgi HS, Prince RC. Sequestration of fermentation CO_2 from ethanol production. *Energy*. **2005**; *30*(10): 1865-1871.

(6) Wyman C. Ethanol Fuel in *Encyclopedia of Energy*; C.J. Cleveland, Ed; Elsevier Academic Press: Boston, 2004; Vol. 2.

(7) Myneni RB, Dong J, Tucker CJ, Kaufmann RK, Kauppi PE, Liski J, Zhou L, Alexeyev V, Hughes MK. A large carbon sink in the woody biomass of northern forests. *P. Natl. Acad. Sci. U.S.A.* **2001**; *98*(26): 14784-14789.

(8) International Boreal Conservation Campaign. Carbon storage in Canada's boreal forest. http://www.interboreal.org/globalwarming/BorealForest-CarbonMap-Soil.pdf (accessed March 2008).

(9) Tilman D, Hill J, Lehman C. Carbon negative biofuels from low-input high-diversity grassland biomass. *Science.* **2006**; *314*(5805): 1598.

(10) Zhu JY. On energy consumption for size reduction and enzymatic saccharification of woody biomass. Presented at 31st Symposium on Biotechnology for Fuels and Chemicals, San Francisco, CA, May 4, 2009; 3-01.

(11) Lemus R, Lal R. Bioenergy crops and carbon sequestration. *Crit. Rev. Plant Sci.* **2005**; *24*(1): 1-21.

(12) Miller SD, Goulden ML, Menton MC, Da Rocha HR, De Freitas HC, Figueira AMES, de Sousa CAD. Biometric and micrometeorological measurements of tropical forest carbon balance. *Ecol. Appl.* **2004**; *14*(4): S114-S126.

(13) Aden A, Ruth M, Ibsen K, Jechura J, Neeves K, Sheehan J, Wallace B, Montague L, Slayton A, Lukas J. *Lignocellulosic biomass to ethanol process design and economics utilizing co-current dilute acid prehydrolysis and enzymatic hydrolysis for corn stover*. Report no: TP-510-32438. National Renewable Energy Laboratory: Golden, CO, 2002.

(14) *Greenhouse Gases, Regulated Emissions, and Energy Use in Transportation Model (GREET)*, version 1.8b; Argonne National Laboratory, 1999. http://www.transportation.anl.gov/modeling_simulation/GREET/ (accessed 2009).

(15) Spatari S, Zhang Y, MacLean H. Life cycle assessment of switchgrass and corn stover derived ethanol-fueled automobiles. *Environ. Sci. Technol.* **2005**; *39*(24): 9750-9758.

(16) DeLuchi MA. *Emissions of Greenhouse Gases From the Use of Transportation Fuels and Electricity, Vol. 1*. Report no: ANL/ESD/TM-22; Center for Transportation Research, Argonne National Laboratory: Argonne, IL, 1991.

(17) Lal R. Soil carbon sequestration impacts on global climate change and food security. *Science.* **2004**; *304*(5677): 1623-1627.

(18) Ranney JW, Mann LK. Environmental considerations in energy crop production. *Biomass Bioenerg.* **1994**; *6*(3): 211-228.

(19) Hendriks CA, Blok K, Turkenburg WC. Technology and cost of recovering and storing carbon dioxide from an integrated gasifier, combined-cycle plant. *Energy,* **1991**; *16* (11-12): 1277-1293.

(20) Avallone EA, Baumeister T. Fuels and Furnaces. In *Marks' Standard Handbook for Mechanical Engineers*, 10th ed. McGraw-Hill: 2008. Accesssed May 24, 2008 from Digital Engineering Library, 7-11.

(21) Office of Transportation and Air Quality, 2005. Emission Facts - Average Carbon Dioxide Emissions Resulting From Gasoline and Diesel Fuel. http://www.epa.gov/otaq/climate/420f05001.htm (accessed May 2008).

(22) Searchinger T, Heimlich R, Houghton RA, Dong FX, Elobeid A, Fabiosa J, Tokgoz S, Hayes D, Yu TH. Use of U.S. Cropland for Biofuels Increases Greenhouse Gases Through Emissions From Land-Use Change. *Science,* **2008**; *319*(5867): 1238-1240.

Chapter 9.

Conclusions

9.1. Summary of key developments and findings

Although pretreatment is critical to the successful conversion of biomass to ethanol, the deconstruction of biomass during dilute acid and hydrothermal pretreatment is not well understood. During these pretreatments, little cellulose is hydrolyzed, significant amounts of hemicellulose are hydrolyzed, and a portion of lignin is extracted. The complex composition and structure of cellulosic biomass and hundreds of possible side reactions and degradation reactions make it difficult to determine the mechanisms of hemicellulose and lignin deconstruction. In order for a cellulosic ethanol facility to be economically viable, the hemicellulose sugars, in addition to cellulose sugars, must be converted to ethanol in high yields; therefore it is important to understand the hydrolysis of hemicellulose in order to optimize sugar yields. Lignin content, composition, and integration strongly influence enzymatic digestibility of *Populus*[1] thus it is important to understand lignin deconstruction during pretreatment. Although hemicellulose shares hydrogen bonds with cellulose and covalent bonds with lignin, discussions of pretreatment implicitly treat each cell wall polymer as an independent substrate. The interactions between these polymers affect the results of pretreatment and thus greater knowledge would support the development of less recalcitrant feedstocks and more efficient pretreatment strategies.

The first objective of this thesis was to identify a system for high throughput pretreatment and enzymatic hydrolysis in order to screen thousands of plant and enzyme combinations. A custom-built metal 96 well plate was selected as the most promising design. This well plate in combination with the development of downscaled analytical

techniques revolutionized biomass analysis[1] enabling multiple studies[2, 3, 4, 5] by other researchers that were previously impossible.

The development of the metal well plate was accompanied by the implementation of indirect steam heating for pretreatment. By comparing the results of enzymatic hydrolysis after pretreatment with indirect steam heating or pretreatment with heating by conventional fluidized sand bath it was discovered that glucose and xylose yields from *Populus trichocarpa* were independent of heating technique. However, it was also found that indirect steam heating resulted in faster heat-up, more stable temperatures during pretreatment, and more reproducible temperature profiles; therefore when heating is critical, indirect steam heating is preferable.

Flowthrough pretreatment with a fixed bed reactor offers a unique opportunity to track biomass deconstruction as a function of time. After establishing baseline-operating conditions, *Populus trichocarpa*, holocellulose, and birchwood xylan were subjected to flowthrough pretreatment. The differences in the total xylooligomer production, rate of xylooligomer production, and distribution of xylooligomer sizes between *P. trichocarpa* and holocellulose indicated that lignin-hemicellulose interactions impeded xylooligomer production at the start of pretreatment; this is in agreement with Liu and Wyman's[6] hypothesis. Although not previously studied, hydrogen bonding between hemicellulose and cellulose also limits xylan hydrolysis during pretreatment as shown by the greater xylooligomer production from birchwood xylan relative to holocellulose and the lack of xylooligomers with a degree of polymerization less than seven in birchwood xylan hydrolysate.

The pretreatment of *P. trichocarpa* was also compared to the pretreatment of cellulolytic enzyme lignin (CEL). Of the three mechanisms, reaction, phase transition, or solubilization, previously suggested for lignin extraction during pretreatment, it appeared that the reactive mechanism is the primary one. This is evidenced by the detection of phenol monomers in the hydrolysate, and the significant differences in the molecular weight, composition, and structure of the pretreated CEL relative to the raw CEL. By limiting the residence time of products in the bulk liquid phase the extent of condensation reactions was reduced. Given the branched, cross-linked structure of lignin, it is logical that any relocation of lignin due to softening can only occur after bond breakage begins. Finally, the differences in lignin removal from native *P. trichocarpa* and CEL demonstrate that the hemicellulose-lignin interactions increased lignin extraction and increased the extractability of syringyl groups relative to guaiacyl groups.

The final objective of this thesis was to address the misconception that the production and use cellulosic ethanol results in carbon dioxide emissions greater than emissions from the production and use of gasoline. Comparison of ethanol production from two feedstocks, poplar and switchgrass, grown on three land types, cropland, temperate forest, and marginal land, to gasoline production from conventional and nonconventional feedstocks revealed that carbon dioxide emissions from ethanol production were substantially lower than emissions from gasoline production. In addition, depending upon the biomass and land type, cellulosic ethanol production and use could sequester significant amounts of carbon dioxide.

9.2. The influence of cell wall interactions during pretreatment

There are hydrogen bonds between hemicellulose and cellulose and covalent bonds, such as ester and ether linkages, between hemicellulose and lignin[7] making the plant cell wall highly cross-linked. Previous kinetic studies of hemicellulose hydrolysis found that the rate of hydrolysis slowed substantially leading authors to propose that hemicellulose consists of an easily hydrolyzed fraction and a difficult to hydrolyze fraction; the associated models are referred to biphasic models. Proposed causes of the differences in reactivity include heat or mass transfer limitations, changes in the interfacial surface area or different intrinsic reactivities.[8] The last is the most frequently cited and hypotheses for these different reactivities include lignin-carbohydrate bonds[9, 10, 11], hemicellulose-cellulose interactions[11], or the number and types of hemicellulose side chain substituents[9, 11]. In this thesis, pretreatment of *P. trichocarpa* and model substrates showed that lignin-hemicellulose and to a lesser extent cellulose-hemicellulose interactions limit the amount and reduce the degree of polymerization of xylooligomers produced during pretreatment. These inhibitory effects support that the hypothesis that cross-linking between hemicellulose and the other cell wall components limits hemicellulose hydrolysis.

9.3. Future work

Although this thesis has identified interactions of hemicellulose with cellulose and lignin as important influences on hemicellulose hydrolysis, additional research is needed to more fully understand the process. This thesis was performed using a single batch of *P. trichocarpa,* however the diversity of biomass is staggering, even within a single

species[3]. Examination of other *Populus* species with varying compositions and cell wall structures as well as other feedstocks such as grasses or softwoods could shed more insight into the interactions between cell wall components. Comparison of *Populus* samples with variations in hemicellulose composition would help to further define the interaction between hemicellulose and the other cell wall components. For example pretreatment of *Populus* with a larger proportion of less substituted xylan, which would be more tightly associated with cellulose[7], would further delineate the interaction between hemicellulose and cellulose. The composition and structure of hemicellulose and lignin in softwoods and grasses is substantially different from that in hardwoods. For example, unlike hardwoods, softwood hemicellulose has a high proportion of mannose and galactose and softwood lignin is predominately guaiacyl derived.[12] Pretreatment of softwoods and relevant model substrates would provide further insight into the reactivity of guaiacyl units.

Lignin-hemicellulose bonds were shown in this thesis to limit the production of xylooligomers but increase the extraction of lignin. Investigation of the solid-liquid equilibria of lignin and hemicellulose derived polymer fragments in water could yield important insights. Previous studies found the solubility of synthetic lignin polymers to increase in sugar solutions prior to the formation of lignin-hemicellulose bonds.[13, 14, 15] Therefore it is still unknown if the observations in this thesis are due to lignin-hemicellulose bonds or simply the presence of polymer fragments. To determine this, the results of xylan pretreatment with an aqueous solution of phenols, CEL pretreatment with

an aqueous solution of xylooligomers, and *P. trichocarpa* pretreatment with hydrolysate should be compared.

Although this thesis demonstrated that depolymerization and condensation reactions of lignin has the greatest influence on the extraction of lignin from *P. trichocarpa* during pretreatment, the macroscopic changes in morphology also demonstrated that lignin phase transition and redistribution occurs. Although challenging, it would be valuable to study the rheology of lignin within the cell wall during pretreatment as rheology can be used to predict the physical and processing characteristics of polymers[16]. By characterizing lignin rheology, especially over a range of temperatures, it may be possible to identify a pretreatment temperature that facilitates the redistribution of lignin. Molecular dynamic simulations will most likely be necessary to study the extrusion of lignin from the cell wall during pretreatment due to the limitations of experimental techniques.

Existing kinetic models of pretreatment treat each cell wall polymer independently without any reactions between the polymers. Developing elementary reactions for every possible reaction during pretreatment would be extremely challenging given the complexity of the system. However, the assumption of independent fractions, demonstrated to be incorrect by this thesis, is likely partially responsible for the limited applicability of the current models. Current biphasic hemicellulose hydrolysis models could be improved by replacing α, the ratio of easily hydrolyzed xylan to total xylan, with a measurement of the degree of cell wall cross-linking. Quantifying this cross-

linking will be very difficult; NMR could be one analytical technique. At the same time, care must be taken to avoid improving model fit by simply adding additional parameters.

9.4. Closing remarks

This thesis has demonstrated that the cell wall architecture significantly influences the progress of biomass deconstruction during pretreatment. Lignin-hemicellulose interactions limit the production of xylooligomers from *P. trichocarpa* and increase the proportion of released xylooligomers with a degree of polymerization less than seven (chapter 6). These same interactions increase the extraction of lignin from *P. trichocarpa* relative to that from CEL and increase the reactivity of syringyl lignin units relative to guaiacyl lignin units (chapter 7). Cellulose-hemicellulose interactions were also shown to limit the production of xylooligomers and promote the production of short chain xylooligomers (degree of polymerization less than seven) during pretreatment (chapter 6), although to a lesser extent than lignin-hemicellulose interactions.

Lignin removal is primarily through a reactive cycle of depolymerization and condensation (chapter 7). However, there is also visual evidence of phase transition and coalescence, which is enabled by the breaking of lignin and lignin-hemicellulose bonds (chapter 7).

These observations suggest several possible modifications to *Populus* to improve ethanol production. Although cellulose-hemicellulose interactions limit xylan hydrolysis, they do so to a lesser extent than lignin-hemicellulose interactions. The interactions are also beneficial as they promote the production of short chain xylooligomers, which have been shown to be less inhibitory during enzymatic hydrolysis than long chain

xylooligomers.[17] Therefore, increasing the cellulose content and reducing the lignin content may improve hemicellulose hydrolysis during pretreatment; this would also be beneficial as a greater cellulose content would result in a greater ethanol production per ton of biomass. Alternatively, modifying the hemicellulose structure to promote hydrogen bonding with cellulose and limit covalent bonding with lignin could improve hemicellulose sugar recovery during pretreatment.

Flowthrough pretreatment produces much more digestible biomass batch pretreatment but the amount of water consumption makes flowthrough pretreatment unsuitable for commercial implementation.[18] Previous studies have attempted to reduce water use during flowthrough pretreatment by applying a flow of water for limited periods of pretreatment either in the middle of pretreatment[18] or at the end[19] of pretreatment. This thesis found that the majority of xylooligomer production and lignin removal occurs during the initial stages of pretreatment at 180^{o}C. Therefore, it may be more beneficial to apply a flow of water at the start of pretreatment to remove the majority of extractable hemicellulose and lignin and limit side and degradation reactions before applying batch conditions to hydrolyze the more recalcitrant fractions of biomass. Another pretreatment strategy to increase delignification could be to perform pretreatment with recycled hydrolysate if it is shown that solubility of lignin can be increased by the presence of dissolved polysaccharides.

The polymers of plant cell walls and bonds between them are complex structures that are not easily decomposed. However, this decomposition to fermentable sugars must be done efficiently for minimal cost in order for cellulosic ethanol and its numerous

benefits to be realized. Lignin-hemicellulose bonds and cellulose-hemicellulose bonds, to a lesser extent, limit xylan hydrolysis but the lignin-hemicellulose bonds may also improve lignin extraction. Knowledge of these interactions suggests possibilities for less recalcitrant feedstocks and advanced pretreatment strategies that could lead to the successful commercialization of cellulosic ethanol.

9.5. References

(1) DeMartini JD. Chemical and structural features of plants that contribute to biomass recalcitrance. Ph.D., University of California Riverside, Riverside, CA, Dec 2012.

(2) DeMartini JD, Wyman CE. Changes in composition and sugar release across the annual rings of Populus wood and implications on recalcitrance. *Bioresource Technol*. **2011**; *102*: 1352-1358.

(3) Studer MH, DeMartini JD, Dvis MF, Sykes RW, Davison B, Keller M, Tuskan GA, Wyman CE. Lignin content in natural *Populus* variants affects sugar release. *P. Natl. Acad. Sci. USA*. **2011**; *108*: 6300-6305.

(4) DeMartini JD, Wyman CE. Composition and hydrothermal pretreatment and enzymatic saccharification performance of grasses and legumes from a mixed-species prairie. *Biotechnology for Biofuels*. **2011**; *4*. DOI 10.1186/1754-6834-4-52.

(5) Lindedam J, Andersen SB, DeMartini JD, Bruun S, Jorgensen H, Felby C, Magid J, Yang B, Wyman CE. Cultivar variation and selection potential relevant to the production of cellulosic ethanol from wheat straw. *Biomass Bioenerg*. **2012**; *37*: 221-228.

(6) Liu C, Wyman CE. The effect of flow rate of compressed hot water on xylan, lignin, and total mass removal from corn stover. *Ind. Eng. Chem. Res*. **2003**; *42*(21): 5409-5416.

(7) Albersheim P, Darvill A, Roberts K, Sederoff R, Staehelin A. *Plant cell walls from chemistry to biology*. Garland Science: New York, 2011.

(8) Maloney MT, Chapman TW, Baker AJ. Dilute acid hydrolysis of paper birch: kinetics studies of xylan and acetyl group hydrolysis. *Biotechnol. Bioeng*. **1985**; *27*: 355-361.

(9) Chen X, Lawoko M, van Heiningen A. Kinetic and mechanism of autohydrolysis of hardwoods. *Bioresource Technol*. **2010**; *101*: 7812-7819.

(10) Conner AH. Kinetic modeling of hardwood prehydrolysis: Part I. Xylan removal by water prehydrolysis. *Wood Fiber Sci*. **1984**; *16*: 268-277.

(11) Lee YY, Iyer P, Torget RW. Dilute-acid hydrolysis of lignocellulosic biomass. *Adv. Biochem. Eng. Biot*. **1999**; *65*: 93-115.

(12) Fengel D, Wegener G. *Wood: Chemistry, ultrastructure, reactions.* Walter de Gruyter & Co: Berlin, 1983.

(13) Barakat A, Chabbert B, Cathala B. Effect of reaction media concentration on the solubility and the chemical structure of lignin model compounds. *Phytochemistry*. **2007**; *68*(15): 2118-2125.

(14) Barakat A, Winter H, Rondeau C, Saake B, Chabbert B, Cathala B. Studies of xylan interactions and cross-linking to synthetic lignins formed by bulk and end-wise polymerization: a model study of lignin carbohydrate complex formation. *Planta*. **2007**; *226*(1): 267-281.

(15) Cathala B, Monties B. Influence of pectins on the solubility and molar mass distribution of dehyrogenative polymers (DHPs, lignin model compounds). *Int. J. Biol. Macromol*. **2001**; *29*(1): 45-51.

(16) Shaw MT. *Introduction to polymer rheology*. John Wiley & Sons: Hoboken, NJ, 2012, 1-14.

(17) Qing Q, Wyman CE. Hydrolysis of different chain length xylooligomers by cellulase and hemicellulase. *Bioresource Technol.* **2011**; *102*: 1359-1366.

(18) Liu C, Wyman CE. Partial flow of compressed hot water through corn stover to enhance hemicellulose sugar recovery and enzymatic digestibility of cellulose. *Bioresource Technol.* **2005**; *96*: 1978-1985.

(19) Yu Q, Zhuang X, Yuan Z, Wang W, Qi W, Wang Q, Tan X. Step-change flow rate liquid hot water pretreatment of sweet sorghum bagasse for enhancement of total sugars recovery. *Appl. Energ*. **2011**; *88*: 2472-2479.